Numerical modelling of mining subsidence, upsidence and valley closure using UDEC

Walter Keilich
University of Wollongong

NUMERICAL MODELLING OF MINING SUBSIDENCE, UPSIDENCE AND VALLEY CLOSURE USING UDEC

A thesis submitted in fulfillment of the
requirements for the award of the degree

DOCTOR OF PHILOSOPHY

from

UNIVERSITY OF WOLLONGONG

by

Walter Keilich, BE Hons (Mining)

SCHOOL OF CIVIL, MINING AND ENVIRONMENTAL ENGINEERING

2009

THESIS CERTIFICATION

I, Walter Keilich, declare that this thesis, submitted in fulfilment of the requirements for the award of Doctor of Philosophy, in the School of Civil, Mining and Environmental Engineering, University of Wollongong, is wholly my own work unless otherwise referenced or acknowledged below. The document has not been submitted for qualifications at any other academic institution.

Walter Keilich

9/09/2009

TABLE OF CONTENTS

LIST OF FIGURES

LIST OF TABLES

LIST OF SYMBOLS

A	=	Cross sectional area (m^2)
C_1	=	Closure from one side of valley (m)
c	=	Cohesion (MPa)
D	=	Distance of inflection point relative to goaf edge (m)
E	=	Young's Modulus (GPa)
$+E_{max}$	=	Maximum tensile ground strain (mm/m)
$-E_{max}$	=	Maximum compressive ground strain (mm/m)
G	=	Shear Modulus (GPa)
G_{max}	=	Maximum ground tilt (mm/m)
H	=	Depth of cover (m)
ITS	=	Indirect Tensile Strength (MPa)
JCS	=	Joint Wall Compressive Strength
JRC	=	Joint Roughness Coefficient
K	=	Bulk Modulus (GPa)
K1	=	Tensile strain factor
K2	=	Compressive strain factor
K3	=	Tilt factor
K4	=	Radius of ground curvature factor
l	=	Length of plate (m)
P_W	=	Pillar width (for multiple panel layouts) (m)
ϕ_1	=	Tilt of block adjacent to valley (radians)
ϕ	=	Friction angle (°)
Φ	=	Abutment angle (°)
θ	=	Change in tilt between two blocks
q	=	Constant (0.5 for both ends of plate clamped)
R_1	=	Depth of valley (m)
R_{min}	=	Minimum radius of ground curvature (km)
r	=	Radius or height of valley wall (m)
S_{goaf}	=	Goaf edge subsidence (m)
S_{max}	=	Maximum developed subsidence (mm)
s	=	Length of arc (m)

σ_c	=	Unconfined Compressive Strength (MPa)
σ_α	=	Axial stress required for buckling (MPa)
σ_H	=	Horizontal stress (MPa)
T	=	Extracted seam thickness (m)
t	=	Thickness of plate (m)
UCS	=	Unconfined Compressive Strength (MPa)
υ	=	Poisson's Ratio
UTS	=	Uniaxial Tensile Strength (MPa)
VL2F	=	20 cm field sonic velocity
W	=	Width of underground opening (m)
W_L	=	Panel width + pillar width (m)
x_1	=	Distance between block corners (m)
y_1	=	Subsidence at corner of block (m)
y_{11}	=	Subsidence at corner of block (m)

ABSTRACT

Ground subsidence due to mining has been the subject of intensive research for several decades, and it remains to be an important topic confronting the mining industry today. In the Southern Coalfield of New South Wales, Australia, there is particular concern about subsidence impacts on incised river valleys – valley closure, upsidence, and the resulting localised loss of surface water under low flow conditions. Most of the reported cases have occurred when the river valley is directly undermined. More importantly, there are a number of cases where closure and upsidence have been reported above unmined coal. These latter events are especially significant as they influence decisions regarding stand-off distances and hence mine layouts and reserve recovery.

The deformation of a valley indicates the onset of locally compressive stress conditions concentrated at the base of the valley. Compressive conditions are anticipated when the surface deforms in a sagging mode, for example directly above the longwall extraction; but they are not expected when the surface deforms in a hogging mode at the edge of the extraction as that area is typically in tension. To date, explanations for valley closure under the hogging mode have considered undefined compressive stress redistributions in the horizontal plane, or lateral block movements and displacement along discontinuities generated in the sagging mode. This research is investigating the possibilities of the block movement model and its role in generating compressive stresses at the base of valleys, in the tensile portion of the subsidence profile.

The numerical modelling in this research project has demonstrated that the block movement proposal is feasible provided that the curvatures developed are sufficient to allow lateral block movement. Valley closure and the onset of valley base yield are able to be quantified with the possibility of using analytical solutions. To achieve this, a methodology of subsidence prediction using the Distinct Element code UDEC has been developed as an alternative for subsidence modelling and prediction for isolated longwall panels. The numerical models have been validated by comparison with empirical results, observed caving behaviour and analytical solutions, all of which are in good agreement. The techniques developed in the subsidence prediction UDEC models have then been used to develop the conceptual block movement model.

The outcomes of this research have vast implications. Firstly, it is shown that valley closure and upsidence is primarily a function of ground curvature. Since the magnitude of curvature is directly related to the magnitude of vertical subsidence there is an opportunity to consider changes in the mine layout as a strategy to reduce valley closure. Secondly, with further research there is the possibility that mining companies can assess potential damage to river valleys based on how close longwall panels approach the river valley in question. This has the added advantage of optimising the required stand off distances to river valley and increasing coal recovery.

ACKNOWLEDGEMENTS

There are many people that I would like to thank for their advice and support over the past six years:

- My principal supervisor Associate Professor Naj Aziz from the School of Civil, Mining and Environmental Engineering, University of Wollongong. My association with Naj began when I commenced my undergraduate mining engineering degree in 1998, and he has been the driving force behind my decision to undertake further study. I would like to thank Naj for his continued support and motivation which has gained my admiration and respect.
- My secondary supervisor Associate Professor Ernest Baafi from the School of Civil, Mining and Environmental Engineering, University of Wollongong. Ernest's advice on numerical modelling, particularly in the early stages of the project was invaluable.
- Dr Ross Seedsman from Seedsman Geotechnics for his financial support, invaluable technical advice and guidance. Without Ross's help, I doubt this project would be where it is now, let alone finished.
- The Australian Coal Association Research Program for their financial support in the first eighteen months of the research project.
- Dr Michael Coulthard from MA Coulthard and Associates. Michael's extremely helpful technical advice on UDEC quite often got the ball rolling again when all seemed lost.
- Johnson Lee, my research partner for the first eighteen months of this project. Johnson's advice on numerical modelling helped me avoid many traps that befall those who are new to the art of numerical modelling.
- The staff at Strata Control Technology for providing access to their drill cores and logs.
- The staff at Metropolitan Colliery for allowing me access to sensitive areas above longwall panels. This experience gave me an appreciation of the enormity of the problem that I was researching.

- The staff at the CSIRO Exploration & Mining (Queensland Centre for Advanced Technologies) for cultivating a further interest in mining geomechanics, giving me time to work on the project and providing excellent computing facilities.
- The staff at Snowden Mining Industry Consultants who encouraged me to finish the project and provided the resources to do so.

Last but not least I would like to thank my family and friends that helped me through what was sometimes a very testing and difficult period. Your support and patience never ceased to amaze me, and for that I remain grateful.

PUBLICATIONS ARISING FROM RESEARCH PROJECT

The outcomes of this research work have resulted in the publication of four papers in mining/geotechnical conferences and one industry based report. Another conference paper and a journal article are in preparation at this time.

- Keilich, W & Aziz, N I 2007, 'Numerical modelling of mining induced subsidence', *Proceedings IMCET 2007*, Ankara, Turkey, June 2007.
- Keilich, W, Seedsman, R W & Aziz, N I 2006, 'Numerical modelling of mining induced subsidence in areas of high topographical relief', *Proceedings of the AMIREG 2006 – 2nd International Conference*, Hania, Greece, September 2006.
- Keilich, W, Seedsman, R W & Aziz, N I 2006, 'Numerical modelling of mining induced subsidence', *Proceedings of the Coal 2006 - 8th Underground Coal Operator's Conference*, Wollongong, NSW, July 2006.
- Keilich, W, Lee, J W, Aziz, N I & Baafi, E Y 2005, 'Numerical modelling of undermined river channels – a case study', *Proceedings of the Coal 2005 – 6th Underground Coal Operator's Conference*, Brisbane, QLD, April 2005.
- Aziz, N I, Baafi, E Y, Keilich, W & Lee, J W 2004, 'University of Wollongong Report on ACARP Project 22083 – Development of Protection Strategies, Damage Criteria and Practical Solutions for Protecting Undermined River Channels', ACARP Research Project No. 22083, *Australian Coal Association Research Program, Brisbane, Queensland, Australia*.

CHAPTER 1
INTRODUCTION

1.1 PROBLEM STATEMENT AND OBJECTIVE

In the Southern Coalfield of New South Wales there is particular concern about subsidence impacts on incised river valleys – valley closure (the two sides of the valley moving horizontally towards the valley centreline), upsidence (upward movement of the valley floor), and the resulting localised loss of surface water under low flow conditions (Figure 1.1 and Figure 1.2). The resulting visual effects of subsidence impacts on river valleys can be quite dramatic with visible presence of water loss, and cracking and buckling of river beds and rock bars. Most of the reported cases have occurred when the river valley is directly undermined but there are a number of cases where valley closure and upsidence have been reported above old mined longwall panels and unmined coal. These latter events are especially significant as they influence decisions regarding stand-off distances and hence mine layouts and reserve recovery.

To date, the explanations offered for these valley closure and upsidence events above unmined coal and old longwall panels involved an increase of undefined horizontal compressive stresses, en masse rock movements and movement along discontinuities. There has been no published study which verifies any of these proposed mechanisms.

The horizontal compressive stress model of Waddington and Kay (2002) can be considered valid when a river valley is situated in the sagging portion of the subsidence profile, as horizontal compressive stress conditions are anticipated when the ground surface deforms in the sagging mode due to the horizontal shortening of the ground surface over the longwall panel. In other portions of the subsidence profile the dominant horizontal stress change is tensile and when the valley is not located above the longwall panel, the traditional horizontal stress redistribution model appears inappropriate.

Fig. 1.1 – Water level reduction in river valley affected by longwall mining

Fig. 1.2 – Unsightly cracking of rock bars in river valley affected by longwall mining

For this thesis, two alternative explanations were considered.

The first alternative explanation for valley closure and upsidence in the tensile portion of the subsidence profile (the hogging phase) includes a redistribution of compressive stresses in the horizontal plane. In this case, compressive stress increases above unmined coal and decreases above mined panels provided that the stress concentrations for valleys are aligned radial to the goaf. This does not explain the valley closure and upsidence events observed above old longwall panels, and will not be pursued further.

The second alternative involves block movements. It is proposed that the horizontal shortening of the ground surface in the sagging phase results in blocks of rock being pushed up the side of the subsidence bowl and into the free face provided by the valley, resulting in valley closure and possible upsidence over unmined coal. This alternative could also explain why valley closure and upsidence occur over old longwall panels as well.

The objective of this thesis is to investigate with numerical modelling whether the block movement proposal is feasible, and if so, provide a credible alternative explanation to the currently used horizontal compressive stress theory.

1.2 METHODOLOGY

There were seven distinct phases in this project:

- The first phase (Chapter 2) involved a review of subsidence theory with particular reference to the Southern Coalfield.
- The second phase (Chapter 3) reviewed valley closure, upsidence and the associated empirical prediction technique. The shortcomings of the currently used model were identified and a new theory of block movements was introduced.
- The third phase (Chapter 4) established the principles of developing a numerical modelling approach. A review of modelling papers related to mining subsidence was also conducted to assist in the selection of the numerical modelling code.
- The fourth phase (Chapter 5) was centred on developing a full scale UDEC subsidence model for isolated single longwall panels that was able to be verified

with empirical data. An audit was conducted on the models (Appendix A) and an example of the modelling code is contained in Appendix B.

- The fifth stage (Chapter 6) involved using the key characteristics from the full scale subsidence models and the creation of a simplified set of models that simulated river valley response with respect to river valley position compared to longwall position. The results from the river valley models were compared to the empirical predictions and kinematic concepts detailed in Chapter 3. A parametric study on the joint properties was also performed. Examples of the code are contained in Appendix C and Appendix D.
- The sixth stage (Chapter 7) applied the voussoir beam analogue and a plate buckling solution to test the numerical models against analytical solutions. The voussoir beam theory is contained in Appendix E.
- The seventh and final stage (Chapter 8) of the project saw the formulation of a summary and conclusion.

1.3 OUTCOMES AND POTENTIAL APPLICATIONS

The expected outcomes of this project are:

- A subsidence prediction tool for isolated longwall panels in flat terrain,
- A greater understanding of the mechanisms behind mining induced subsidence in the Southern Coalfield,
- A feasible explanation for valley closure based on numerical modelling, and
- The confirmation that valley closure and the onset of valley base yield can be assessed with analytical solutions.

CHAPTER 2
MINE SUBSIDENCE IN THE SOUTHERN COALFIELD

2.1 INTRODUCTION

Mine subsidence has long been considered a problem, but only since the 1950's has there been a concerted effort to predict the degree of subsidence and the associated effects on the surface environment.

The concepts and theories of mining subsidence date back to the 1850's, with the earliest concepts appearing to be of Belgian and French origin. Other countries with significant coal industries (Germany, Poland and the United Kingdom) also contributed to the scientific research and findings. A comprehensive review of the development of subsidence theory is given by Whittaker and Reddish (1989).

In terms of subsidence prediction, a major milestone was the publication of the National Coal Board Subsidence Engineers' Handbook in 1966 which has since been revised (National Coal Board 1975). This empirical model was based on observations from around 200 sites in several U.K. coalfields. This method has been widely used in other countries but is generally limited in its application to U.K. strata.

Locally, this prompted the development of similar empirical methods, most notably for the Southern Coalfield of New South Wales (Holla & Barclay 2000, Waddington & Kay 1995) and the Newcastle District of the Northern Coalfield of New South Wales (Kapp 1984). This involved obtaining subsidence parameter values from a series of charts and graphs according to specified mine layouts and surface geometries.

This chapter will present a review of Southern Coalfield geology; subsidence theory associated with longwall mining and discusses the widely used empirical methods of Holla and Barclay (2000) and Waddington and Kay (1995).

2.2 SUBSURFACE MOVEMENT

During longwall mining, a large void in the coal seam is produced and this disturbs the equilibrium conditions of the surrounding rock strata, which bends downward while the floor heaves.

When the goaf reaches a sufficient size, the roof strata will fail and cave. Seedsman (2004) reports that caving does not necessarily occur vertically above the extracted longwall panel and in many cases, caving is defined by a goaf angle that is measured from vertical and trends inward over the goaf. This angle is most likely a function of the bedding structure of the roof and the orientation of the goaf with respect to sub vertical jointing. In the Newcastle Coalfield, the average goaf angle is 12º with a standard deviation of 8º. Numerical modelling by CSIRO Exploration and Mining and Strata Control Technology (1999) of the caving in the Southern Coalfield appears to support a goaf angle value of 12º. Further numerical modelling by Gale (2005) in an unspecified coalfield also supports this value. Caving will cease when the goaf angle encounters a stratigraphic unit strong enough to bridge what is now the effective span. This concept is illustrated in Figure 2.1. The goaf and overburden strata will then compact over time and become stabilised.

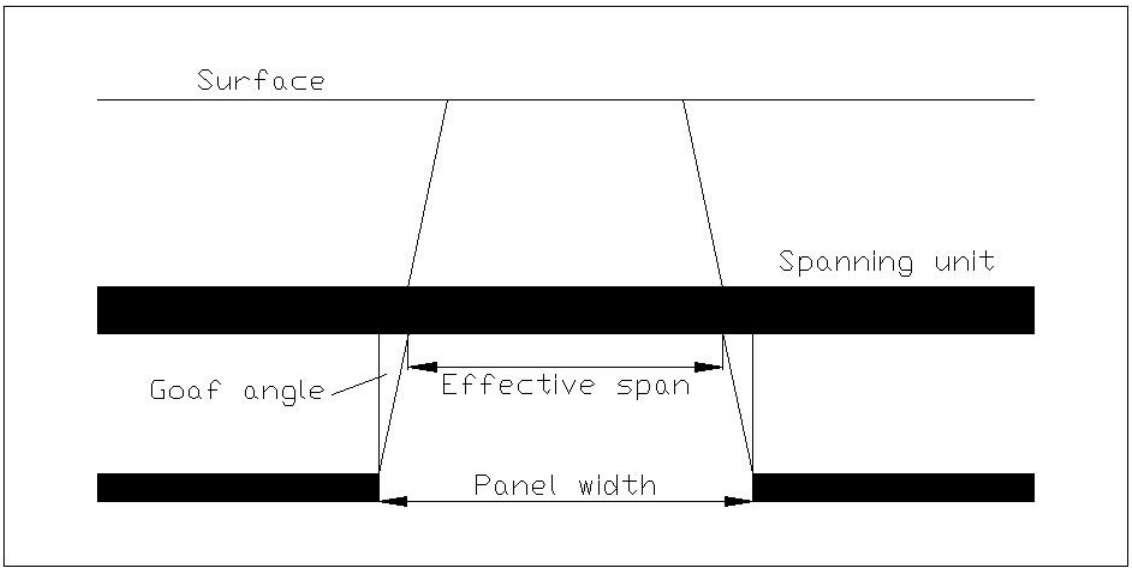

Fig. 2.1 – Relationship between panel width, goaf angle and effective span

2.2.1 Zones of movement in the overburden

The caving of the roof strata as previously described gives rise to several zones within the overburden strata. The number of zones varies in the literature with Kratzsch (1983) describing six zones, Peng (1992) describing four zones, and Kapp (1984) describing three zones. These zones are not distinct but there is a gradual transition from one to another.

In the Southern Coalfield, Holla and Barclay (2000) report on the monitoring of subsurface movements over five longwall panels at Tahmoor Colliery. The borehole in which the monitoring equipment was installed was located above the third longwall panel. It was found that most of the strata dilation and separation took place up until the third longwall panel was extracted, and then the subsurface movements changed to an en masse nature when the fourth and fifth longwall panels were extracted. It was also found that the overburden from the surface to a depth of 112 m suffered almost no dilation. This was explained as being a result of the stratigraphic nature of the overburden to that depth, and it could also be explained by the deflection of a massive spanning unit in the overburden.

Various researchers have used different vertical distances to define the transition points from one zone to another. Overall, regardless of the number of zones, the vertical fracture profile gives a similar representative picture (Figure 2.2).

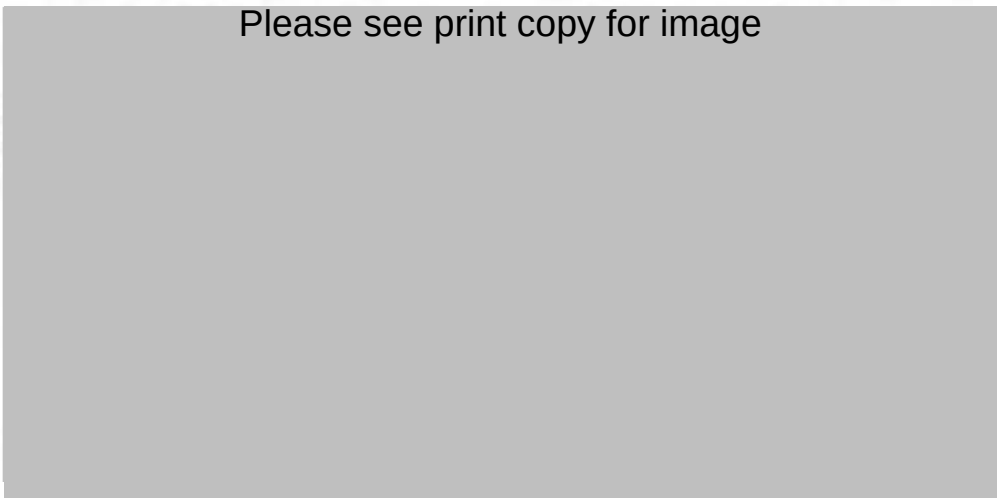

Fig. 2.2 – Overburden movement above a longwall panel (Peng 1992)

2.2.2 Caving in the Southern Coalfield and its significance on subsidence development

Seedsman (2004) reported on the existence of a massive unit in the strata of the Newcastle Coalfield and presented an alternative way of predicting subsidence based on the voussoir beam analogue. For this method to be applied, it is assumed that the massive unit remains elastic and all caving takes place underneath the massive unit. Therefore, it is implied that the developed subsidence is a function of the deflection of the massive unit provided the massive unit remains elastic and does not fail.

Unfortunately, the amount of information on the caving characteristics in the Southern Coalfield is somewhat limited. Microseismic results from the CSIRO Exploration and Mining Division, and Strata Control Technology, in an Australian Coal Association Research Program (ACARP) project provided some useful information on the caving behaviour at Appin Colliery, which is located in the Southern Coalfield (CSIRO Exploration & Mining & Strata Control Technology 1999). The longwall panel that was monitored was 200 m wide and extracted the 2.3 m thick Bulli Seam at a depth of about 500 m. The monitoring included the installation of 17 triaxial geophones and nine geophones in a borehole drilled from the surface to the Bulli Seam and two perpendicular surface strings of four geophones each. The period of monitoring was approximately four months, during which there was 700 m of face retreat.

From the monitoring, it was seen that the majority of fracturing extended approximately 50 m to 70 m above the Bulli Seam with no fracturing exceeding approximately 290 m, and to a depth of 80 m to 90 m into the floor. Figure 2.3 illustrates the microseismic events in a cross section of the monitored longwall panel.

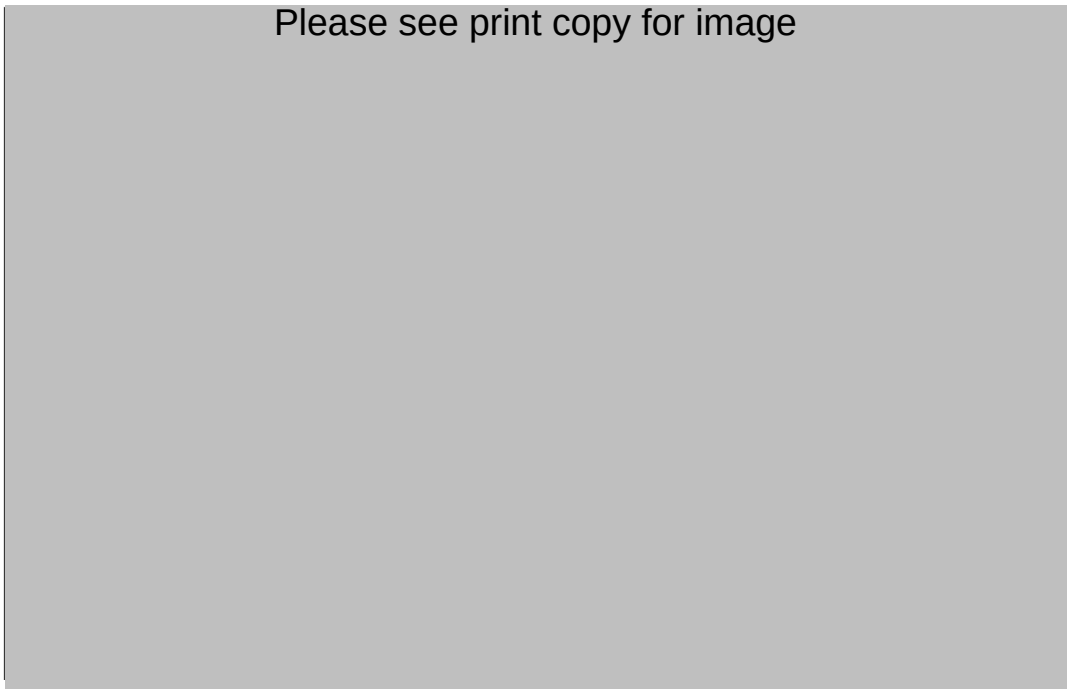

Fig. 2.3 – Cross section of longwall panel with microseismic event location (CSIRO Exploration & Mining & Strata Control Technology 1999)

An analysis of Holla and Barclay (2000) indicates that the Bulgo Sandstone is the most massive unit in the stratigraphy of the Southern Coalfield, with a thickness ranging from approximately 90 m to 200 m, and located at a distance between 90 m and 120 m above the Bulli Seam at Appin Colliery. It is also the strongest of the larger units. If the position of the Bulgo Sandstone were overlain onto Figure 2.3, it would be seen that the majority of the fracturing in the goaf is below the Bulgo Sandstone with some isolated fracturing events above this level. This would seem to suggest that the Bulgo Sandstone is acting as the massive spanning unit, therefore all potential subsidence development can be theoretically derived from a voussoir analysis of the Bulgo Sandstone. This is discussed in Appendix E with the voussoir theory and its potential use as a verification tool for the numerical model.

2.3 SURFACE DEFORMATIONS

The subsidence basin that is formed when an underlying area is extracted usually extends beyond the limits of the underground openings. The subsidence profile in theory is symmetrical about the longwall panel centreline with the maximum subsidence

(S_{max}) occurring at the trough centre (Holla & Barclay 2000). The components of trough subsidence are illustrated in Figure 2.4.

The main parameters of ground movement are:

- Maximum subsidence (S_{max}),
- Maximum ground tilt (G_{max}),
- Maximum tensile and compressive ground strains ($+E_{max}$ & $-E_{max}$), and
- Minimum radius of ground curvature (R_{min}).

The value of the maximum subsidence essentially depends on the extracted seam thickness (T), depth of cover (H), width of the underground opening (W) and degree of goaf support. The tilt of the ground surface between two points is calculated by dividing the difference in reduced levels by the distance between the points. Tilt can also be calculated by taking the first derivative of the subsidence curve. Accordingly, maximum tilt occurs at the point of inflection on the subsidence curve, which is also the point where the subsidence is approximately equal to one half of S_{max}.

Strains result from horizontal movements. Horizontal strain is defined as the change in length per unit of the original horizontal length of ground surface. Compressive strains occur over the extracted area due to the downward and inward movement of the surface, and tensile strains occur over goaf edges and in the area of trough margin. The point of inflection on the subsidence curve also represents the transition from compressive strain to tensile strain.

Strain and tilt (Equations 2.1 to 2.3) have been found to be directly proportional to the maximum subsidence and inversely proportional to the cover depth (National Coal Board 1975):

$$+E_{\max} = \frac{1000 \times K1 \times S_{\max}}{H} \qquad [2.1]$$

$$-E_{\max} = \frac{1000 \times K2 \times S_{\max}}{H} \qquad [2.2]$$

$$G_{\max} = \frac{1000 \times K3 \times S_{\max}}{H} \qquad [2.3]$$

Where,

K1 = Tensile strain factor (non-dimensional)

K2 = Compressive strain factor (non-dimensional)

K3 = Tilt factor (non-dimensional)

The curvature is the rate of change of tilt (second derivative of the subsidence curve) and it is concave above part of the extracted area and convex in the area of trough margin and over goaf edges. The curvature (1/R) has been found to be directly proportional to the depth of mining (Equation 2.4):

$$\frac{1}{R_{\min}} = \frac{K4 \times E_{\max}}{H} \qquad [2.4]$$

Where,

K4 = Curvature factor (non-dimensional)

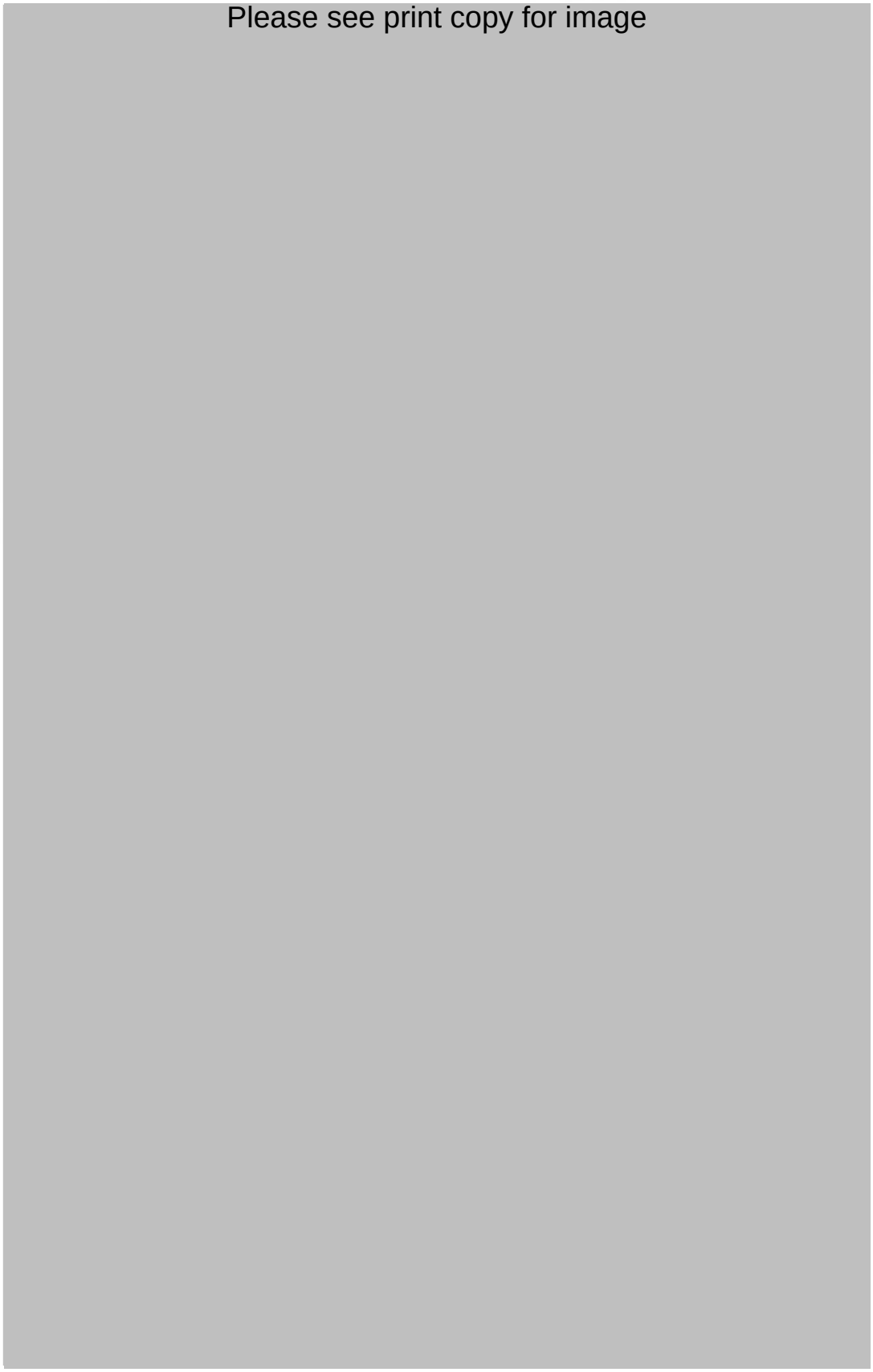

Fig. 2.4 – Characteristics of trough subsidence (Holla 1985)

2.3.1 Angle of draw

The angle of draw (or the limit of mining influence) is defined as the angle between the vertical and the line joining the extraction edge with the edge of the subsidence trough. In practice, the angle of draw is difficult to measure and implement because the subsidence profile is asymptotic to the original surface, and small errors in surveying measurements may result in a large range of draw angles.

Holla and Barclay (2000) stated “The trough margin is regarded as the point where a clear subsidence of 10 or 20 mm can be found by levelling, provided there is no question of ground settlement through non-mining causes”. This statement seems practical as most structures can withstand certain amount of movements without damage. Even in areas not affected by mining, studies in New South Wales have shown that movements up to 20 mm can occur from climatic variations (Holla & Barclay 2000). It must be noted that the origin of the 20 mm cut-off limit for subsidence appears to originate from Kratzsch (1983).

The magnitude of the angle of draw varies widely between coalfields. In the Southern Coalfield of New South Wales, the draw angle varies between 2° and 56°, assuming a cut-off subsidence of 20 mm. The average draw angle was 29° with nearly 70 % of the observed values below 35° (Holla & Barclay 2000). In the Newcastle District of the Northern Coalfield, Kapp (1984) recorded draw angles varying from 21.3° - 44.4° whilst imposing a cut-off subsidence of 5 mm.

Whittaker and Reddish (1989) compiled the variation in draw angles for different coalfields:

- Yorkshire Coalfield (U.K.): 32°- 38°,
- South Limburgh Coalfield (U.K): 35° - 40°,
- Indian coalfields: 4° - 21°,
- US coalfields: 12° - 34°, and
- Czechoslovakian coalfields: 25° - 30°.

It must be noted about the measurement of draw angles in coalfields other than the Southern Coalfield of New South Wales, it is not known whether a 20 mm cut-off subsidence limit was imposed.

As can be seen, the once common practice of applying the National Coal Board values for draw angles in Australia whilst performing subsidence predictions is no longer valid. Due to the different geological characteristics of each coalfield, it is imperative that the empirical methods developed for that particular coalfield are used instead.

2.3.2 Extraction area

There are three classifications of extraction area that influence the characteristics of the subsidence trough. These classifications are expressed in terms of the extraction width/depth of cover ratio (W/H). The three classifications are:

- Sub-critical extraction,
- Critical extraction, and
- Super-critical extraction.

Sub-critical extraction is defined as an extraction that has a W/H ratio less than 1.4. A sub-critical extraction is insufficient to produce maximum subsidence (S_{max}) at the longwall panel centre due to the degree of strata arching/bending across the longwall panel. Critical extraction is defined as an extraction that has a W/H ratio of approximately 1.4 – 2.0. A critical extraction is one that is just large enough to produce maximum subsidence at the longwall panel centre (Holla & Barclay 2000). The magnitude of the critical width depends on the geological characteristics of the overburden. Super-critical extraction is defined as an extraction that has a W/H ratio larger than 2.0. A super-critical extraction allows development of the full potential subsidence. The main difference between critical and super-critical extractions is the shape of the subsidence trough. In a super-critical extraction, the maximum subsidence will occur over a length on the surface, instead of at one point as characterised by critical extractions. A comparison of sub-critical, critical and super-critical trough shapes and strain profiles is illustrated in Figure 2.5.

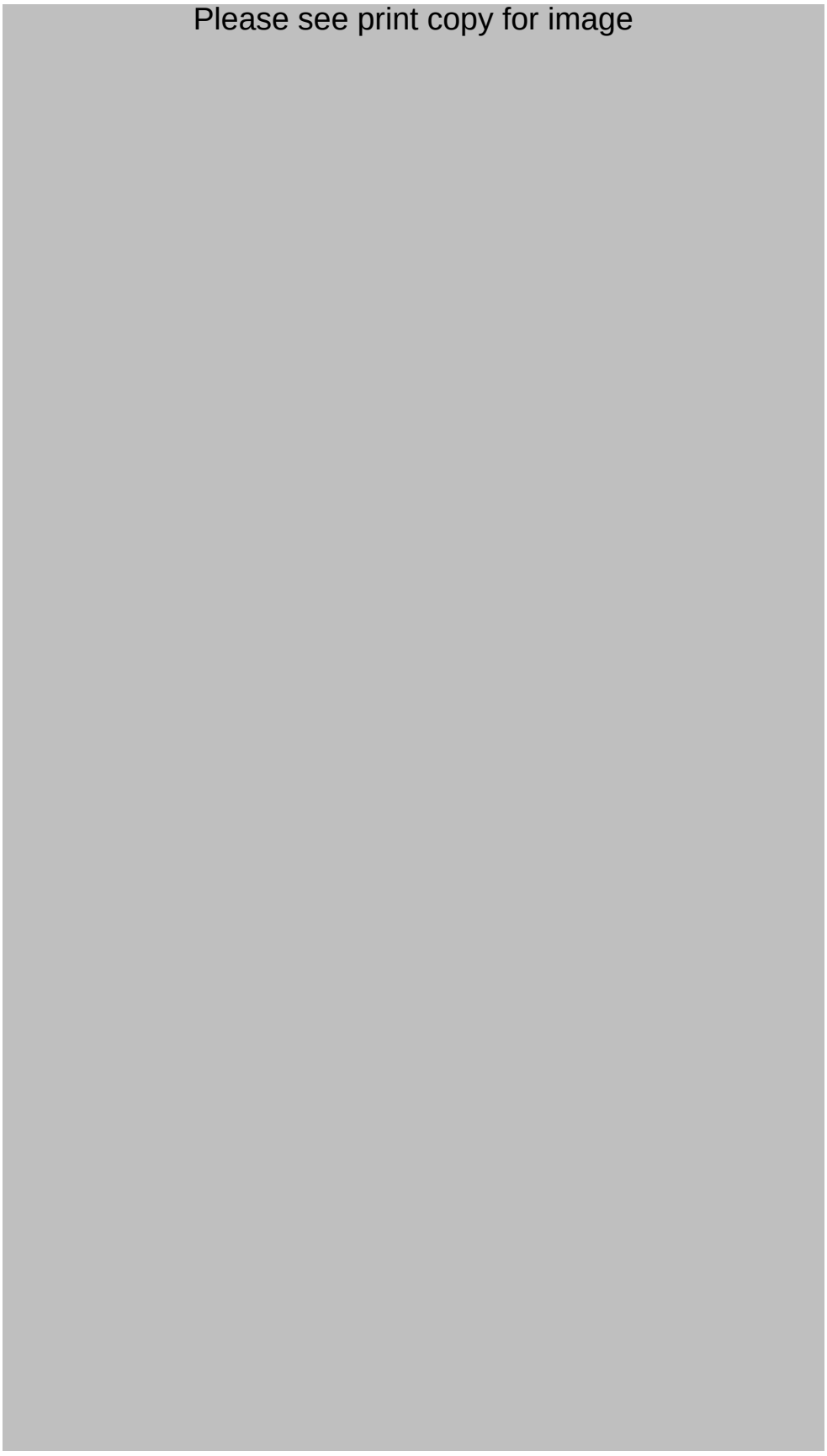

Fig. 2.5 – Sub-critical, critical and super-critical trough shapes (Whittaker & Reddish 1989)

2.3.3 Stationary and dynamic subsidence profiles

When considering a longwall panel, it can be seen that a subsidence profile can be drawn in two directions: across the longwall panel (transverse) and along the longwall panel (longitudinal). The transverse profiles are called stationary profiles because they lie across the already mined extraction edges and associated movements are permanent. The longitudinal profiles are called dynamic profiles because they lie lengthways along the longwall panel, following the advancing longwall face. The movements associated with dynamic profiles are variable. Figure 2.6 and Figure 2.7 illustrate the formation of stationary and dynamic subsidence profiles respectively.

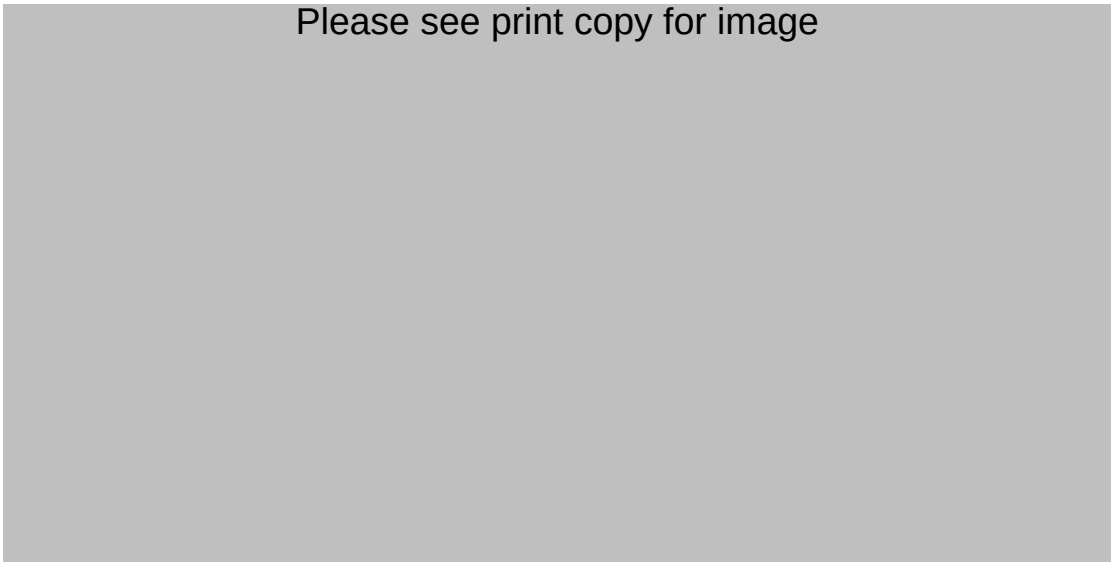

Fig. 2.6 – Stationary subsidence profiles (Peng 1992)

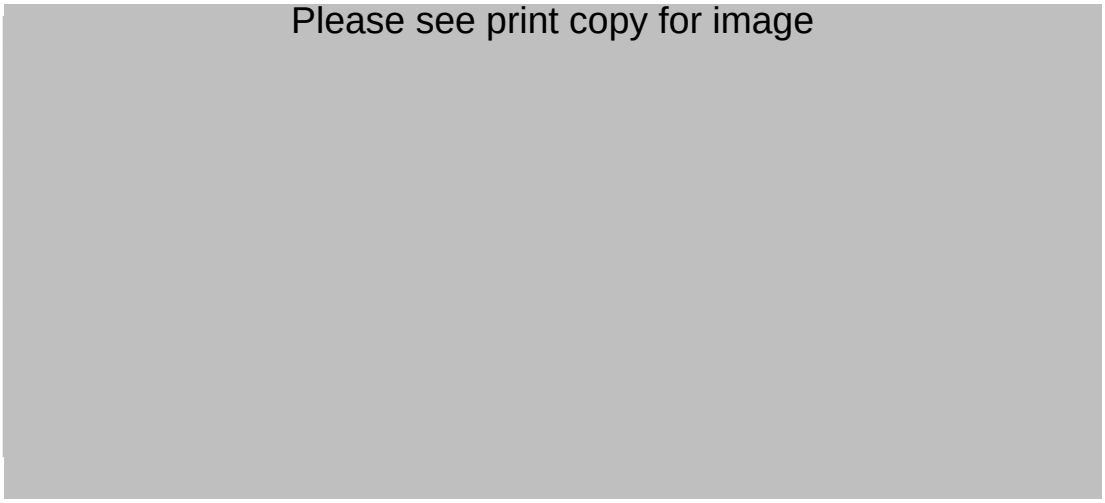

Fig. 2.7 – Dynamic subsidence profiles (Peng 1992)

2.4 SOUTHERN COALFIELD GEOLOGY

The geology of the Sydney Basin has been studied extensively by numerous authors such as Hanlon (1953), Packham (1969), Bowman (1974), Reynolds (1977), Jones and Rust (1983), Ghobadi (1994), and Holla and Barclay (2000). Between these authors, a comprehensive description of the geology, stratigraphy, stratigraphic nomenclature, geological mapping and engineering properties of various stratigraphic units have been established. The Southern Coalfield is one of five coalfields within the Sydney Basin. A summary based on the above mentioned authors will be given in this chapter.

2.4.1 The Sydney Basin

The Sydney Basin comprises the Southern part of the much larger Sydney-Bowen Basin, which extends from Batemans Bay in Southern New South Wales to Collinsville in Queensland. The Sydney Basin contains gently folded sedimentary rocks of Permian (270 million years ago) and Triassic (225 million years ago) ages deposited upon an older basement. The Sydney Basin extends from Batemans Bay to a line between Muswellbrook and Rylstone. The sedimentary rocks of the Sydney Basin have been derived from erosion. Erosion produces fragments, in which the finer proportion may dissolve in water and therefore be transported in solution. Sedimentary rocks are formed by the deposition of these fragments, along with the precipitation of the dissolved material. The formation of sedimentary rocks produces a layered structure known as bedding or stratification. Each layer is a bed or stratum and represents the sediment deposited in a certain interval of time commenced and terminated by a change in the character of the conditions under which the sediment was being deposited or in the character of the material being deposited. The Sydney Basin is about 3000 m deep in its central area. The major rock units or groups of strata are thick towards the centre of the basin and thin towards the margins, and individual beds show local variations in thickness (Reynolds 1977).

Sedimentary Rocks

Sedimentary rocks can be classified according to grain size. The coarsest are the conglomerates comprising large and small pebbles. Then follow sandstones which may

be of various types; for example, quartzose sandstone, if the mineral known as quartz is the dominant constituent, or lithic sandstone, if the individual fragments in the sandstone are themselves particles of very fine-grained rock. Then follow the very fine-grained sedimentary rocks, siltstones and claystones. When such a sedimentary rock is made up of silt particles or clay particles and displays lamination is it called shale. In relation to rocks generally, they are referred to as massive if there is no lamination, being uniform when viewed from any direction. As well as the main minerals forming sedimentary rocks, there is the matrix of the rocks, the finer sedimentary material which helps to bond the rock together, the most common being clay. The rock may be further consolidated by the introduction of chemical cement such as calcium carbonate or silica (Reynolds 1977).

Coal

Coal is always associated with other sedimentary rocks and occurs as beds called seams. Where strata contains coal seams the strata are traditionally known as coal measures. Coal may be described as a sedimentary rock derived from carbonaceous plant material. Initially, luxuriant growths of plants under swamp conditions are buried under succeeding layers of sediment and form in the first stage peat. As the deposit increases in age and sinks deeper, the beds are covered by greater masses of sediment. The pressure and temperatures involved may progressively convert the original peat into lignite, bituminous coal such as is found in the Sydney Basin, and ultimately anthracite (Reynolds 1977).

Structures

There are three geological structures which need to be mentioned – folds, faults and joints. Most folds are formed when a rock sequence is subjected to tectonic forces; the rocks respond to these forces by buckling. This buckling may be expressed as gentle flexures or as wrinkles on both large and small scales, depending upon the degree of deformation. Fractures may occur in association with, or in place of folding. A fracture along which no movement has occurred is called a joint but when the rock on one side of the break has moved relative to the other side, the fracture is called a fault. It is generally accepted that faulting in rocks occurs because of stresses which may be

relieved either by folding if rocks are sufficiently plastic or by faulting if the rocks are brittle. In the Southern Coalfield, faults are relatively common but not intensive. A joint is defined as a break of geological origin in the continuity of a body of rock occurring singly or more frequently in a set or system but not attended by observable displacement. Alteration, emplacement and/or decomposition products may occur along joint surfaces, which in some instances may bond the joint (Reynolds 1977).

2.4.2 The Southern Coalfield

The Southern Coalfield is one of the five major coalfields within the Sydney-Gunnedah Basin. The principal coal-bearing sequence in the Southern Coalfield is the Illawarra Coal Measures which outcrops along the Illawarra Escarpment in steep slopes below the base of the prominent Hawkesbury Sandstone cliffs. The Illawarra Coal Measures consists of four coal seams of proven or potential economic significance, namely the Bulli Seam, Balgownie Seam, Wongawilli Seam and Tongarra Seam in descending order. The Bulli Seam has been extensively mined in the northern part of the coalfield due to its coking properties and low ash content. The Balgownie seam is not identifiable everywhere and the known economic development is confined to the eastern side of the field north of Wollongong. The Wongawilli Seam also has coking properties and is used in blends with coal from the Bulli Seam. Except for localised variations, the typical thickness and section of the seam persist throughout the entire coalfield. Its quality, however, is acceptable throughout only part of the coalfield. The Tongarra Seam is of inferior quality over most of the coalfield (Holla & Barclay 2000).

An idealised stratigraphic column is presented in Figure 2.8.

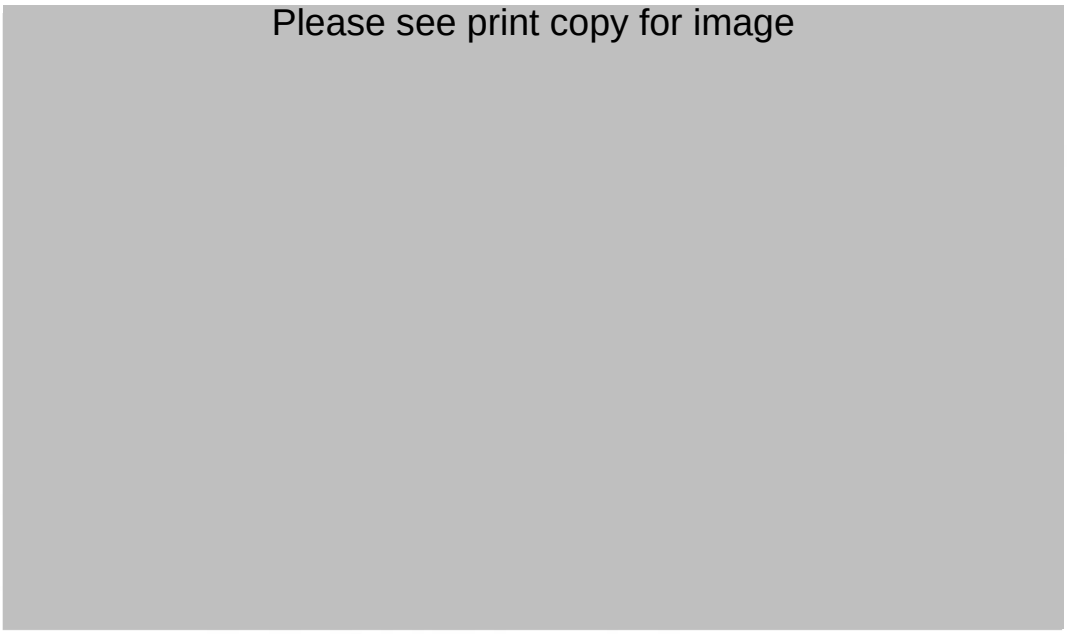

Fig. 2.8 – Idealised stratigraphic column of the Southern Coalfield (Holla & Barclay 2000)

2.4.2.1 Illawarra Coal Measures

The Illawarra Coal Measures form the south-eastern segment of the Sydney Basin. This area is bounded on the east and south by the outcrop of the coal measures which appear above sea level at Coal Cliff, 20 km north of Wollongong, and traverses the escarpment of the Illawarra Coastal Range. The coal measures are of Permian age and lie conformably upon the Shoalhaven Group. Triassic rocks lie conformably upon the coal measures. The basal formation of the Triassic System is the Coal Cliff Sandstone of the Narrabeen Group.

The stratigraphic sequence of the Illawarra Coal Measures is shown in Table 2.1.

Table 2.1 – Stratigraphic units of the Illawarra Coal Measures in the Southern Coalfield (Packham 1969, MacGregor & Conquest 2005)

Stratigraphic Unit	Thickness At Mt Kembla (m)
SYDNEY SUB-GROUP	
Bulli Seam	1.5
Loddon Sandstone	9.2
Balgownie Seam	0.9
Lawrence Sandstone	
Cape Horn Seam	
Unnamed Member	15.2
Hargrave Seam	
Unnamed Member	
Wongawilli Seam	9.8
Kembla Sandstone	15.2
American Creek Seam	2.1
Unnamed Member	27.4
Tongarra Seam	9.2
Wilton Formation:	
Unnamed Member	16.9
Woonona Seam	4.6
CUMBERLAND SUB-GROUP	
Erins Vale Formation	29.0
Pheasants Nest Formation:	
Cordeaux Seam	1.2
Unnamed Member	18.3
Unanderra Seam	4.3
Unnamed Member	48.8

Pheasants Nest Formation

The Pheasants Nest Formation is the lowest formation of the coal measures and usually is tuffaceous sandstone resting conformably upon the underlying rocks. The distinguishing feature of the basal coal-measure sediments is the irregular bedding of light coloured tuffs and sandstones, compared with the thick, massive, greenish and brownish Broughton Sandstone of the Gerringong Volcanics, or farther west, the grey silty sandstone of the Berry Formation. The sequence of beds below the Unanderra Seam is irregular and it is doubtful whether individual beds occur laterally to any extent. The rocks are chiefly tuffaceous sandstones, shales and tuffs. A bed of conglomerate may also occur. Fine interbedding is common, as is also a transition from one rock type to another.

Thin intermittent coal seams have been observed within the sequence of the Pheasants Nest Formation. The Unanderra Seam is the lowest named seam in the coal measures. It is known in the Mt Kembla – Mt Keira area where is occurs about 45 m above the base of the coal measures. It consists predominately of carbonaceous shale with thin plies of coal.

The sequence above the Unanderra Seam consists of irregularly interbedded tuffaceous sandstones, shales and tuffs. Individually the beds are thin and insignificant. Knowledge of these beds is also confined to the Mt Kembla area. A minor coal seam, up to 10 cm thick, occurs in this sequence. The Cordeaux Seam is a thin seam of carbonaceous and tuffaceous shale containing coal bands. It is only known in the Mt Kembla – Mt Nebo area. Its thickness is variable up to a maximum of 1.2 m. The maximum recorded thickness of the Pheasants Nest Formation is 120 m (Packham 1969).

Erins Vale Formation

This formation apparently marks the commencement of a more stable depositional environment. Bedding becomes more regular and the sediments are not so distinctly tuffaceous. Calcite, although present, does not occur so prominently as veins and facings as in the lower sediments. Nevertheless, individual beds are not persistent. The rocks in the sequence are tuffaceous sandstones, which predominate, and shales. Gritty and conglomeratic sandstones appear occasionally, especially in the upper part of the formation. The maximum recorded thickness of the formation is 120 m (Packham 1969).

Wilton Formation

The Woonona Seam, the basal member of the Wilton Formation and of the Sydney Sub-Group, is much more persistent than any of the lower seams. It outcrops above sea level at Thirroul in the north and extends to about Macquarie Pass in the south. It has not been found on the southern edge of the coalfield. The seam is up to 6 m thick and is subject to splitting in some areas. It consists of coal and shaly coal and usually, although not always, contains numerous bands of shale. The most economic development of the seam is in the Mt Kembla area where it is 4.6 m thick, with a workable section 2.5 m

thick, which contains 24 % ash, excluding shale bands. The seam, however, is not worked at the moment. The coal has weak coking properties.

The interval between the Woonona Seam and the Tongarra Seam consists of beds of shales and sandstones which, although distinct in local areas, do not persist laterally. Generally sandstone is the subordinate rock type. The thickness of the strata varies between 15 m and 75 m (Packham 1969).

Tongarra Seam

The Tongarra Seam is subject to splitting by a bed of sandstone in some areas. Usually the seam consists of coal of variable quality and shale bands. It apparently occurs throughout most of the coalfield but less is known of its characteristics in the western half of the field. It is the lowest seam occurring on the southern edge of the field. Thickness varies from 1.2 m to 6.7 m. Its best development is in the Tongarra and Avondale areas where parts of the seam are of quality suitable for mining. Here the worked section, excluding shale bands, contains approximately 20 % ash. The coal has medium coking properties.

The interval between the Tongarra and American Creek Seams consist essentially of dark grey shale containing minor beds of sandstone. A significant bed of yellowish white tuffaceous shale of 30 cm average thickness occurs about 4.6 m above the Tongarra Seam. It has not been identified over the whole field but where it can be recognised it serves as a valuable marker horizon. The sediments vary in thickness between 9 m and 30 m (Packham 1969).

American Creek Seam

The American Creek Seam consists chiefly of carbonaceous shale and coal. In the past, the seam has been worked as a source of oil shale in the Mt Kembla area. The seam varies in thickness and character, lateral variation in places being sudden. Although it occurs throughout the whole field its development is discontinuous, presumably owing to local washouts or areas of non-deposition. Its thickness ranges usually up to a maximum of 7.5 m (Packham 1969).

Kembla Sandstone

The Kembla Sandstone is usually a massive, light-grey, medium-grained sandstone, occasionally coarse or with conglomeratic phases, which grades vertically upwards through a sandy shale to a carbonaceous shale immediately below the Wongawilli Seam. In places a basal shale member may also exist. The thickness of the Kembla Sandstone varies between 4.5 m and 15 m (Packham 1969).

Wongawilli Seam

The Wongawilli Seam extends over the whole coalfield. Its thickness ranges from 6 m in the south to 15 m in the northeast. Over most of the field, however, a range of 9 m to 11 m is maintained. The seam consists of coal plies of varying quality, separated by bands or beds of shale, mostly carbonaceous or coal or tuffaceous. One bed, which is a hard, sandy, cream-coloured tuff, known colloquially as the Sandstone Band, characterises the seam. Over part of the field the lowest 1.8 m to 3.7 m of the seam contains coal of commercial quality. In collieries where the seam is mined, the worked section contains 20 % to 30 % ash. The coal plies, that is, excluding shale bands, contain 15 % to 25 % ash and have strong coking properties. In some localities a system of sills intrudes the seam over wide areas.

The interval between the Wongawilli Seam and the Balgownie Seam consists of shale, sandstone and one or two minor coal seams. In the northern coastal area the two minor coal seams are known as the Cape Horn and Hargrave Seam and divide the sequence as shown in Table 2.2.

Table 2.2 – Interval between Wongawilli and Balgownie Seams (Packham 1969)

Stratigraphic Unit	Thickness (m)
Balgownie Seam	
Lawrence Sandstone: Medium-grained massive sandstone overlain by shale	11
Cape Horn Seam	1.2
Dark-grey shale containing sandstone beds	3.0
Hargrave Seam	0.3
Interbedded sandstone and shale	7.0
Wongawilli Seam	

The thicknesses quoted are for the Scarborough area. The total thickness is 23 m compared with 27 m in the Helensburgh area to the north where the Lawrence Sandstone remains constant in thickness while the other sediments thicken. South and west of this area the coal seams become less definite although in any particular locality, except perhaps in the far south, some coal is always present.

In the central part of the field, a thin coal seam of 30 cm average thickness is overlain by sandstone and underlain by shale. The seam extends over a wide area and may prove to be the extension of the Cape Horn Seam. The overlying sandstone, which is about 6 m thick, may thus correspond to the Lawrence Sandstone. In the central and southern parts of the field the interval between the Wongawilli and Balgownie Seams is reduced to 15 m and less (Packham 1969).

Balgownie Seam

The Balgownie Seam exceeds 1.5 m in thickness in the extreme north eastern part of the field but shows a steady decrease in thickness to the south and west. South of Macquarie Pass it is less than 30 cm thick, although generally it is of good quality. It usually consists of un-banded clean coal and contains about 15 % ash. The coal is of medium coking quality. Commercially the Balgownie Seam is attractive from the aspect of coal quality but unattractive from the aspect of thickness.

Like the Balgownie Seam, the formation between it and the Bulli Seam decreases in thickness from the northeast to the west and south. Its thickness averages 9 m varying

between 4.5 m to 15 m. The formation consists essentially of light-grey, medium-grained massive sandstone called the Loddon Sandstone. This is invariably overlain by a bed of dark-grey shale, usually less than 3 m thick, which at the top becomes carbonaceous to form the floor of the Bulli Seam (Packham 1969).

Bulli Seam

The Bulli Seam is the topmost formation in the Illawarra Coal Measures. Commercially it is the most important of the coal seams and has been extensively mined. Thickness of the seam is a maximum of 4 m in the northern part of the field with a regional decrease to the south. In the vicinity of Mt Kembla such decrease becomes rapid and farther south of this point the seam is represented by about 60 cm of coal and shale. In the far south the seam is less than 30 cm thick and consists chiefly of carbonaceous shale. In the extreme southwest part of the field the seam is absent, and owing to contemporaneous erosion, the section overlying the Wongawilli Seam has been replaced by Triassic rocks. North of its rapid thickness change near Mt Kembla the seam is over 1.5 m thick.

In its areas of best development, that is, north of Mt Kembla, the Bulli Seam consists essentially of clean coal containing in places thin shale bands. Its ash content is remarkably consistent, only rising above the general range of 9 % to 12 % at the northern end of the field. Its coking properties vary generally from medium to strong but are weak in one or two localities. The Bulli Seam is overlain by the Coal Cliff Sandstone of the Narrabeen Group (Packham 1969).

2.4.2.2 Narrabeen Group

The Narrabeen Group is known to occur throughout the Sydney Basin. It extends along the Illawarra coastal escarpment and also outcrops to the west of the escarpment. This group includes the main sequence of rocks along the coastal cliffs between Stanwell Park and Scarborough, where it is particularly well exposed. The lowest units of the Narrabeen Group are Late Permian and the upper unit is Middle to Late Triassic in age. The thickness of the Narrabeen Group decreases to the south.

The Narrabeen Group includes the Coal Cliff Sandstone, Wombarra Shale, Otford Sandstone Member, Scarborough Sandstone, Stanwell Park Claystone, Bulgo Sandstone, Bald Hill Claystone, Garie Formation and the Newport Formation. The Hawkesbury Sandstone overlies the Narrabeen Group (Ghobadi 1994).

Coal Cliff Sandstone

The Coal Cliff Sandstone is the basal unit of the Narrabeen Group and overlies the Illawarra Coal Measures. The thickness of the unit ranges between 6 m and 20 m (Hanlon 1953). The Coal Cliff Sandstone is a light grey, fine to medium grained, quartz-lithic and lithic sandstone with a number of pebble and shale bands. It crops out in the coastal section near Clifton and passes below sea level north of Coalcliff. Angular siderite fragments up to 10 cm in size are common in the basal Coal Cliff Sandstone. This unit forms the roof of some colliery workings and is exposed underground for several kilometres to the west of the Illawarra escarpment. In some places colliery roofs are less stable because the fine sandstone near the base of the Coal Cliff Sandstone sometimes grades into shale (Ghobadi 1994).

Wombarra Shale

The Coal Cliff Sandstone is overlain by 6 m to 30 m of greenish-grey shale with lithic sandstone interbeds. It is well exposed in road cuttings and cliffs south of Coalcliff. The sandstone interbeds are generally quite thin, lenticular, fine-grained and carbonate-cemented. Towards the top of the formation, a thicker sandstone unit is called the Otford Sandstone Member (Ghobadi 1994).

Scarborough Sandstone

The Scarborough Sandstone overlies the Wombarra Shale. Commonly the Scarborough Sandstone is conglomeratic with coloured chert clasts especially in the basal half. It consists of beds up to several metres in thickness which becomes finer upwards. This unit comprises lithic to quartz-lithic sandstone with pebbles and minor amounts of grey shale (Ghobadi 1994).

Stanwell Park Claystone

This unit overlies the Scarborough Sandstone. It consists of interbedded green to chocolate shale and sandstone. Three claystone intervals and two sandstone beds can be recognized. The lower section of the unit consists of greenish-grey claystone and sandstone which slowly changes upward into red-brown claystone and clay. The sandstone beds are composed of weathered lithic fragments and are usually light greenish-grey in colour. The relative proportion of claystone and sandstone varies but overall they are sub-equal (Bowman 1974).

Bulgo Sandstone

The Bulgo Sandstone, which rests on the Stanwell Park Claystone, is the thickest unit of the Narrabeen Group on the Illawarra coast. It forms prominent outcrops in the area and between Coalcliff and Clifton. It consists of thickly bedded sandstone with intercalated siltstone and claystone beds up to 3 m thick. Conglomerate is also present, especially toward the base. The Bulgo Sandstone has a higher proportion of quartz than of rock fragments. Sandstone beds rarely exceed 4 m in thickness while the siltstone and shale interbeds are usually less than 1 m thick (Ghobadi 1994).

Bald Hill Claystone

The Bald Hill Claystone, which overlies the Bulgo Sandstone, outcrops in the hills near Otford and on the Mt Ousley road to the south. This formation is about 15 m thick in the Bald Hill area (Hanlon 1953). It consists almost entirely of claystone, but lithic sandstone interbeds are found towards the base of the unit. Mottled chocolate and green claystone zones are common (Ghobadi 1994).

Garie Formation

Toward the top of the Bald Hill Claystone, thin beds of light coloured claystone become more common. This upper zone passes into a mid-grey slightly carbonaceous massive claystone, which is overlain in turn, by the Newport Formation. The Garie Formation is

usually less than 3 m thick but it is a very good marker horizon in the southern Sydney Basin (Ghobadi 1994).

Newport Formation

The mid-grey shale and minor interbedded lithic sandstone of the Newport Formation overlies the Garie Formation. Mud-rocks of this formation are thinly bedded. The dark-grey mud-rocks contain plentiful plant fossils. Claystone beds consisting of sand-sized flakes of kaolinite, with a large original porosity, are common in the Newport Formation (Bowman 1974).

2.4.2.3 Hawkesbury Sandstone

This unit is flat-lying Middle Triassic quartz sandstone that crops out at the top of most the Illawarra escarpment. It forms a resistant plateau to the west of the escarpment, which gently dips to the northwest. The formation has a thickness of about 180 m at Stanwell Park. It contains a minor amount of mudstone, interbedded with fine sandstone, but it consists dominantly of sandstone beds (Jones & Rust 1983) typically 2 m to 5 m but up to 15 m in thickness. Transition into conglomerate is seen in some of the sandstone beds. Strong cross-bedding is common in the Hawkesbury Sandstone. The interbedded mudstone is very prone to weathering upon exposure and the Hawkesbury Sandstone is often involved in rock falls from the escarpment.

2.5 CURRENT PREDICTION TECHNIQUES USED IN THE SOUTHERN COALFIELD

Empirical a. based on observation or experiment, not on theory.

Empirical prediction methods provide an instrument in which reasonably accurate subsidence predictions can be made, provided the user is aware of the limitations of such methods. Subsidence prediction in the Southern Coalfield by empirical methods is mainly limited to the guidelines proposed by Holla and Barclay (2000), published by the New South Wales Department of Primary Industries (formerly the New South Wales Department of Mineral Resources), and the Incremental Profile Method

(Waddington & Kay 1995) that was developed by Mine Subsidence Engineering Consultants (formerly Waddington Kay and Associates). The Incremental Profile Method attempts to address the shortfalls of the New South Wales Department of Primary Industries empirical method, mainly in the areas of multiple longwall panel subsidence and longwall mining effects on river valleys. This section will cover both empirical methods.

2.5.1 New South Wales Department of Primary Industries Empirical Technique

The method devised by the New South Wales Department of Primary Industries has been in existence since the mid 1980's (Holla 1985). Since then, the method has been refined with the addition of subsidence data (up to June 2000), and a discussion on the effects of mining induced subsidence on public utilities, dwellings and water bodies. Whilst not accounted for in the prediction technique, there is also a discussion on the major factors modifying the theoretical subsidence behaviour such as faults, dykes, and gullies. Several case studies are also presented to illustrate these factors in action.

2.5.1.1 Overview of method

The subsidence data and resulting graphs in this method were obtained from collieries in the area between the Illawarra Escarpment and the Burragorang Valley. This data was collected over a period of thirty years. The majority of the mines included in the analyses were mining the Bulli seam except in two cases for which the workings were in the Wongawilli seam. The predominant method of mining was by longwall mining, although some pillar extraction data has been included.

The basic inputs that are required for this method are:

- Width of longwall panel (W),
- Depth of cover (H),
- Mined seam height (T), and
- Pillar width (P_w) (multiple longwall panel layouts).

Once these parameters are known, it is possible to predict the following parameters for a given single longwall panel mining layout:

- Maximum developed subsidence (S_{max}),
- Maximum tensile strain ($+E_{max}$),
- Maximum compressive strain ($-E_{max}$),
- Maximum ground tilt (G_{max}),
- Radius of ground curvature (R_{min}),
- Location of inflection point, and
- Goaf edge subsidence (S_{goaf}).

With these parameters it is possible to produce a subsidence profile as shown in Figure 2.9. It must be noted that only the maximum developed subsidence can be predicted for multiple longwall panels.

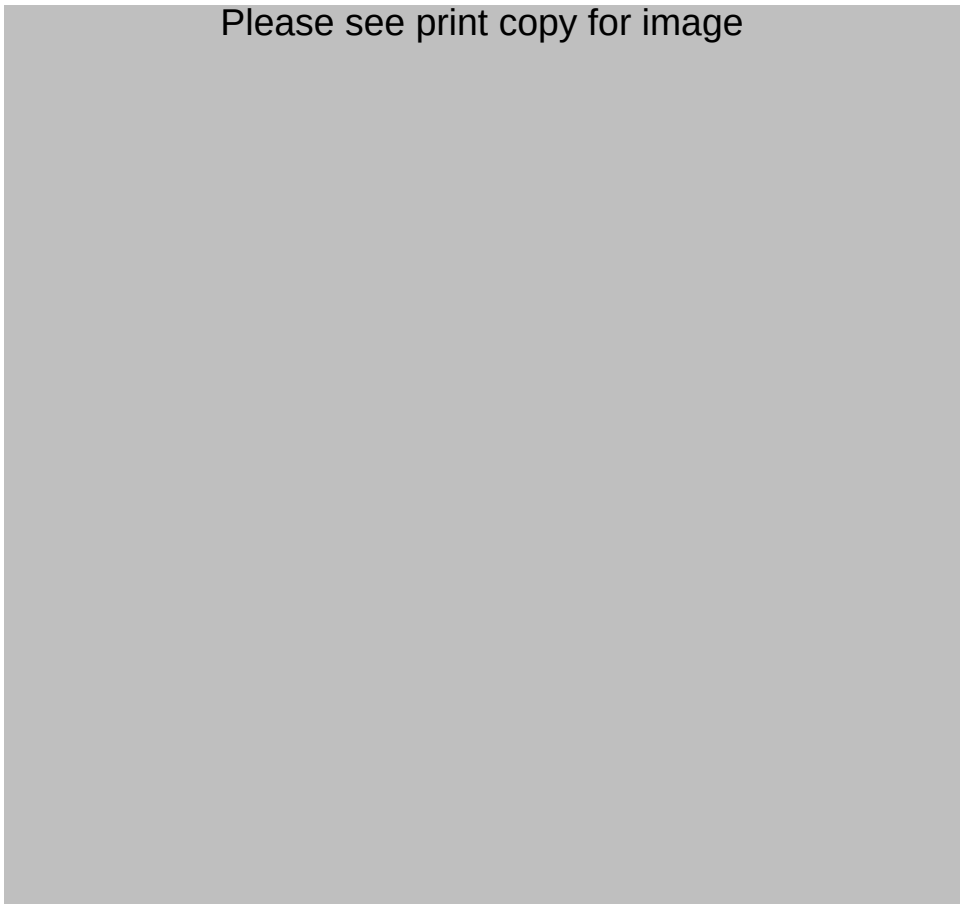

Fig. 2.9 – Formation of a subsidence trough above an extraction panel (Holla & Barclay 2000)

2.5.1.2 Maximum developed subsidence for single longwall panels

Maximum developed subsidence is a function of the longwall panel width to depth of cover ratio (W/H) and the extracted thickness (T). Generally, the larger the W/H ratio, the greater the subsidence. If a longwall panel is fixed at a depth of 400 m and is 200 m wide, it would generally produce greater subsidence than if the same longwall panel was 150 m wide. This is mainly due to the bridging capability of the strata above the extracted longwall panel.

Figure 2.10 is used for predicting the maximum developed subsidence over a single longwall panel. It can be seen in Figure 2.10 that the subsidence factor (S_{max}/T) increases substantially for W/H ratios greater than 0.5. This would suggest that subsidence is no longer controlled by the elastic deformation/sag of the strata and that the bridging capability of the strata is reached at this value.

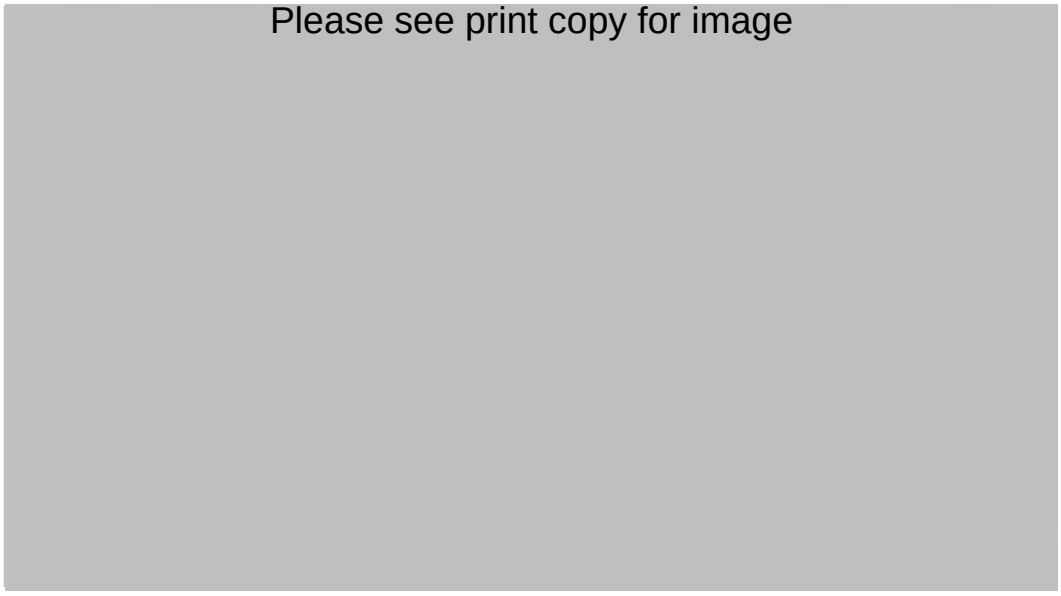

Fig. 2.10 – Relationship between W/H ratio and S_{max}/T for single panels (Holla & Barclay 2000)

It can be seen from Figure 2.10 that the largest longwall W/H ratio still falls into the sub-critical category (W/H < 1.4). This is a result of the deep mining conditions in the Southern Coalfield, and although data exists for W/H ratios between 0.5 and 0.9, the

resulting scatter suggests that subsidence prediction would be more accurate for W/H ratios less than 0.5.

Another point to note, and which has been addressed by Holla and Barclay (2000), is that Figure 2.10 suggests that the maximum developed subsidence from pillar extraction is greater than that for longwall extraction. One reason given argues that for longwall extraction, unmined coal is concentrated in chain pillars and for pillar extraction; unmined coal is spread out over the goaf area in the form of stooks. The reason for the greater developed subsidence from pillar extraction is simply that chain pillars, by their dimensions, are inherently stronger than smaller stooks. Another reason that is raised is the validity of the pillar extraction data. It is pointed out that in some cases, old workings next to new pillar extraction panels may have influenced the quality of the data set, and in many cases was difficult to identify.

2.5.1.3 Maximum developed subsidence for multiple longwall panels

More often than not, the need to predict the subsidence produced by one single isolated longwall panel in virgin coal is not that great. In practise, it is not uncommon for a series of ten or more longwall panels to be mined. These longwall panels are separated by chain pillars and it has been observed by Holla and Barclay (2000) that the subsidence over multiple longwall panel layouts is controlled primarily by the compression of pillar coal and strata located both above and below the seam. Longwall panels in the Southern Coalfield are generally narrow enough to allow the strata to bridge between the pillars, reducing the sag component of subsidence while increasing pillar compression.

It can be seen from Figure 2.11, and noted by Holla and Barclay (2000), that the maximum subsidence does not develop until four to five longwall panels have been mined for a particular geometry. This is a result of the incremental loading of pillars as mining progresses, up to a point where the pillar stress reaches a maximum (in this case after four to five longwall panels). At this stage, the differences in the maximum subsidence for different layouts are due to differences in pillar loads and stresses, therefore implying that pillar deformation is the significant contributor to the maximum developed subsidence. Recently, this characteristic has been noted by Mills and

Huuskes (2004) at Metropolitan Colliery, where the overall magnitude of subsidence is controlled by the elastic compression of the chain pillars and the strata above and below the chain pillars. It was proposed that subsidence occurs in response to the 'super-panel' effect of multiple longwall panels, rather than in response to individual longwall panels. Figure 2.11 and Figure 2.12 are used to predict the subsidence for multiple longwall panel layouts.

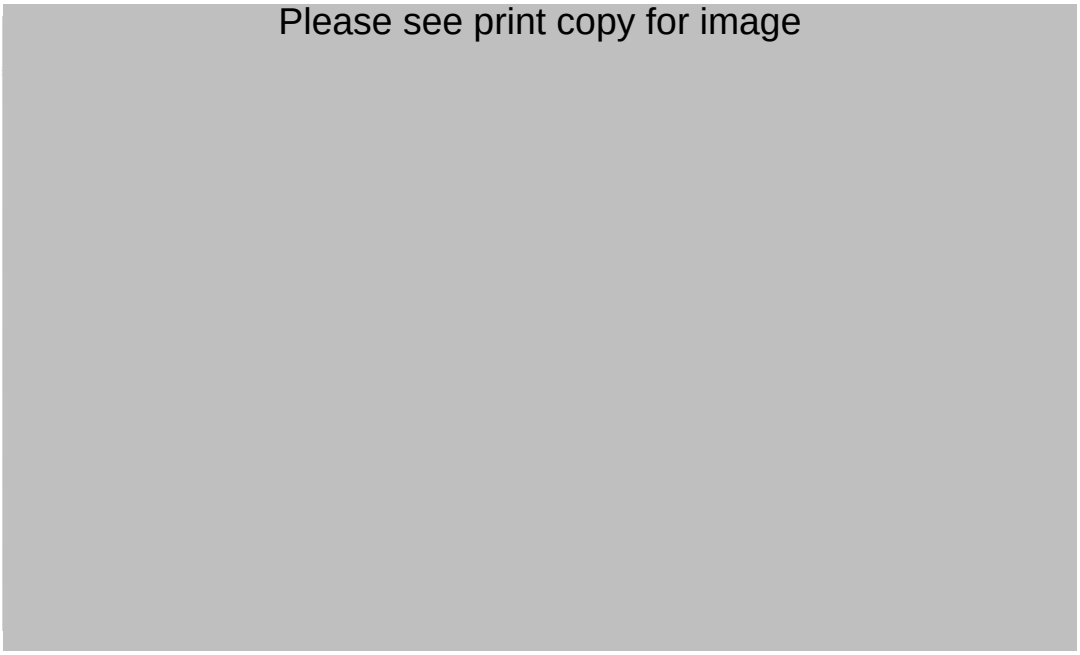

Fig. 2.11 – Relationship between W/H and S_{max}/T for multiple panels (Holla & Barclay 2000)

Given the important role that chain pillars play in subsidence development, a relationship was established between the loading on the pillar and the subsidence factor (S_{max}/T). This can be seen in Figure 2.12.

The area of overburden loading a pillar in a multiple longwall panel layout is given by Equation 2.5:

$$Area = W_L H - \left(W^2 \times \tan\left(\frac{\Phi}{4}\right)\right) \qquad [2.5]$$

Where,

W_L = Longwall panel width + pillar width (m)

H = Depth of cover (m)

Φ = Abutment angle (°)

For mines operating in the Bulli Seam where H is greater than 350 m, it is recommended that 21˚ should be used for the abutment angle (Colwell Geotechnical Services 1998).

However, for this value of the abutment angle the second term ($(W)^2$ x tan(Φ/4)) is small compared to the first term (W_LH). Therefore, pillar load can be taken as a function of (W_LH) and the pillar stress (W_LH/P_W).

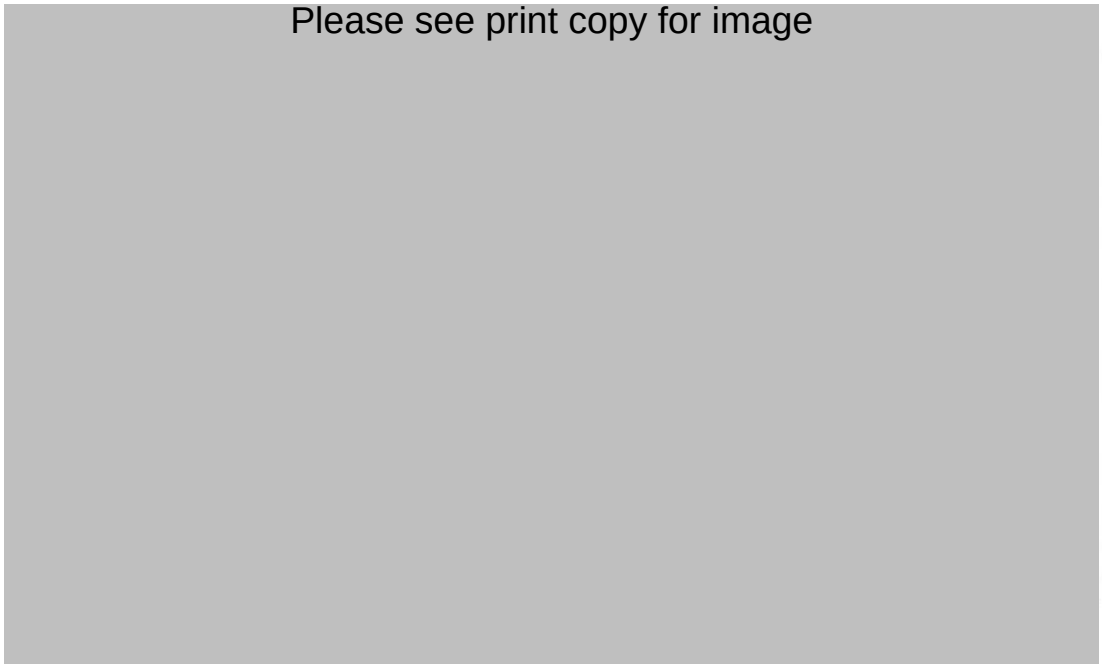

Fig. 2.12 – Relationship between pillar stress factor (W_LH/P_w) and S_{max}/T for multiple panel layouts (Holla & Barclay 2000)

2.5.1.4 Maximum strains

Strains are caused by differential horizontal movements. Horizontal strain is generally not critical in the design of structure, but must be accounted for in the design of linear structures like pipelines. Horizontal strain is the change in length per unit of the original horizontal length of ground surface. Compressive strains occur above the extracted area and tensile strains occur over the goaf edges and trough margin.

According to Holla and Barclay (2000), surface strains are directly proportional to the amount of subsidence developed and inversely proportional to the depth of cover, a relationship that is given by Equation 2.1 and Equation 2.2.

Figure 2.13 and Figure 2.14 illustrate the relationship between W/H and, K1 and K2 respectively. These graphs were derived by calculating K1 and K2 from Equation 2.1 and Equation 2.2, respectively for all the available data. Anomalous values were defined as being affected by streams, gullies, gorges and hills. It can be seen that curves can be drawn to include most of the non-anomalous values.

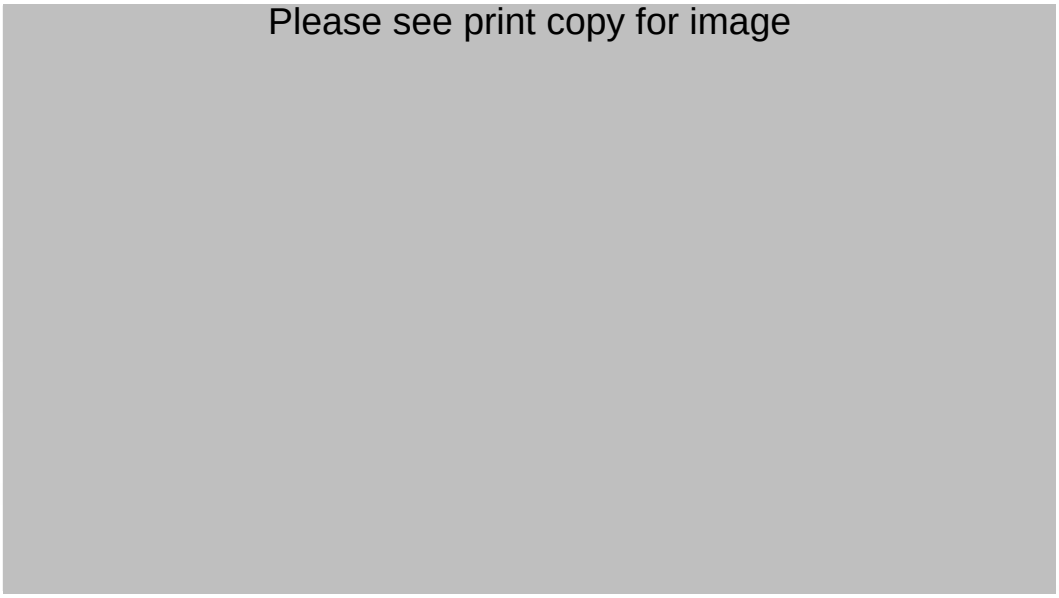

Fig. 2.13 – Relationship between W/H ratio and K1 (Holla & Barclay 2000)

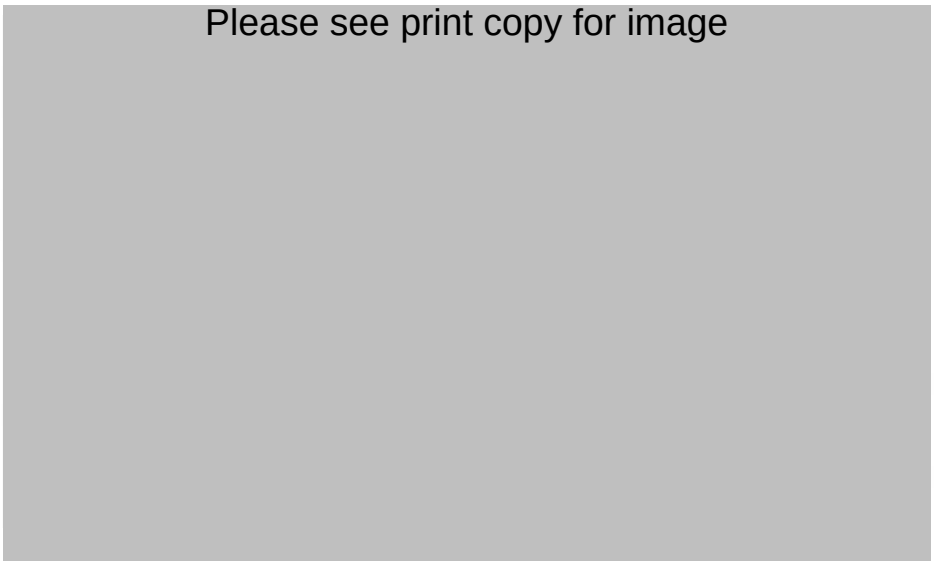

Fig. 2.14 – Relationship between W/H ratio and K2 (Holla & Barclay 2000)

2.5.1.5 Maximum tilt

Tilt of the ground surface between two points is found by dividing the difference in subsidence at the two points by the distance between them. The maximum tilt occurs at the point of inflection where the subsidence is approximately one half of S_{max}. The relationship can be found in Equation 2.3.

The values of K3 were calculated in the same manner as for strain. The results can be seen in Figure 2.15.

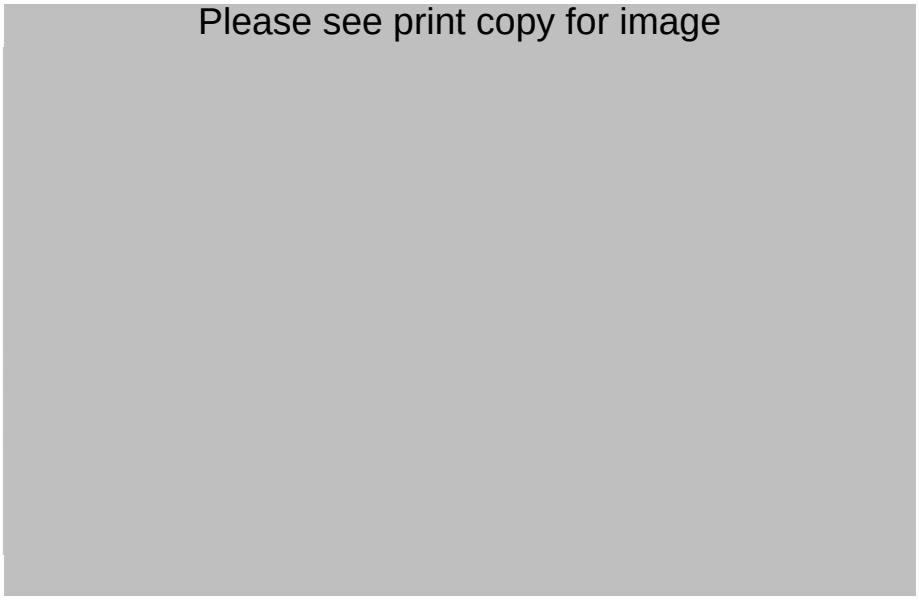

Fig. 2.15 – Relationship between W/H ratio and K3 (Holla & Barclay 2000)

2.5.1.6 Radius of ground curvature

The curvature is defined as the rate of change of tilt. It is concave above part of the extracted area and convex in the area of trough margin and over goaf edges. A regression analysis was performed by Holla and Barclay (2000) on the available data and resulted in a K4 value of 22 with a reasonably high confidence level. Based on this value of K4, the radius of curvature, R_{min}, is shown for different mining depths in Figure 2.16.

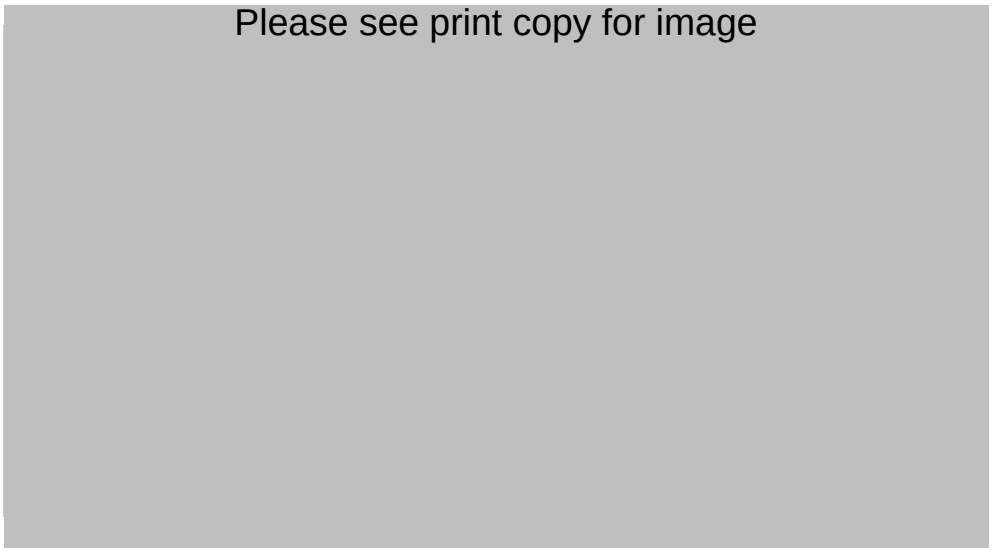

Fig. 2.16 – Relationship between maximum strain and minimum radius of curvature (Holla & Barclay 2000)

2.5.1.7 Location of inflection point

The inflection point is the point where tensile strains become compressive, and vice versa. For W/H ratios more than 0.5, the inflection point is located within the goaf. For smaller ratios it moves outside the goaf, and the smaller the W/H ratio, the farther out from the goaf edge. Figure 2.17 shows the location of inflection point from the goaf edge over main and tailgates for various values of W/H.

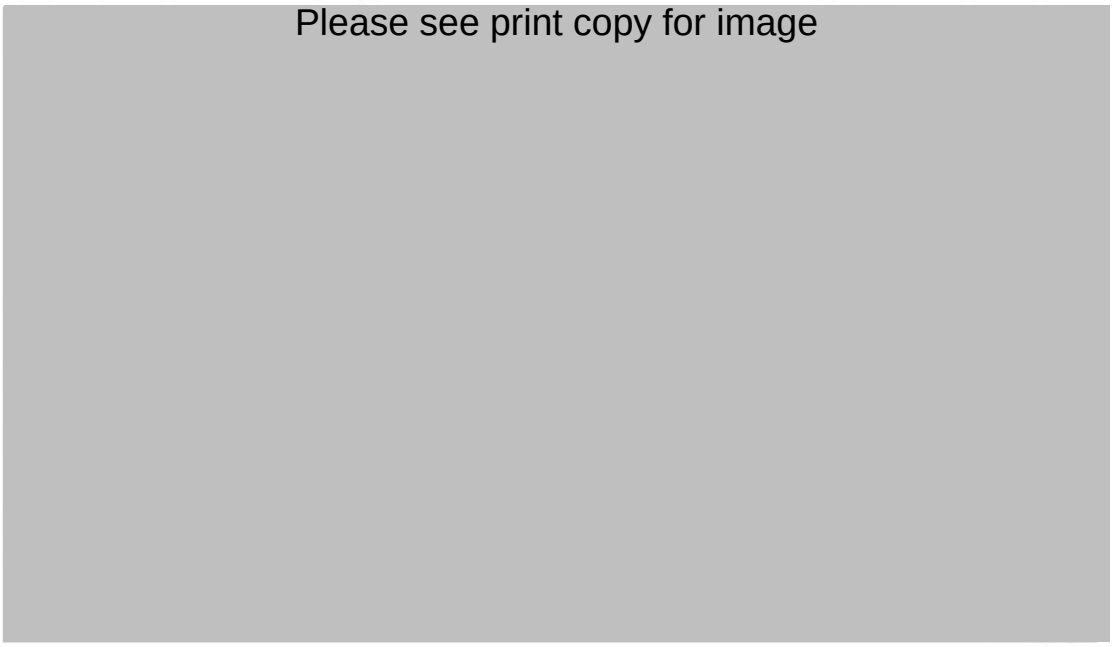

Fig. 2.17 – Location of inflection point (Holla & Barclay 2000)

2.5.1.8 Goaf edge subsidence

Goaf edge subsidence values for various W/H ratios can be seen in Figure 2.18. It is noted that for subcritical longwall panels, the goaf edge subsidence forms much of the maximum developed subsidence.

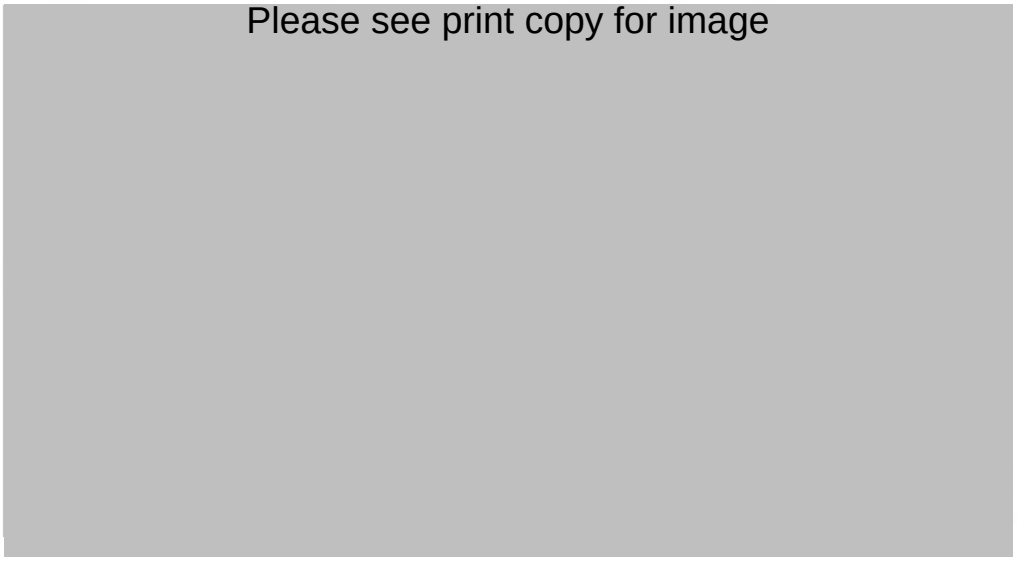

Fig. 2.18 – Goaf edge subsidence (Holla & Barclay 2000)

2.5.2 The Incremental Profile Method

The Incremental Profile Method was developed by MSEC (formerly Waddington Kay and Associates) in 1994 during the course of a study for BHP Collieries Division, the Water Board and AGL (Waddington Kay and Associates 2002). The purpose of the study was to develop an empirical model that could predict subsidence, tilts, curvatures, strains and surface effects as a result of longwall mining at Appin and Tower Collieries.

2.5.2.1 Overview of method

Historical subsidence data from Appin, Tower, Tahmoor, West Cliff, Cordeaux and South Bulli Collieries was studied and plotted in a variety of ways in order to identify a regular pattern of ground behaviour. The most significant patterns were found in the shapes of the incremental subsidence profiles measured along survey lines transversely across the longwall panels.

The incremental subsidence profile for each longwall panel was derived by subtracting the initial subsidence profile measured before mining the longwall panel, from the final subsidence profile measured after mining the longwall panel. The incremental subsidence profile for a longwall panel shows the change in the subsidence profile caused by the mining of the longwall panel.

Figure 2.19 is an illustration of typical incremental subsidence profiles.

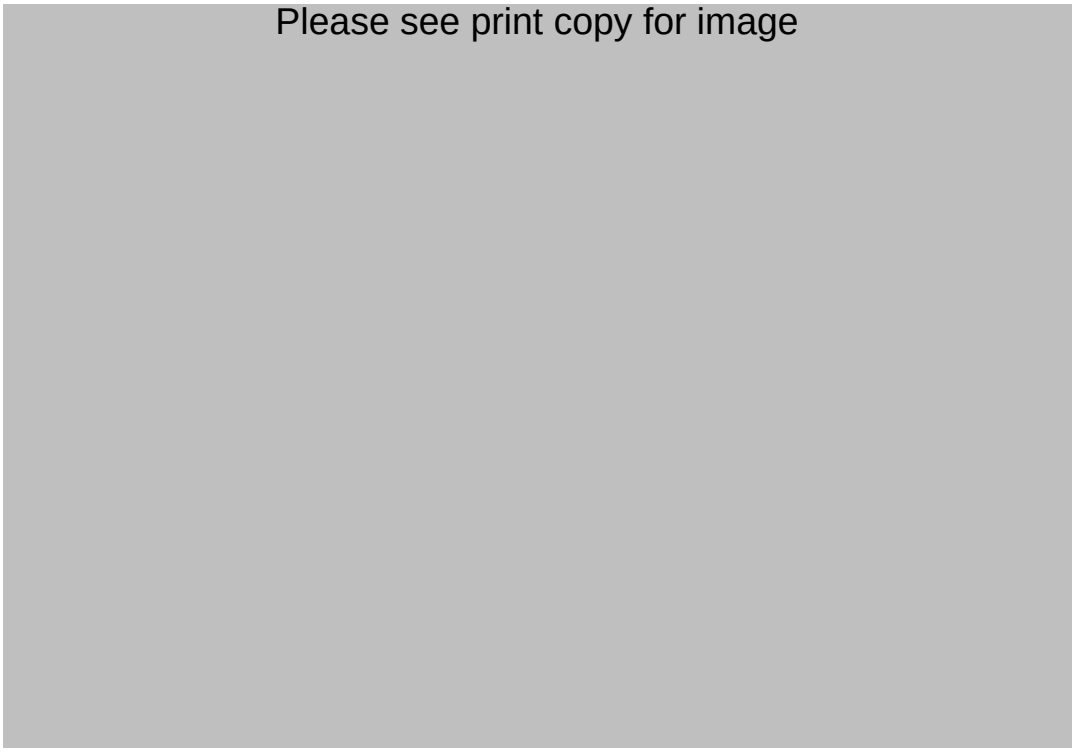

Fig. 2.19 – Typical incremental subsidence profiles, NSW Southern Coalfield (Waddington Kay & Associates 2002)

The Incremental Profile Method is based on predicting the incremental subsidence profile for each longwall panel in a series of longwall panels and then adding the respective incremental profiles to show the cumulative subsidence profile at any stage in the development of a series of longwall panels. Incremental tilts, curvatures and strains can also be predicted. Profiles in both the transverse and longitudinal directions can be predicted, thereby allowing predictions to be made on any point on the surface above a series of longwall panels.

Initially designed for the Southern Coalfield, the method has been applied to the Newcastle Coalfield and used to predict subsidence at West Wallsend, Cooranbong, Wyong and South Bulga Collieries. Further research by the authors of this method has involved the potential application of the Incremental Profile Method in multi-seam situations. It was found that the multi-seam profiles are generally greater in amplitude than single seam profiles and differ in shape from the standard profile over single seams.

The incremental profiles have been modelled in two halves, the point of maximum subsidence being the point at which the two halves of the profile meet. A library of mathematically defined profile shapes has been established, which allows the incremental profiles to be modelled, depending on the width to depth ratio of the longwall and the position of the longwall panel in the series. The mathematical formulae that define the profile shape are of the form given in Equation 2.6. The library of profile shapes comprise the values of *a* to *k* in these formulae.

$$y = \frac{a + cx + ex^2 + gx^3 + ix^4 + kx^5}{1 + bx + dx^2 + fx^3 + hx^4 + jx^5} \qquad [2.6]$$

Different formulae apply, with unique *a* to *k* values, for first, second, third, fourth, and fifth or subsequent longwall panels in a series, and for different width to depth ratios, within the range of 0.3 to 5.0. For second, third, fourth and fifth or subsequent longwall panels, the left and right hand side of the profiles have different formulae.

The library of profile shapes contains *a* to *k* values for 693 different half-profile shapes for single-seam mining operations. The library also contains 236 different half-profile shapes for a range of multi-seam mining situations. A selection of model incremental subsidence profiles for various width to depth ratios is shown in Figure 2.20.

It has been acknowledged by the authors that the method has a tendency to over-predict the subsidence parameters as a conservative view was adopted in drafting the graph (Figure 2.21) that is used for predicting the maximum incremental subsidence. Figure 2.21 shows the maximum incremental subsidence, expressed as a proportion of seam thickness, versus longwall panel width to depth ratio.

Since Figure 2.21 is used to determine the amplitude of the incremental subsidence profile, any over-prediction of the maximum subsidence value also leads to over-predictions of the tilt, curvature and strain values. Once the geometry of a longwall panel is known, the shapes of the two halves of the incremental subsidence profile of the longwall panel can be determined from the appropriate formulae to provide a smooth non-dimensional subsidence profile across the longwall panel.

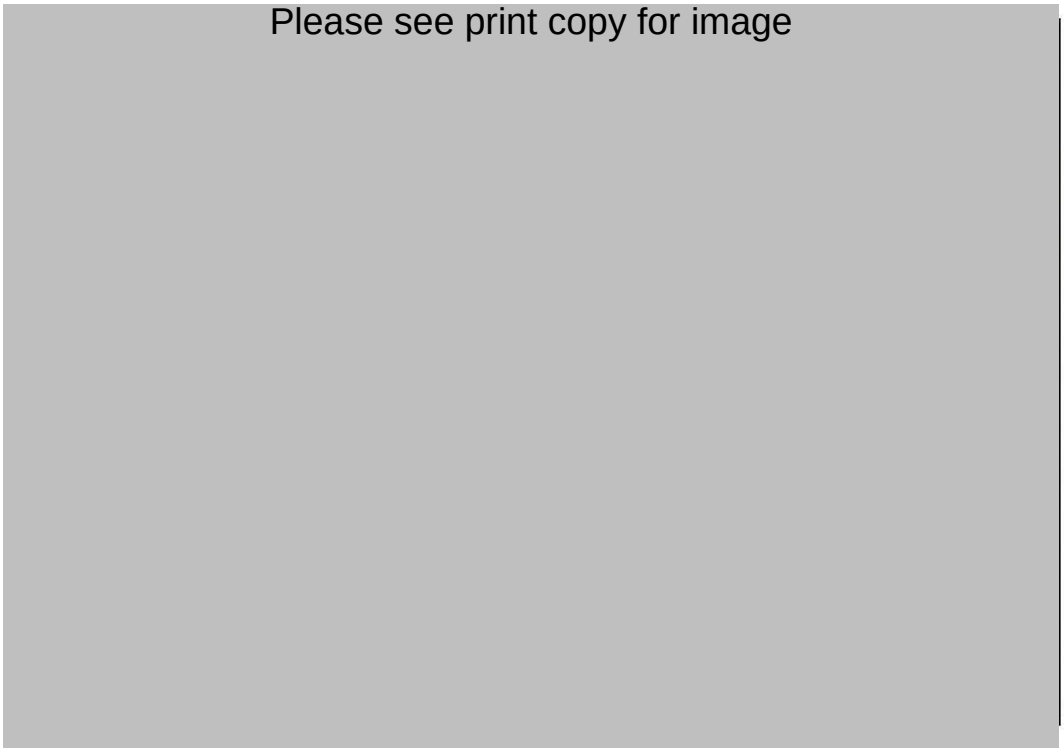

Fig. 2.20 – Incremental subsidence profiles obtained using the Incremental Profile Method (Waddington Kay & Associates 2002)

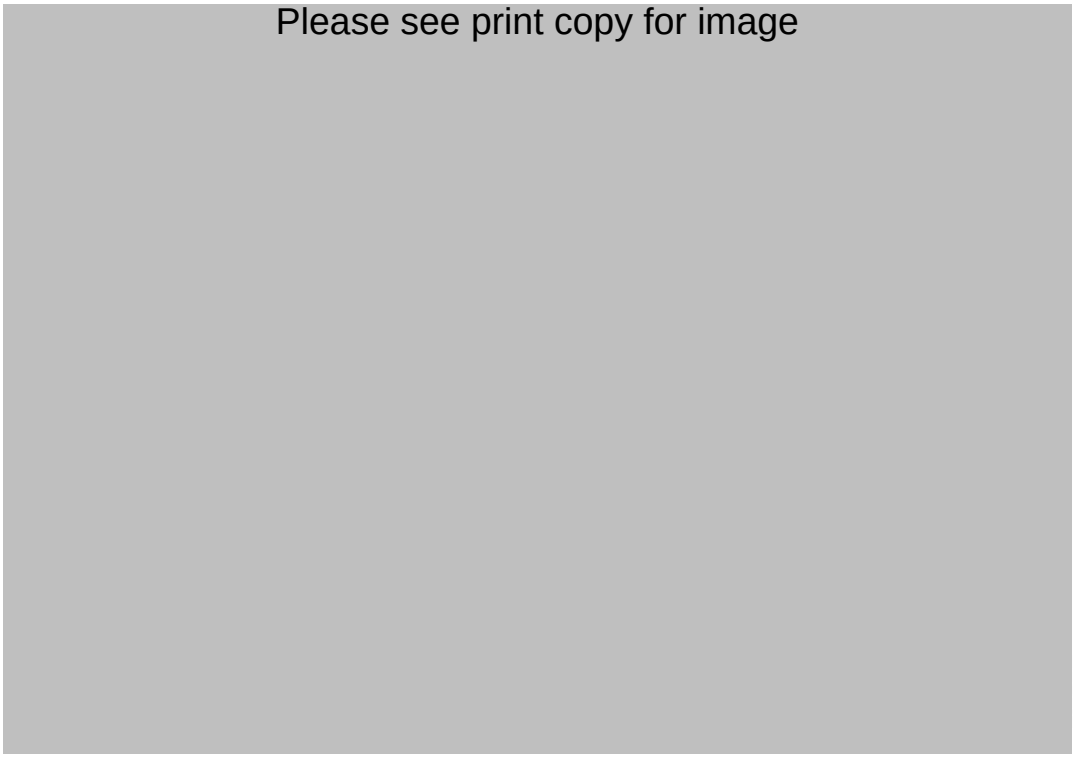

Fig. 2.21 – Prediction curves for maximum incremental subsidence (Waddington Kay & Associates 2002)

The actual incremental profile is obtained by multiplying vertical dimensions by the maximum incremental subsidence value and horizontal dimensions by the local depth of cover. Smooth tilt and curvature profiles are obtained by taking the first and second derivatives of the subsidence profile.

The amplitude and position of the incremental profile relative to the advancing goaf edge of the longwall is determined by a factor known as the overlap factor, the profile moving further towards the previous longwall panel as the overlap factor increases. This factor is an empirically derived factor, which is a function of the longwall panel width, pillar width and the depth of cover.

In order to determine strain values from the curvature graphs, it is necessary to select an empirical relationship that will generally provide conservative results. The NCB Subsidence Engineers' Handbook (National Coal Board 1975) adopts a relationship in which the reciprocal radius of curvature, *K*, is equal to strain squared divided by 0.024. The authors state this relationship does not provide a good fit when predicted strains, derived from predicted curvatures are compared with measured values, and a better fit is obtained if a linear relationship of strain = 15 x curvature is chosen, which equates to the bending strain in a beam of 30 m depth bending about its centre line.

The authors point out that the relationship of 15 times curvature is also reasonably close to the graph of radius of curvature versus maximum strain (Figure 2.16) for depths of cover between 300 m and 400 m. It has been found that a multiplying factor of 10 gives better results in the Newcastle Coalfield.

Predicted horizontal displacements in the direction of the prediction line can be derived by accumulating the predicted strains multiplied by the bay lengths, after distributing any displacement closure errors over all bay lengths in proportion to the predicted strains. Alternatively, the predicted horizontal ground movement profiles can be derived by applying a proportionality factor to the predicted tilt profiles, which they resemble in both magnitude and direction. If the latter method is adopted, it is stated that it should be realised that the actual shapes of the horizontal displacement profile and the tilt profile are different and that the predicted horizontal movements at low tilt values could be understated.

The authors state that the predicted subsidence and tilt profiles obtained using the Incremental Profile Method usually match the observed profiles reasonably accurately, and it is not possible to match the predicted and observed curvature and strain profiles to the same standard, due to the large amount of scatter in the measured data, although the range of strains are adequately predicted.

2.6 SUMMARY

In this chapter, subsidence theory was reviewed and particular attention was paid to the caving characteristics of the Southern Coalfield. The caving characteristics have been identified as one of the distinguishing features in terms of numerical model validation. The empirical methods of Holla and Barclay (2000) and Waddington and Kay (2002) were also reviewed and the following is a summary of the advantages and disadvantages regarding the empirical methods.

DPI Empirical Method Advantages

- Easy to use,
- Reasonably accurate for W/H < 0.5 (a variation of 10 % should be accounted for),
- Predictions can be made in a relatively short time (when compared to other methods such as numerical modelling, influence and profile functions), and
- A complete subsidence profile can be obtained for a single longwall panel extraction.

DPI Empirical Method Disadvantages

- Only applicable to longwall mining,
- Large scatter in data evident in Figures 2.10, 2.13, 2.14, 2.15, 2.17 and 2.18 (S_{max}/T for single longwall panels, K1, K2, K3, inflection point and goaf edge subsidence respectively),
- Predicted limit of mining influence affected by the determination of the draw angle (large variation in observed values) and the uncertain extent of horizontal movement,

- Cannot produce a subsidence profile for multiple longwall panel layouts,
- Cannot predict subsidence in topography that is not relatively flat,
- Cannot predict subsidence for multiple seam mining,
- Cannot predict location and depth of surface cracking due to the acknowledged difficulty in predicting surface strains, and
- Cannot predict sub-surface deformations – must rely on assumptions.

Incremental Profile Method Advantages

- Multiple longwall panel application,
- Multiple seam application,
- Can predict transverse and longitudinal profiles anywhere above a series of longwall panels,
- Can predict horizontal displacements,
- Allows for variation in seam thickness, pillar and longwall panel widths, and depths of cover across a series of longwall panels, and
- Applicable to other coalfields (e.g. Newcastle Coalfield).

Incremental Profile Method Disadvantages

- Only applicable to longwall mining,
- Large data scatter problematic for localised strain predictions, and
- Not as simple to use compared to DPI method.

CHAPTER 3
VALLEY CLOSURE AND UPSIDENCE

3.1 INTRODUCTION

Valley closure and upsidence are phenomena that occur when mining approaches and undermines river valleys. The most common effects of valley closure and upsidence are cracking and buckling of river beds and rock bars, localised loss of water flow and adverse effects on the local ecosystem (Figures 3.1 to 3.3). In most cases, the loss of water flow into voids beneath the base of the valley is caused by the cracking and buckling of the valley base. The magnitude of water loss is dependant on the gradient of the creek/river, relative water table levels and the magnitude of the water flows. Where losses occur it is generally temporary and this water re-joins the creek/river further downstream (Waddington & Kay 2001). The most common method of rehabilitation involves the injection of some type of grout to try and seal the mining induced rock fracture network and restore water flow.

Fig. 3.1 – Buckling of rock bars resulting in low angle fractures

Fig. 3.2 – Buckling of rock bars leading to vertical cracks

Fig. 3.3 – Reduction in creek water level due to mining

To date, the most comprehensive review on valley closure and upsidence due to mining was performed by Waddington Kay and Associates as part of ACARP Project No. C9067. These research reports culminated in a handbook for the undermining of cliffs, gorges and river systems (Waddington Kay & Associates, CSIRO Petroleum Division & University of New South Wales 2002) and contain a conceptual model for valley closure and upsidence, along with an empirical method to predict valley closure, upsidence, compressive strain and regional horizontal movement for river valleys that have been undermined.

3.2 CURRENT MODELS

3.2.1 Horizontal stress model

In Waddington Kay and Associates (2002), it is summarised that during the formation of a river valley, the horizontal stresses in the valley sides redistribute to the valley base, causing an increase in horizontal compressive stress. This phenomenon is not new and is commonly referred to as the 'notch effect'. As the base of the valley is a free surface, it is able to expand vertically. This upward movement of the valley base is generally termed upsidence. Upward movement also occurs in the sides of the valley and for some distance beyond.

When a river valley is directly undermined by a longwall panel, the conceptual model stipulates that the longwall panel extraction causes a redistribution of horizontal compressive stress above and below the mined out seam. The horizontal compressive stress that is distributed below the longwall panel contributes to buckling and failure of the floor of the extraction, whilst the horizontal compressive stress distributed above the longwall panel adds to the already high horizontal compressive stress at the base of the valley. This conceptual model is illustrated in Figure 3.4.

Depending on the bedding plane spacing and strength of rock in the valley base, the increase in horizontal compressive stress may be enough to buckle and fail the valley base (Figure 3.5 and Figure 3.6). Failure of the strata in the valley base continues downwards until equilibrium is achieved. This can occur if a stronger bed is reached or

the depth of failure reached provides enough vertical confinement to prevent compressive failure.

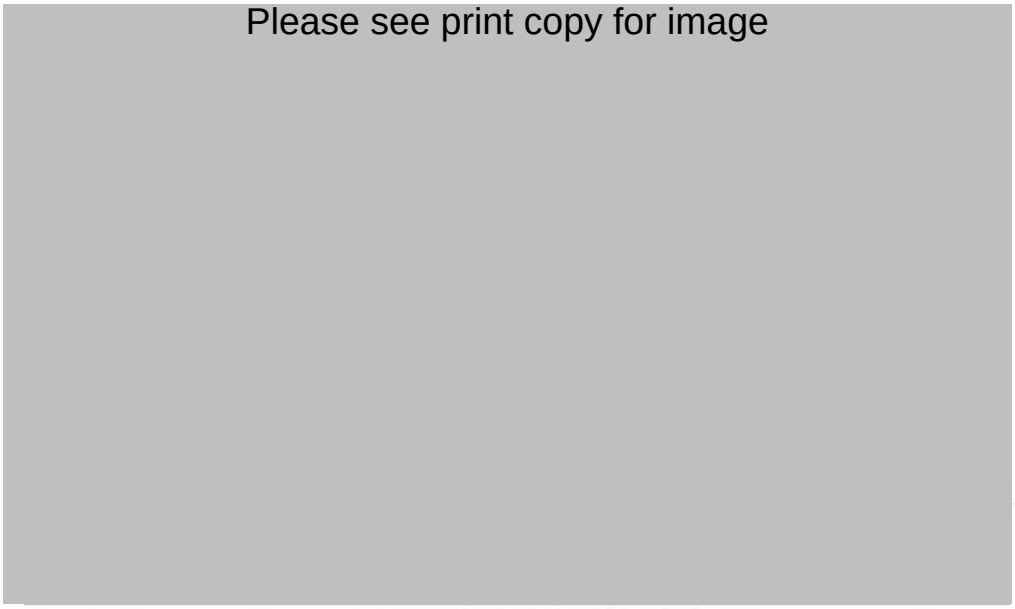

Fig. 3.4 – Notch effect on horizontal stress field (Holla & Barclay 2000)

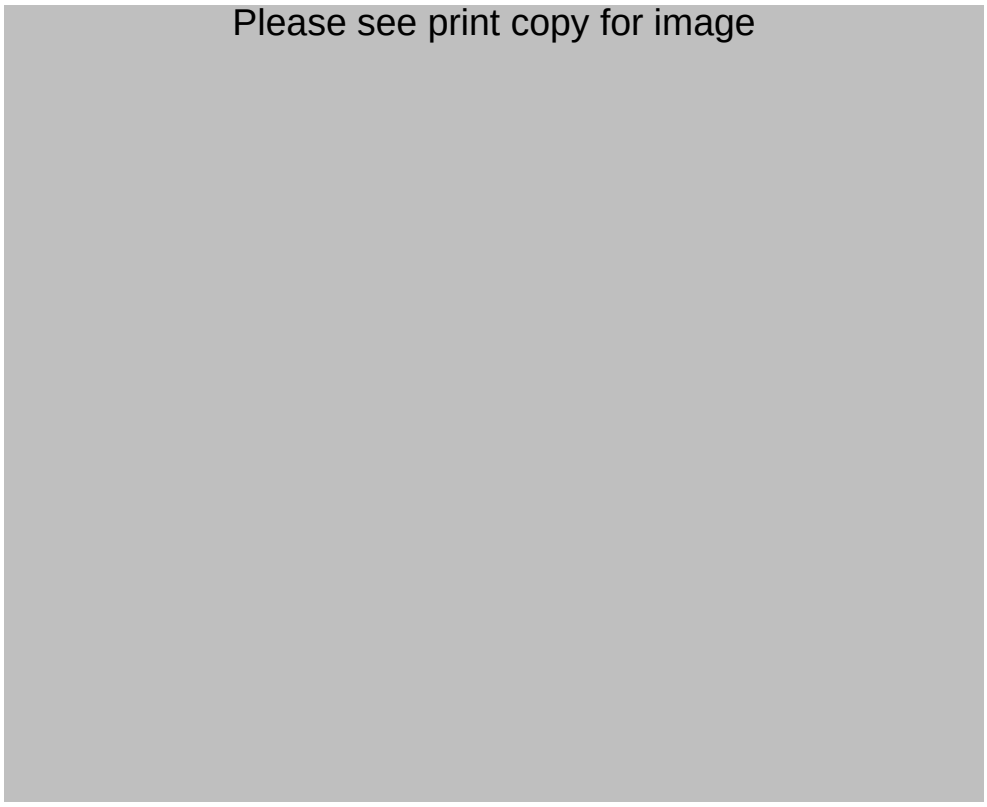

Fig. 3.5 – Strata buckling mechanism due to in-situ horizontal stress (Waddington Kay & Associates 2002)

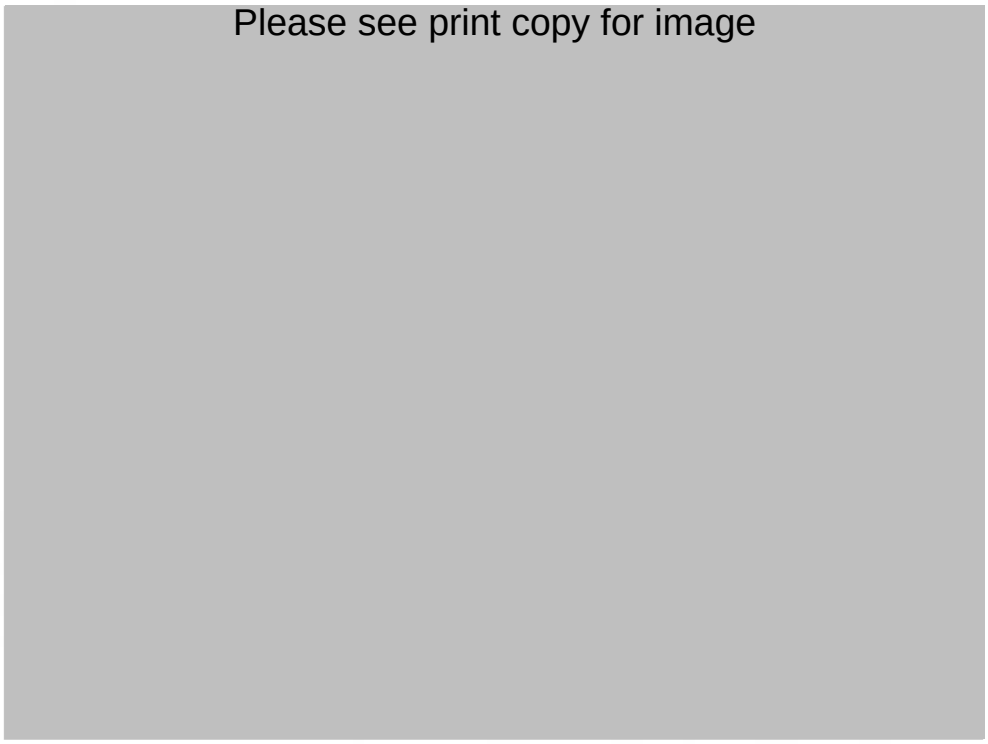

Fig. 3.6 – Possible failure mechanisms in the bottom of a valley (Waddington Kay & Associates 2002)

The buckling and failure of the valley base can create voids below the base of the valley. This failure of the valley base allows some relaxation of the sides of the valley to occur, resulting in valley closure.

3.2.2 Empirical predictions

In Waddington Kay and Associates (2002), an empirical method to predict valley closure and upsidence has been developed. This method is based on upper-bound measured values and is anticipated to over-predict in areas of lower horizontal stress. The prediction method for valley closure and upsidence is based on a series of graphs that show the interrelationships between closure/upsidence and a number of contributory factors. The contributing factors include:

- Longitudinal distance from travelling, commencing or finishing goaf end,
- Valley depth (incised gorges), and
- Maximum incremental subsidence of mined longwall panel.

The contributing factors are plotted on graphs and serve as adjustment factors to predict valley closure and upsidence.

The distance measurement convention used in the predictions is shown in Figure 3.7.

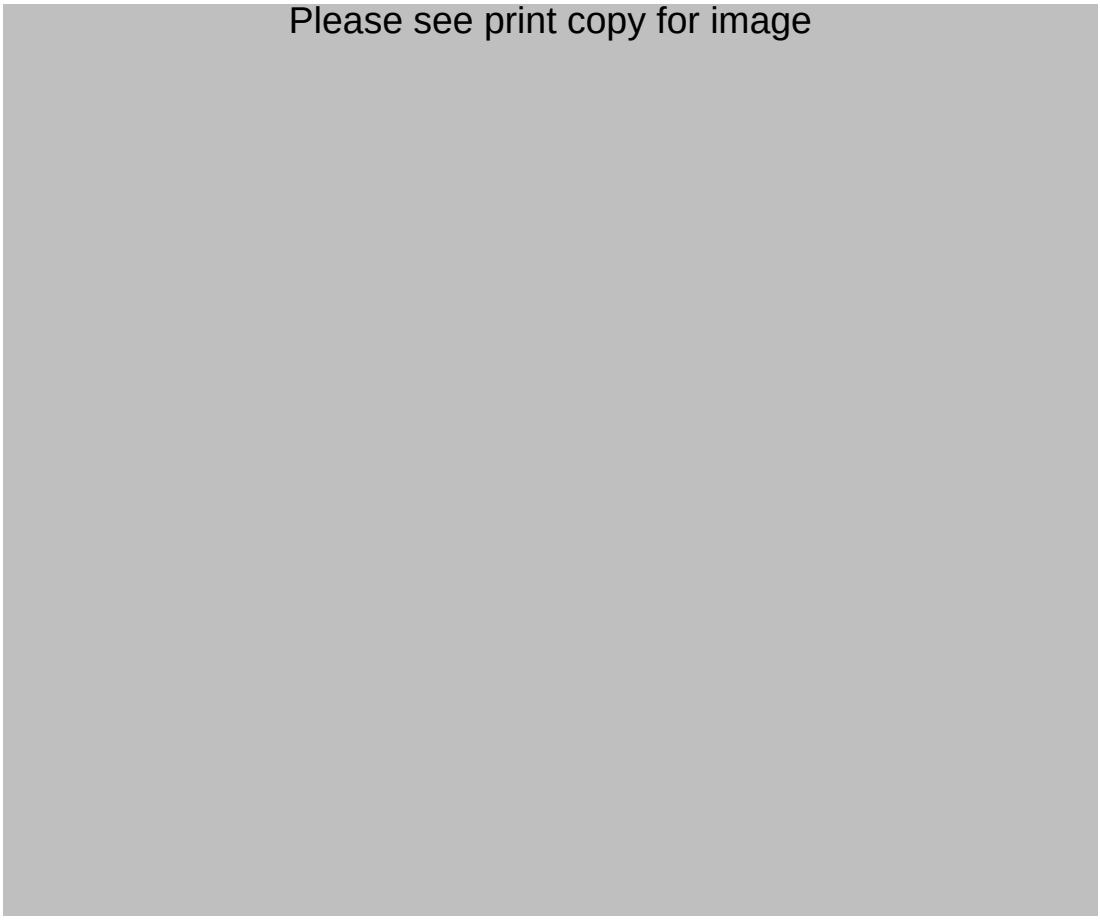

Fig. 3.7 – Distance measurement convention for valley closure and upsidence predictions (Waddington Kay & Associates 2002)

The transverse distances for points A, B, C and D in Figure 3.7 are -270 m, 115 m, 460 m and 680 m respectively. Distances outside the goaf are negative. The longitudinal distances for points A, B, C and D are 450 m, 350 m, 160 m and -130 m respectively. Distances outside the goaf are also negative.

The graphs used to predict valley closure are shown in Figures 3.8 to 3.11 and the graphs used to predict upsidence are shown in Figures 3.12 to 3.15. The base data used to prepare these plots are not available in the literature. It is also important to note that

the plots include the raw data (blue) as well as so called adjusted data that was produced by Waddington Kay and Associates in the formulation of their empirical models.

To make a prediction of valley closure or upsidence at a point in the base of a creek or river valley, the following information is necessary:

- Distance of the point from the advancing edge of the longwall panel,
- Longitudinal distance from the nearest end of the longwall panel,
- Valley depth,
- Maximum incremental subsidence of the longwall panel that is being mined, and
- Longwall panel and pillar widths.

The initial prediction of valley closure is made using Figure 3.8. The value of valley closure is then adjusted by multiplying it by the adjustment factors obtained in Figures 3.9 to 3.11. The procedure followed for predicting upsidence is the same as predicting valley closure.

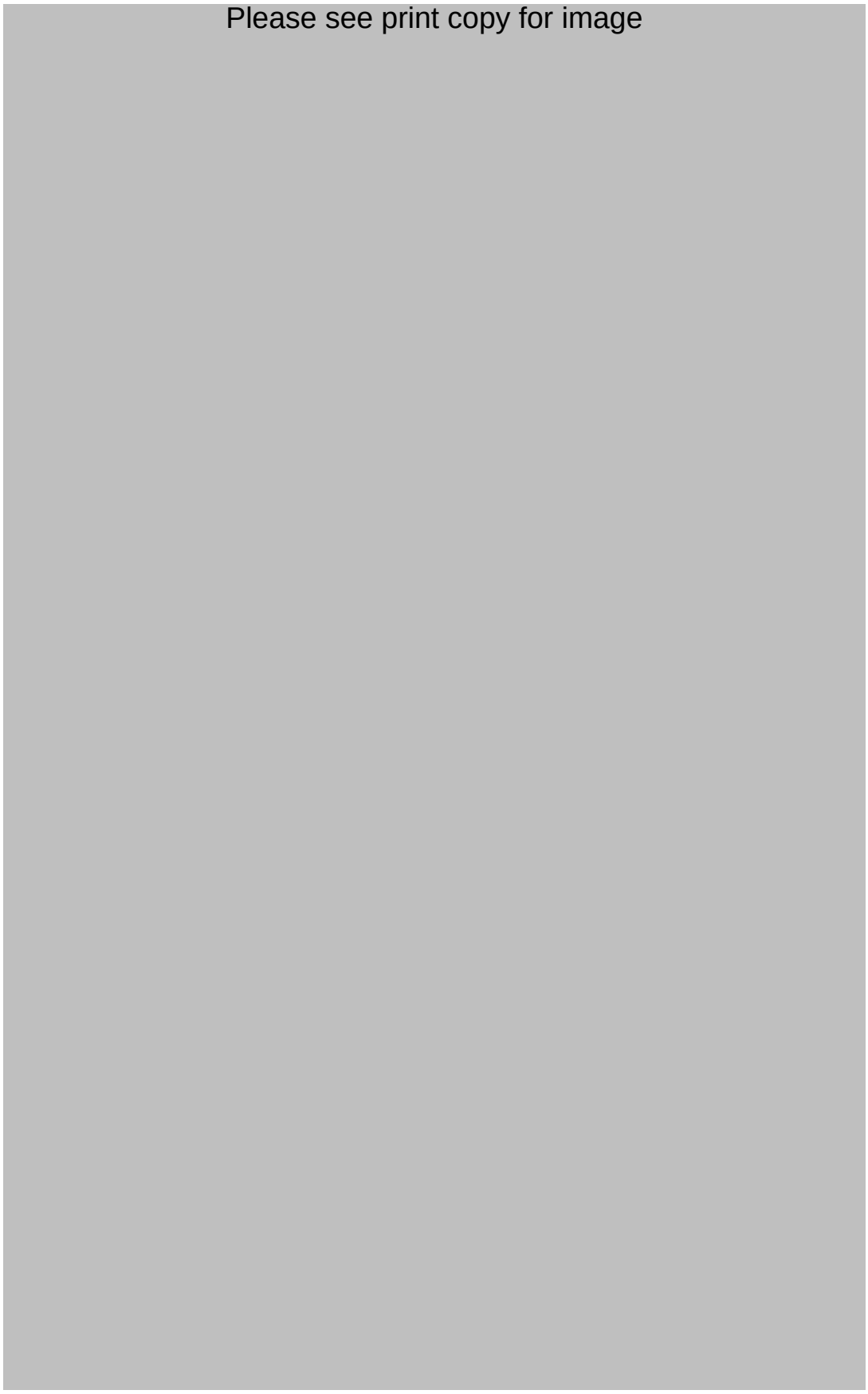

Fig. 3.8 – Valley closure versus transverse distance from the advancing goaf edge (Waddington Kay & Associates 2002)

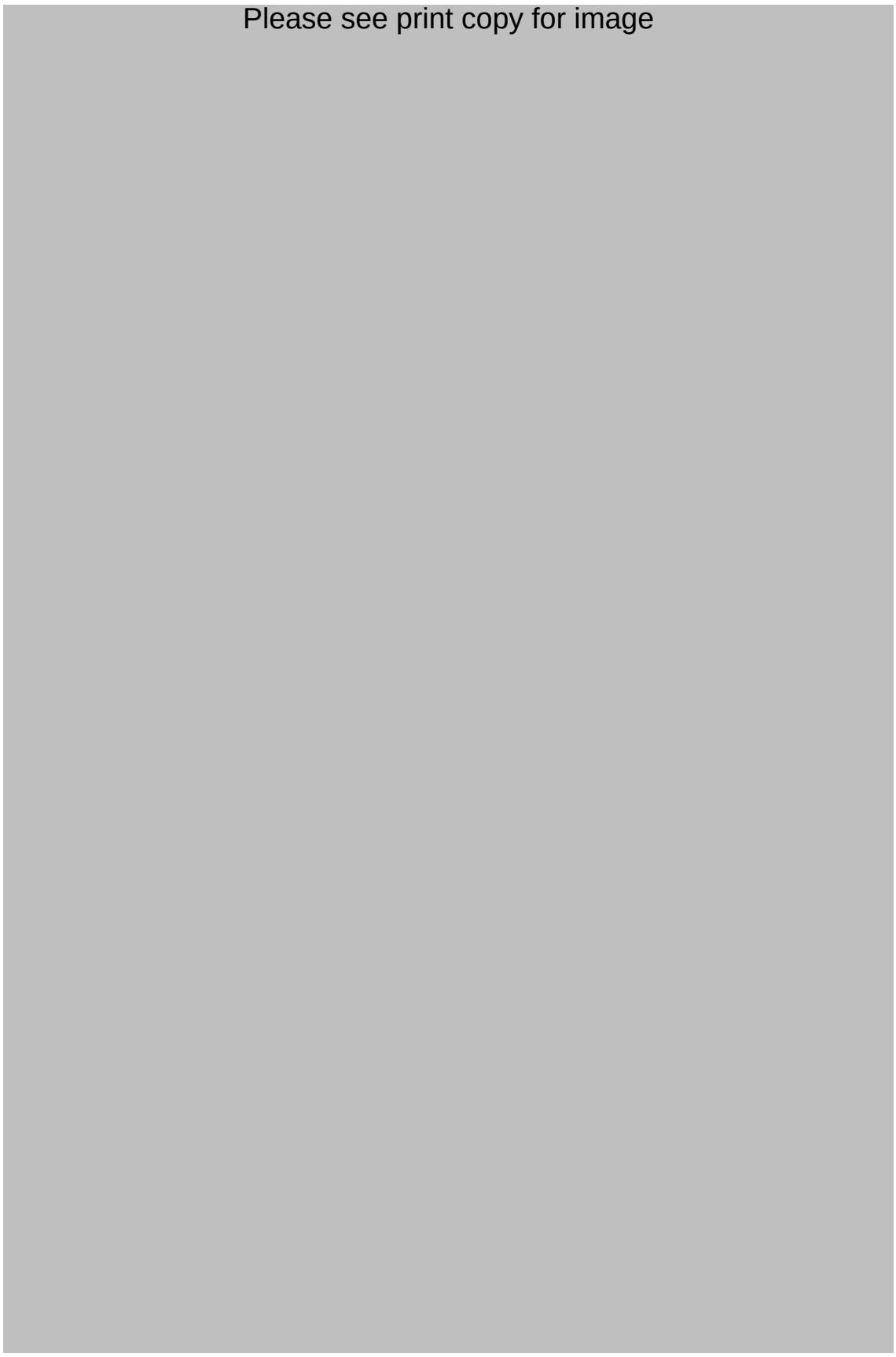

Fig. 3.9 – Valley closure adjustment factor versus longitudinal distance (Waddington Kay & Associates 2002)

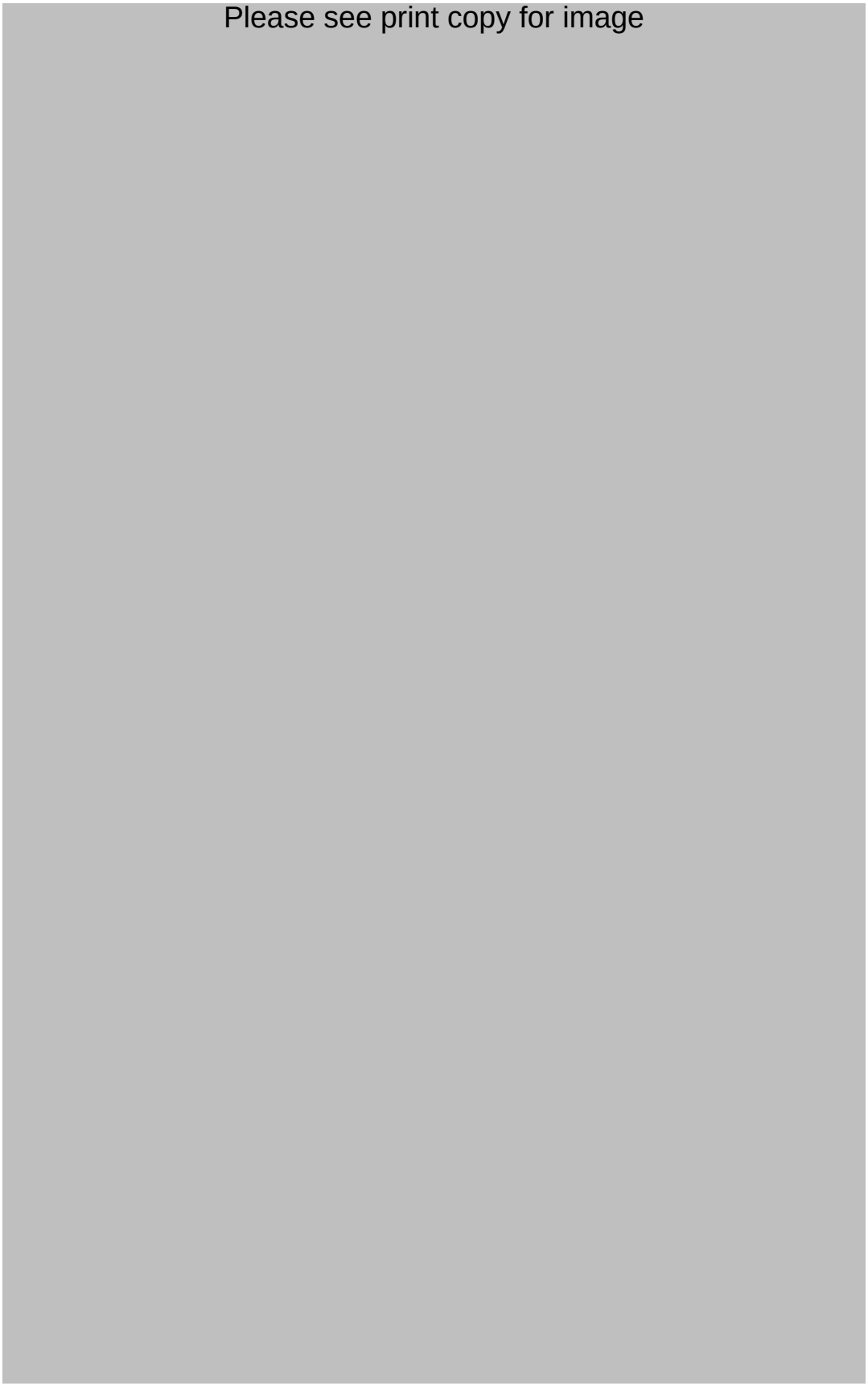

Fig. 3.10 – Valley closure adjustment factor versus valley depth (Waddington Kay & Associates 2002)

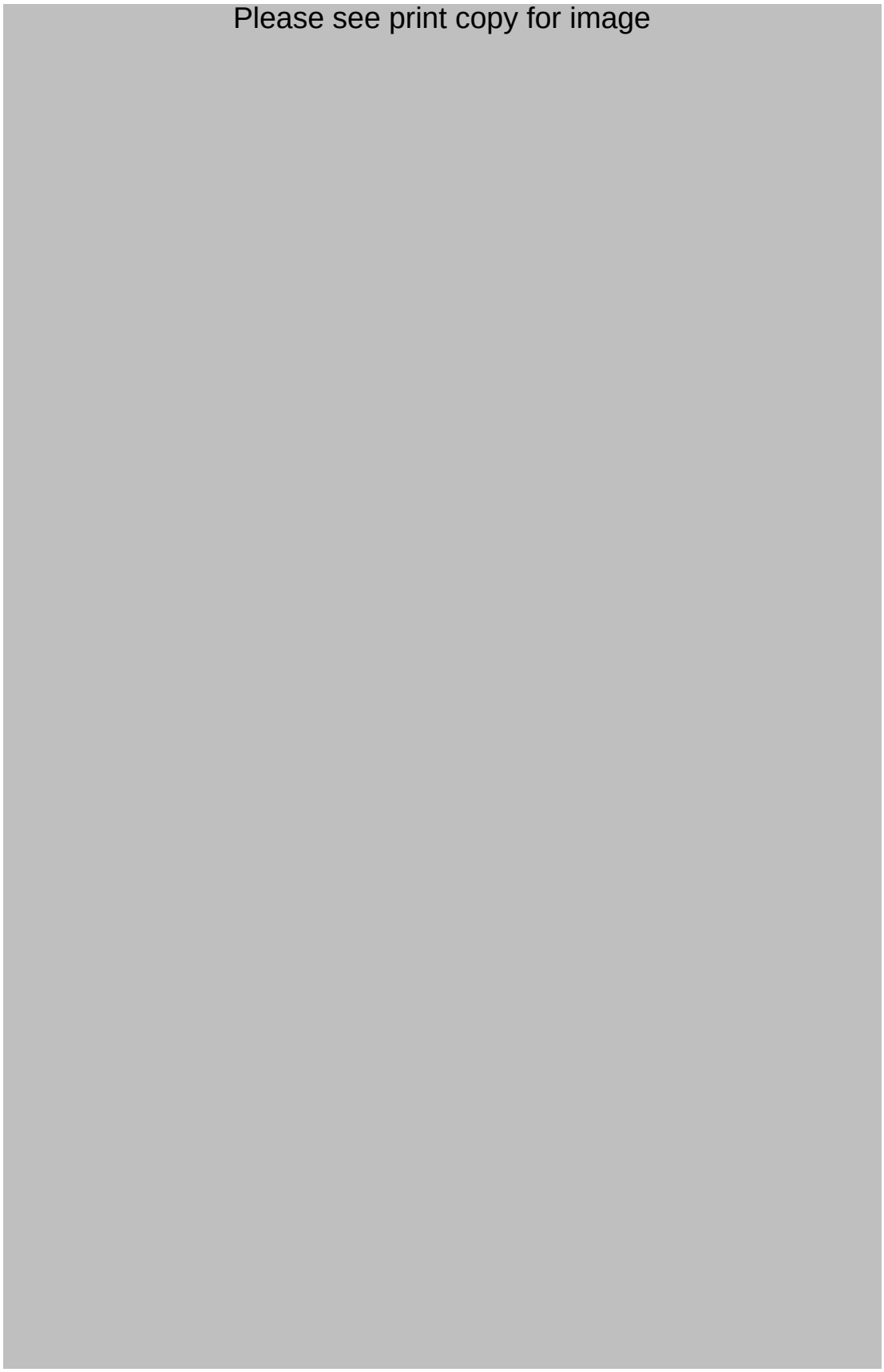

Fig. 3.11 – Valley closure adjustment factor versus maximum incremental subsidence (Waddington Kay & Associates 2002)

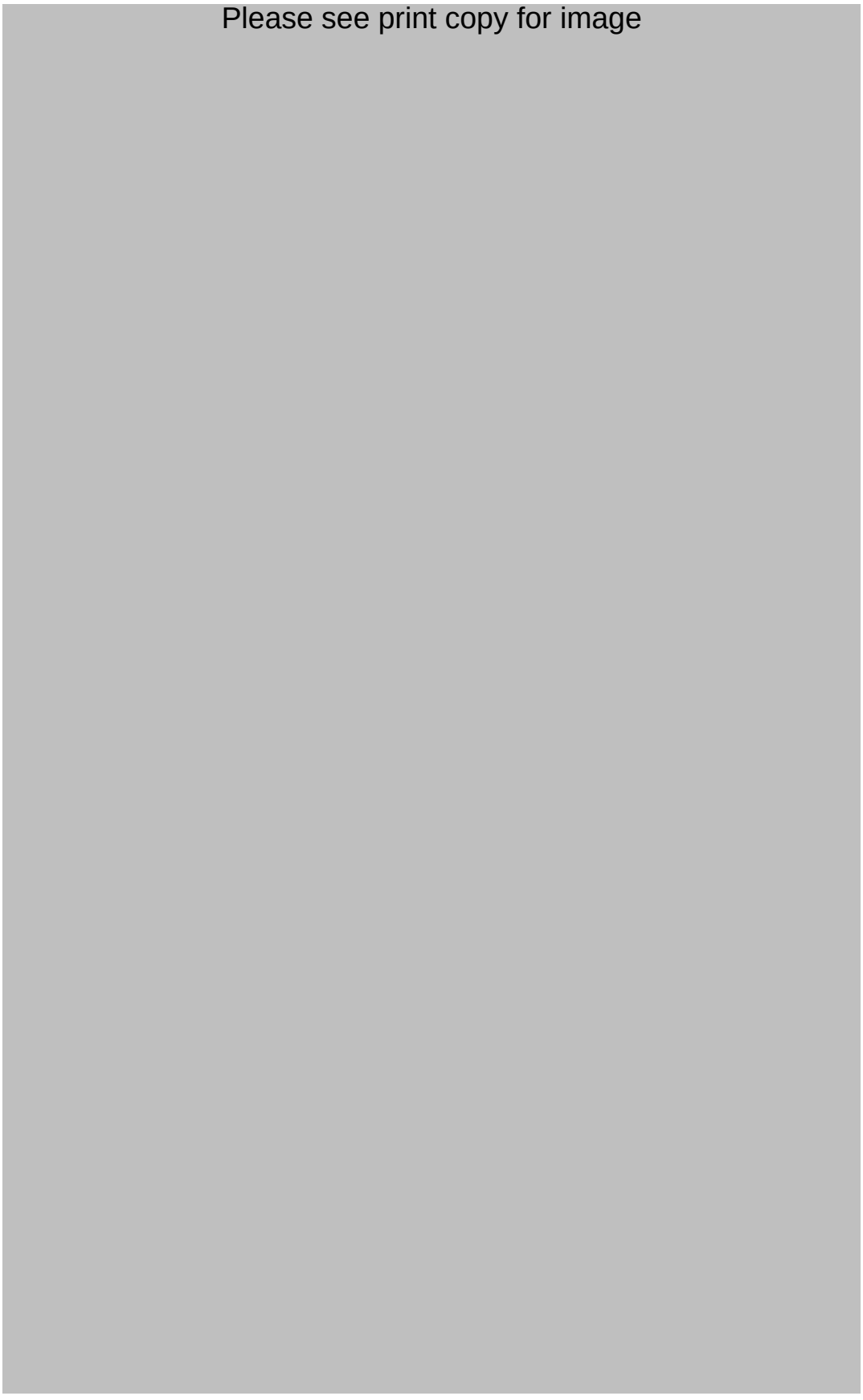

Fig. 3.12 – Upsidence versus transverse distance from the advancing goaf edge (Waddington Kay & Associates 2002)

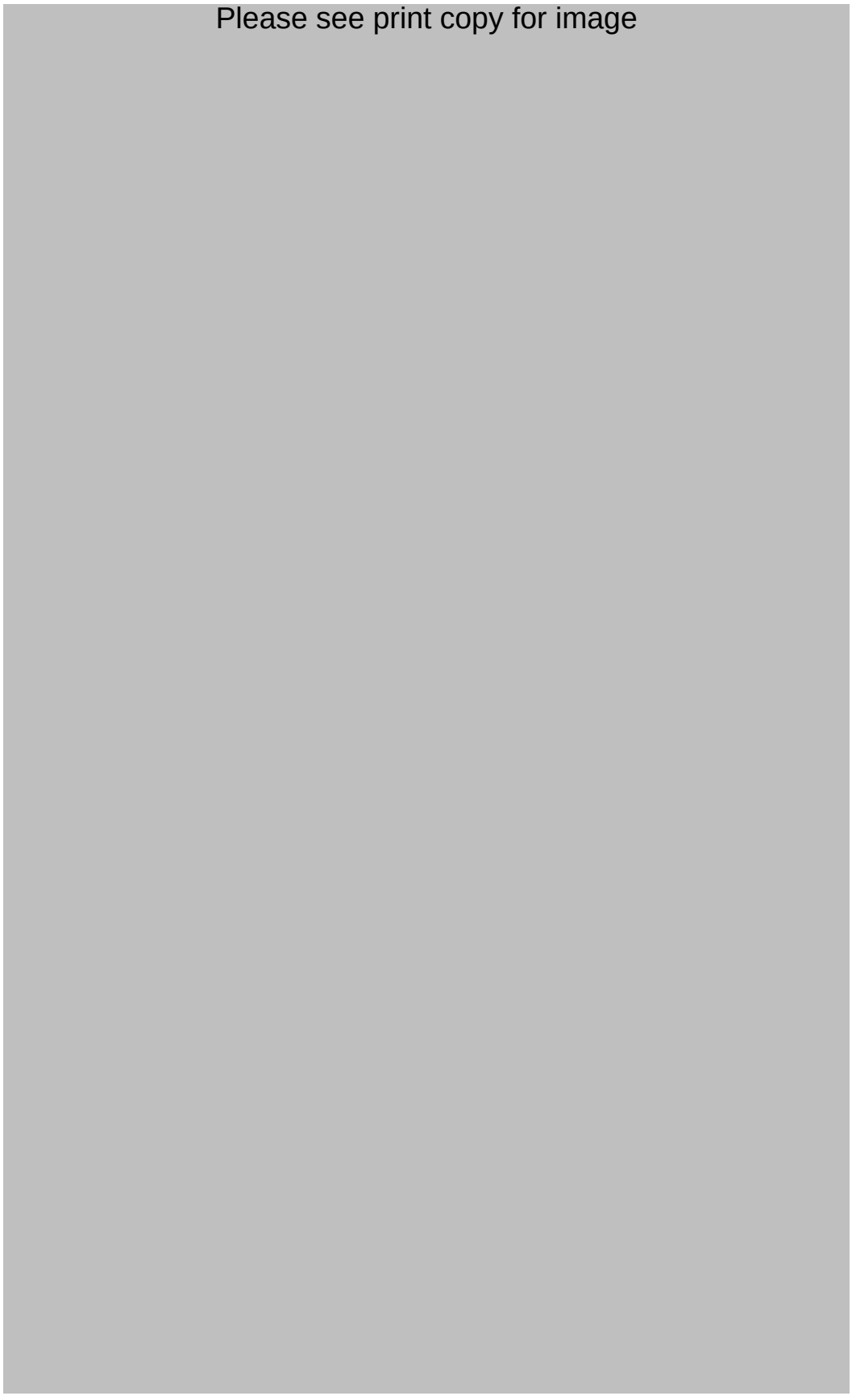

Fig. 3.13 – Upsidence adjustment factor versus longitudinal distance (Waddington Kay & Associates 2002)

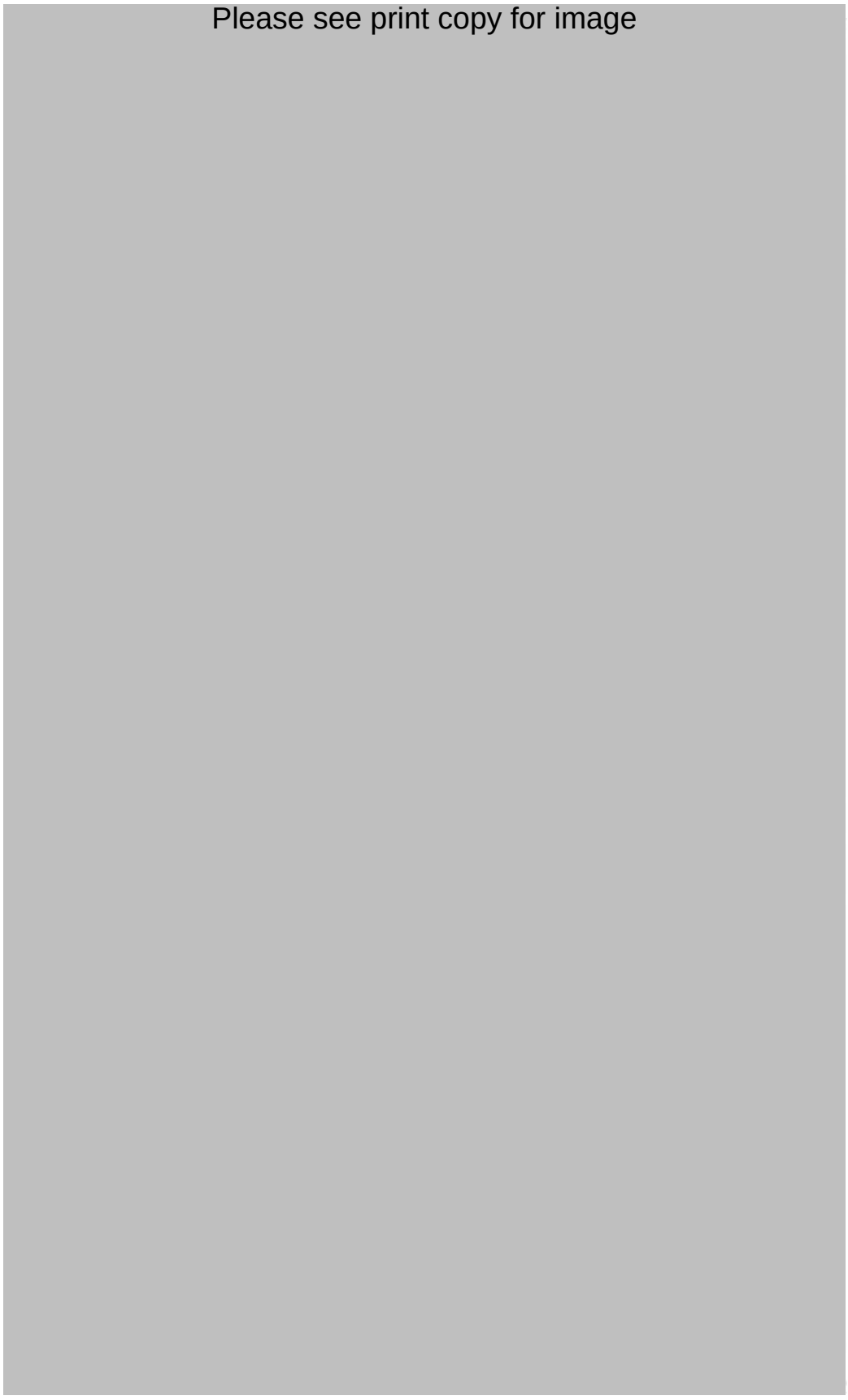

Fig. 3.14 – Upsidence adjustment factor versus valley depth (Waddington Kay & Associates 2002)

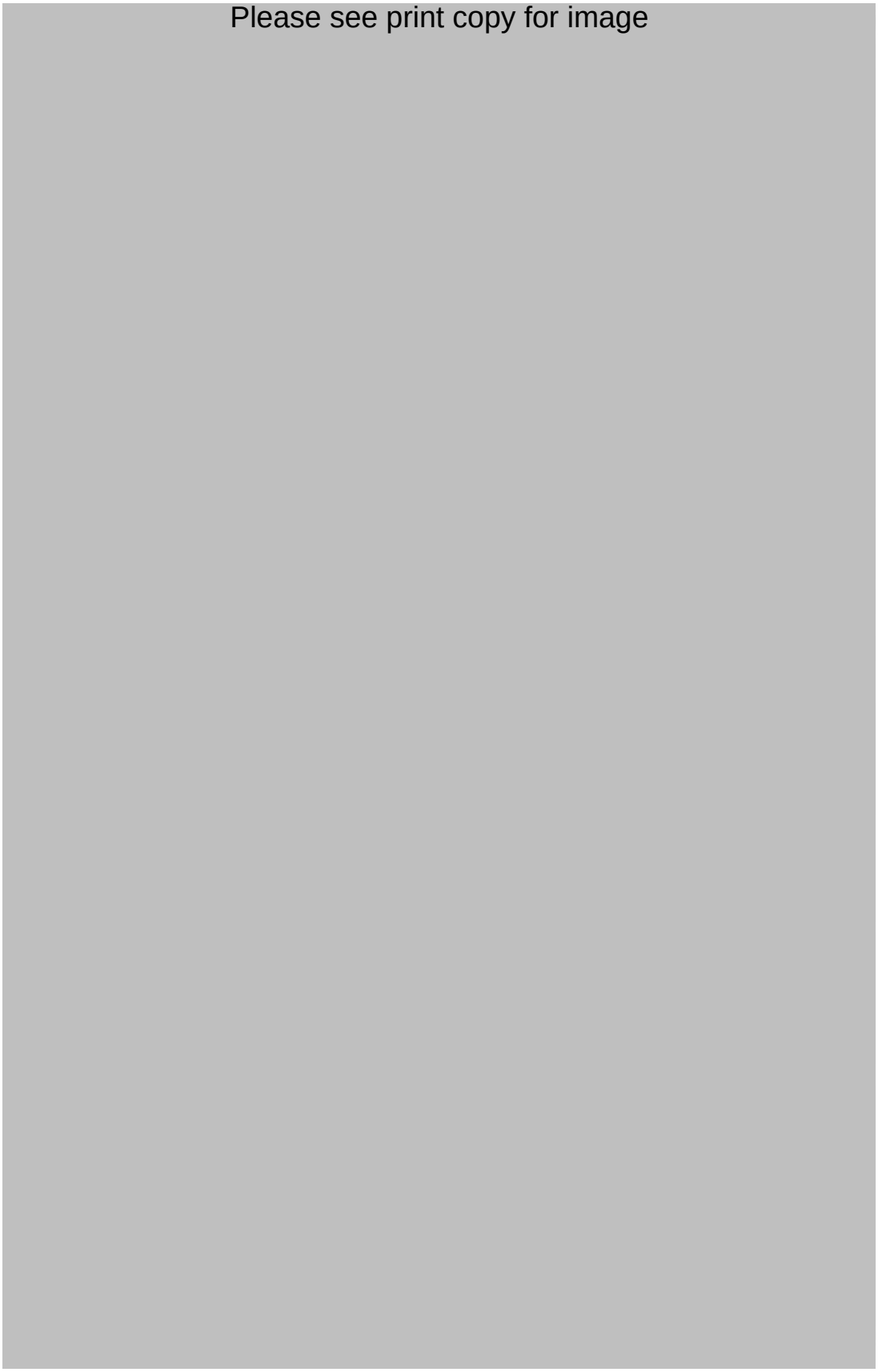

Fig. 3.15 – Upsidence adjustment factor versus maximum incremental subsidence (Waddington Kay & Associates 2002)

3.2.3 Limitations

For a river valley that is directly undermined by a longwall panel, the horizontal stress model is valid. By virtue of geometry, it would be expected that horizontal stresses are predominately compressive in the base of a valley that is located in the sagging portion of the subsidence profile. Results from the empirical study (Waddington Kay & Associates 2002) show that cases of valley closure and upsidence occur well outside the goaf edge in unmined coal and also over old longwall panels (Figure 3.8 and Figure 3.12). These events largely occur in the hogging portion of the subsidence profile, where the horizontal stresses are predominately tensile.

The significance of these valley closure and upsidence events above unmined coal is considerable. There is an increase in the environmental footprint, which is usually seized upon by environmental, community and anti-mining groups. The increase in environmental footprint may lead to problems in defining the limit of mining influence using the traditional 20 mm vertical subsidence cut-off limit. This in turn potentially leads to policies defining mining barriers and stand-off distances, as environmental groups like the RIVERS SOS coalition seek the establishment of a one kilometre protection zone around rivers in the Southern Coalfield (Mineral Policy Institute 2005). Mining barriers lead to increased roadway development to access coal reserves on the other side of protected rivers, and these results in inefficient mine designs and most importantly, sterilisation of coal reserves. An example of this can be seen in Figure 3.16, which illustrates BHP Billiton Illawarra Coal's original mine layout for the Douglas Project which undermined the Nepean River, and the amended layout which does not undermine the Nepean River at all (BHP Billiton 2005).

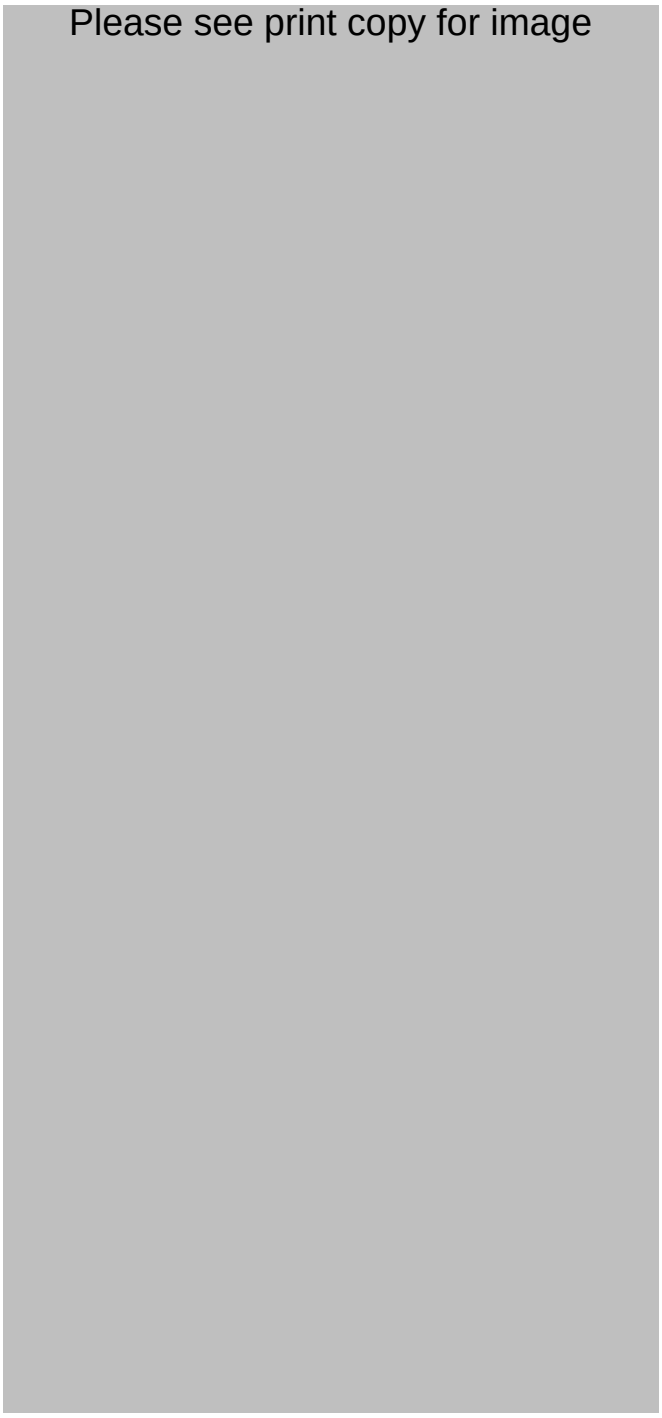

Fig. 3.16 – Original and amended plan for mining near the Nepean River (BHP Billiton 2005)

The conceptual model of redistributed horizontal compressive stress in two dimensions cannot explain the upsidence and closure events in the hogging phase, the lack of valley closure and upsidence over currently mined longwall panels, or explain why valley closure occurs if there is no valley base failure. It is simply not sufficient to assume that

all valley closure and upsidence events occur because of horizontal compressive stress. It is also not sufficient to assume that valley closure and valley base failure are related.

3.2.4 Recent developments

A review was published on the Southern Coalfield Enquiry (SCI) in July 2008 (NSW Department of Planning 2008). This independent enquiry was established because of concerns held by the NSW Government over both past and potential future impacts of mine subsidence on significant natural features in the Southern Coalfield. These concerns first surfaced in the community in 1994 when the bed of the Cataract River suffered cracking and other subsidence impacts.

The enquiry conducted a state of the art review of subsidence impacts of significant natural features and recognised the fact that valley closure and upsidence in the far-field are difficult to predict, and the mechanisms are not fully understood.

A review of the mechanisms behind valley closure and upsidence referenced the horizontal compressive stress model of Waddington Kay and Associates (2002) as the most likely mechanism if the valley is located above the mining area. It was recognised that valley closure and upsidence in the far field was not fully understood. The following possible mechanisms were listed but not expanded upon:

- Simple elastic horizontal deformation of the strata within the exponential ‘tail’ of the subsidence profile that applies in conventional circumstances,
- Influence of valleys and other topographical features which remove constraints to lateral movement and permit the overburden to move en masse towards the goaf area, possibly sliding on underlying weak strata layers,
- Unclamping of near-surface horizontal shear planes,
- Influence of unusual geological strata which exhibit elasto-plastic or time dependant deformation,
- Stress relaxation towards mining excavations,
- Horizontal movements aligned with the principal in-situ compressive stress direction,
- Valley notch stress concentrations,

- Movements along regional joint sets and faults, and
- Unclamping of regional geological plates.

It was concluded that the coal mining industry should escalate research into the prediction of non-conventional subsidence effects in the Southern Coalfield and their impacts and consequences for significant natural features, particularly in respect of valley closure, upsidence and other topographical features.

Shortly after the conclusion of the enquiry, The Metropolitan Coal Project Review Report was published (NSW Planning Assessment Commission 2009). This report contained the proposal known as the Metropolitan Coal Project, which related to the future life of mine planning for Metropolitan Colliery. It is the first mining proposal in the Southern Coalfield since the SCI was published in 2008.

A review of subsidence and far-field events like valley closure and upsidence was conducted but mostly drew from the SCI. This illustrates that progress on identifying and verifying a mechanism that explains valley closure and upsidence events over unmined coal is not progressing swiftly.

3.3 ALTERNATIVE MODEL

Due to the inability of the horizontal compressive stress model to explain upsidence and valley closure over unmined coal and old longwall panels, the new conceptual model involves investigating whether block movements in the sagging phase contributes to upsidence and valley closure in the hogging phase.

The basic concept of this model is illustrated in Figure 3.17.

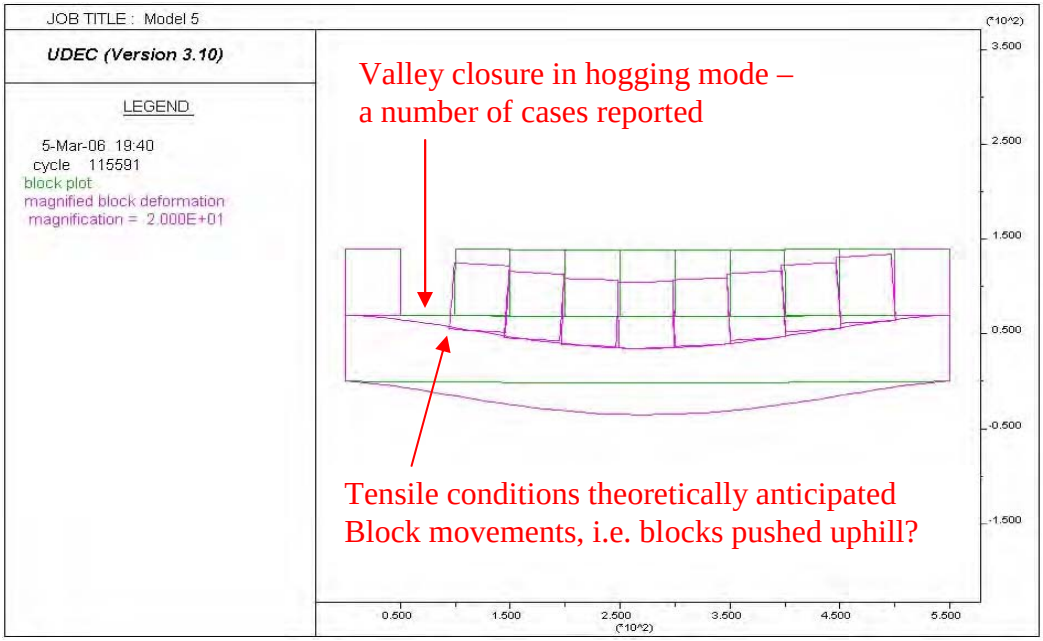

Fig. 3.17 – New conceptual model for upsidence and valley closure in the hogging phase

This conceptual model proposes that if a translation plane is present at the base of the valley, the closure observed above unmined coal is a result of rock blocks being pushed into the void provided by the valley, due to the horizontal shortening of the ground surface directly above the mined longwall panel. Upsidence is not expected to occur due to the translation plane dissipating any built up horizontal stress generated by the movement of the blocks.

If the translation plane is not present at the base of the valley, but located beneath the base of the valley, it is proposed that upsidence will be the dominant feature present above unmined coal. Rock blocks will still have horizontal stresses exerted on them by the horizontal shortening of the ground surface, forcing them in an outward direction, but as no translation plane exists to dissipate the horizontal stress, there will be a concentration in horizontal compressive stress at the base of the valley causing upsidence, and possibly valley base failure. It is anticipated that valley closure above unmined coal is a function of translation plane location, curvature of the ground surface and valley depth. Likewise, upsidence above unmined coal is thought to be a function of translation plane location and curvature of the ground surface.

The assumption that a translation plane exists below the ground surface is based on what is reported in the literature. In Holla and Barclay (2000), it is reported that surface wrinkles at Tahmoor Colliery were a result of a plane of weakness below the ground surface. It was also reported that a nearby borewell was damaged by horizontal shearing of the borehole wall.

A similar occurrence was also reported in Mills and Huuskes (2004) where monitoring instruments in a valley base at Metropolitan Colliery were replaced due to horizontal shearing. In a previous report by Mills (2002) it was noted that there was a loss of drilling water recirculation and low RQD observed in the core at around 6 m below the base of the valley in the same area.

In Holla and Armstrong (1986), it was reported that a borehole at West Cliff Colliery became impassable to a logging probe at 80 m below the ground surface.

This proposed model is compatible with the data in the empirical method described earlier in this chapter as it will provide an explanation for valley closure and upsidence over unmined coal and old longwall panels and take into account the presence of a translation plane below and at the base of a valley.

3.3.1 Kinematics of a particle moving along a known path

The kinematics of a particle moving along a known path is described in this section and is reproduced from Hibbeler (1997). The main principle can be readily adapted to blocks moving along a known path, i.e. the subsidence profile.

Planar motion

Consider the particle *P* shown in Figure 3.18, which is moving in a plane along a fixed curve, such that at a given instant it is located at position *s*, measured from point *O*. Consider a coordinate system that has its origin at a fixed point on the curve, and at the instant considered this origin happens to coincide with the location of the particle. The *t* axis is tangent to the curve at *P* and is positive in the direction of increasing *s*. This positive direction is designated with the unit vector u_t. A unique choice for the normal

axis can be made by considering the fact that geometrically the curve is constructed from a series of differential arc segments *ds*.

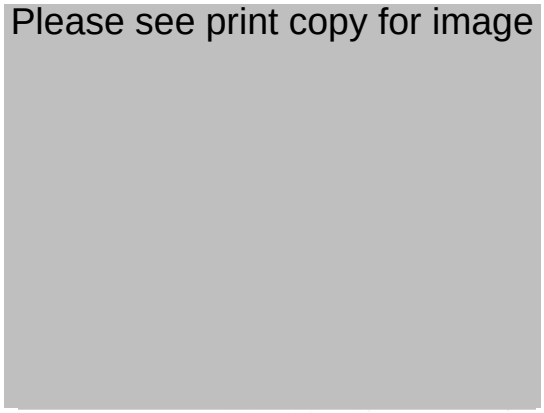

Fig. 3.18 – Position (Hibbeler 1997)

As shown in Figure 3.19, each segment *ds* is formed from the arc of an associated circle having a radius of curvature ρ and centre of curvature *O'*. The normal axis *n* which will be chosen is perpendicular to the *t* axis and is directed from *P* toward the centre of curvature *O'*, Figure 3.18. This positive direction, which is always on the concave side of the curvature, will be designated by the unit vector u_n. The plane which contains the n and t axes is referred to as the osculating plane, and in this case it is fixed in the plane of motion.

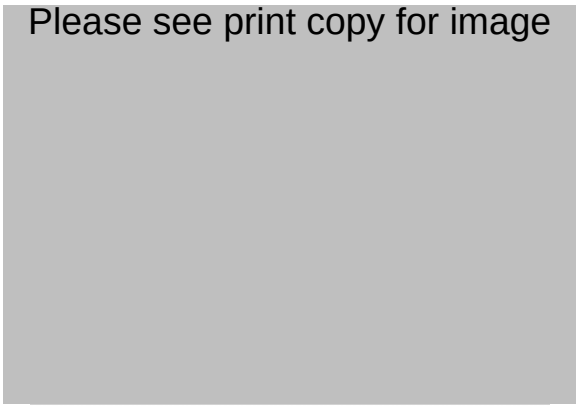

Fig. 3.19 – Radius of curvature (Hibbeler 1997)

Velocity

Since the particle is moving, *s* is a function of time. The particle's velocity *v* has a direction that is always tangent to the path, Figure 3.20, and a magnitude that is determined by taking the time derivative of the path function *s = s(t)*, i.e. *v = ds/dt* (Equation 3.1 and Equation 3.2).

Hence,

$$v = \upsilon u_t \qquad [3.1]$$

Where,

$$\upsilon = \dot{s} \qquad [3.2]$$

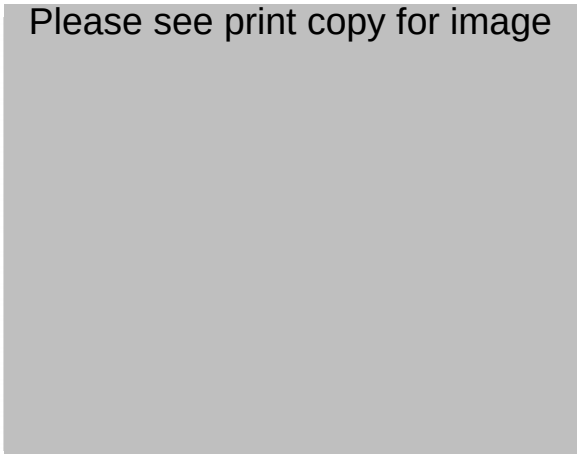

Fig. 3.20 – Velocity (Hibbeler 1997)

Acceleration

The acceleration of the particle is the time rate of change of the velocity (Equation 3.3),

$$a = \dot{v} = \dot{\upsilon} u_t + \upsilon \dot{u}_t \qquad [3.3]$$

In order to compute the time derivative $\dot{u}_t$, note that as the particle moves along the arc *ds* in time *dt*, u_t preserves its magnitude of unity; however, it changes its direction, so that it becomes u_t', Figure 3.21.

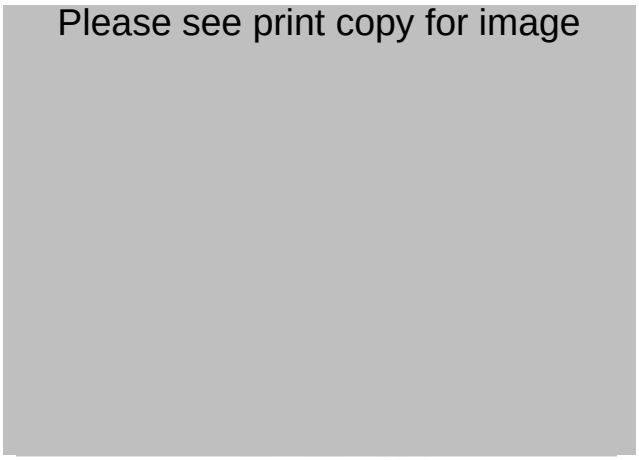

Fig. 3.21 – Time derivative (Hibbeler 1997)

As shown in Figure 3.22, we require $u_t' = u_t + du_t$. Here du_t stretches between the arrowheads of u_t and u_t', which lie on an infinitesimal arc of radius $u_t = 1$. Hence du_t has a magnitude of $du_t = (1)d\theta$, and its direction is defined by u_n.

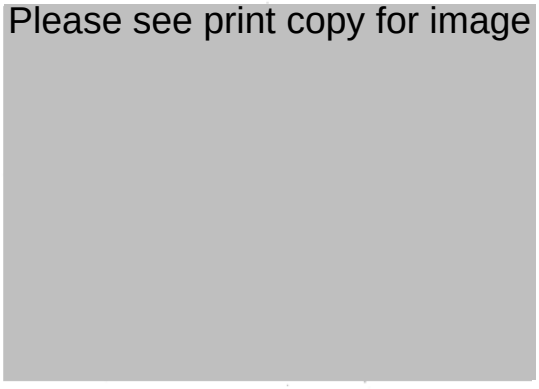

Fig. 3.22 – Time derivative components (Hibbeler 1997)

Consequently, $du_t = d\theta u_n$, and therefore the time derivative becomes $\dot{u}_t = \dot{\theta} u_n$. Since $ds = \rho d\theta$, then $\dot{\theta} = \dot{s}/\rho$, and consequently (Equation 3.4),

$$\dot{u}_t = \dot{\theta} u_n = \frac{\dot{s}}{\rho} u_n = \frac{v}{\rho} u_n \qquad [3.4]$$

Substituting into Equation 3.3, *a* can be written as the sum of its two components (Equations 3.5 to 3.7),

$$a = a_t u_t + a_n u_n \qquad [3.5]$$

Where,

$$a_t = \dot{v} \text{ or } a_t = v\frac{dv}{ds} \qquad [3.6]$$

and,

$$a_n = \frac{v^2}{\rho} \qquad [3.7]$$

These two mutually perpendicular components are shown in Figure 3.23, in which case the magnitude of acceleration (Equation 3.8) is the positive value of:

$$a = \sqrt{a_t^2 + a_n^2} \qquad [3.8]$$

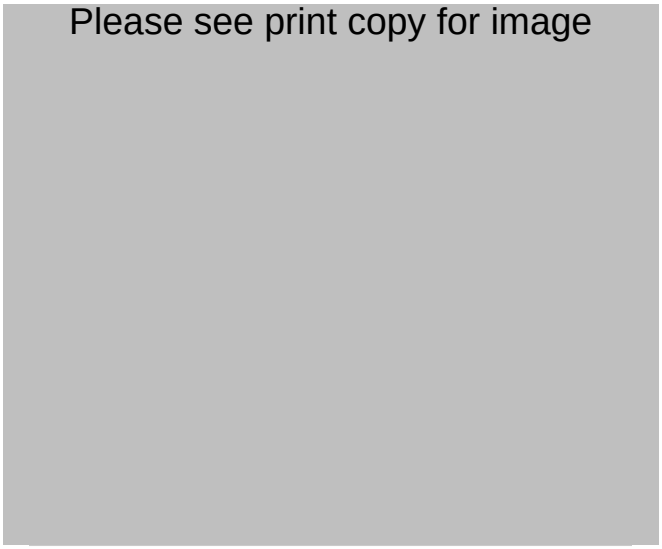

Fig. 3.23 – Acceleration (Hibbeler 1997)

3.3.2 Adaptation to blocks moving along a known path

It can be seen from Equations 3.1 to 3.8 that the kinematics of a particle moving along a known path is highly dependant on the shape of the path and the radius of curvature that is produced from the change of shape in the path. In a mining situation, the shape of the path becomes the subsidence profile. The tilt or radius of curvature can be derived from the subsidence profile as discussed in Chapter 2.

When blocks that represent river valleys are placed on the subsidence profile (Figure 3.24), the blocks will rotate against each other (Figure 3.25) resulting in blocks being pushed into the free face provided by the valley. Holla and Barclay (2000) report that monitoring of horizontal movement of the valley sides in an un-named creek was almost constant, indicating a rigid-body-type movement. This observed behaviour supports the notion of en masse block movements.

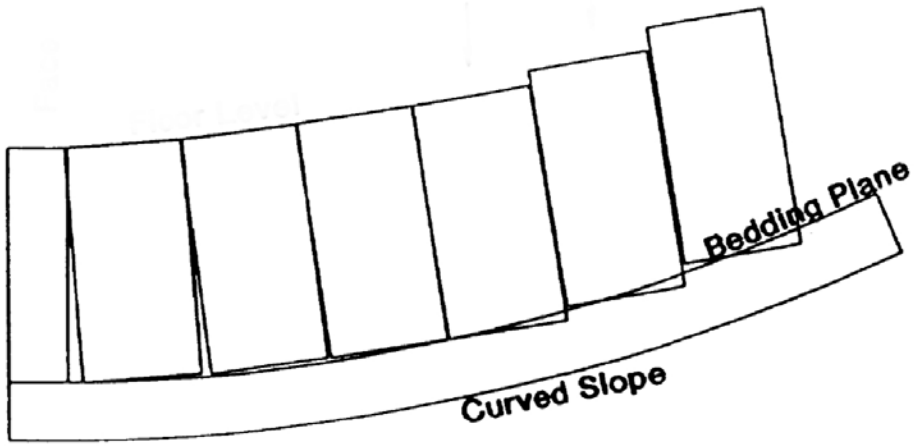

Fig. 3.24 – Magnified block displacements on curved slope (after Nemcik 2003)

Please see print copy for image

Fig. 3.25 – Area of contact between rotating blocks (Nemcik 2003)

The actual kinematics of rock blocks sliding along a translation plane to produce valley closure needs to be further investigated. It can be readily deduced that the movement of each individual block is a function of the radius of curvature or tilt of the subsidence profile, and the height of each individual block.

From simple trigonometry (Figure 3.26), in a circle of radius *r*, the length of the arc *s* opposite the angle θ at the centre is defined by Equation 3.9.

$$s = r\theta \qquad [3.9]$$

Where θ is in radians.

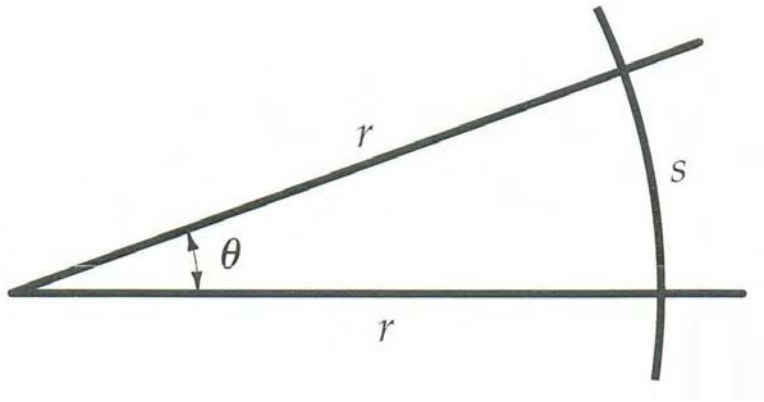

Fig. 3.26 – Length of an arc

Adapting the above theory to block rotations and simplifying to enable simple trigonometric analysis (Figure 3.27):

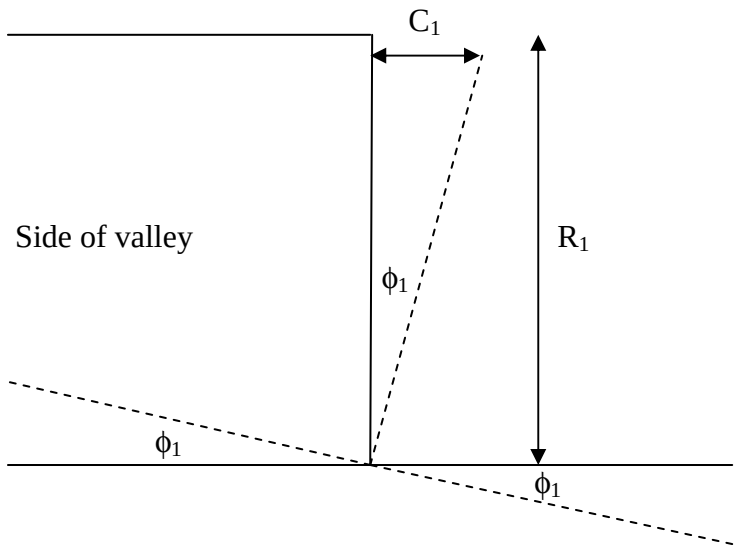

Fig. 3.27 – Exaggerated view of valley tilt and resulting closure

Where,

R_1 = Depth of valley (m)

ϕ_1 = Tilt of block adjacent to valley (radians)

C_1 = Closure from one side of valley (m)

To determine the tilt experienced by one half of a valley, consider Figure 3.28.

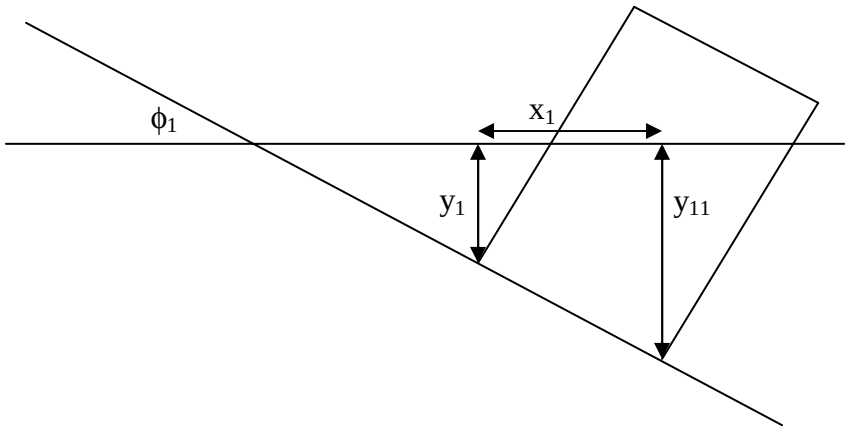

Fig. 3.28 – Components of valley tilt

Where,

y_1 = Subsidence at corner of block (m)

y_{11} = Subsidence at corner of block (m)

x_1 = Distance between block corners (m)

Using simple trigonometry, the angle of tilt can be calculated from Equation 3.10 and Equation 3.11, and the resulting closure can be calculated from Equation 3.12.

$$\tan\phi_1 = \frac{y_{11} - y_1}{x_1} \qquad [3.10]$$

$$\phi_1 = \left(\frac{y_{11} - y_1}{x_1}\right) \cdot \tan^{-1} \qquad [3.11]$$

$$C_1 = R_1\left[\left(\frac{y_{11} - y_1}{x_1}\right) \cdot \tan^{-1}\right] \qquad [3.12]$$

If the expression for ϕ_1 in Equation 3.11 is substituted into Equation 3.12, it can be seen that the final expression for closure takes on the form of Equation 3.9.

Equation 3.12 could possibly be used to calculate the inward closure of the valley wall that is furthest from the longwall panel, as the proposed block movement mechanism postulates that the side of the valley closest to the longwall panel is pushed away from the longwall panel and into the free face provided by the valley, hence adding displacements along the translation plane as an extra consideration. An exception would be when the valley is located directly above the longwall panel, and then Equation 3.12 could be used to calculate the inward displacement of both walls, and hence total valley closure.

3.4 REQUIRED WORK PROGRAM

As the alternative block movement model does not need to consider out-of-plane stresses, it is amenable to two-dimensional numerical modelling. Therefore, it is proposed to investigate the alternative block movement theory by numerical modelling. In order for this to occur, the viability and credibility of the models created by the chosen numerical code needs to be established.

The numerical modelling will take place in two stages. The first stage will involve the creation of single longwall panel subsidence models that can be verified with the DPI Southern Coalfield empirical method and analytical methods.

The second stage will involve the creation of simplified subsidence models that incorporate river valleys and translation planes at different depths. These models will be based on the single longwall panel subsidence models for consistency.

An emphasis will be placed on the models being transparent for credibility purposes. All the material properties, assumptions and processes used in the creation of the models will be fully traceable so that the results from the models will be beyond reproach.

3.5 SUMMARY

The widely accepted conceptual model was reviewed and it was quickly identified that this model cannot explain upsidence and valley closure over unmined coal, a phenomenon that is evident in the field data gathered by Waddington Kay and Associates (2002). A review of recent developments revealed that no substantial progress has been made in identifying the mechanism behind valley closure and upsidence above unmined coal. The proposed alternative explanation of block movements was introduced and is the subject of further investigation using numerical modelling in the following chapters.

CHAPTER 4
DEVELOPMENT OF A NUMERICAL MODELLING APPROACH

4.1 INTRODUCTION

The numerical modelling of a geotechnical engineering problem can often be fraught with uncertainties not only about the choice of the model but also the choice of the values of input parameters and quite often assumptions are made without proper justification. In order to avoid falling into this trap, the proposed numerical modelling in this thesis will be developed in accordance to the principles outlined in Hudson, Stephansson and Andersson (2005). A literature review (in chronological order) of numerical modelling in mining subsidence related problems is also undertaken to determine what numerical modelling code is most suitable for the modelling of single isolated longwall panels and river valleys. The audits for the numerical modelling in this thesis can be found in Appendix A.

4.2 MODELLING PRINCIPLES

The development of a numerical modelling approach for isolated single longwall panels and the block movement model is based on the principles outlined in Hudson, Stephansson and Andersson (2005). The principles stipulate that the numerical modelling itself is not the most important aspect, but the conceptualisation of the problem, material properties and parameters should be paramount in any investigation. It is also stressed that the engineering problem at hand should be subjected to ‘soft’ and ‘hard’ audits.

The soft audit establishes an overview of the modelling work and determines whether well known issues of importance and difficulty in characterising and modelling rock masses have been addressed at the outset. The hard audit is similar to the soft audit but requires justifications to the answers given. The audits are designed to ensure that the numerical modelling is transparent and traceable through the audit trail.

Several references that deal with numerical modelling of mining subsidence or mining related activities with UDEC, FLAC or similar software are reviewed. The aim of this chapter is to make a decision on which numerical code is better suited to modelling mining induced subsidence for isolated single longwall panels and block movements based on the examples given.

4.3 LITERATURE REVIEW

4.3.1 Coulthard and Dutton (1988)

In this paper, the numerical modelling programs FLAC and UDEC are used to calculate the subsidence over a longwall panel for a range of longwall panel widths. The results from the numerical modelling were compared to the empirical predictions for the NSW Southern Coalfield.

Holla's empirical work on subsidence prediction in the Southern Coalfield indicated there was a large increase in the maximum developed subsidence as longwall panel widths increase from subcritical to critical.

At the moment, there are no critical width longwall panels in the Southern Coalfield, but the authors argue that subsidence prediction will only become feasible if it can capture the subsidence characteristics for a range or different mining geometries and geological conditions.

From the results of their numerical modelling, the authors reproduced the results of earlier workers that dismissed elastic analyses because of the shallow subsidence profile produced, and the unrealistic calibration of material properties required to fit the elastic analyses to observed subsidence profiles.

On the other hand, it was found that modelling a non-linear material with FLAC, containing horizontal ubiquitous joints, produced a large increase in the maximum developed subsidence, as characterised by Holla's work. It was also found that UDEC produced this large increase as well.

In conclusion, the authors felt that both the FLAC and UDEC models have the potential of predicting subsidence in new geological environments, but UDEC was favoured because of its ability to model roof behaviour. The authors found that the key factors governing the UDEC predictions were highly dependant on the material properties (joint friction angle and elastic modulus of the rock mass) and jointing pattern selected (finer upper strata increased subsidence magnitude).

4.3.2 Johansson, Riekkola and Lorig (1988)

In this paper, the authors discuss their experience in the design of multiple parallel caverns using explicit finite difference methods. The two programs that were used were FLAC and UDEC.

After the site characterisation was complete, preliminary modelling was performed on several major cross sections using FLAC. The purpose of this preliminary modelling was to identify potential areas where stability problems may arise. Once critical areas were identified, more detailed analyses were performed. Where joint spacing was relatively wide, UDEC was employed. Where rock was highly fractured, FLAC was used.

The purpose of this paper was to demonstrate how valuable numerical modelling can be in the design process.

4.3.3 Alehossein and Carter (1990)

In this paper, the authors discuss the difference between implicit and explicit modelling of joints (horizontal and vertical) in a rock mass. The numerical model used is a simple trench style excavation, with one-half of the problem discretised because of symmetry. The rock material was assumed to be an isotropic, linear elastic material, and the joints were assumed to conform to the elasto-plastic Mohr-Coulomb failure criteria. Joints were modelled implicitly as part of the constitutive model, i.e. ubiquitous, and explicitly. Joint spacing was varied in each model.

From the modelling of horizontal joints, it was found that jointing had little effect on overall horizontal movements, and the predictions from both the implicit and explicit modelling were quite close. On the other hand, it was found that vertical movement was sensitive to explicit joint spacing, compared to implicit joint spacing. From the modelling of vertical joints, it was found that both implicit and explicit joints produced similar results.

In conclusion, the authors suggested that the computationally more efficient method of implicit joint modelling was adequate for many practical problems. It was also noted that the accuracy of the implicit method depended of the spacing of the joints relative to a typical dimension of the excavation.

4.3.4 Brady et al. (1990)

In this paper, the authors used UDEC to model static and dynamic behaviour of jointed rock. The results from the modelling were then compared with the analytical solutions.

Four problems have been used for the study. These included:

- Jointed block subject to cyclical loading (static),
- Circular excavation intersected non-diametrically by a joint (static),
- Plane shear wave normally incident on a joint in an elastic solid (dynamic), and
- Explosive source located near a slip-prone joint (dynamic).

The joint deformation model used in the analysis was the Coulomb strength model. In all cases, the numerical simulation matched well with the analytical solutions.

From the results of the modelling, it was concluded that UDEC can simulate the mechanics of jointed rock, but the study did not confirm that UDEC is a valid simulation of the engineering behaviour of jointed rock.

4.3.5 Choi and Coulthard (1990)

In this paper, the authors examined the results of distinct element modelling applied to a simple trap door problem, and compared the results with Cosserat continuum limit load calculations. Distinct element studies of mining-induced subsidence were also discussed.

The authors reviewed the three different methods of modelling a jointed rock mass: explicit modelling, equivalent continuum modelling, and generalised continuum modelling. The general conclusion drawn was that explicit modelling of joints is the best method where block separation, rotation and slip, and large relative motions may occur. Equivalent continuum models were regarded as unreliable unless the joint spacings were very small compared with other system lengths. The generalised continuum method was viewed as a somewhat promising approach, as it was able to represent internal structure without being limited by the assumption that the structure is very small relative to system lengths.

From the results of their numerical modelling with UDEC, the DE analysis matched the Cosserat continuum method for the active case (simple mechanism), but not for the passive case (complex mechanism). It was concluded that for the passive case, the material in the upper part of the model should be treated as a continuum.

It was concluded that a discontinuum can be modelled as a generalised continuum where the structure is reasonable simple and the assumed mechanism is correct. If the structure is more complex and the mechanism not easily predicted, distinct element methods or finite element methods (incorporating the Cosserat theory) should be used.

The authors then discussed the applicability of distinct element modelling to subsidence, with reference to the Angus Place Case Study. Again, elastic models were discounted as reliable means of subsidence prediction due to their inability to model roof strata behaviour. The credibility of distinct element models was demonstrated by the comparison of DE modelling results and physical models in Australian rock conditions.

It was found that the major factors affecting the results of the UDEC modelling were the suitable spacing of bedding planes and sub-vertical jointing. Even so, the UDEC modelling matched the trends in surface subsidence better than continuum models. It was also noted that the method of excavation may produce different behaviour.

4.3.6 O'Conner and Dowding (1990)

In this paper, the authors described their findings from numerical modelling which complemented a field study that carried out extensive deformation measurements during the excavation of a longwall panel. The purpose of the numerical modelling was to try and simulate mining induced subsidence and to demonstrate the influence of discontinuities on the rock mass.

The authors used a hybrid code that combined the Northwestern University Rigid Block Model with the rigid block model developed by Peter Cundall. The main feature of this hybrid code is the edge-to-edge contacts between blocks. When all the edge-edge contacts of a block have satisfied one of three failure criteria (pure tensile failure, shear failure and rotation-tension failure) the block can undergo large displacements and rotations and develop corner-edge contact with any other block.

The subsidence model was based on a transverse cross section of the longwall panel. The bedding planes were approximated from borehole geophysics and mapping data. The joint sets were obtained from mapping of rock exposures. Six different scenarios were carried out, and these varied the number of strata types, joint and bedding plane stiffness, joint density, and shear resistance.

In conclusion, the authors found that the rigid block model was capable of simulating the general trend of vertical displacements within the overburden, but could not simulate fracturing and shearing above the zone of block caving. It was also found that the rigid block model behaved more stiffly than the actual rock mass, and consequently, the models which contained relatively low stiffness values produced the best agreement between measured and calculated displacements. Lastly, it was found that increasing the density of vertical joints or reducing the rigid block contact roughness did not improve the agreement between measured and simulated displacements.

4.3.7 Coulthard (1995)

In this paper, Coulthard reported on his work from the Angus Place Case Study. In this study, several scientists and engineers were invited to predict the developed subsidence over two longwall panels mined in virgin coal. The author chose UDEC to develop numerical models and subsidence predictions.

The author justified his choice of program by discussing the fact that distinct element methods such as UDEC can model the discontinuum behaviour that forms a key part of the mechanical response of a rock mass to longwall mining. The purpose of this study was to evaluate the potential of this numerical method for predicting subsidence in environments where no empirical data are available.

Parameters that were changed in the model (to fine tune) included DE sizes and shapes in the lower roof strata to produce bulking, joint constitutive model for sub-vertical jointing, and the finite difference zoning within the blocks. It was noted that little information was available on jointing in the rock mass apart from the sub-horizontal bedding planes, therefore the model did not attempt to represent the detailed geology of the rock strata. Average rock properties were used in all regions.

The blocks were governed by the Mohr-Coulomb elasto-plastic constitutive model. The bedding planes were modelled as standard UDEC joints, with initial elastic behaviour and with slip and separation determined by a Mohr-Coulomb shear strength criterion with tensile cut-off. The sub-vertical joints were modelled with UDEC's 'intact rock' constitutive model.

In conclusion, it was found that the UDEC analyses yielded good qualitative agreement with the main aspects of the field measurements, including:

- Magnitude and asymmetry of subsidence,
- The narrowness of the subsidence peaks, and
- Collapse of immediate roof strata and trends in deformations in the central borehole.

The model was not calibrated after field results became available. It was also noted that the model was able to produce asymmetry in the subsidence profile, something that was not possible in an elastic continuum analysis.

The main limitations of the UDEC models were found to be:

- Failure to reproduce bulking of the collapsed goaf,
- Failure to match borehole displacements in the upper strata, and
- Considerable underestimates of subsidence over the chain pillar.

It was proposed to increase the orientation of potential crack planes by defining multiple sets of intersecting joints in the lower roof. It was suggested that this can allow some block rotation to develop and increase the bulking of the goaf.

4.3.8 Bhasin and Høeg (1998)

In this paper, the authors performed a parametric study on the joint constitutive model for a large cavern in the Himalayas using UDEC. The joint constitutive models that were compared were the Mohr-Coulomb and the Barton-Bandis models. The results of the parametric study indicated that deformations around an opening were dependant on the size or the number of blocks adjacent to the excavation. It was also found that in a model where the block size is small compared to the excavation dimensions, the failure mechanism in jointed rock masses was strongly influenced by volume changes when approaching failure, and these volume changes were generally determined by the dilation along pre-existing discontinuities. This dilation along the joints caused a build-up of high normal stresses which in underground openings can cause interlocking of the blocks and inhibit further deformation. This situation may be relieved by using the Mohr-Coulomb joint constitutive model instead of the Barton-Bandis model, as the Barton-Bandis model allows for the build-up of stress caused by dilatant behaviour. This may be particularly useful when modelling underground longwall excavations.

4.3.9 Alejano et al. (1999)

In this paper, the authors used FLAC to develop subsidence models for flat coal seam longwall mining in British basins. These FLAC models were validated from empirical methods (SEH). The authors also developed models for slightly inclined coal seams and for steeply inclined coal seams. The slightly inclined coal seam models were also validated by empirical observations, but the steeply inclined models were not. The numerical models were based on longwall mines from the Midlands coalfields in central England. There was a large amount of material properties data and empirical predictions available.

The authors chose an elasto-plastic material model with the following features:

- Transversely isotropic elastic pre-failure behaviour,
- Anisotropic yield surface, yield may occur by joints or material itself, and
- Isotropic elastic post-failure behaviour.

To assess the quality of the rock mass, the GSI rating was used. The strength parameters of the Coal Measures rock mass were determined by the Hoek-Brown criterion, and equivalent Mohr-Coulomb parameters calculated. Joint strength was determined by scaling the results of laboratory testing.

The calculation of pre-failure (E_x, E_y, υ_{xy}, υ_{yx} and G) and post-failure deformability parameters (E) relied on formulas suggested by several authors. It was stated that these formulas simulated rock mass behaviour quite well. It was noted that the material model described is not available in FLAC and must be implemented via subroutines written in an in-built language (FISH).

The implementation of the material model followed a two stage process. First, an isotropic elastic model was assigned to the rock mass, compatible with the ubiquitous joint model. The FLAC model was then run in order to estimate the height of the fractured zone. Any material lying above the fractured zone was then assigned a transversely isotropic elastic model.

It was stated that forty two models were created for coal seams located at 150 m, 200 m, 300 m, 400 m, 500 m and 700 m depth with W/H ratios of 0.4, 0.6, 0.8, 1, 1.25, 1.5 and 2 for each depth. This covered the range of subcritical, critical and supercritical values defined by the SEH.

From the results of the numerical modelling, it was found that the subsidence troughs produced by FLAC fit the empirical observations quite well, with the maximum differences always smaller than 10 % of the seam thickness. On the other hand, horizontal displacements did not match well at all. It was found that the maximum horizontal displacement for the supercritical case was overestimated, whilst for the subcritical case the opposite took place. The authors suggested that the occurrence of surface tension cracks may account for these differences, in effect turning a continuous material into a discontinuous material.

Other parameters that were compared to SEH results were fractured zone height, subsidence factor, rib-side subsidence, limit angle, and maximum horizontal displacement in trough. It was stated by the authors that the FLAC results agree or follow general trends given by the SEH results, with the exception of limit angle and maximum horizontal displacement. The limit angle predicted by FLAC was within the range of 30° – 45°, whereas the SEH assumed the limit angle to be constant at 35°. The reasons for the difference in horizontal displacement had been covered previously.

In conclusion, the authors stated that subsidence due to longwall coal mining can be adequately modelled by the described methodology, but there were still some issues to be overcome. These included:

- The problem of modelling a discontinuum with a continuum code. The authors argued that given the large scale of the models involved, continuum modelling can be representative of the actual rock mass behaviour. Also, it was pointed out that discontinuum models had not been used successfully, most probably due to the lack of knowledge about joint distribution,
- The use of a custom constitutive model, whilst still effective, did not behave exactly as required, and

- Using rock characterisation techniques with accuracy with published data on different Coal Measures rock masses.

4.3.10 Sitharam and Latha (2002)

In this paper, an equivalent continuum model had been incorporated into FLAC via the FISH utility. The equivalent continuum model was verified with three case studies.

It was pointed out by the authors that the requirements for an equivalent continuum model were Hoek & Brown parameters 's' and 'm', JRC, JCS, and SRF (Barton and Bandis model). Such parameters may not be readily available rendering the analysis of such problems impossible. A new equivalent continuum approach was proposed, and this approach required the estimation of only two joint parameters, namely the number of joints in the rock per meter depth and the inclination of the most critical joint set. These two parameters were used in conjunction with the joint roughness or strength parameter to calculate the Joint Factor. The authors stated that the Joint Factor (J_f) can take care of the effects of frequency, orientation and strength of joint. The Joint Factor had been derived from extensive laboratory testing of intact and jointed specimens (plaster of Paris, sandstone and granite).

In the model, the rock mass properties were determined by a set of empirical relations, which expressed the elastic modulus of a jointed rock mass as a function of joint factor and the elastic modulus of intact rock. The authors stated that this model had been validated against experimental results and also with results from explicit modelling. It was also stated that the model worked well for jointed rock masses with different joint fabric and joint orientation.

The implementation of the model involved writing a FISH function that calculated the elastic modulus of the jointed rock in the changing stress field. The function also calculated the modulus ratio, the compressive strength ratio, and the confining pressure of the rock mass. The constitutive model used was the Mohr-Coulomb model with a confining stress dependant hyperbolic relation.

The model had been used in three case studies: two powerhouse excavations and one mine excavation. The values of the joint factor ranged from 13 to 111. It was found that the numerical analysis estimated the field behaviour very well. The authors concluded that the joint factor model can be confidently applied for solving excavation problems in jointed rock masses.

4.3.11 CSIRO Petroleum (2002)

Numerical modelling of undermined river valleys with UDEC and FLOMEC (three dimensional continuum code) was performed by CSIRO Petroleum in order to replicate observed behaviour in the Cataract and Nepean Gorges. Only the UDEC models will be discussed as three dimensional modelling is beyond the scope of this thesis. The modelling was carried out in two stages, the first being a geomechanical run, and the second being a geomechanical fluid flow run.

Parametric variations to the UDEC geomechanical models included:

- Gorge wall slope,
- Joint strength,
- Presence of ubiquitous joints,
- Magnitude of horizontal in-situ stress,
- Mining sequence, and
- Bedding plane and vertical joint geometry.

Parametric variations to the UDEC geomechanical fluid flow models included:

- Gorge wall slope,
- Shallow river valley geometry,
- Flat horizontal ground surface,
- Additional parallel joint set in gorge wall, dipping 10 to 30 degrees,
- Strength of 30 degree joints,
- Ubiquitous joints in gorge wall dipping 30 degrees towards gorge,
- Magnitude of horizontal in-situ stress,
- Depth of water table,

- Permeability of Bald Hill Claystone, and
- Poro-elastic and steady state responses to mining.

In both cases, the parameters that were found to have the greatest effect on model response were the magnitude of horizontal in-situ stress, the presence of ubiquitous joints, joint strength and permeability. The authors concluded that the numerical modelling provided greater understanding of general strata mechanisms that occurred during the undermining of surface topographical features. It was also concluded from the modelling that horizontal movements from valley closure induced by undermining were predominately associated with bedding plane shear at shallow depth, and these sheared bedding planes acted as conduits for ground water, and may impact on local hydrology.

It was noted that the numerical models were not verified in any way, and although the purpose of the exercise was to investigate valley closure outside longwall panels, no explanation was given for why this occurred.

4.4 SUMMARY

From the reviewed references, the following points are deduced regarding numerical modelling of mining induced subsidence:

- Elastic models are considered unsuitable for subsidence prediction due to the unrealistic calibration of material properties required in order to fit predicted subsidence profiles to observed profiles,
- Continuum codes like FLAC have been used to predict surface subsidence successfully, but subsurface behaviour or horizontal movement cannot be evaluated because of the continuum nature of the code,
- It has also been shown that FLAC is unable to reproduce the large increase in subsidence that occurs in the transition between subcritical and critical extraction widths in the Southern Coalfield,
- An equivalent continuum model has been produced, and it is claimed that it is suitable for modelling jointed rock. This method seems to be limited to simple excavations where large block movements are not expected,

- It has also been demonstrated that the computationally more efficient method of implicit joint modelling is adequate for many practical problems. It is also noted that the accuracy of the implicit method depends of the spacing of the joints relative to a typical dimension of the excavation. Again, this method is restricted to simple problems where large block movements are not expected,
- Distinct Element codes like UDEC were found to be generally more accurate than FLAC because of their ability to model discontinuous rock masses, therefore allowing evaluation of subsurface movements and roof behaviour,
- Key factors governing UDEC predictions were highly dependant on the material properties (joint friction angle and elastic modulus of the rock mass) and jointing pattern selected (finer upper strata increased subsidence magnitude),
- UDEC was able to produce asymmetry in the subsidence profile, something which is not possible in an elastic continuum analysis (Angus Place Case Study),
- UDEC modelling matched the trends in surface subsidence better than continuum models. It was also noted that the method of excavation may produce different behaviour (Angus Place Case Study), and
- From UDEC verification studies, it is concluded that UDEC can simulate the mechanics of jointed rock, but the study does not confirm that UDEC is a valid simulation of the engineering behaviour of jointed rock.

From the above summary, it can be concluded that UDEC is the most suitable code to develop a subsidence model in flat terrain and in areas of high topographical relief, provided verification can be undertaken. Even though FLAC has the capability of predicting surface subsidence quite well with equivalent continuum routines, the incorporation of such a routine introduces a range of additional parameters that have to be estimated, which in turn introduces a higher degree of uncertainty. Poor correlation with horizontal movements restricts the use of FLAC in modelling undermined river valleys due to resultant valley closure and horizontal movement of rock blocks.

Furthermore, UDEC has the advantage of being able to incorporate field properties directly into the model without calibration, eg. in-situ stress field, bedding plane spacing, joint spacing, sub vertical joint orientation, material and joint properties.

CHAPTER 5
SINGLE LONGWALL PANEL MODELS WITH NO RIVER VALLEY

5.1 INTRODUCTION

In this chapter, the approach used for modelling single longwall panel extractions in flat terrain is developed and discussed. The selection of single longwall panel extractions for modelling was such that it can be verified by the empirical method developed by Holla and Barclay (2000), which was discussed in Chapter 2. The results from the models are also discussed. An example of the modelling script used can be found in Appendix B.

5.2 NUMERICAL MODELLING STRATEGY

The approach used in the numerical modelling of single longwall panels in flat terrain was to try and replicate the DPI empirical model (single longwall prediction) in an attempt to see whether UDEC was capable of modelling a relatively complex process without the extensive calibrations that are sometimes required to get a model to 'fit' empirical observations. This step was necessary as it established the credibility of the numerical models, and also provided a base on which river valleys can be modelled (in terms of subsidence and curvatures).

Holla and Barclay (2000) provided a list of mines and extraction details, from which ground movement data were collected and the subsidence curves derived (single longwall panel only). The majority of the mines extracted the Bulli Seam using the longwall method of mining. The data that was derived from pillar extraction and Wongawilli Seam extraction was excluded from the modelling. It should be noted that the extraction details are approximate figures only.

Holla and Barclay (2000) also provided the thickness of the stratigraphic units in the overburden, grouped according to colliery. This was used for the derivation of the

thickness of rock units above the Bulli seam for different mines. The details for the rock units below the Bulli seam was derived from the literature and field geotechnical characterisations.

5.3 MATERIAL PROPERTIES FOR INTACT ROCK

A great deal of information has been published on the material properties of the stratigraphic units above and including the Bulgo Sandstone (Pells 1993). Most of this data is derived from civil engineering works in and around Sydney, not specifically the Southern Coalfield. A Mohr-Coulomb constitutive model has been used and this will be continued. Most recently, a drilling program has been completed which contains the geotechnical characterisation of several boreholes that were drilled over Appin and Westcliff collieries (MacGregor & Conquest 2005). This geotechnical characterisation resulted in a complete set of material properties for the:

- Hawkesbury Sandstone,
- Bald Hill Claystone,
- Bulgo Sandstone,
- Scarborough Sandstone,
- Coal Cliff Sandstone, and
- Loddon Sandstone.

UDEC requires the following material properties to be defined (for the Mohr-Coulomb block model):

- Density (kg/m^3),
- Young's Modulus (GPa),
- Poisson's Ratio,
- Bulk Modulus (GPa),
- Shear Modulus (GPa),
- Friction Angle ($^\circ$),
- Dilation Angle ($^\circ$),
- Cohesion (MPa), and
- Tensile Strength (MPa).

Typically, the parameters derived from multi-stage triaxial testing are Young's Modulus, unconfined compressive strength, Poisson's Ratio, friction angle and cohesion. The Mohr-Coulomb block model allows a specification of a dilation angle, but if none is specified then the value used defaults to zero, i.e. for plastic yield to be treated via a non-associated flow rule. In the absence of other information the dilation angle has been set to zero. The other parameters such as bulk and shear moduli, and tensile strength can be derived from formulae or tables (McNally 1996).

Complete material properties were missing for the Newport Formation, Bulli Seam and Cape Horn Seam. The Stanwell Park Claystone, Wombarra Shale and Kembla Sandstone were missing the values for friction angle and cohesion. The material properties for the Balgownie Seam, Lawrence Sandstone, Cape Horn Seam, UN2, Hargraves Coal Member, UN3, and the Wongawilli Seam were also derived. For simplicity, the Balgownie Seam and Hargraves Coal member were assumed to have the same material properties as the Bulli Seam, and the Lawrence Sandstone was assumed to have the same material properties as the Loddon Sandstone.

Density

The densities of the various stratigraphic units have been well defined in the geotechnical characterisation (MacGregor & Conquest 2005) and Pells (1993). The density of coal was assumed to be 1500 kg/m^3 (CSIRO Petroleum 2002). The densities of UN2 and UN3 were derived from the sonic logs that formed part of the geotechnical characterisation.

Unconfined Compressive Strength (UCS)

The missing UCS values were obtained by an examination of the sonic UCS for the relevant borehole. MacGregor and Conquest (2005) provide an exponential relationship (Equation 5.1) between the inferred UCS and the 20 cm field sonic velocity (VL2F). This relationship is based on 142 samples established by BHP Illawarra Coal.

$$InferredUCS = 1.3217 \times EXP^{(0.00094 \times VL2F))} \qquad [5.1]$$

For the BHP Illawarra Coal database, it was stated that the average error is 12.5 MPa. When comparing the laboratory derived UCS values to the sonic UCS values provided in the geotechnical characterisation (MacGregor & Conquest 2005), it was found that the average error is 10.8 MPa. Therefore, the use of the above relationship can be considered satisfactory to determine the missing UCS values. This approach was used for UN2 and UN3. The UCS for the Newport Formation was taken from Pells (1993) and the UCS for the Bulli and Wongawilli seams were taken from Williams and Gray (1980).

Young's Modulus

Once the UCS values had been determined, it was possible to estimate the Young's Modulus using the guide in Table 5.1 (McNally 1996):

Table 5.1 – Estimation of Young's Modulus

Modulus Ratio, E / UCS	
500 +	Exceptionally brittle cherty claystone
300	Strong, massive sandstone and conglomerate
200	Most coal measures rock types, especially sandstone
200	Strong, uncleated coal, UCS > 30 MPa
150	Medium to low strength coal
100	Weak mudstone, shale, non-silicified claystone

A modulus ratio of 200 was assumed for UN2 and UN3. These two units were the only ones to have their Young's Modulus derived in this way as these units were not tested and their descriptions did not resemble any close rock units. The Young's Modulus for the remaining units were either derived from the literature or assumed to be the same as neighbouring similar rock types.

Tensile Strength

If the tensile strength of the rock was not known, the values in Table 5.2 were used (McNally 1996):

Table 5.2 – Estimation of tensile strength

UCS / ITS	UCS / UTS	
20	14	Strong sandstone and conglomerate
20	14	Strong coal
15	10	Sedimentary rock generally
15	10	Medium to low strength coal
12	8	Shale, siltstone, mudstone
10	7	Weak shale, siltstone, mudstone

It can be seen that the majority of rocks in the Southern Coalfield possess a tensile strength approximately one tenth of their uniaxial compressive strength. This relationship was used in the derivation of tensile strength for most of the stratigraphic sequence with the exception of the Bulli and Wongawilli Seams, whose tensile strengths is given by Williams and Gray (1980).

Poisson's Ratio

If the Poisson's Ratio was unknown, the values in Table 5.3 were used (McNally 1996):

Table 5.3 – Estimation of Poisson's Ratio

Poisson's Ratio	
0.35	Stronger coals
0.30	Weaker coals
0.30	Stronger sandstones
0.25	Most coal measures lithologies

This approach was used for the Newport Formation, Bulli Seam, Balgownie Seam, Cape Horn Seam, UN2, Hargraves Coal Member, UN3 and the Wongawilli Seam.

Bulk and Shear Moduli

The bulk and shear moduli were calculated by the following relationships (Equation 5.2 and Equation 5.3):

$$K = \frac{E}{2(1-2\upsilon)} \qquad [5.2]$$

$$G = \frac{E}{2(1+\upsilon)} \qquad [5.3]$$

Where,

K = Bulk Modulus (GPa)
G = Shear Modulus (GPa)
E = Young's Modulus (GPa)
υ = Poisson's Ratio

Friction Angle

Missing values for the friction angle are best approximated by using values for similar rock types. The Stanwell Park Claystone and Wombarra Shale were assumed to have the same friction angle as the closest laboratory tested claystone unit, namely the Bald Hill Claystone. The Lawrence Sandstone and Kembla Sandstone were assumed to have the same friction angle as the Loddon Sandstone, based on the logic applied to the claystone units. The friction angle for the Bulli Seam was taken from CSIRO Petroleum (2002) and all other coal units were assumed to have the same friction angle. The friction angle for UN2 and UN3 was assumed to be the same as the Loddon Sandstone.

Cohesion

The missing values for cohesion were derived using the Mohr-Coulomb relationship (Equation 5.4):

$$\sigma_c = \frac{2c\cos\phi}{1-\sin\phi} \qquad [5.4]$$

This method was used for the same units where the friction angle was calculated.

Table 5.4 contains a complete set of material properties used in the models.

Table 5.4a – Material properties for stratigraphic rock units

Unit	Density (kg/m^3)	E (GPa)	UCS (MPa)	Poisson's Ratio	Bulk Modulus (GPa)
Hawkesbury Sandstone	2397.00	13.99	35.84	0.29	11.47
Newport Formation	2290.00	11.65	34.00	0.25	7.77
Bald Hill Claystone	2719.00	10.37	28.97	0.46	14.12
Bulgo Sandstone	2527.00	18.00	65.53	0.23	12.60
Stanwell Park Claystone	2693.00	19.20	48.30	0.26	13.22
Scarborough Sandstone	2514.00	20.57	71.75	0.23	16.16
Wombarra Shale	2643.00	17.00	48.10	0.37	24.81
Coal Cliff Sandstone	2600.00	23.78	78.70	0.22	17.07
Bulli Seam	1500.00	2.80	20.00	0.30	2.33
Loddon Sandstone	2539.00	15.07	56.50	0.33	16.76
Balgownie Seam	1500.00	2.80	20.00	0.30	2.33
Lawrence Sandstone	2539.00	15.07	56.50	0.33	16.76
Cape Horn Seam	1500.00	2.00	9.00	0.30	1.67
UN2	2560.00	13.48	67.40	0.25	8.99
Hargraves Coal Member	1500.00	2.80	20.00	0.30	2.33
UN3	2620.00	13.00	65.00	0.25	8.67
Wongawilli Seam	1500.00	2.00	9.00	0.30	1.67
Kembla Sandstone	2569.00	18.15	61.05	0.28	13.79
Lower Coal Measures	2092.00	9.37	40.49	0.29	8.11

Table 5.4b – Material properties for stratigraphic rock units (continued)

Unit	Shear Modulus (GPa)	Friction Angle (°)	Cohesion (MPa)	Tensile Strength (MPa)
Hawkesbury Sandstone	5.65	37.25	9.70	3.58
Newport Formation	4.66	35.00	8.85	3.40
Bald Hill Claystone	4.72	27.80	10.60	2.90
Bulgo Sandstone	7.91	35.40	17.72	6.55
Stanwell Park Claystone	7.63	27.80	14.57	4.83
Scarborough Sandstone	10.80	40.35	13.25	7.18
Wombarra Shale	7.24	27.80	14.51	4.81
Coal Cliff Sandstone	11.44	33.30	19.40	7.87
Bulli Seam	1.08	25.00	6.37	0.84
Loddon Sandstone	6.51	28.90	17.10	5.65
Balgownie Seam	1.08	25.00	6.37	0.84
Lawrence Sandstone	6.51	28.90	17.10	5.65
Cape Horn Seam	0.77	25.00	2.87	0.70
UN2	5.39	28.90	19.89	6.74
Hargraves Coal Member	1.08	25.00	6.37	0.84
UN3	5.20	28.90	19.18	6.50
Wongawilli Seam	0.77	25.00	2.87	0.70
Kembla Sandstone	7.12	28.90	18.02	6.11
Lower Coal Measures	3.83	27.17	12.20	3.75

5.4 PROPERTIES OF THE BEDDING DISCONTINUITIES

The engineering behaviour of rock masses can be dominantly controlled by the properties of the discontinuities – features in the rock mass with zero or negligible tensile strength (Brady & Brown 2006). For sedimentary rock masses, bedding partings and joints are the key discontinuities. Bedding, stratification or layering is one of the most fundamental and diagnostic features of sedimentary rocks. In numerical modelling, it is important to correctly distinguish between bedding as a textural element and bedding partings. Bedding textures are due to vertical differences in grain size, grain shape, packing or orientation. Generally, bedding is layering within beds on a scale of about 1 cm or 2 cm (Tucker 2003 & Selley 2000). Some of the textural features can become partings and these can be within the same lithology or between different lithologies.

Limited information exists about bedding planes in the Southern Coalfield. Most of the information has been derived from civil engineering works and visual examination of outcrops along the coast (Ghobadi 1994). It is also recognised that strata thickness and bedding plane thickness will vary from site to site, so it would be advantageous to derive the required information from a complete geotechnical investigation at one site, if possible.

Several holes were drilled by Strata Control Technology Pty. Ltd. on behalf of BHP Illawarra Coal to determine strata mechanical properties (see Section 5.3). These cores were also logged for discontinuities, but unfortunately bedding planes or drilling induced fractures were not specifically identified. The author was allowed access to the logs and laboratory reports. Neutron and gamma logging was also performed on holes. A site visit was conducted by the author and a visual examination of the core, along with a comparison of the logs was carried out for the Bulgo Sandstone. It was found that there was a good correlation between major bedding planes and partings identified in the core and the corresponding logs. When compared to data provided by Pells (1993) and Ghobadi (1994), there was good agreement apart from the Newport Formation and Bald Hill Claystone. In these instances, it was decided to use the values provided by Pells (1993). The bedding plane spacings that were used in the models are summarised in Table 5.5.

Table 5.5 – Bedding plane spacing

Rock Unit	Bedding Plane Spacing (m)
Hawkesbury Sandstone	9.00
Newport Formation	1.00
Bald Hill Claystone	1.00
Bulgo Sandstone	9.00
Stanwell Park Claystone	3.00
Scarborough Sandstone	4.00
Wombarra Shale	3.00
Coal Cliff Sandstone	3.00

Information on specific shear strength properties of bedding partings are scarce and if the discontinuities are not directly laboratory tested, estimates or values from field studies have to be used. In this thesis, the bedding partings are treated as a subset of joints. Derivation of the joint normal and shear stiffness was done in accordance to the procedures described by Itasca (2000). It appears that the shear stiffness can be approximated as one-tenth of the normal stiffness. This approach has been used by Itasca (2000), and has been used by Coulthard (1995) and Badelow et al. (2005). The derived joint normal and shear stiffness used for each rock unit is shown in Table 5.6.

Table 5.6 – Joint normal and shear stiffness

Rock Unit	Normal Stiffness (GPa/m)	Shear Stiffness (GPa/m)
Hawkesbury Sandstone	21.00	2.10
Newport Formation	140.00	14.00
Bald Hill Claystone	204.00	20.4
Bulgo Sandstone	26.00	2.60
Stanwell Park Claystone	78.00	7.80
Scarborough Sandstone	76.00	7.60
Wombarra Shale	115.00	11.50
Coal Cliff Sandstone	400.00	40.00

It was found through initial testing that the shear stiffness of joints and bedding planes in the immediate rock units above and below the Bulli Seam needed relatively high values to prevent excessive block penetration and to allow the models to obtain a final equilibrium state.

The joint and bedding plane strength parameters have been obtained from Chan, Kotze and Stone (2005), and the relationship derived from Barton (1976) coupled with the spreadsheet solution provided by Hoek (2000) has been used to calculate equivalent Mohr-Coulomb parameters based on the Joint Roughness Coefficient (JRC) and Joint Wall Compressive Strength (JCS) values given by Chan, Kotze and Stone (2005). The bedding plane properties used in the models can be seen in Table 5.7.

Table 5.7 – Bedding plane properties

Bedding Plane Property	Value
Friction Angle (°)	25.00
Residual Friction Angle (°)	15.00
JCS	4.00
JRC	5.00
Cohesion (MPa)	0.29
Residual Cohesion (MPa)	0
Dilation Angle (°)	0
Tensile Strength (MPa)	0

5.5 VERTICAL JOINTS AND PROPERTIES

Very little data exists on the vertical joint spacing in rock units in the Southern Coalfield, and even where geotechnical characterisations have been completed, vertical joint spacing simply cannot be assessed from cores (as in the Strata Control Technology characterisation).

Price (1966) reported on work done in Wyoming, USA, which suggested for a given lithological type, the concentration of joints is inversely related to the thickness of the bed. Examples were given for dolomite where joints in a 10 ft (3.05 m) thick bed occurred at every 10 ft; and joints in a 1 ft (0.305 m) thick bed occurred every 1 ft. Similar results were also reported for sandstone and limestone. The mechanism proposed by Price (1966) assumed that the cohesion between adjacent beds is non-existent and that friction angle, normal stress and tensile strength are all constant. Price (1966) suggests that while these parameters will change in reality, these factors cause only second-order variations in the relationship between joint frequency and bed thickness.

A comprehensive review of the Price model was performed by Mandl (2005). In addition, this review also included Hobbs' model, which is a more complex model that takes into account the elastic modulus and bedding plane cohesion of adjacent beds. Both models predict a joint spacing that scales with bed thickness.

Ghobadi (1994) reported that the vertical joint spacing in the Hawkesbury Sandstone is observed to be 2 m – 5 m, Scarborough Sandstone 1 m – 4 m, Bulgo Sandstone 0.5 m – 1.5 m, Stanwell Park Claystone 0.1 m – 0.5 m, and the Wombarra Shale 0.2 m – 0.6 m apart. It was noted that many of the joints on the escarpment and coastline are filled with calcite and/or clay. These values are not in good agreement with the Price joint model.

Pells (1993) reported that the vertical joint spacing in the Hawkesbury Sandstone is 7 m – 15 m in the Southern catchment area, the Newport Formation 1 m – 3 m, Bald Hill Claystone 1 m, and the Bulgo Sandstone 2 m – 13 m. These values are in good agreement with the Price joint model, therefore the assumption that vertical joint spacing is equal to bedding plane spacing will be used in the numerical model.

The vertical joint spacing for various rock units is shown in Table 5.8.

Table 5.8 – Vertical joint spacing

Rock Unit	Vertical Joint Spacing (m)
Hawkesbury Sandstone	9.00
Newport Formation	1.00
Bald Hill Claystone	1.00
Bulgo Sandstone	9.00
Stanwell Park Claystone	3.00
Scarborough Sandstone	4.00
Wombarra Shale	3.00
Coal Cliff Sandstone	3.00

Vertical joint properties have been estimated in the same manner as for bedding planes.

The vertical joint properties are shown in Table 5.9.

Table 5.9 – Vertical joint properties

Property	Vertical Joint
Friction Angle (°)	19.00
Residual Friction Angle (°)	15.00
JCS	2.00
JRC	8.00
Cohesion (MPa)	0.86
Residual Cohesion (MPa)	0
Dilation Angle (°)	0
Tensile Strength (MPa)	0

For simplicity, vertical joint dip was assumed to be 90°, forming perfectly square blocks (as vertical joint spacing is assumed to be equal to bedding plane spacing). Coulthard (1995) noticed that vertical joint dip played an important role in the caving and bulking of the goaf but ultimately could not produce the required bulking factor.

5.6 IN-SITU STRESS

A thorough review of regional and local in-situ stress has been compiled by the CSIRO for their numerical modelling (CSIRO Petroleum 2002). From 206 measurements across the entire Sydney Basin, the ratio of horizontal stress to vertical stress was found to be in the range of 1.5 – 2.0. Table 5.10 shows the horizontal to vertical stress ratio for the Appin, Westcliff and Tower collieries, measured adjacent to the Cataract – Nepean River gorges.

Table 5.10 – Horizontal to vertical stress ratios (after CSIRO Petroleum 2002)

Colliery	σ_H/σ_V
Appin	1.75
West Cliff	1.40
Tower	3.26

The average of the horizontal to vertical stress ratios in Table 5.10 is approximately two, and in the Southern Coalfield, the horizontal stress is usually considered to be twice the vertical stress so for the numerical models, a horizontal to vertical stress ratio of two was implemented.

5.7 MESH GENERATION

The mesh employed was relatively simple. Each block was subdivided into four constant strain zones. It was noted by Coulthard (1995) that this may result in a unit of large blocks being excessively stiffer than a unit of smaller blocks. If this occurs in the models, the mesh density will be increased in the areas of interest. A typical representation of the mesh can be seen in Figure 5.1.

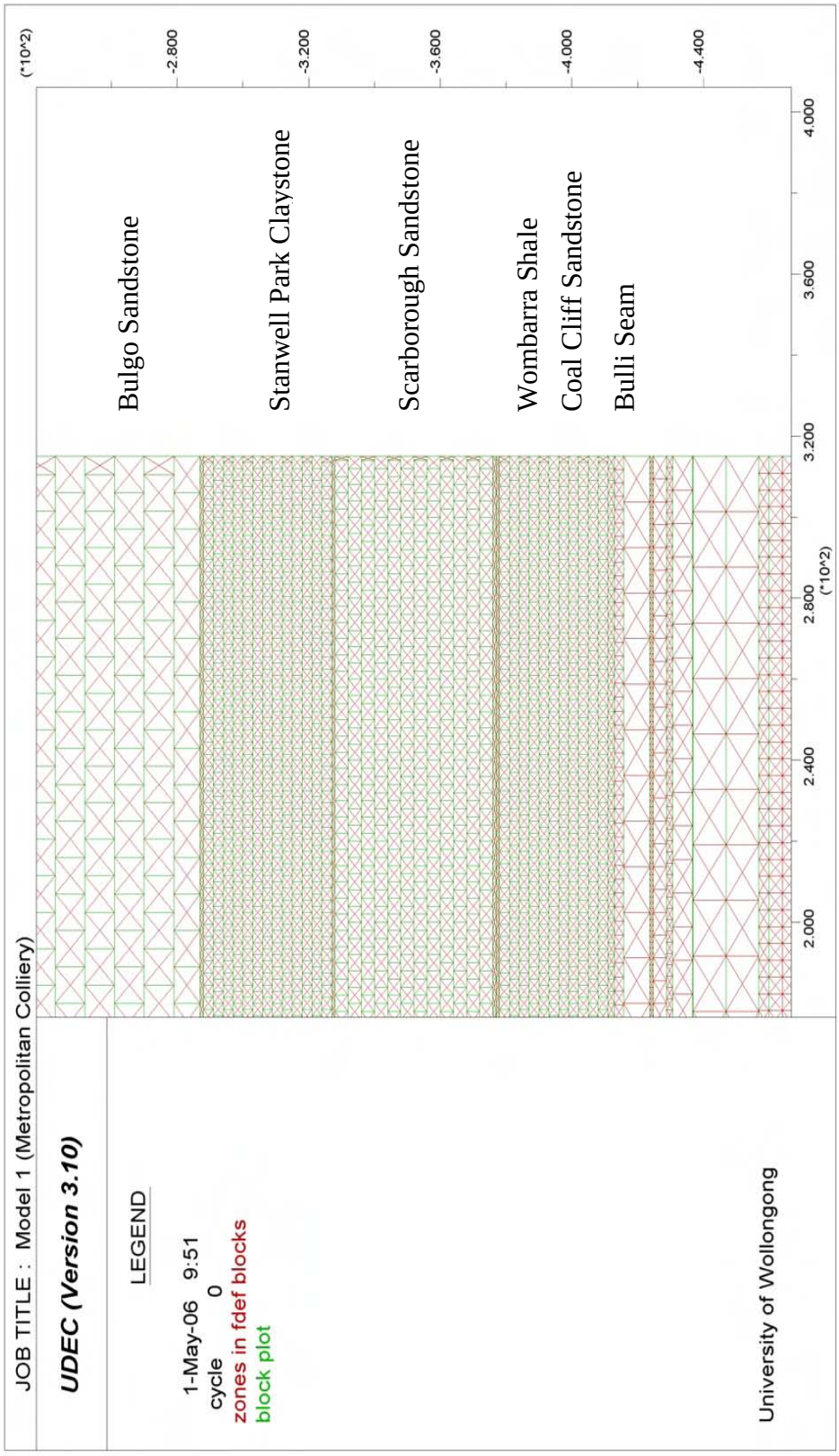

Fig. 5.1 – Typical mesh configuration for all models

5.8 CONSTITUTIVE MODELS

The constitutive model employed for the rock blocks was the standard Mohr-Coulomb model. The constitutive model used for the joints was the Coulomb slip with residual strength model. This model simulates displacement weakening of the joint by the loss of frictional, cohesive and/or tensile strength at the onset of shear or tensile failure (Itasca 2000). This model is suitable for general rock mechanics, including underground excavations. The definition of a discontinuity means that the tensile strength is suitable to be set to zero.

5.9 BOUNDARY CONDITIONS

The models were constrained in the x-direction on the sides of the models, and the bottoms of the models were constrained in the y-direction. The top of each model, representing the ground surface was left as a free surface.

5.10 HISTORIES

History points were placed along the surface at a distance determined by the vertical joint spacing of the Hawkesbury Sandstone (9 m). The history points on the surface monitored movements in the x and y-directions in order to enable the calculation of vertical subsidence (and goaf edge subsidence), strain and tilt.

5.11 MODEL GEOMETRY AND INITIAL TEST MODELS

The data from which Holla and Barclay (2000) derived their single longwall panel, Bulli Seam subsidence curves has been reproduced in Table 5.11. The data that was derived from pillar extraction and Wongawilli Seam extraction will be excluded from the modelling. It is noted that the extraction details are approximate figures only.

Figure 5.2 is a graphical representation of the thickness of the stratigraphic units in the overburden, grouped according to colliery. As the extraction details in Table 5.11 are approximate figures, a reconciliation of the Bulli seam depth (Figure 5.2) and the cover depth (Table 5.11) produced expected errors, in some cases considerable. As Figure 5.2

is the closest approximation of stratigraphic unit thickness for several collieries, it was used for the derivation of the thickness of rock units above the Bulli seam for different mines. The longwall panel widths were derived from Table 5.11 and combined with the information from Figure 5.2 to produce the number of models required.

Excluding mines that utilise pillar extraction, extract the Wongawilli Seam, and whose stratigraphic details do not appear in Figure 5.2, it was concluded that four models can be created from the available data (Table 5.12). Unfortunately, some stratigraphic details were missing for Appin, Tower and South Bulli collieries. It was decided to exclude these mines from the models to reduce uncertainty that would be introduced by estimating the thickness of the missing units. It must be noted that whilst 18 potential models can be created with the available data, four models was considered sufficient to cover the range of W/H ratios represented in the single longwall panel subsidence curve in Holla and Barclay (2000).

Symmetry was utilised to halve the size of the models and run times needed. The plane of symmetry is on the right hand side of the models as can be seen in Figures 5.3 to 5.6. To determine the width of each model, a boundary was placed at an arbitrary distance from the edge of the longwall panel and the model was cycled using the auto damp option to ensure quick solution times. The location of the boundary was then adjusted so a full subsidence profile could be produced. A comparison between the subsidence profile produced by the default local damping, the optional auto damping and local damping combined with a sub-elastic stage (sets joints and zone constitutive models to infinite strength for initial equilibrium cycling) was made for Model 4 and the resulting subsidence profiles can be seen in Figure 5.7.

The auto damping option produced maximum subsidence of 479 mm, whilst the default local damping produced a maximum subsidence of 476 mm. The sub-elastic stage with local damping produced 475 mm of subsidence. The difference in maximum developed subsidence between the highest value (auto damping) and the lowest value (sub-elastic with local damping) was 4 mm or 0.84 %, therefore auto damping was deemed suitable for use with the final models. Model run times with auto damping are significantly lower as well, 7.5 hours compared to eight days with local damping.

Model depth was dependant on stratigraphy and the stratigraphic sequence (in descending order) for the models was as follows:

- Hawkesbury Sandstone,
- Newport Formation,
- Bald Hill Claystone,
- Bulgo Sandstone,
- Stanwell Park Claystone,
- Scarborough Sandstone,
- Wombarra Shale,
- Coal Cliff Sandstone,
- Bulli Seam,
- Loddon Sandstone,
- Balgownie Seam,
- Lawrence Sandstone,
- Cape Horn Seam,
- UN2,
- Hargraves Coal Member,
- UN3,
- Wongawilli Seam, and
- Kembla Sandstone.

Where UN2 and UN3 stand for Un-Named members 1 and 2 respectively.

The stratigraphic sequence below the Bulli Seam has been derived from the geotechnical characterisation performed by MacGregor and Conquest (2005) and will be used for all models.

Table 5.13 contains the thickness of stratigraphic units according to the models listed in Table 5.12.

Table 5.14 contains the finalised width and depth for each UDEC model (designated Model 1, Model 2, Model 3 and Model 4).

Table 5.11 – Details for various mines used in the derivation of the empirical subsidence prediction curves (Holla & Barclay 2000)

Colliery	Panel	Individual Panel Width (m)	Cover Depth (m)	Extracted Thickness (m)
Appin	LWs 1 & 2	150-170	490	2.70
	LWs 5-9	145-150	500	2.80
	LWs 14-18	207	500	2.70
	LWs 21-29	207	490	2.50
Bellambi West	LWs 501-506	110	320	2.50
Bulli	SW 1 & 2*	79-86	300	2.30
Coal Cliff	221-224, & 260***	96-920	460	2.60
Cordeaux	LWs 17-23A	158	450	2.50
Elouera	LW 1	160	330	3.00
Kemira	LWs 4-6	160-189	190-235	2.70
Metropolitan	SW 1**	105-336	470	2.70
Oakdale	LW 5	160	360-410	2.20
South Bulli	200 series LWs	145	440	2.50
	300 series LWs	145	450	2.50
	LWs K to N	145	445-465	2.65
	LWs 9-11	145	400	2.65
Tahmoor	201*	260	430	1.90
	LWs 3-9	190	415-425	2.10
Tower	LWs 1-3	110	485	2.60
	LWs 6-8	155	480	2.60
West Cliff	LW 1	145	470	2.65
	421*	118	455	2.65
	LWs 16-21	205	470-480	2.60

Note 1 – Width refers to the width of individual panels
Note 2 – Values of width, cover depth and extracted seam thickness are approximate * indicates pillar extraction; ** indicates short walls; *** indicates Wongawilli type
Note 3 – The seam extracted was the Bulli seam in all cases except in Elouera and Kemira Collieries where it was the Wongawilli Seam

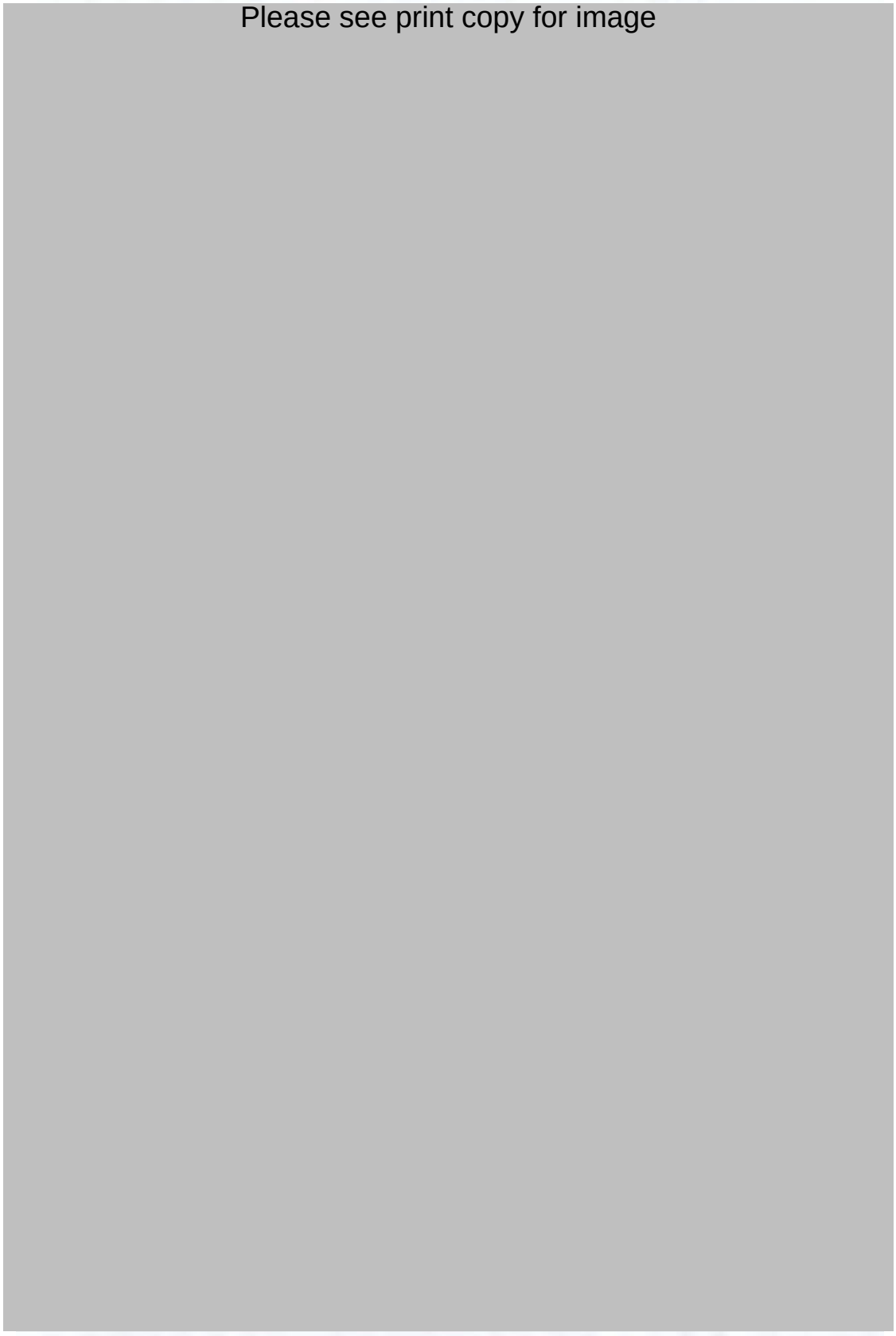

Fig. 5.2 – Thickness of stratigraphic units grouped according to mine (Holla & Barclay 2000)

Table 5.12 – List of models

Model Name	Colliery	W (m)	H (m)	T (m)	W/H
Model 1	Metropolitan	105	413	2.7	0.25
Model 2	Cordeaux	158	450	2.5	0.35
Model 3	Elouera	160	288	3.0	0.56
Model 4	Elouera	175	288	3.0	0.61

Table 5.13 – Thickness of stratigraphic units (m) for each model, in descending order

	Model		
	1	**2**	**3 & 4**
Hawkesbury Sandstone	88.0	153.0	78.0
Newport Formation	20.0	13.0	7.0
Bald Hill Claystone	34.0	23.0	12.0
Bulgo Sandstone	145.0	156.0	92.0
Stanwell Park Claystone	40.0	23.0	11.0
Scarborough Sandstone	50.0	32.0	36.0
Wombarra Shale	16.0	29.0	29.0
Coal Cliff Sandstone	20.0	21.0	23.0
Bulli Seam	2.7	2.5	3.0
Loddon Sandstone	8.0	8.0	8.0
Balgownie Seam	1.0	1.0	1.0
Lawrence Sandstone	4.0	4.0	4.0
Cape Horn Seam	2.0	2.0	2.0
UN2*	6.0	6.0	6.0
Hargraves Coal Member	0.1	0.1	0.1
UN3*	10.0	10.0	10.0
Wongawilli Seam	10.0	10.0	10.0
Kembla Sandstone	3.0	3.0	3.0
Lower Coal Measures	50.0	50.0	50.0
Total Depth	**509.8**	**546.6**	**385.1**

*Un-named member

Table 5.14 – Finalised width and depth of models

Model Name	Total Model Width (m)	Total Model Depth (m)
Model 1	815	509.8
Model 2	874	546.6
Model 3	480	385.1
Model 4	525	385.1

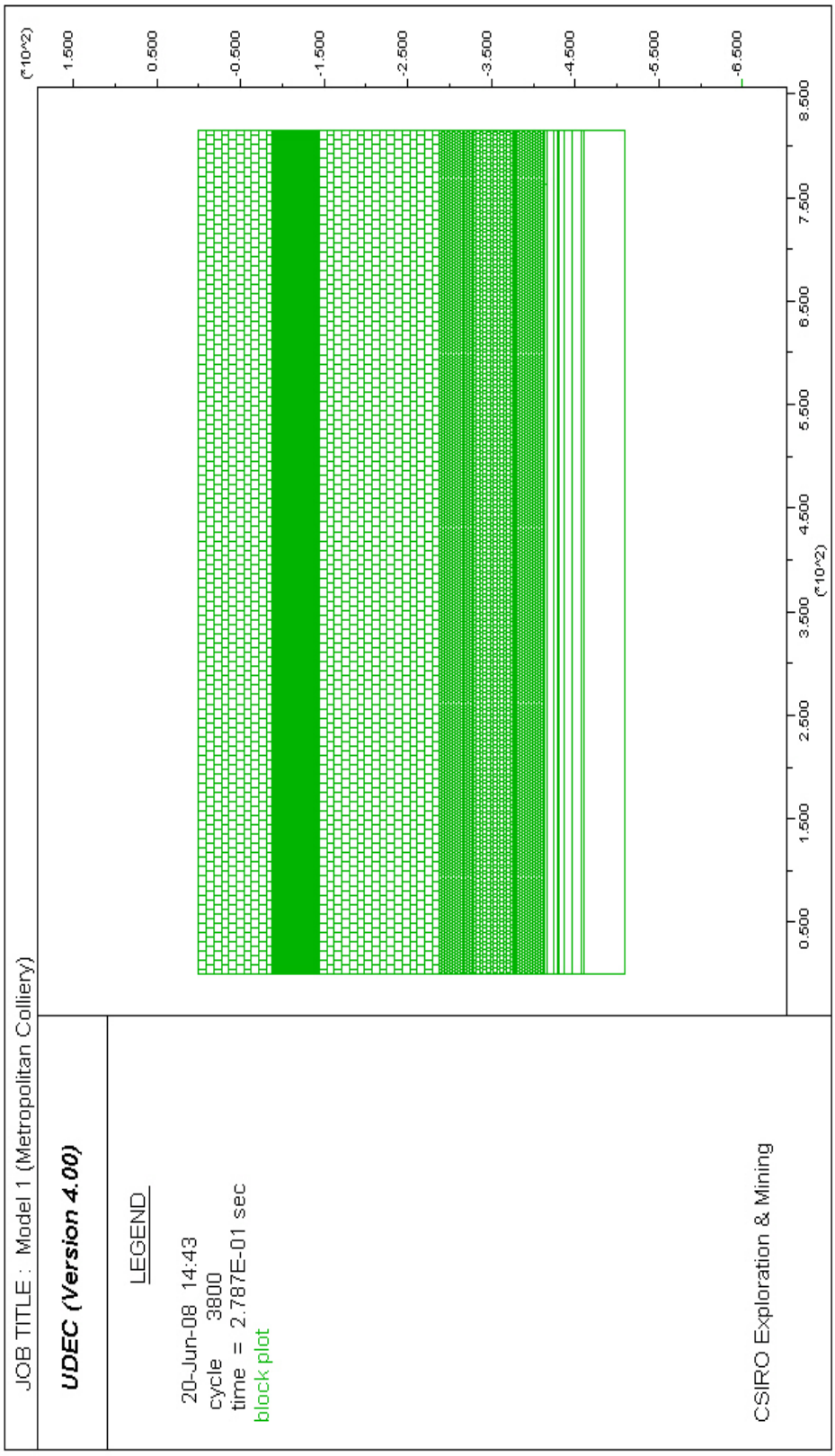

Fig. 5.3 – Model 1 geometry

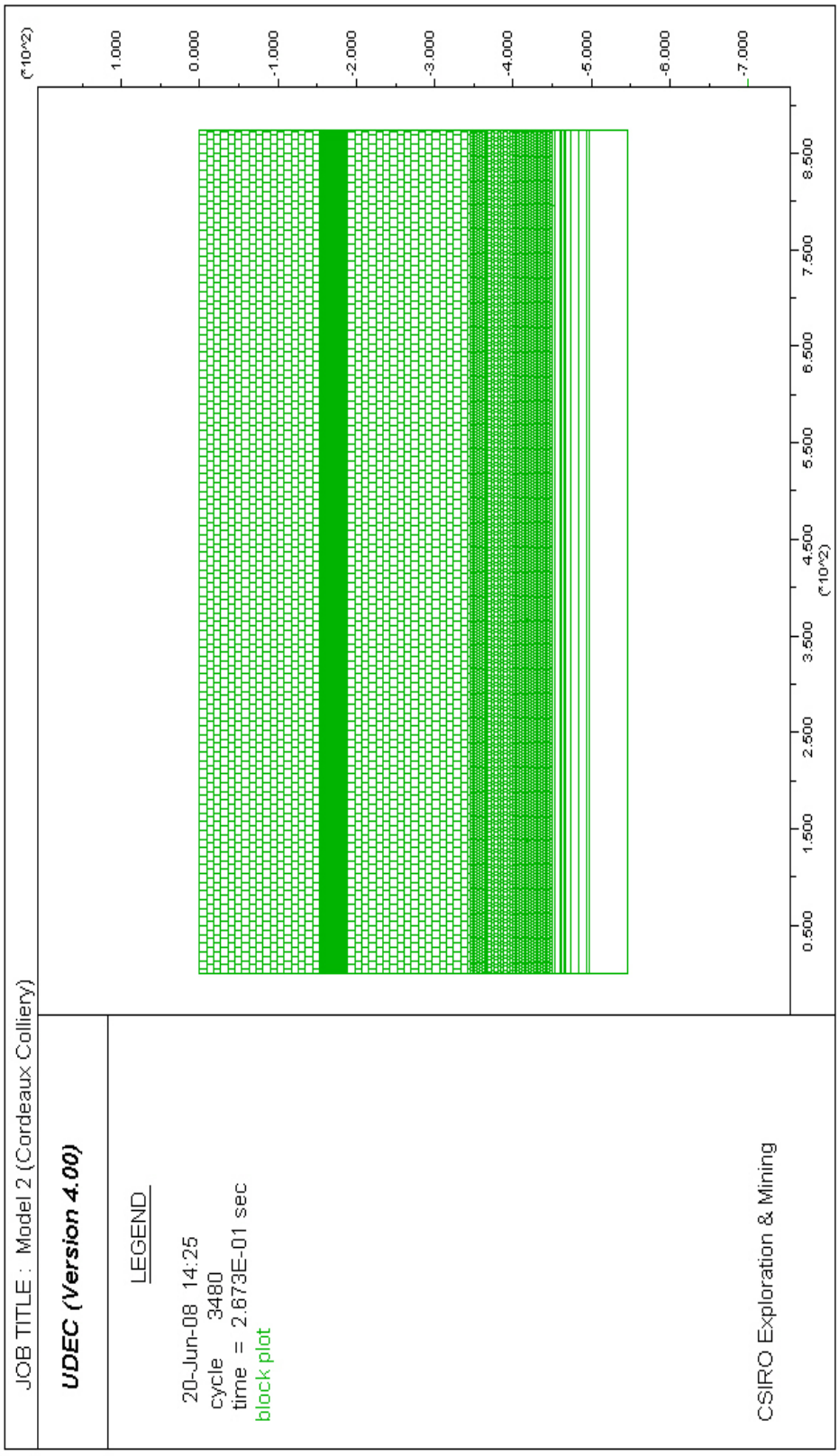

Fig. 5.4 – Model 2 geometry

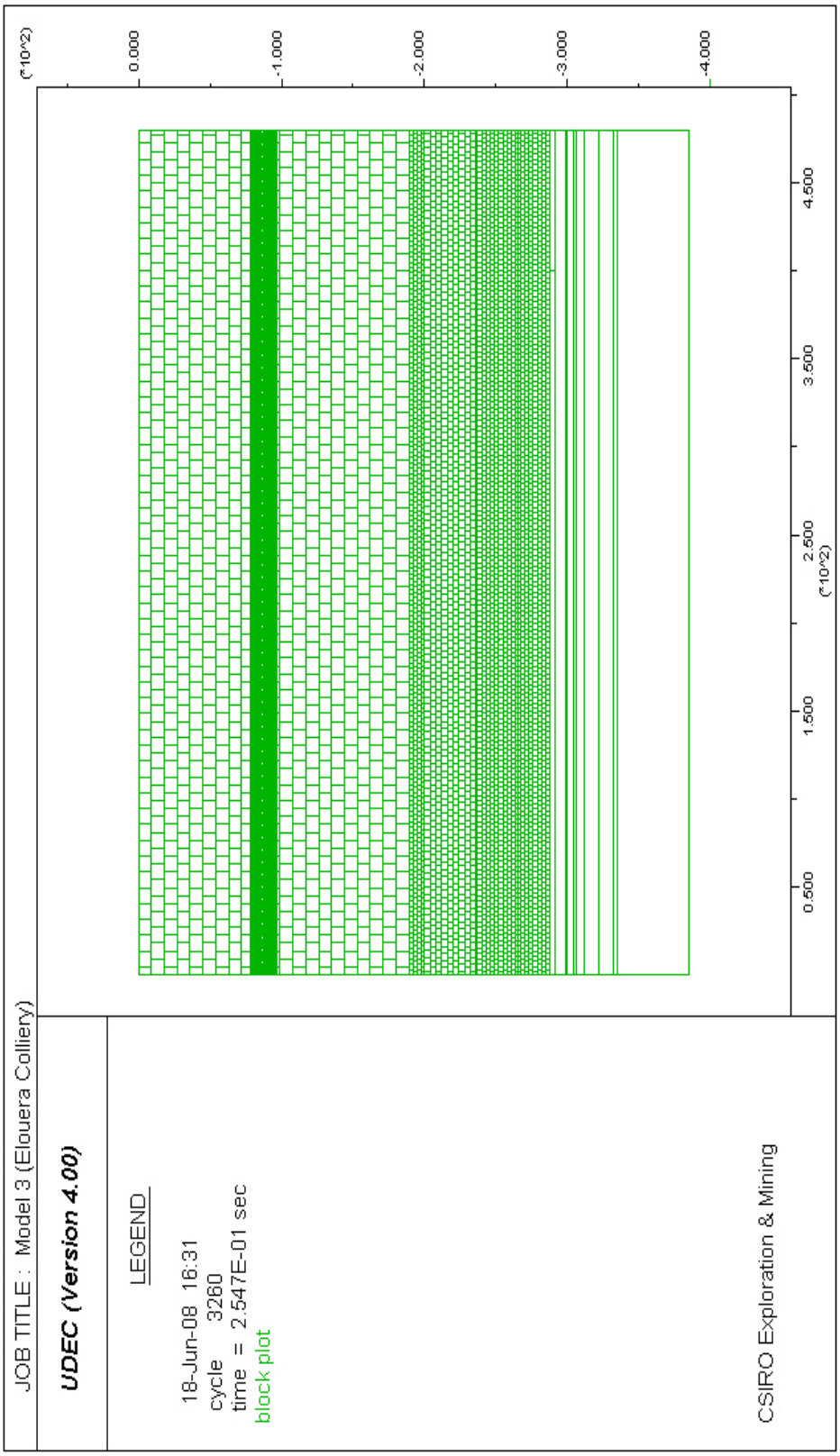

Fig. 5.5 – Model 3 geometry

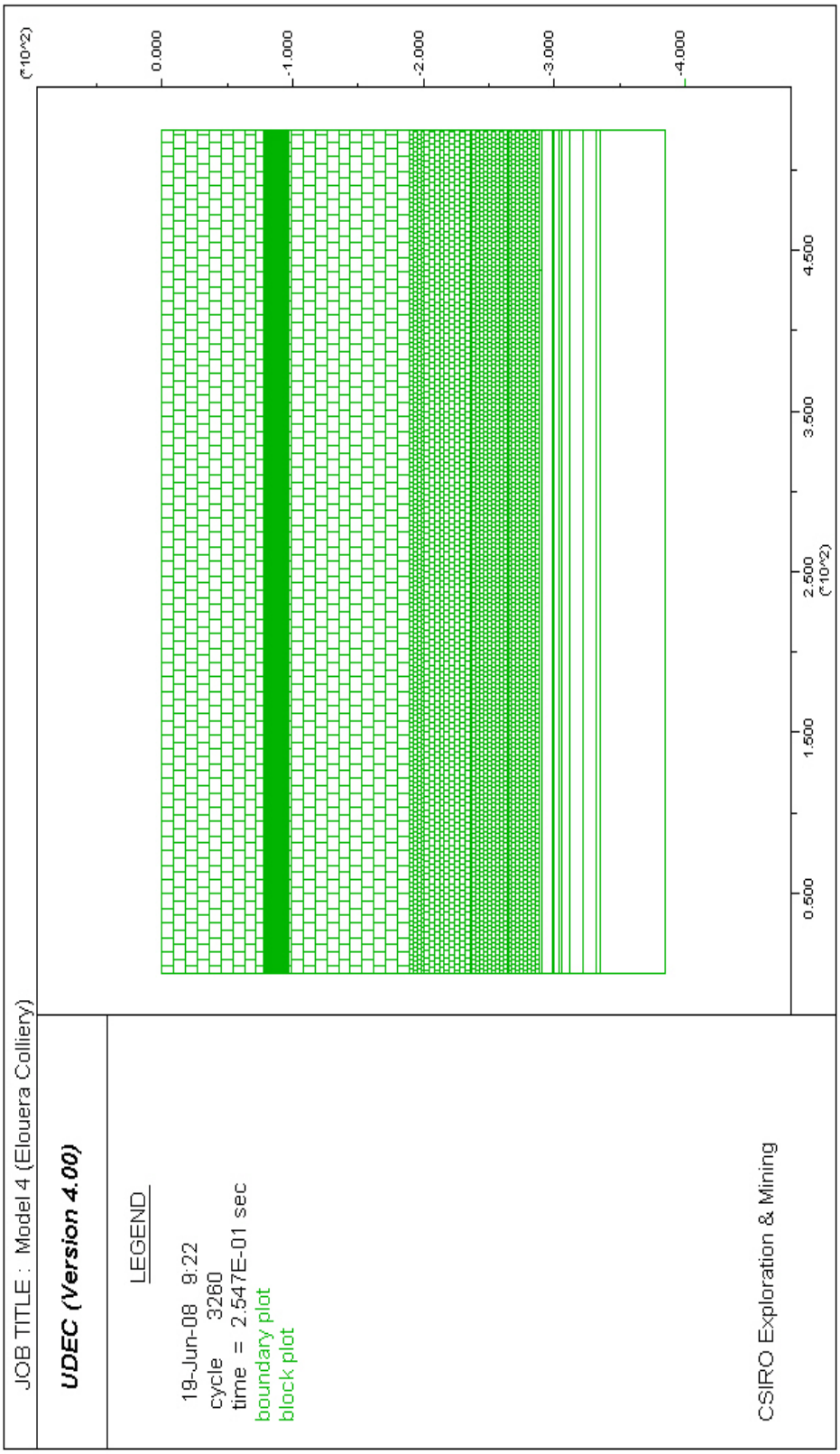

Fig. 5.6– Model 4 geometry

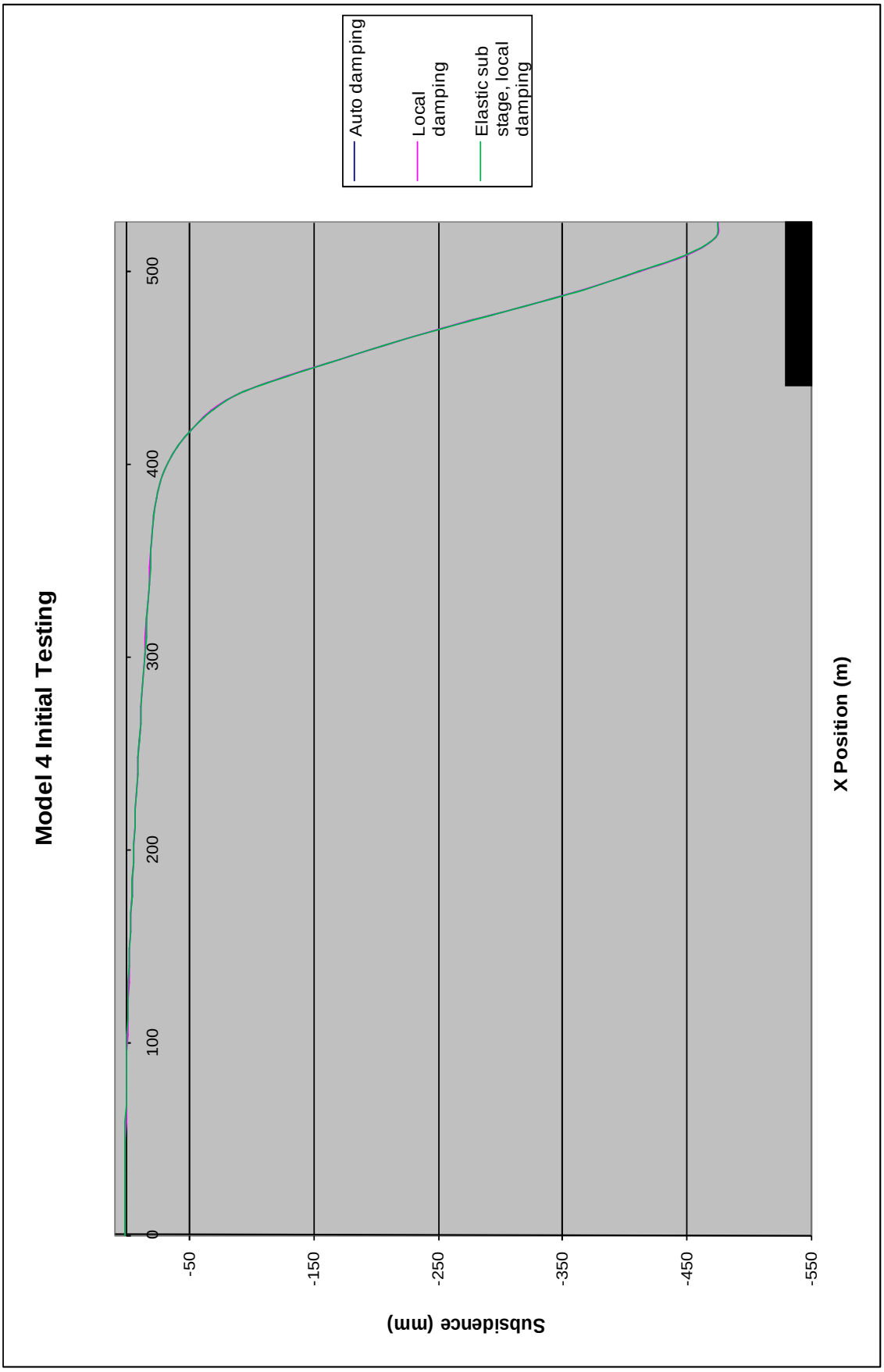

Fig. 5.7 – Subsidence profiles for different damping options

5.12 RESULTS

The details of the single longwall panel flat terrain models can be found in Tables 5.12, 5.13 and 5.14. The results from the four models are presented in Table 5.15.

Table 5.15 – Results from single longwall panel flat terrain models

Parameter	Model 1	Model 2	Model 3	Model 4
W/H	0.25	0.35	0.56	0.61
T (m)	2.70	2.50	3.00	3.00
S_{max} (mm)	39	163	328	479
S_{goaf} (mm)	38	91	89	110
+ E_{max} (mm/m)	0.04	0.07	0.75	1.55
- E_{max} (mm/m)	0.23	0.33	0.58	0.69
G_{max} (mm/m)	0.11	1.13	3.92	5.64
R_{min} (km)	81.62	61.98	17.46	8.45
D (m)	-173.00	-205.50	18.50	26.02
S_{max}/T	0.01	0.07	0.11	0.16
S_{goaf}/S_{max}	0.97	0.56	0.27	0.23
K1	0.42	0.19	0.66	0.93
K2	2.41	0.91	0.51	0.42
K3	1.15	3.11	3.44	3.39
D/H	-0.42	-0.46	0.06	0.09

Where,

W = Width of longwall panel

H = Depth of cover

T = Extracted seam thickness

S_{max} = Maximum developed subsidence over centre of longwall

S_{goaf} = Maximum developed subsidence over goaf edge

E_{max} = Maximum developed strain (+ve tensile, -ve compressive)

G_{max} = Maximum developed tilt

R_{min} = Radius of curvature

D = Distance of inflection point relative to goaf edge (negative values outside goaf, positive values inside goaf)

K1 = Tensile strain factor

K2 = Compressive strain factor

K3 = Tilt factor

To put the results into perspective, the results from Table 5.15 are superimposed onto the corresponding empirical curves from Holla and Barclay (2000). These are shown in Figures 5.8 (subsidence factor), 5.9 (goaf edge subsidence factor), 5.10 (tensile strain factor), 5.11 (compressive strain factor), 5.12 (tilt factor) and 5.13 (location of inflection point).

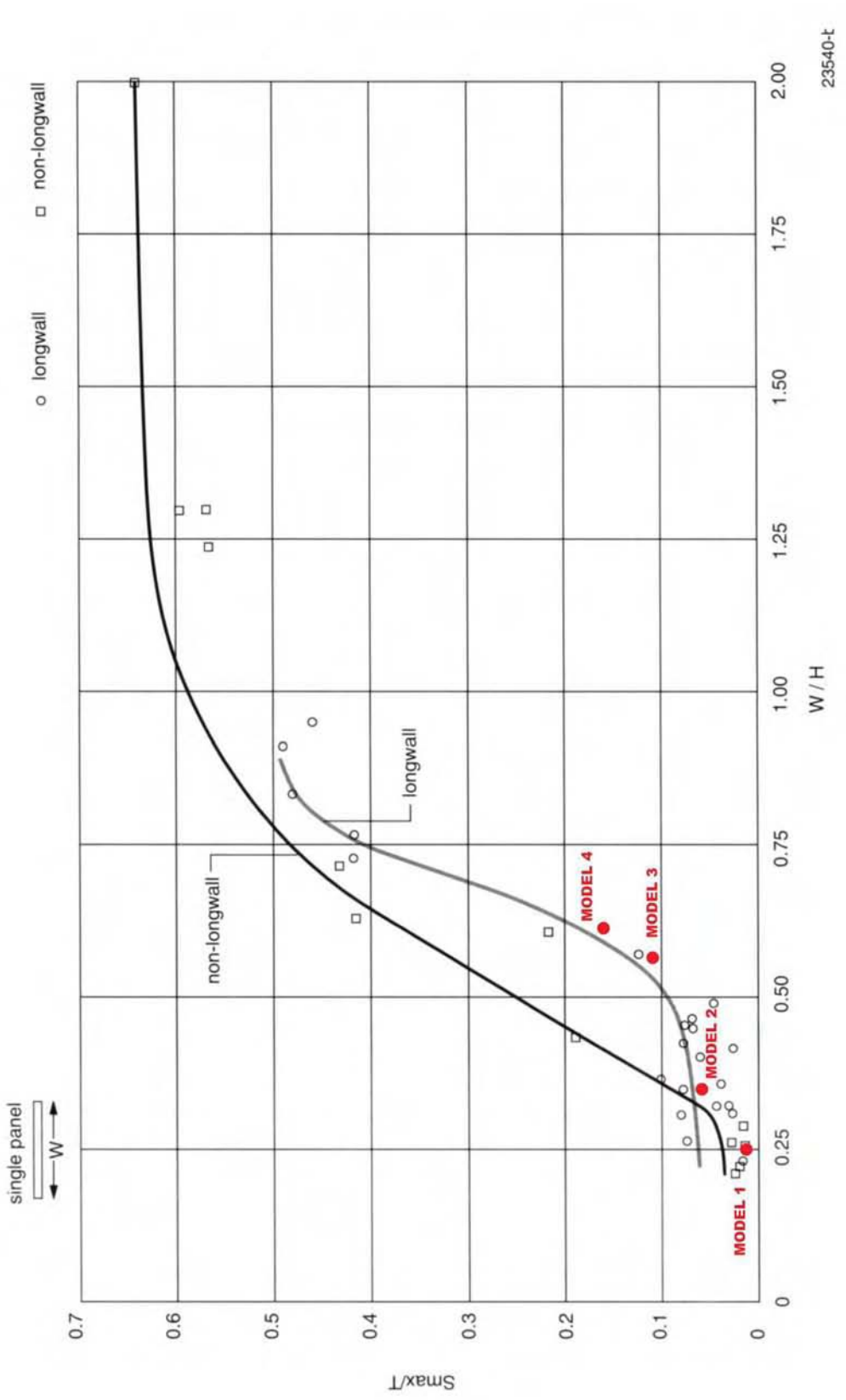

Fig. 5.8 – Superimposed model results for S_{max}/T (after Holla & Barclay 2000)

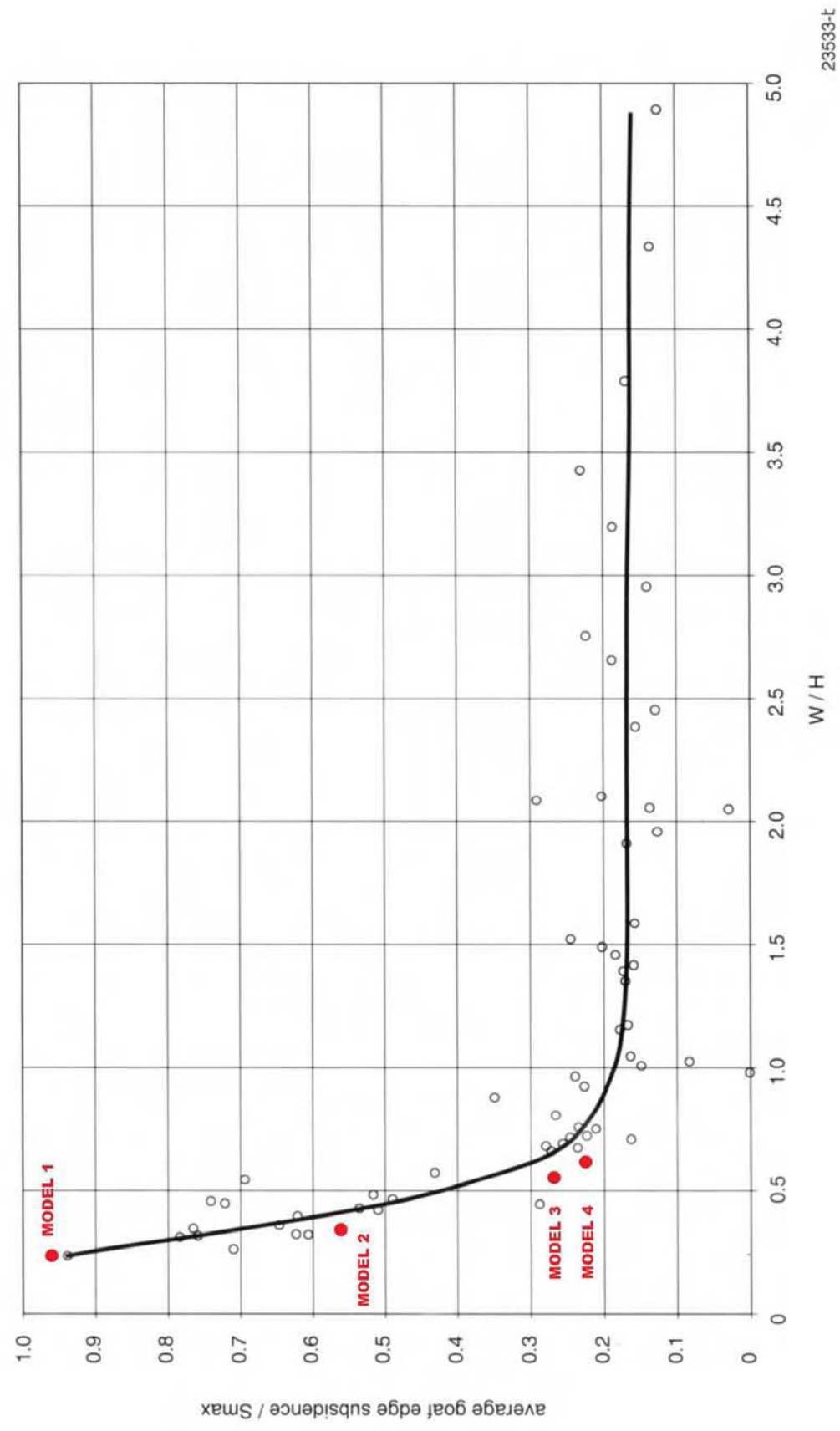

Fig. 5.9 – Superimposed model results for S_{goaf}/S_{max} (after Holla & Barclay 2000)

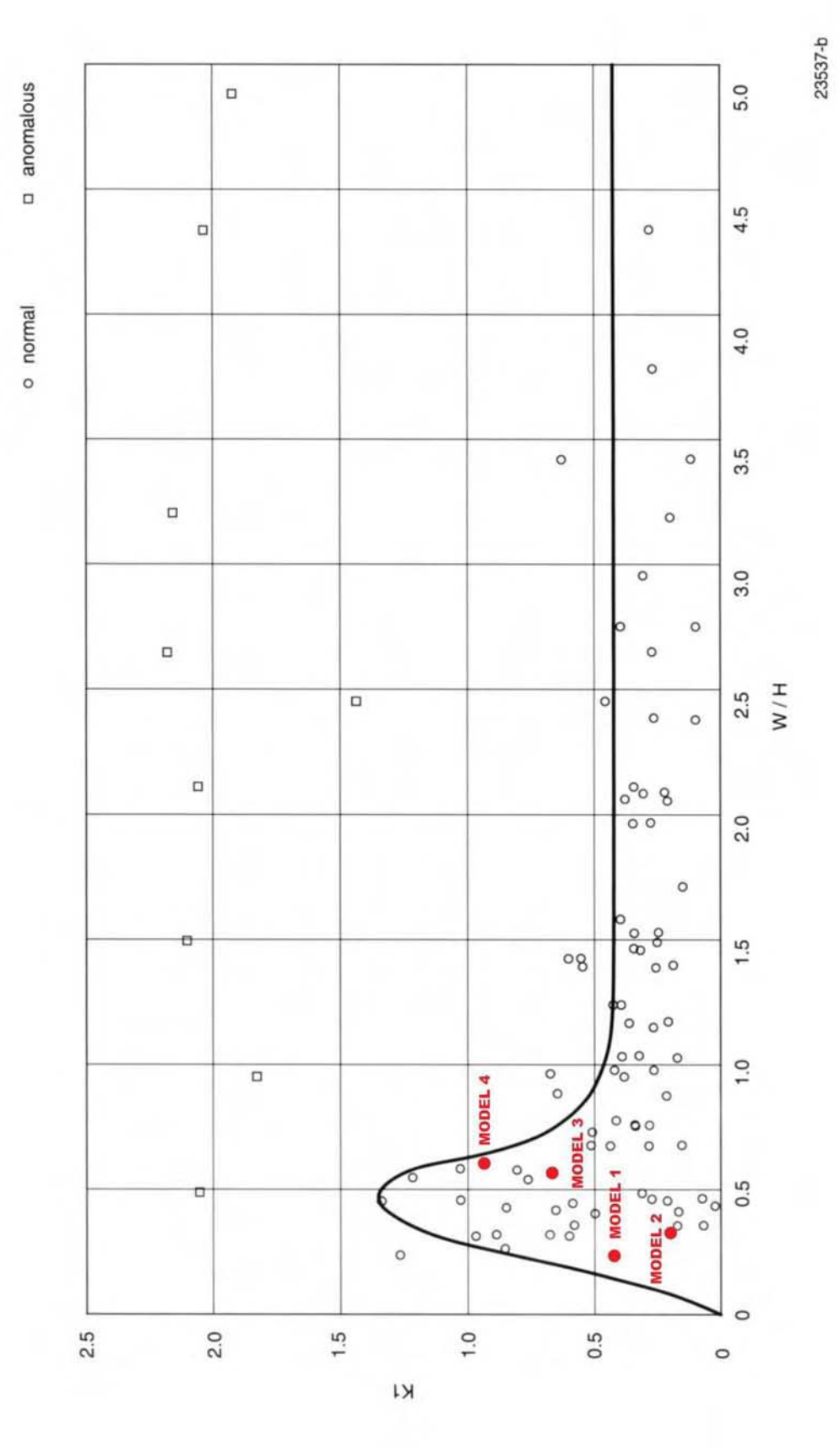

Fig. 5.10 – Superimposed model results for K1 (after Holla & Barclay 2000)

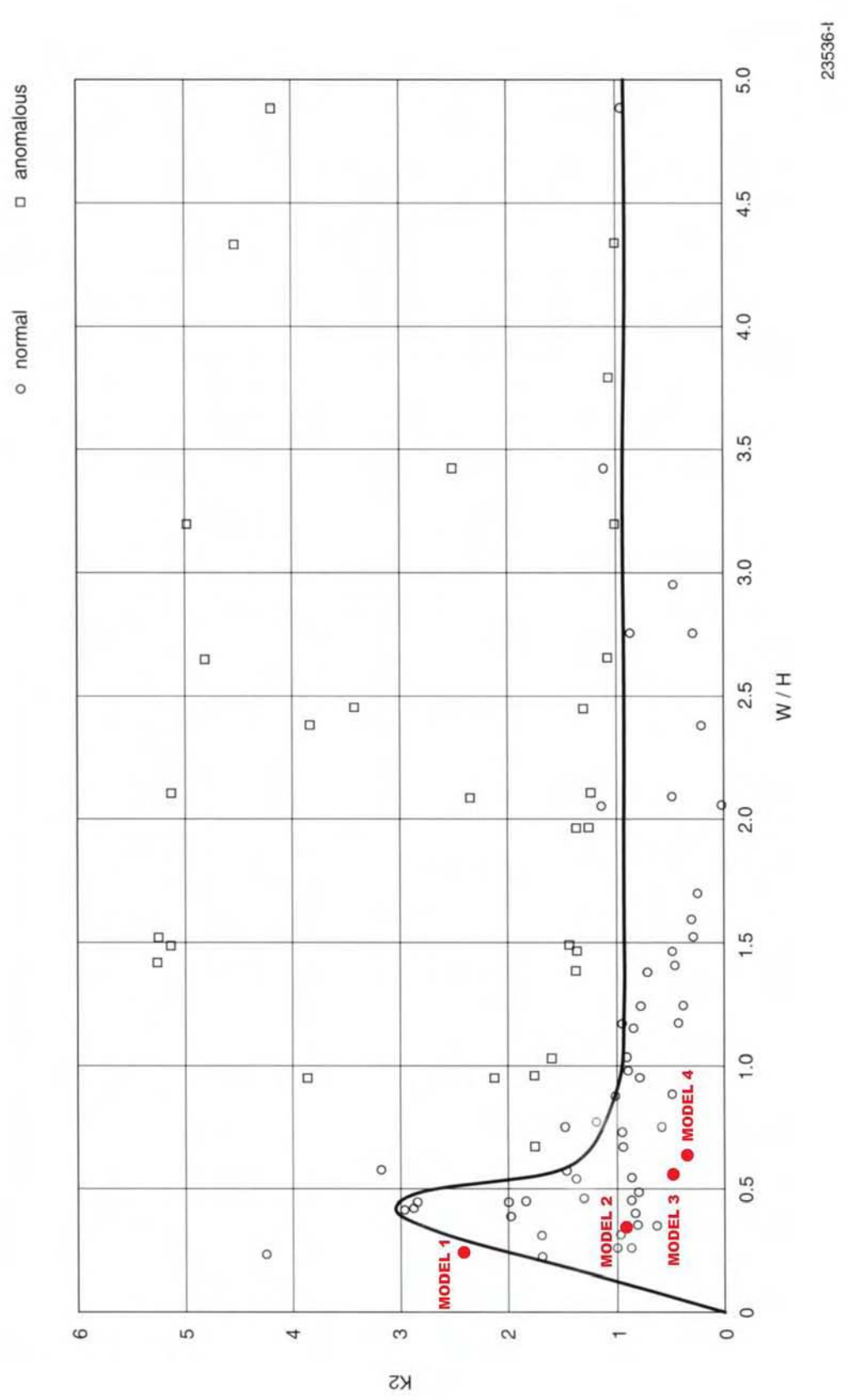

Fig. 5.11 – Superimposed model results for K2 (after Holla & Barclay 2000)

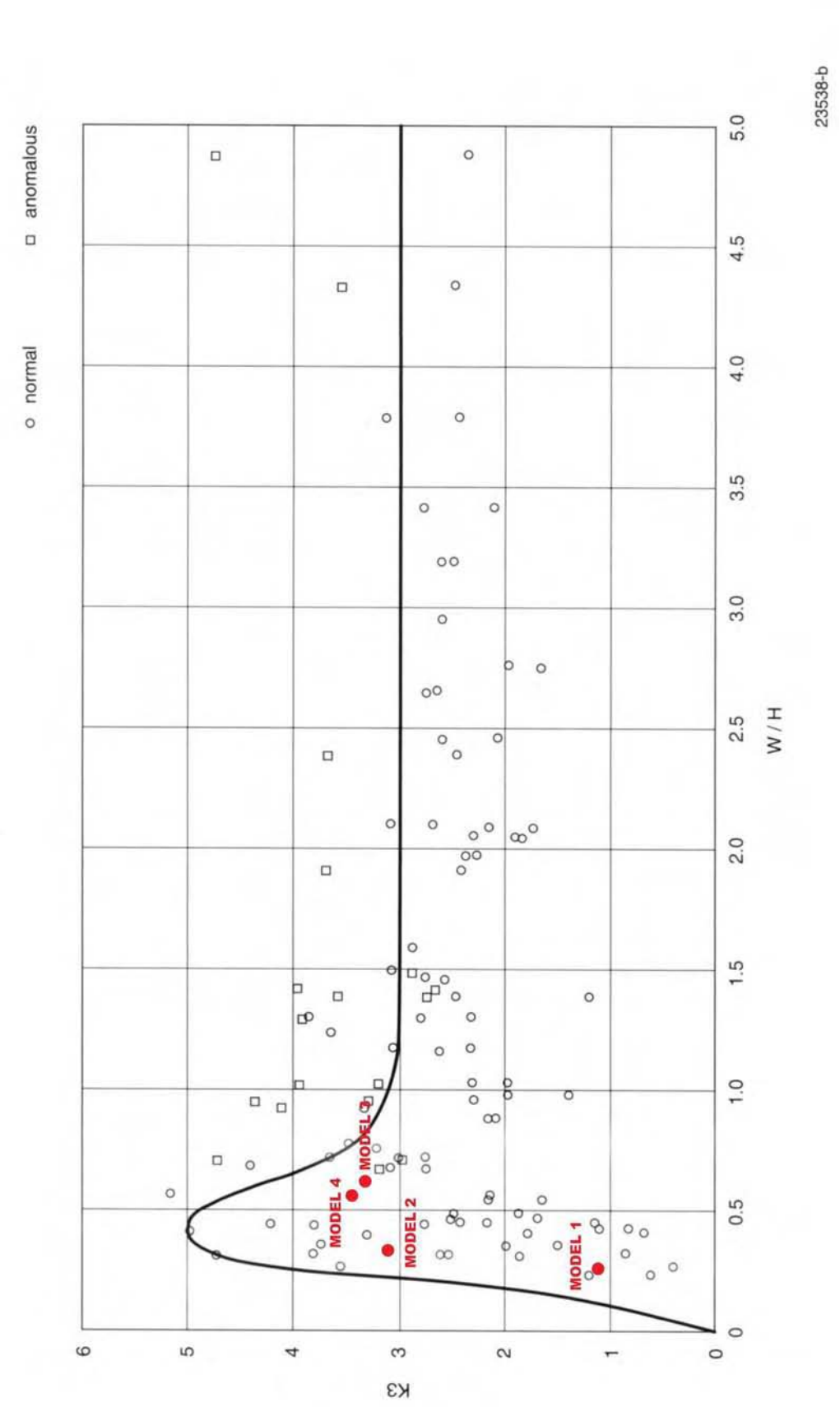

Fig. 5.12 – Superimposed model results for K3 (after Holla & Barclay 2000)

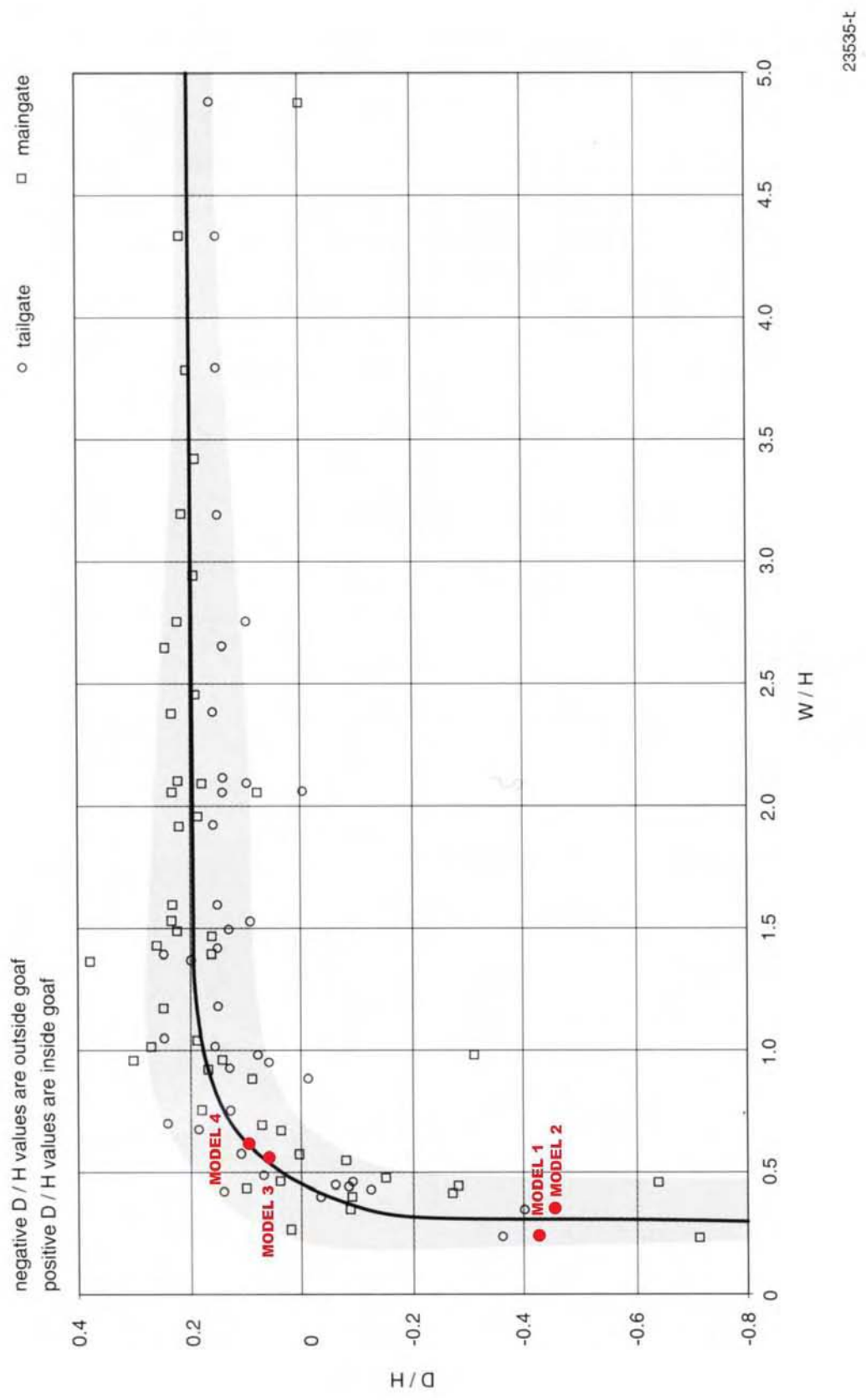

Fig. 5.13 – Superimposed model results for D/H (after Holla & Barclay 2000)

It can be seen from Figure 5.8 and Figure 5.9 that the numerical models predicted maximum developed subsidence and goaf edge subsidence quite well. Given the amount of scatter in the empirical data for the subsidence factor, this was a good result.

Horizontal strain has been previously defined as the change in length per unit of the original horizontal length of ground surface. Tensile strains occur in the trough margin and over the goaf edges. Compressive strains occur above the extracted area. Holla and Barclay (2000) noted that maximum tensile strains are generally not larger than 1 mm/m and maximum compressive strains 3 mm/m, excluding topographical extremes. Strain has been recognized as one of the most difficult parameters to predict due to vertical joints potentially opening up on the surface and the large effect that variations in topography has on the strain profile. Observed strain profiles in the field are never as perfect as theoretical strain profiles due to these factors.

It can be seen from Figure 5.10 and Figure 5.11 that the model results contained considerable scatter in the data points, as did the empirical results for the strain constants. Part of the problem is the use of the K1 and K2 constants which normalize strains to depth and S_{max} – this may not be valid for sub-critical extraction. Another part of the problem is the magnitude of movements being predicted and modelled. Since the magnitude of the movements are in the order of a few millimetres over a distance of several hundred metres, the scatter in the predicted strain constants can be attributed to modelling ‘noise’. Even though there may be difficulty in predicting surface strains, it is encouraging to note that the predicted strains from the numerical models lie within or very close to the empirical curves.

As defined previously, tilt of the ground surface between two points is calculated by dividing the difference in subsidence at the two points by the distance between them. Maximum tilt occurs at the point of inflection where the subsidence is roughly equal to one half of S_{max}. It can be seen in Figure 5.12 that the model results for the tilt constant K3 produced good matches with the empirical predictions.

The point of inflection is the location where tensile strains become positive and vice versa. The results of the position of the inflection point relative to the goaf can be seen in Figure 5.13. It is noted by Holla and Barclay (2000) that the position of the inflection

point falls inside the goaf for W/H ratios greater than 0.5 or outside the goaf for W/H ratios less than 0.5. It can be seen that this observation holds true for Model 1 (W/H = 0.25), Model 3 (W/H = 0.56) and Model 4 (W/H = 0.61), and the predicted location of the inflection point falls within the range of empirical data scatter. The predicted subsidence at the inflection point was roughly one half of predicted S_{max} for all models and this is in agreement with Holla and Barclay (2000).

The calculated angle of draw for the models varied between 18° and 41°. This produced an average value of 29°. The angle of draw was calculated using the 20 mm cut-off limit. The average angle of draw from Holla and Barclay (2000) is also 29°. This was an exact match but it must also be noted that there seems to be no apparent relationship between angle of draw and W/H ratio, the predicted values can only be compared to the empirical values and not be verified in any way.

The UDEC subsidence development history above the centre of the longwall panel, subsidence profile, strain profile, tilt profile, yielded zones and caving development, and joint slip for all four models are shown in Figures 5.14 to 5.41.

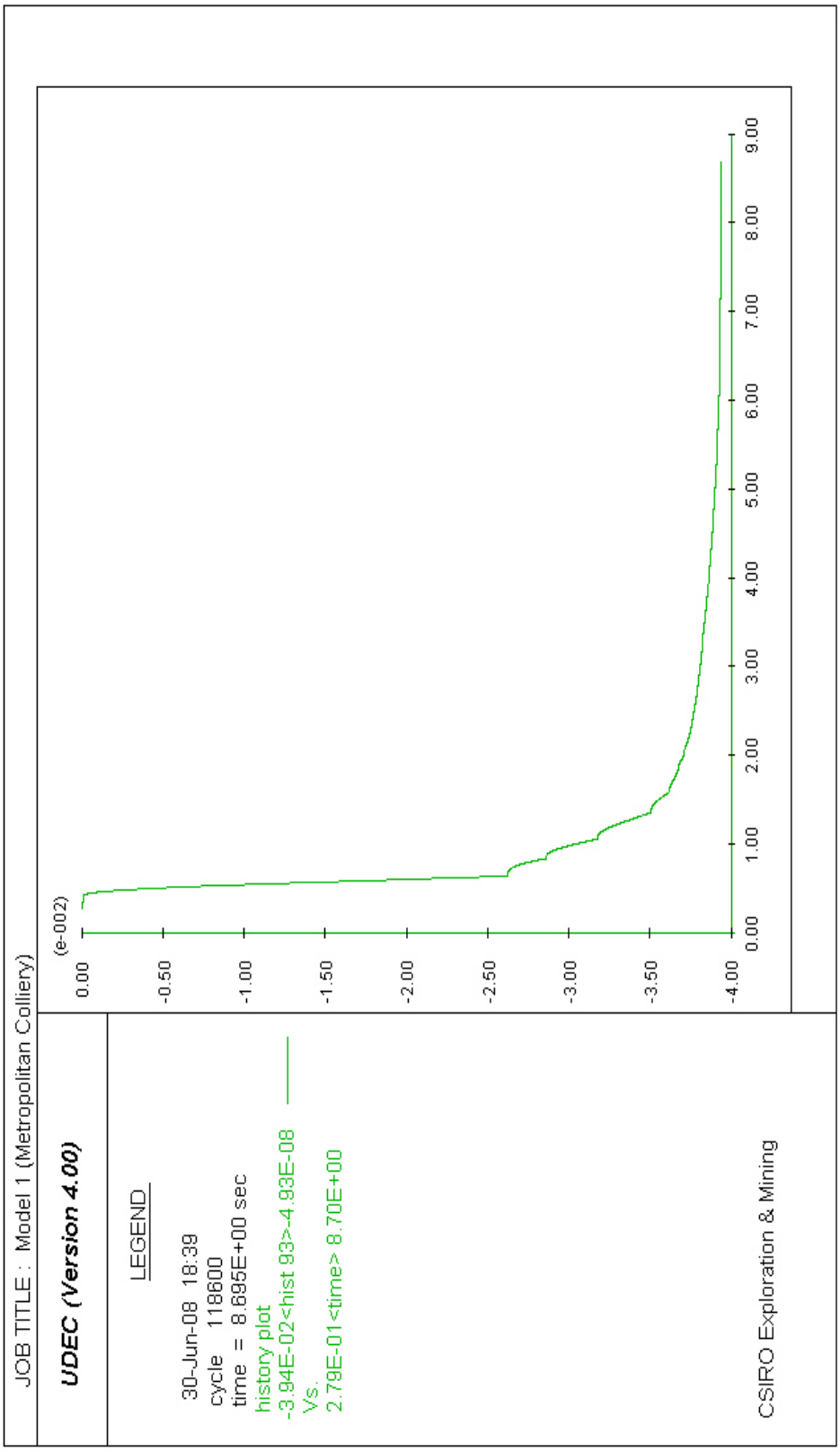

Fig. 5.14 – Development of maximum subsidence in Model 1

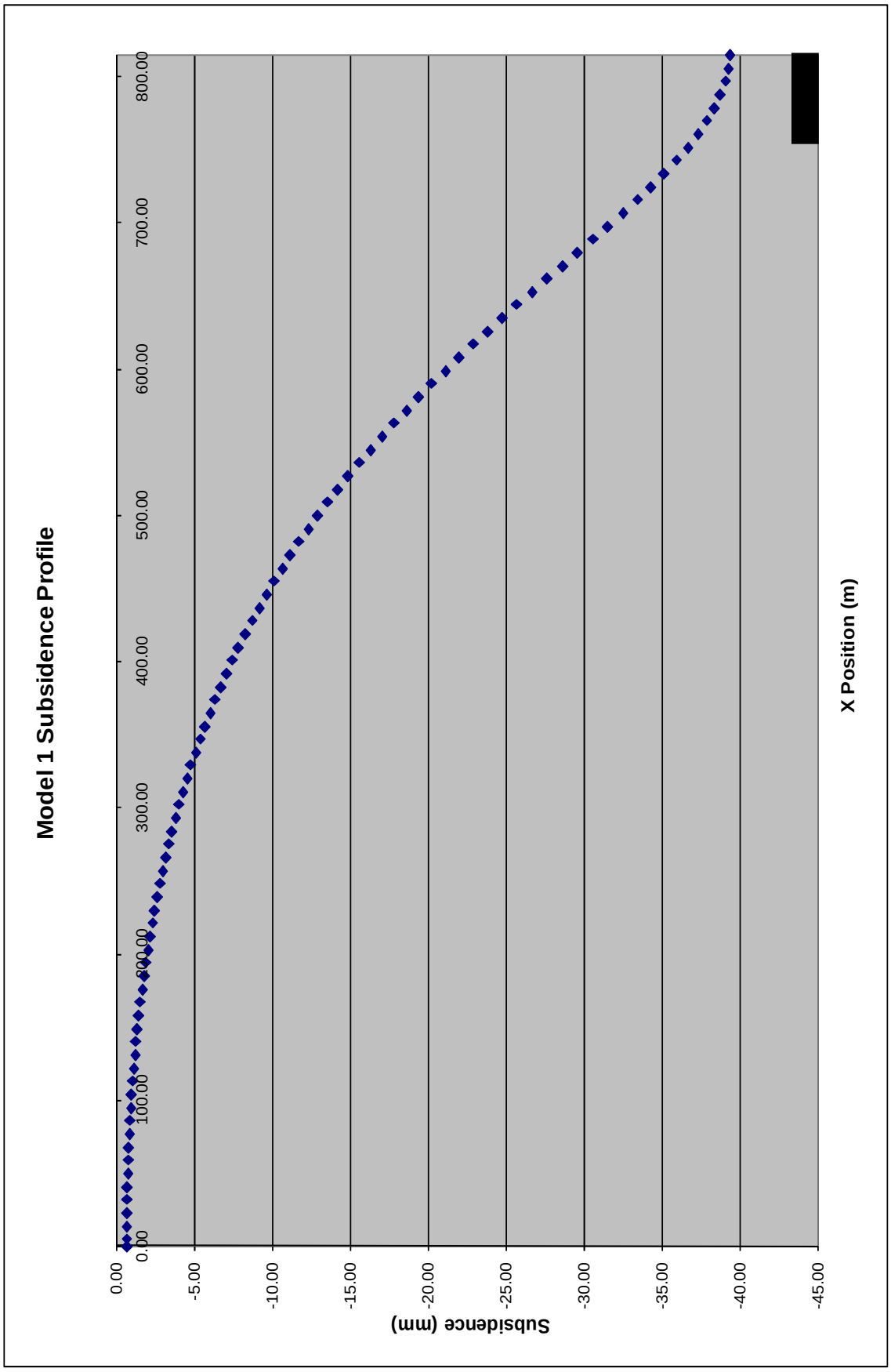

Fig. 5.15 – Subsidence profile for Model 1

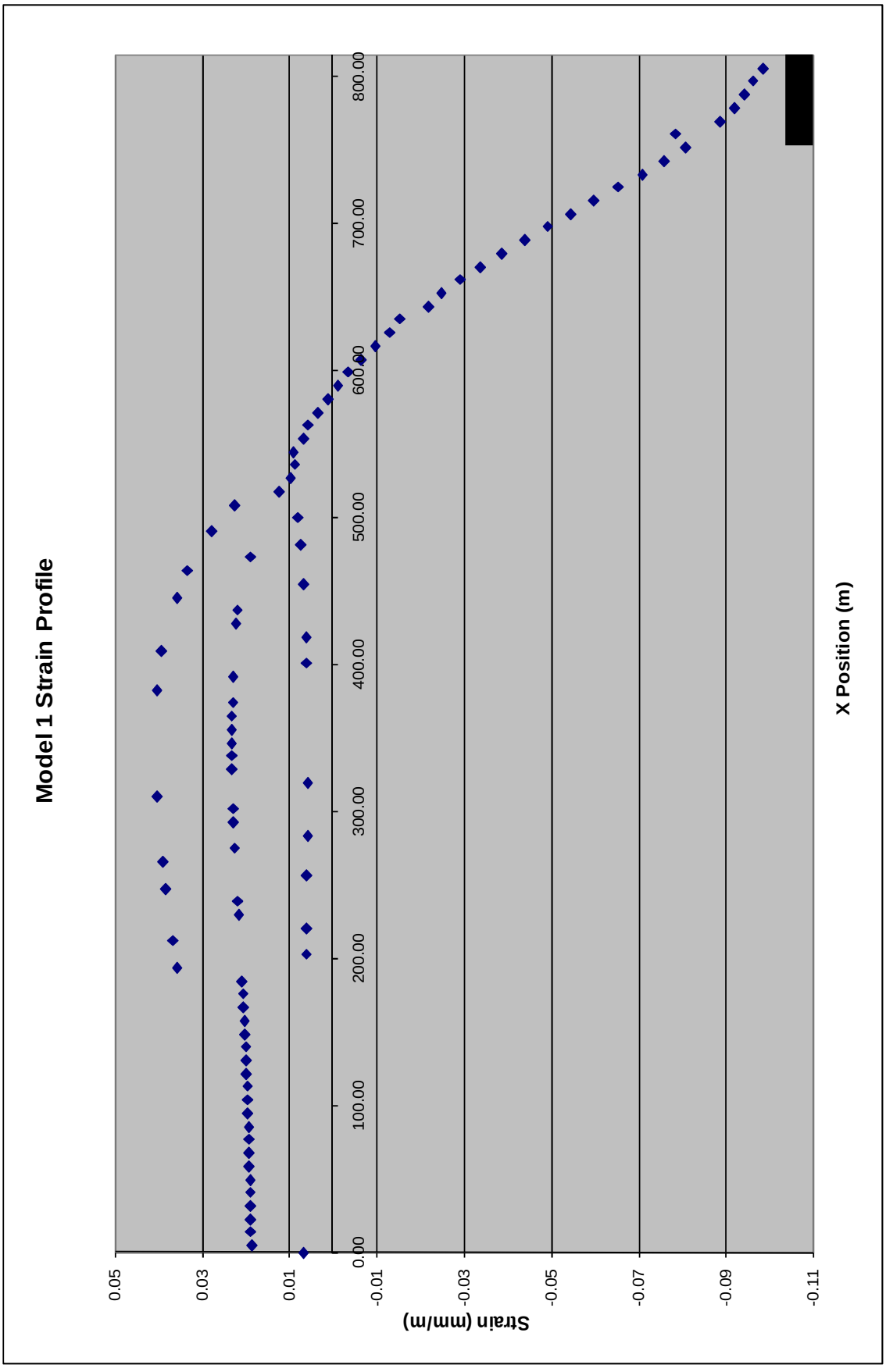

Fig. 5.16 – Strain profile for Model 1

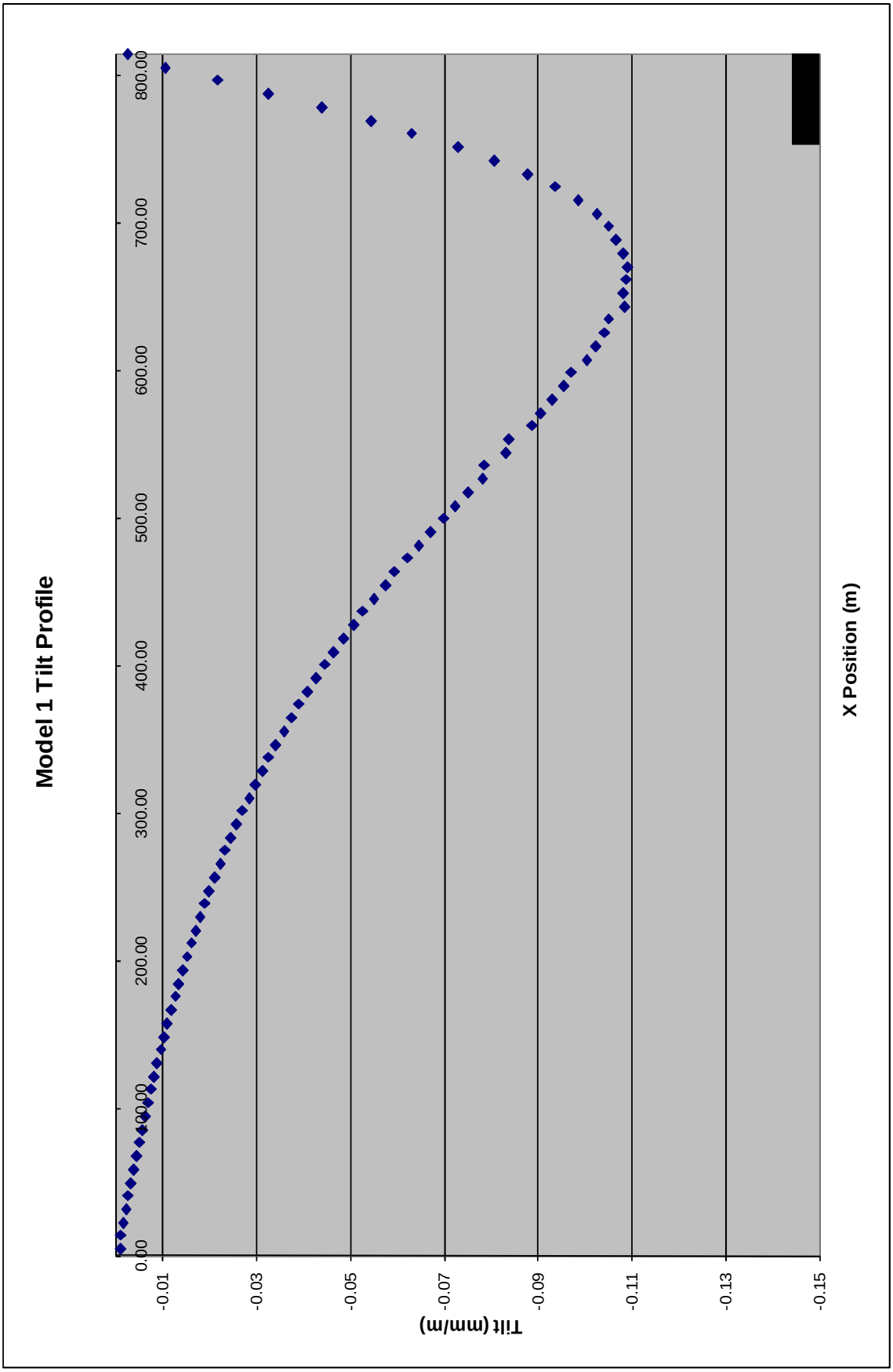

Fig. 5.17 – Tilt profile for Model 1

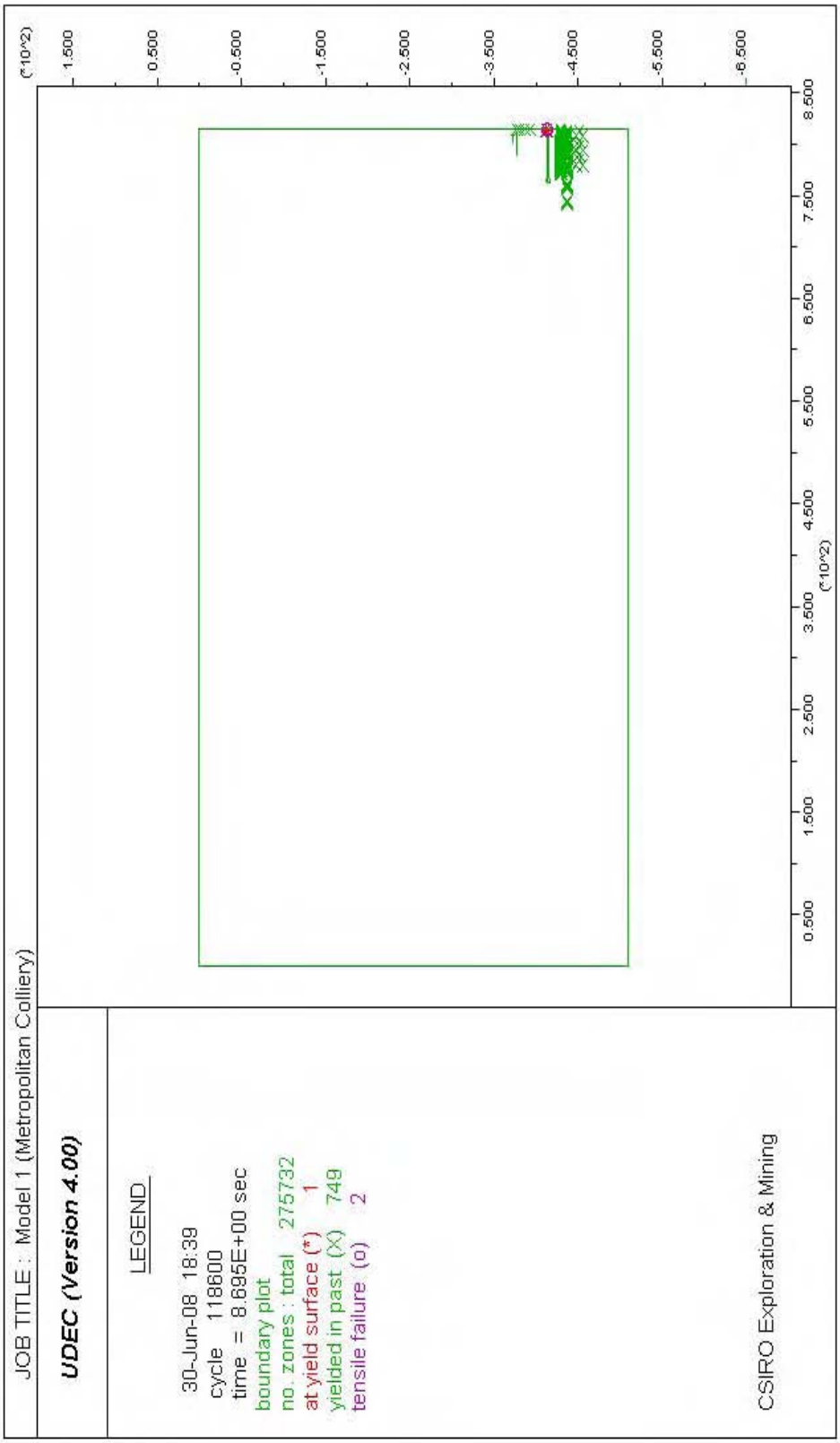

Fig. 5.18 – Yielded zones and caving development in Model 1

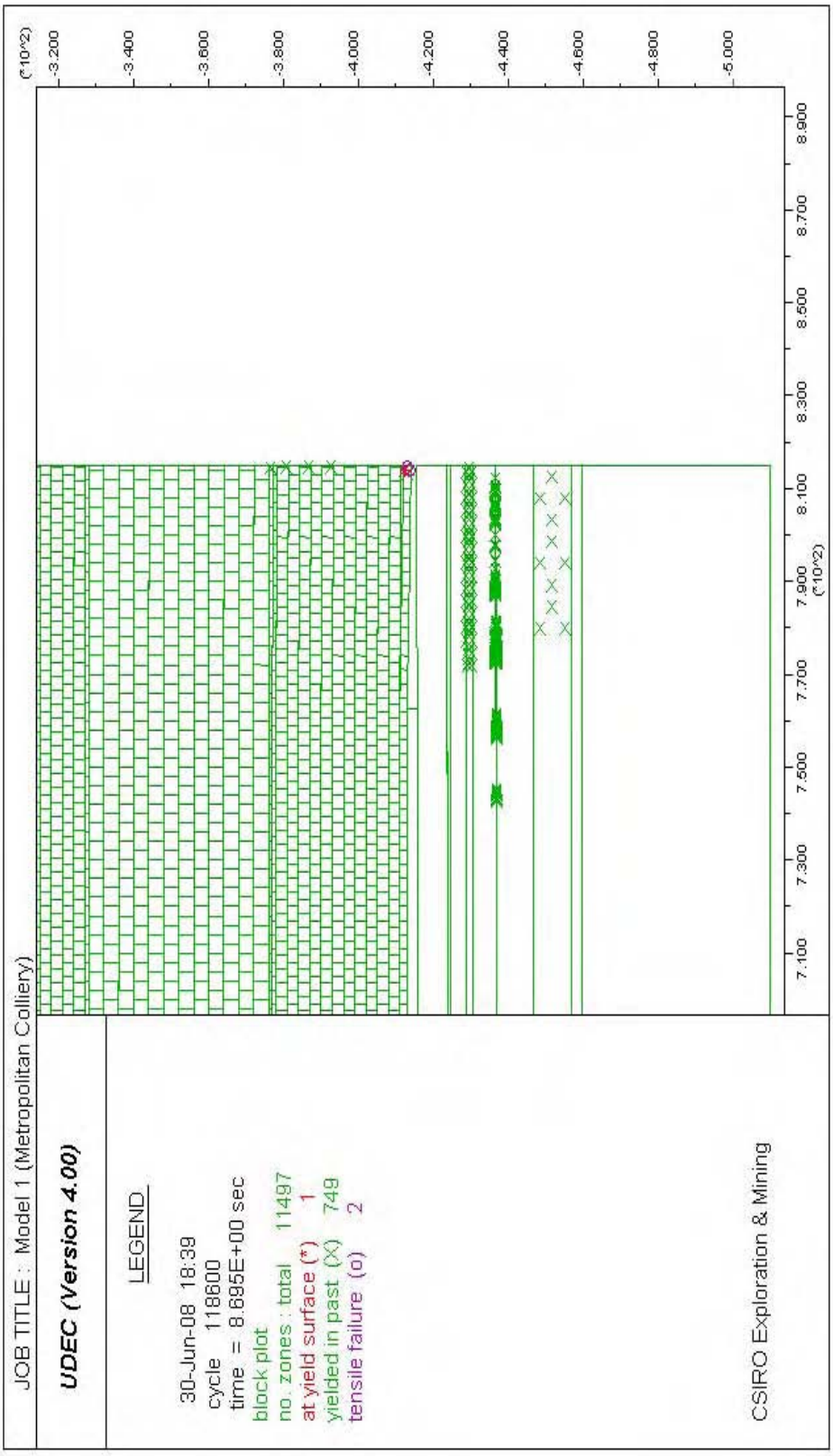

Fig. 5.19 – Detailed view of yielded zones in Model 1

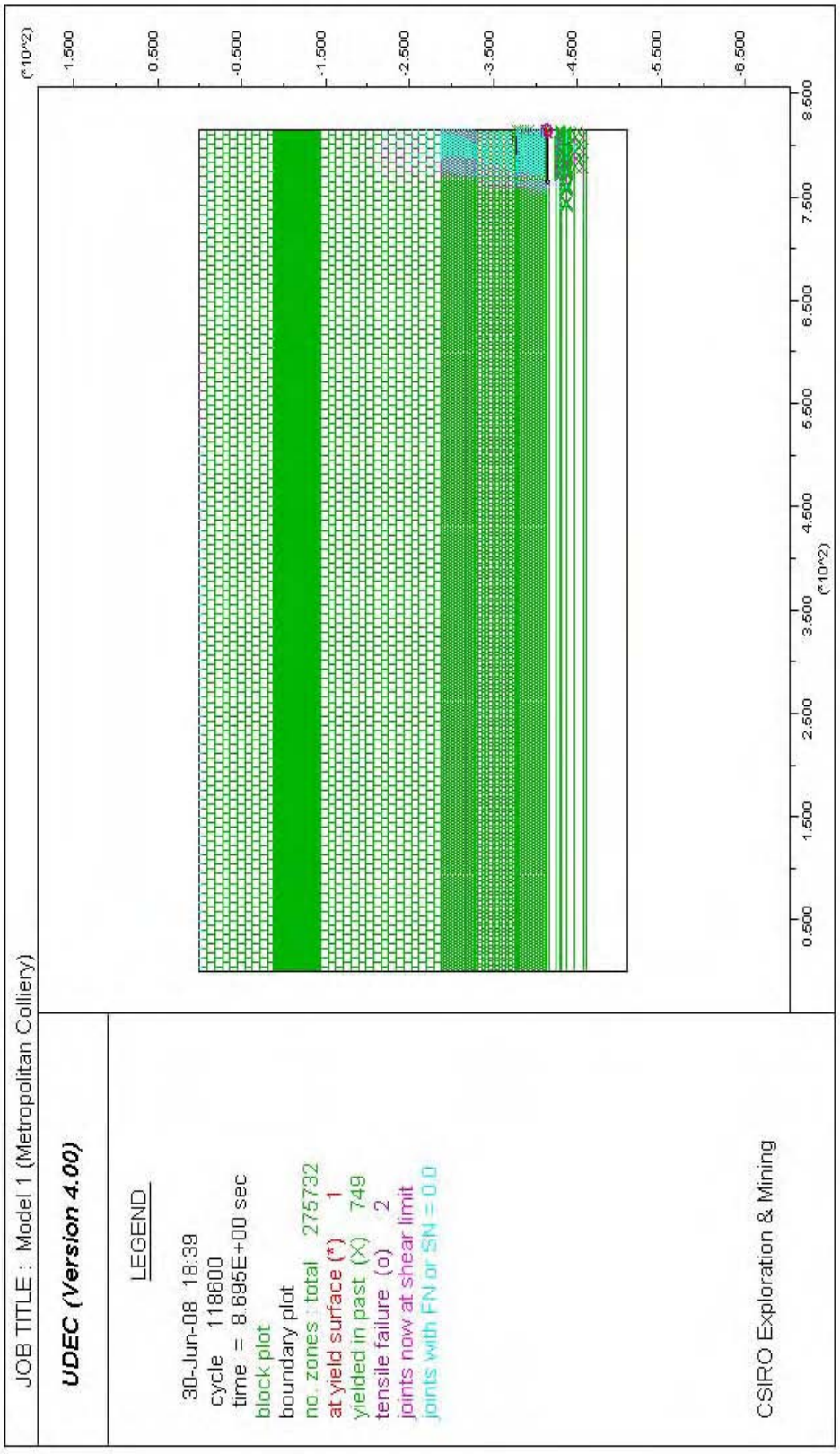

Fig. 5.20 – Yielded zones and joint slip in Model 1

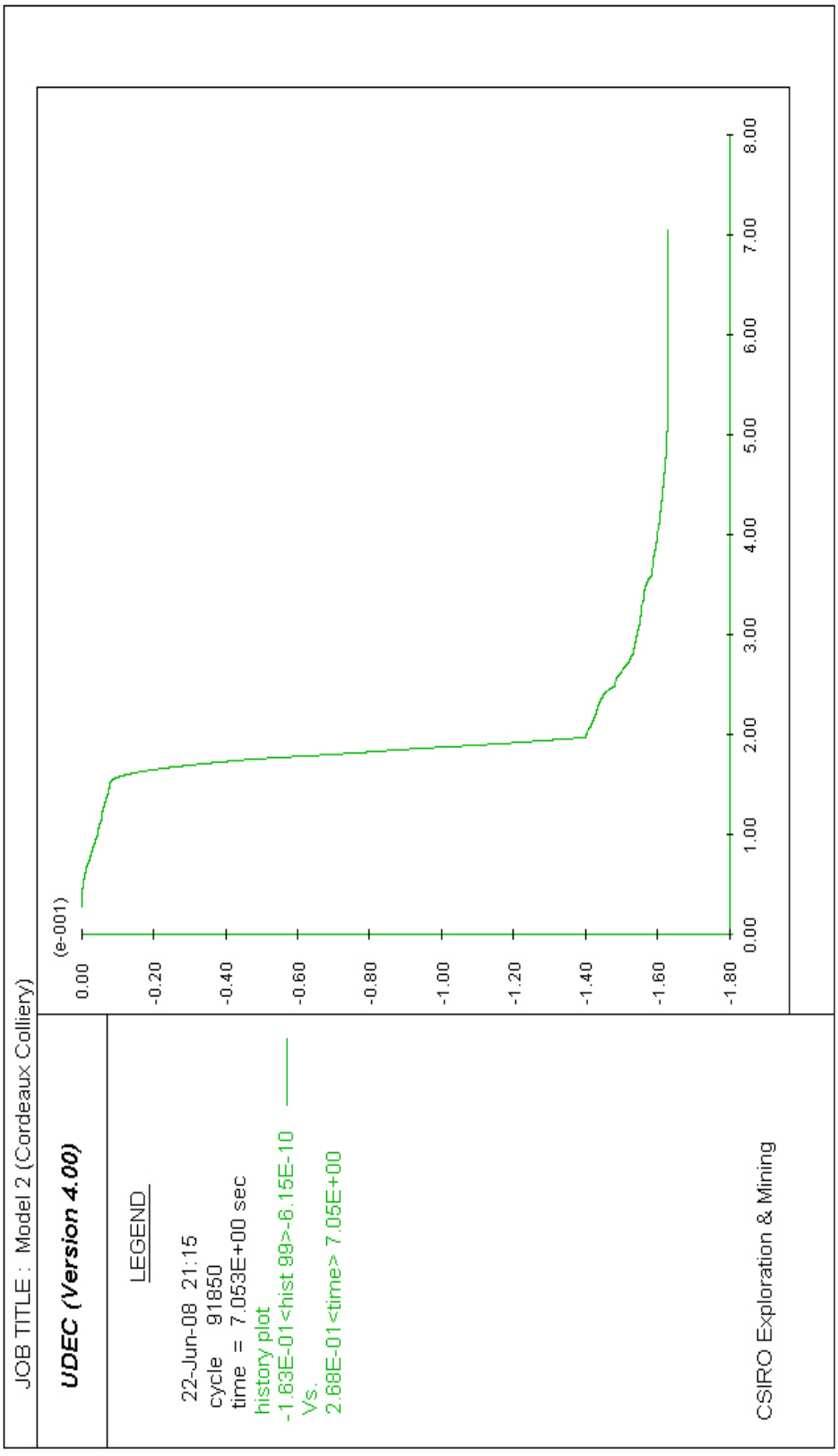

Fig. 5.21 - Development of maximum subsidence in Model 2

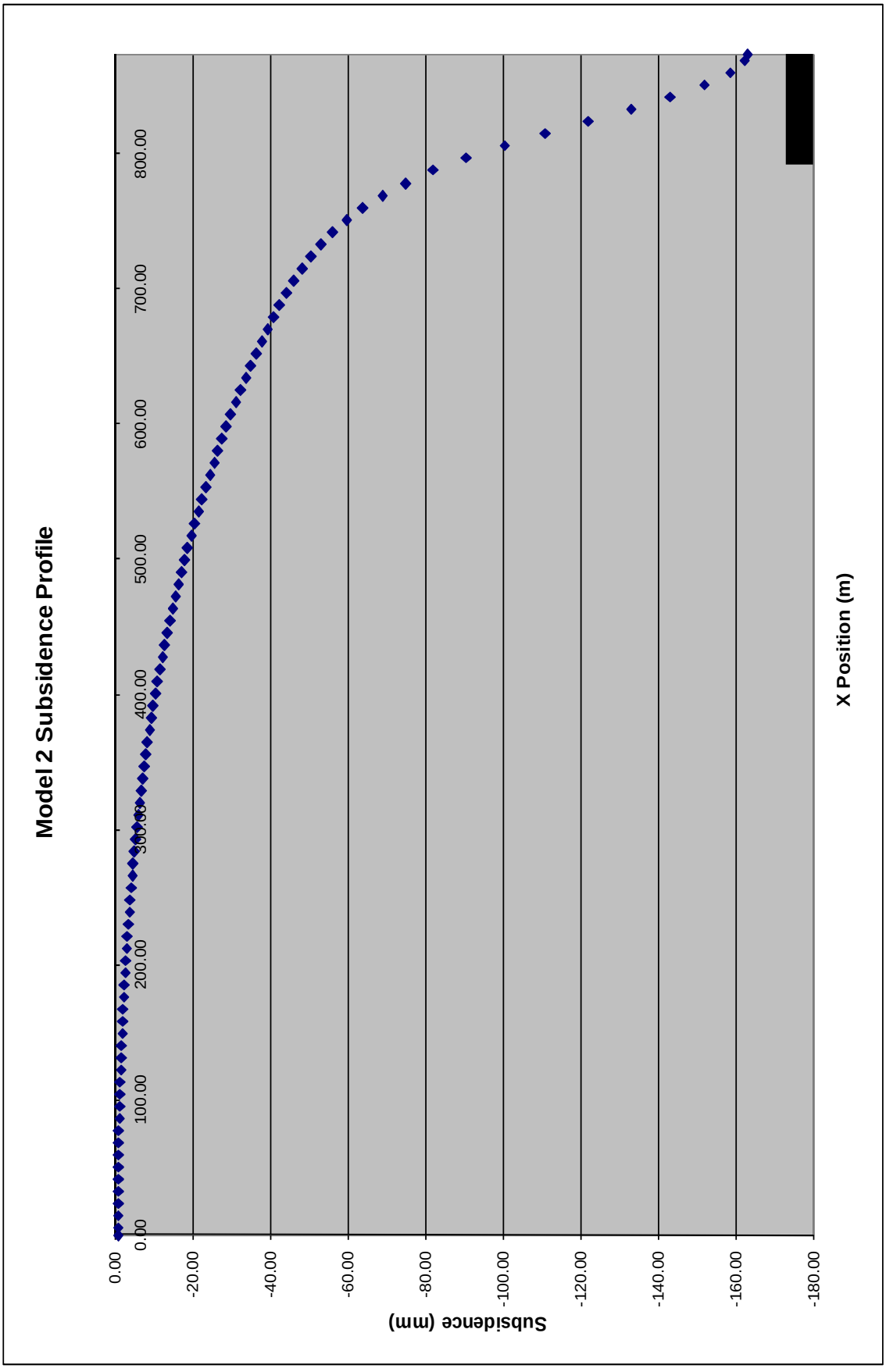

Fig. 5.22 – Subsidence profile for Model 2

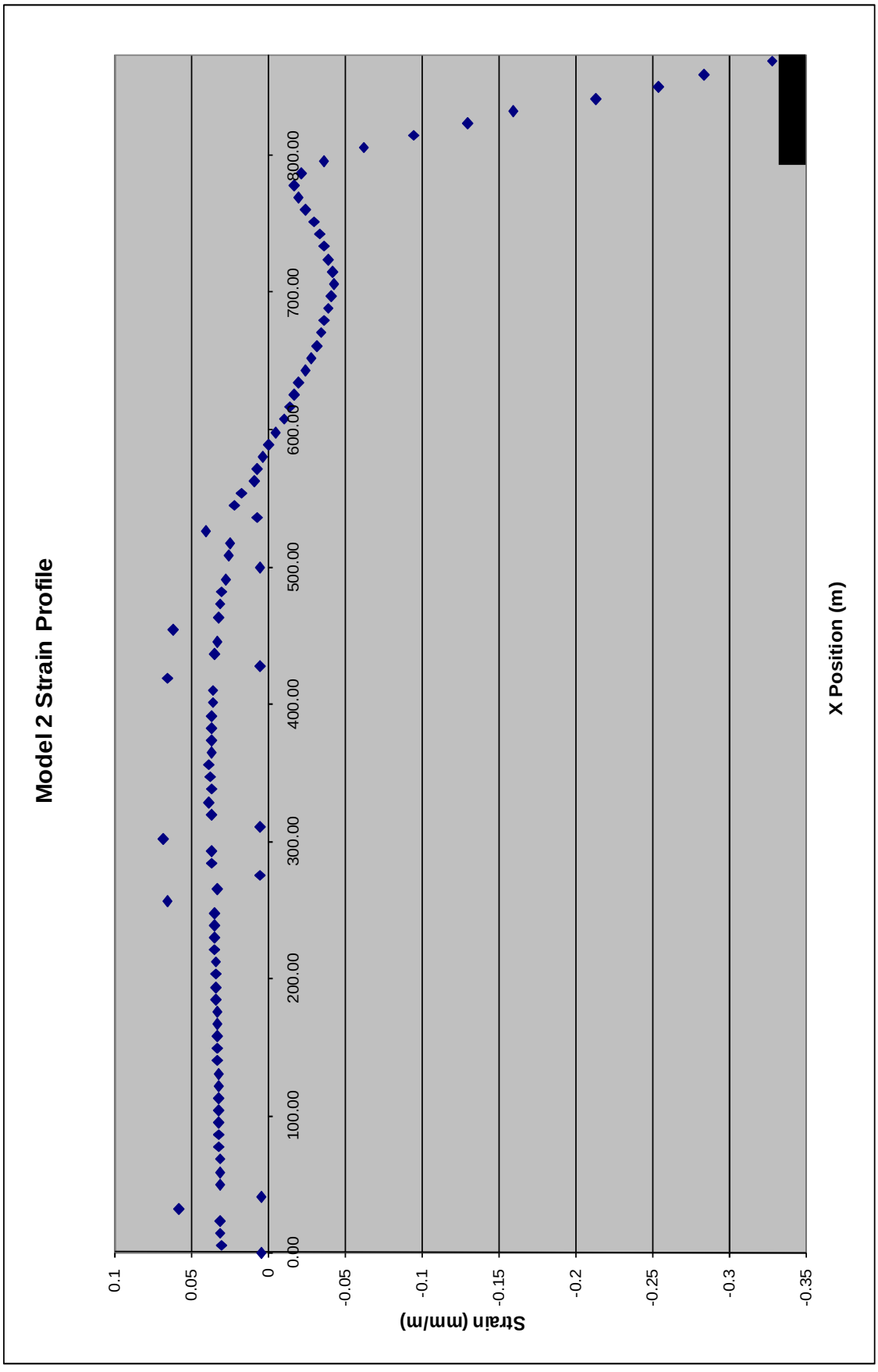

Fig. 5.23 – Strain profile for Model 2

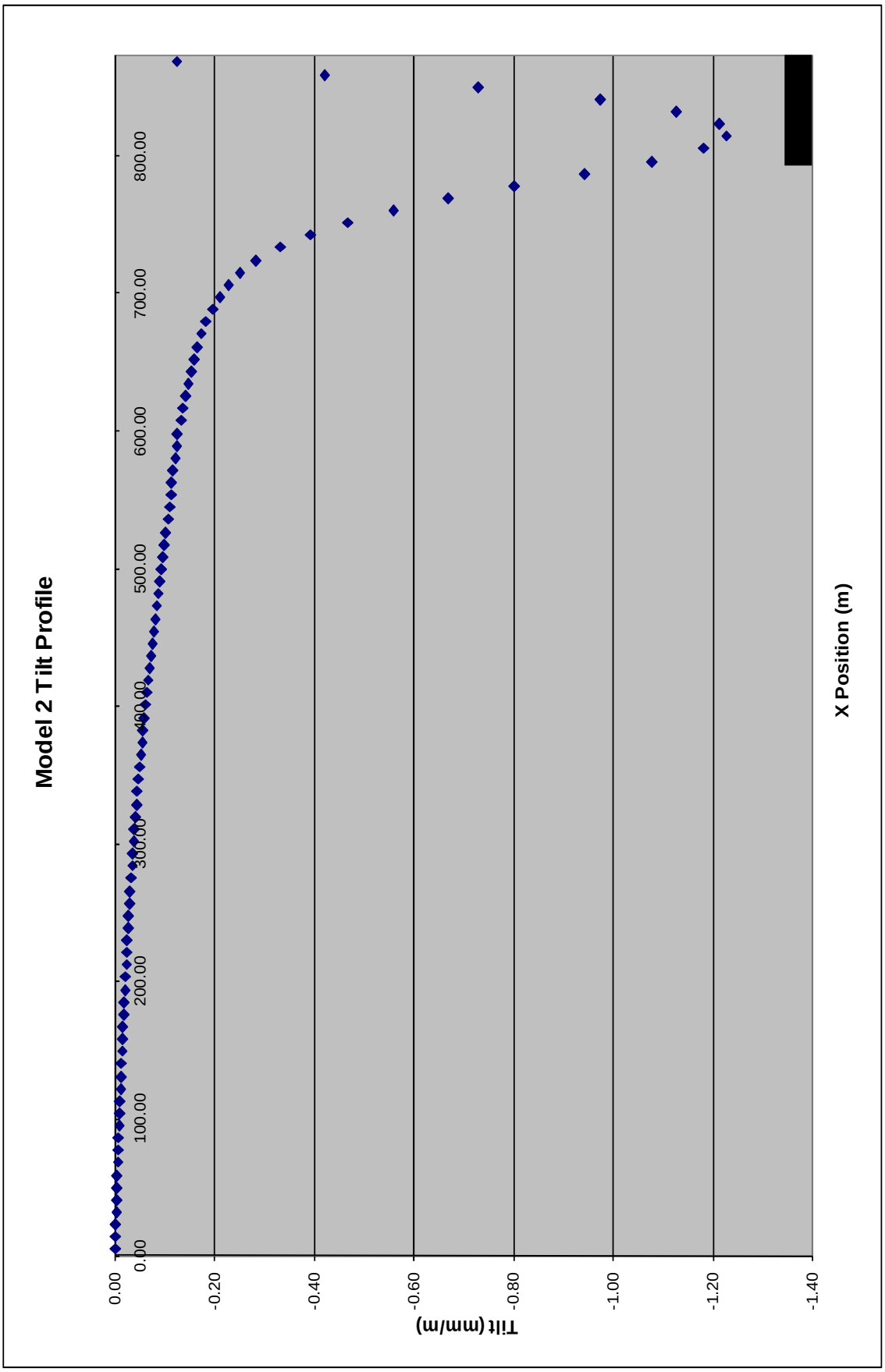

Fig. 5.24 – Tilt profile for Model 2

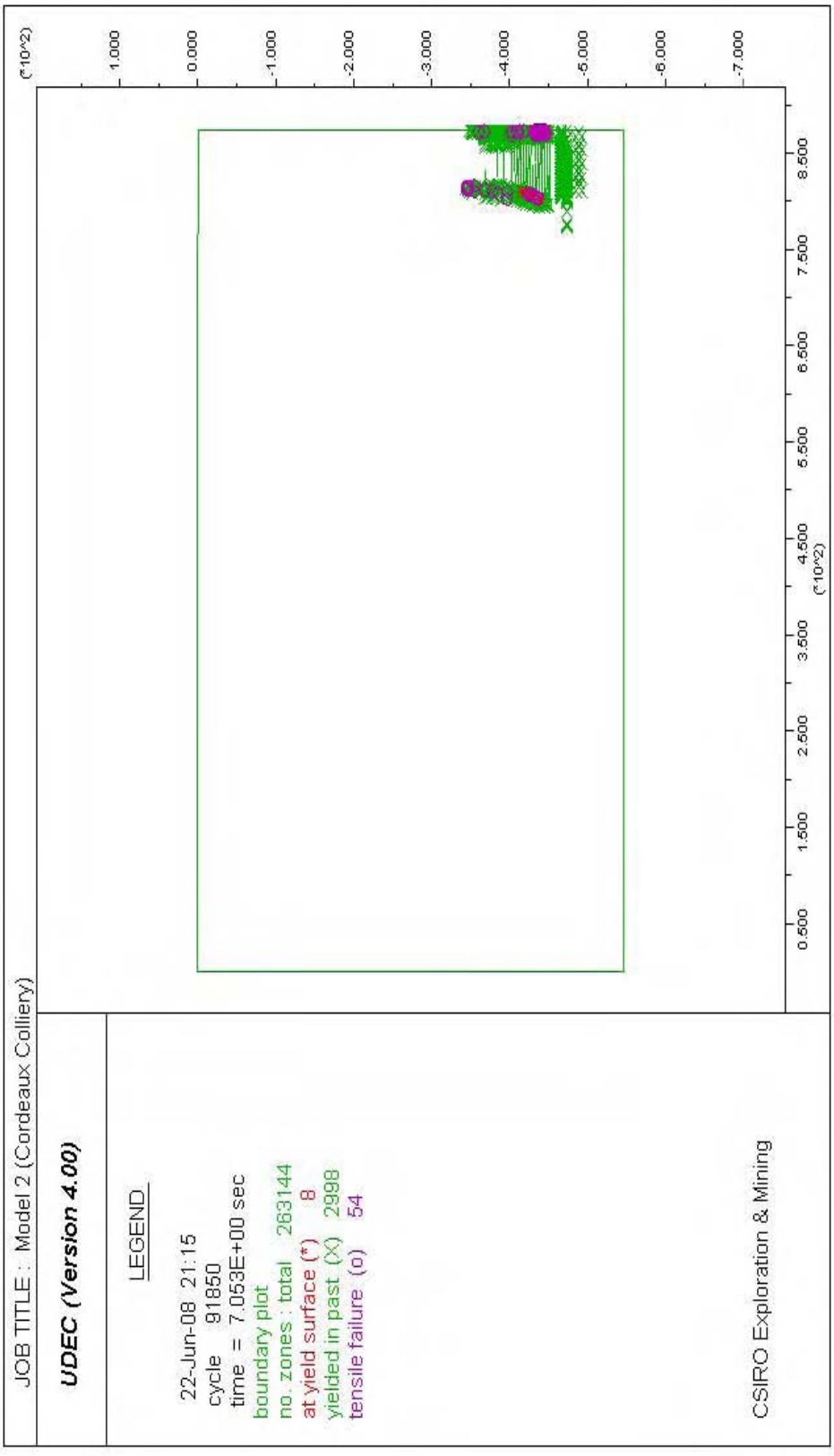

Fig. 5.25 – Yielded zones and caving development in Model 2

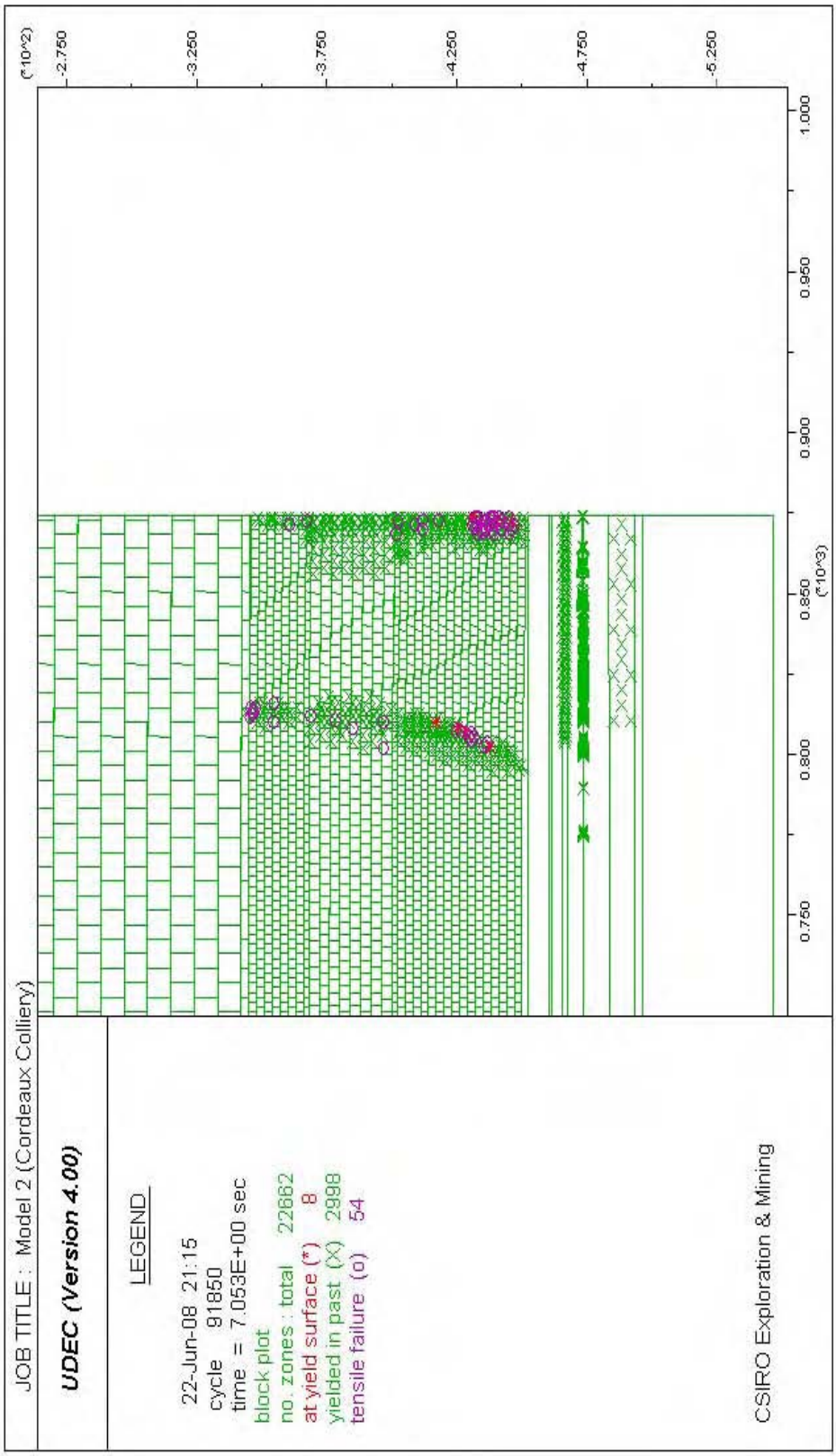

Fig. 5.26 – Detailed view of yielded zones in Model 2

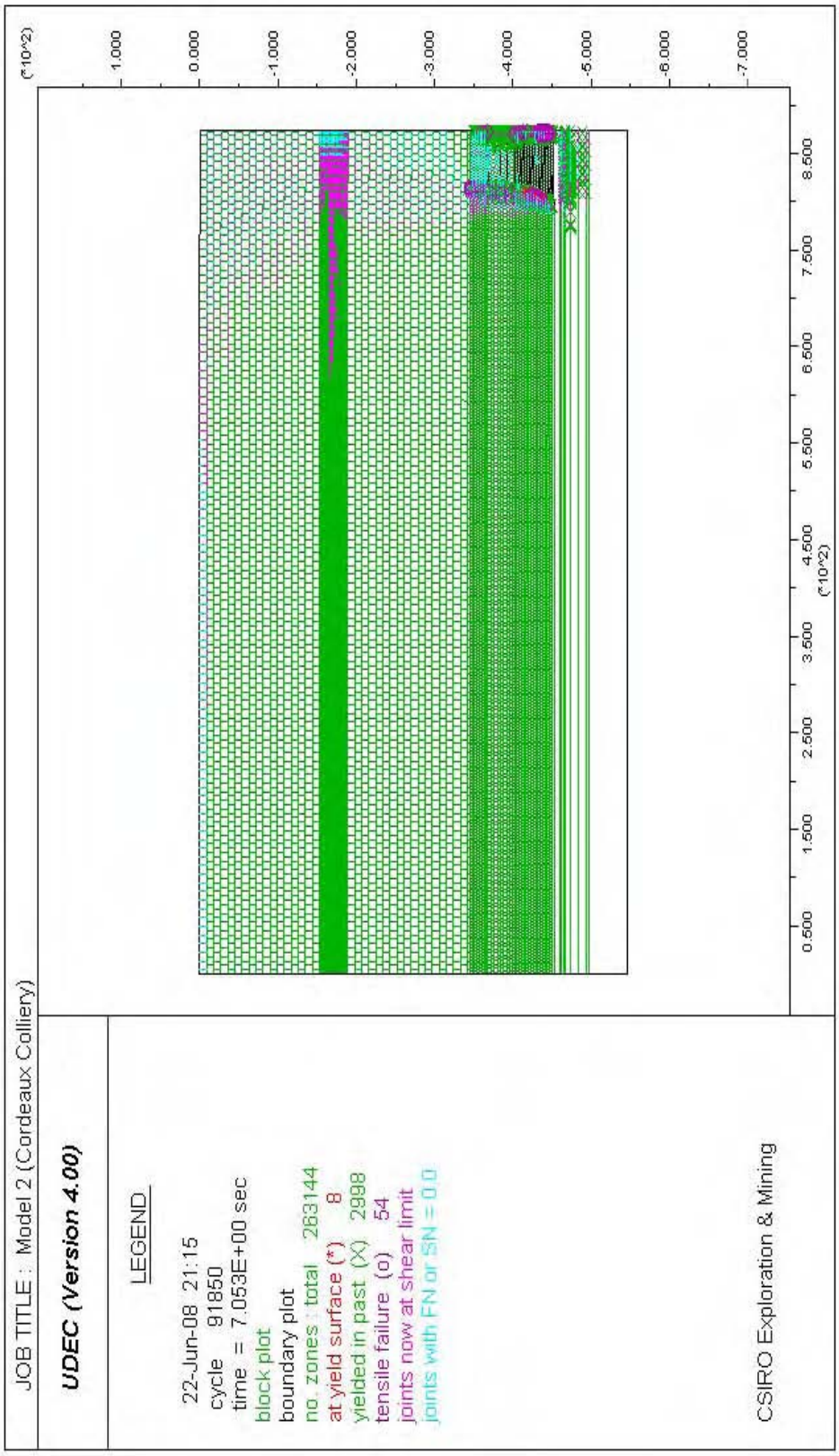

Fig. 5.27 – Yielded zones and joint slip in Model 2

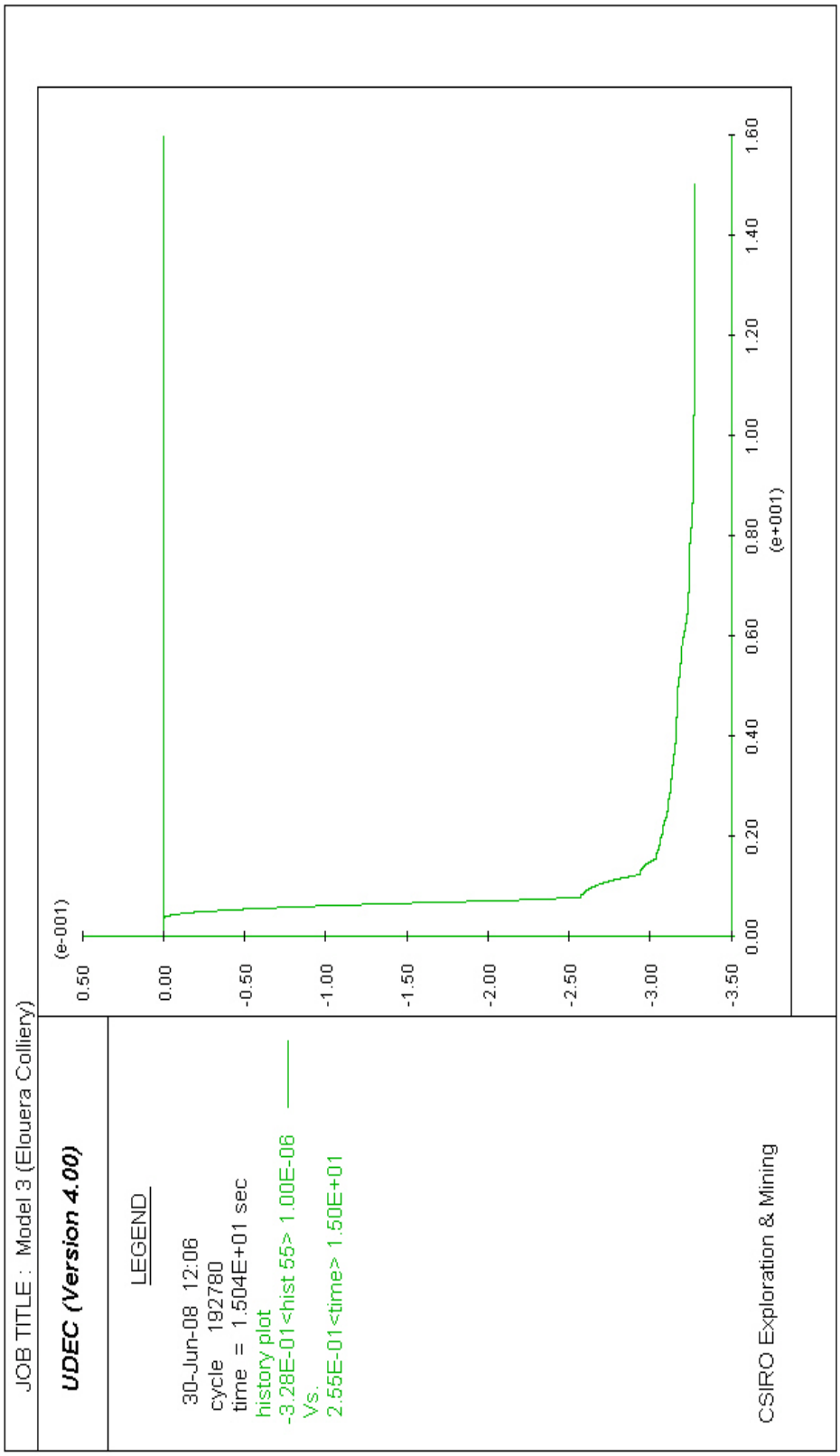

Fig. 5.28 – Development of maximum subsidence in Model 3

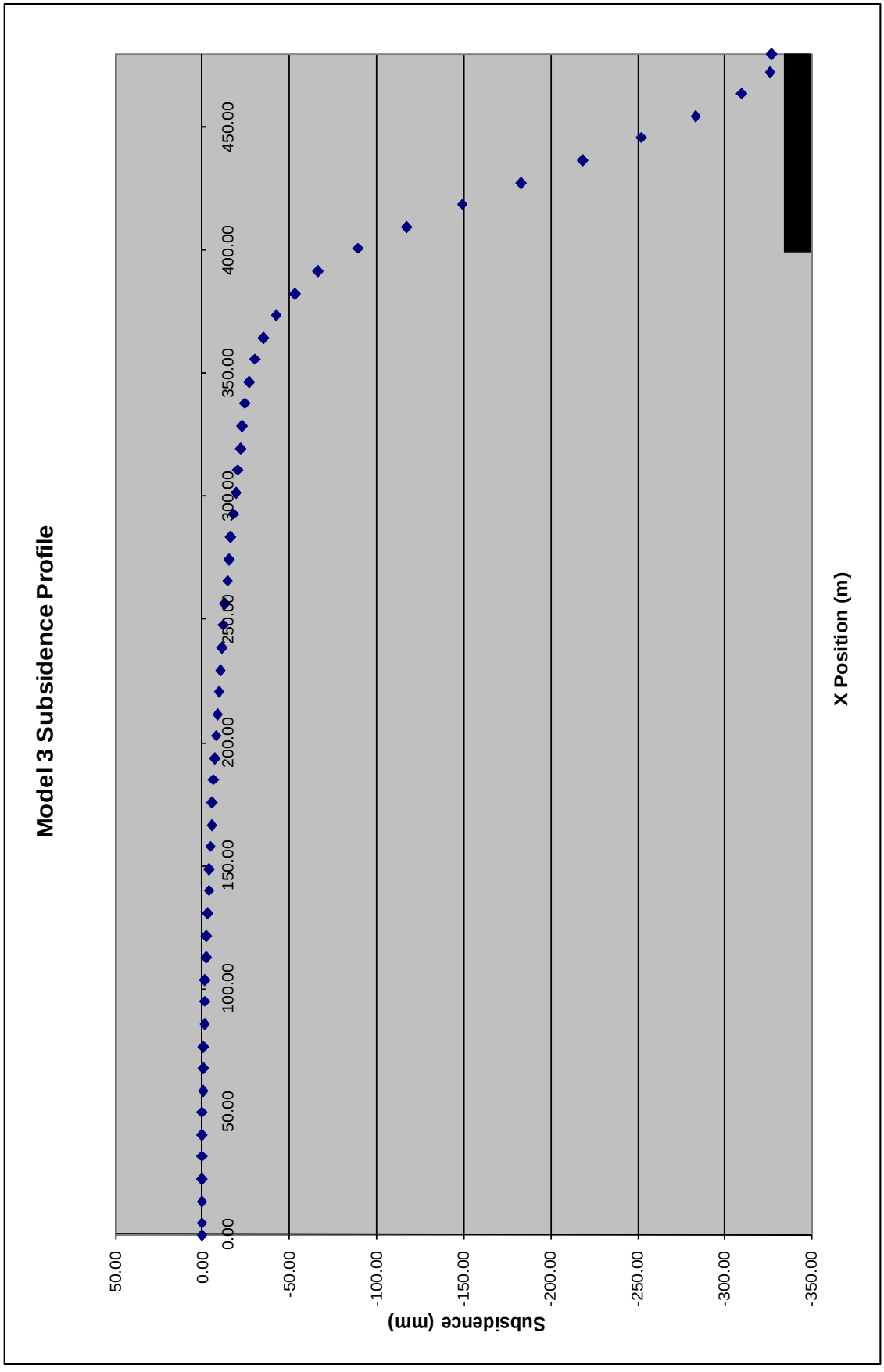

Fig. 5.29 – Subsidence profile for Model 3

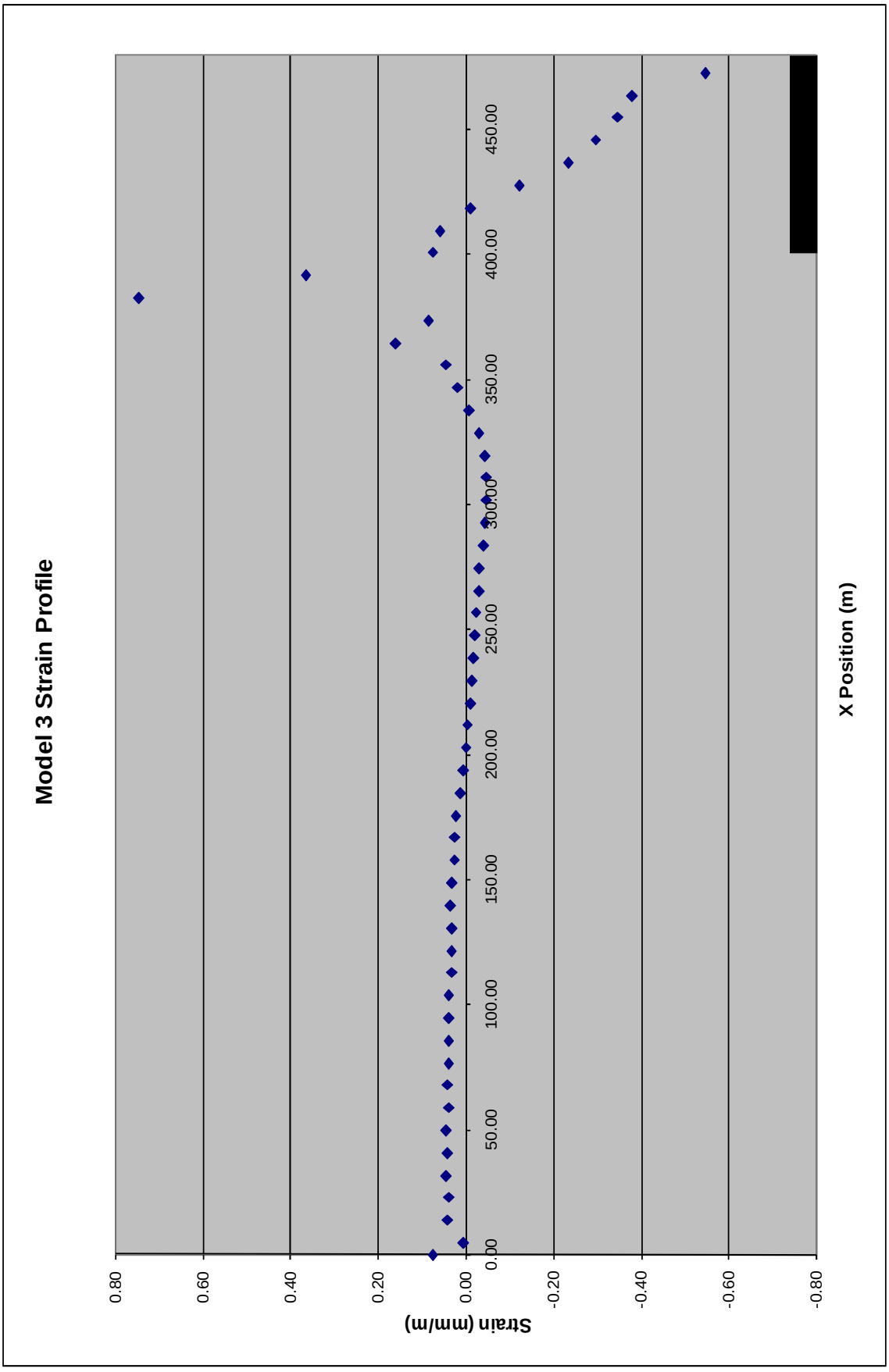

Fig. 5.30 – Strain profile for Model 3

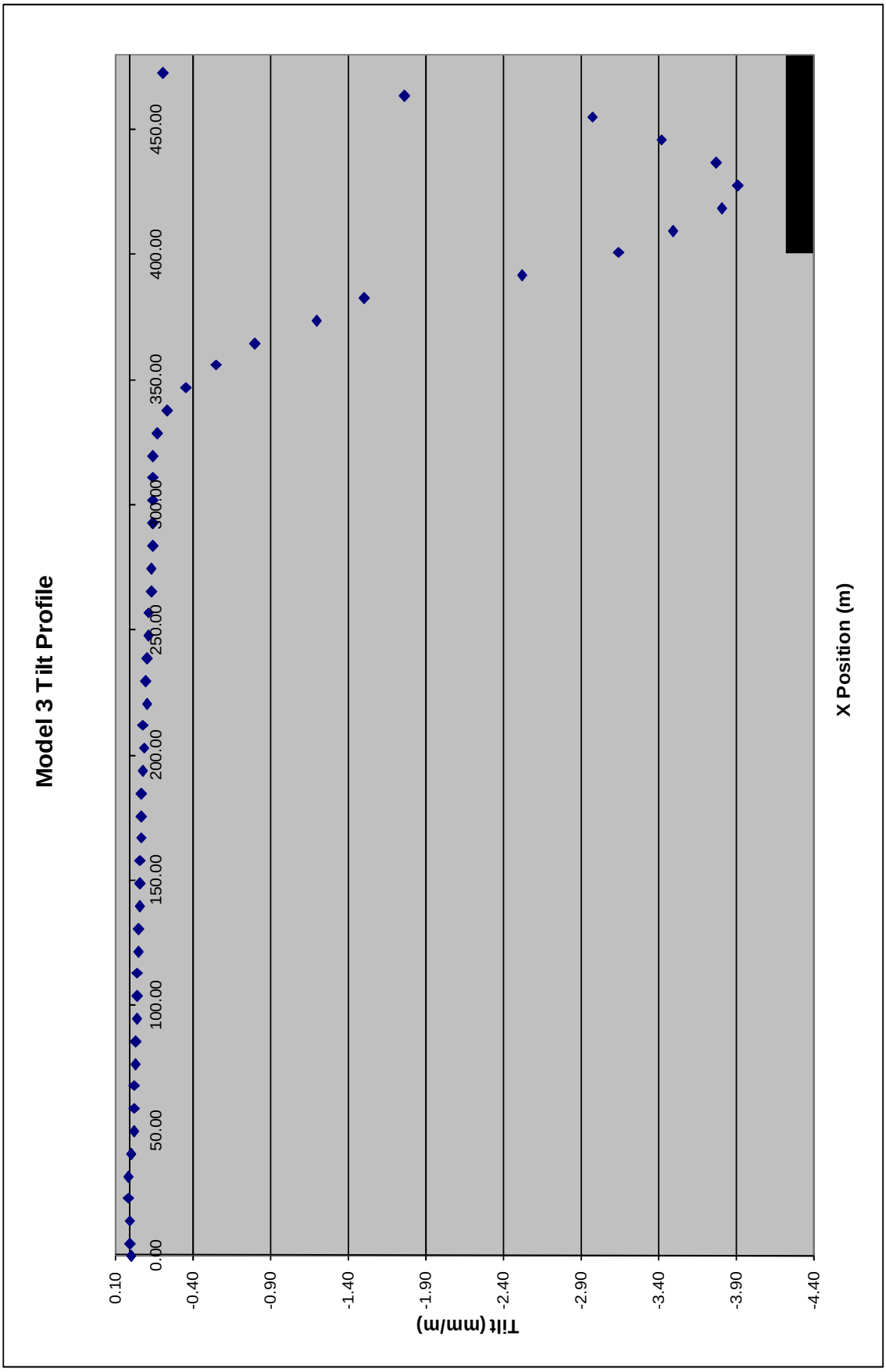

Fig. 5.31 – Tilt profile for Model 3

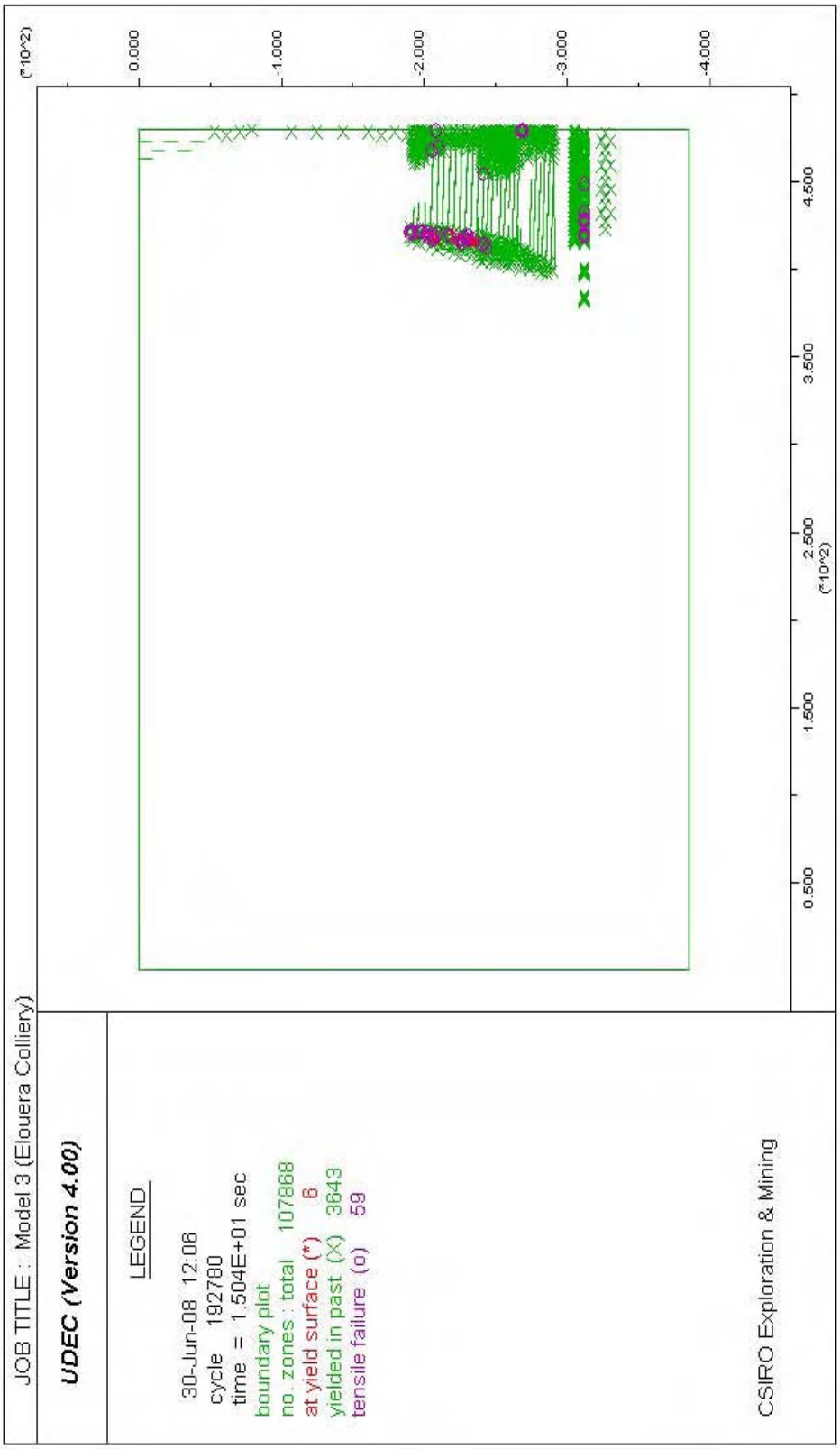

Fig. 5.32 – Yielded zones and caving development in Model 3

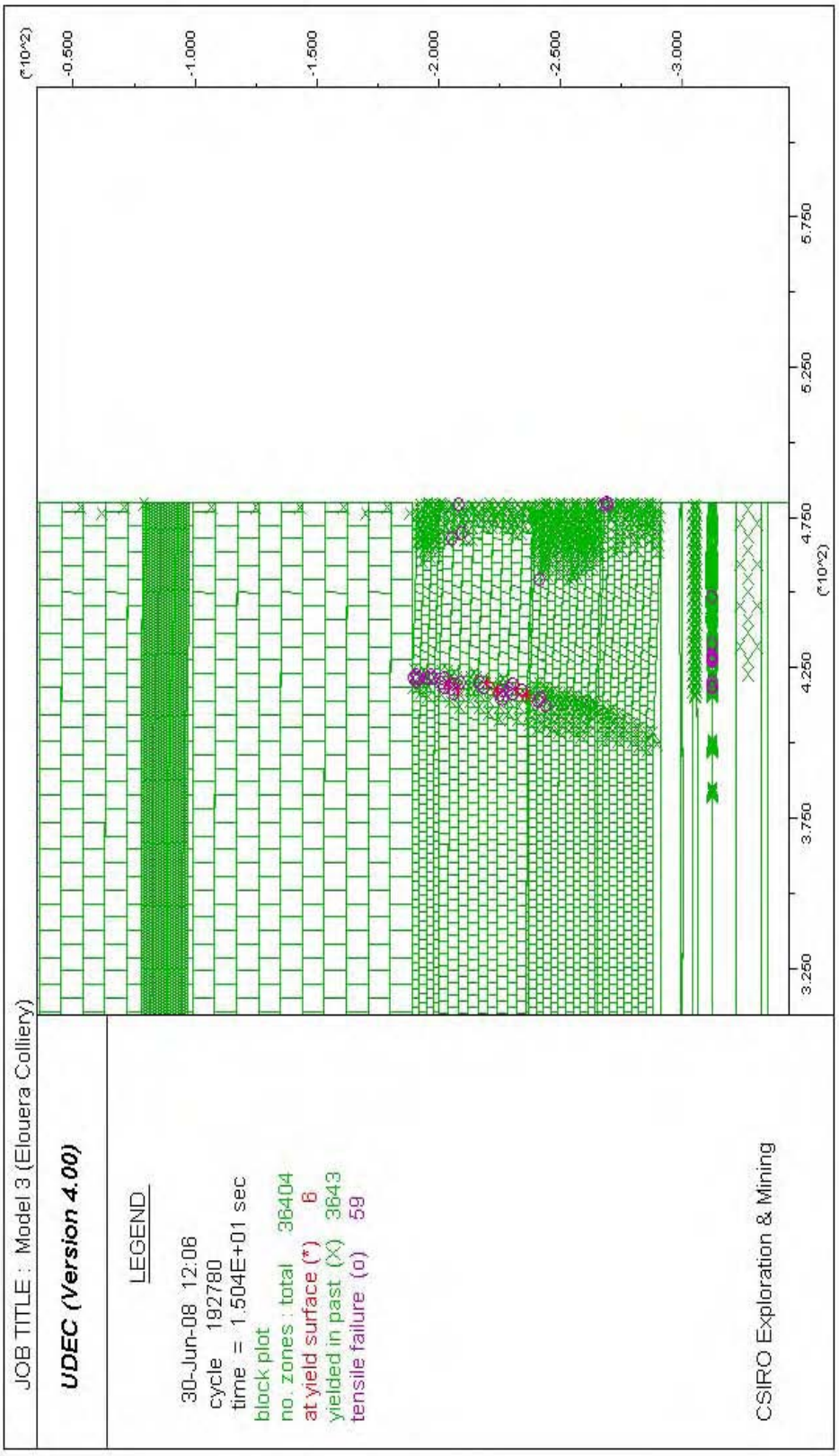

Fig. 5.33 – Detailed view of yielded zones in Model 3

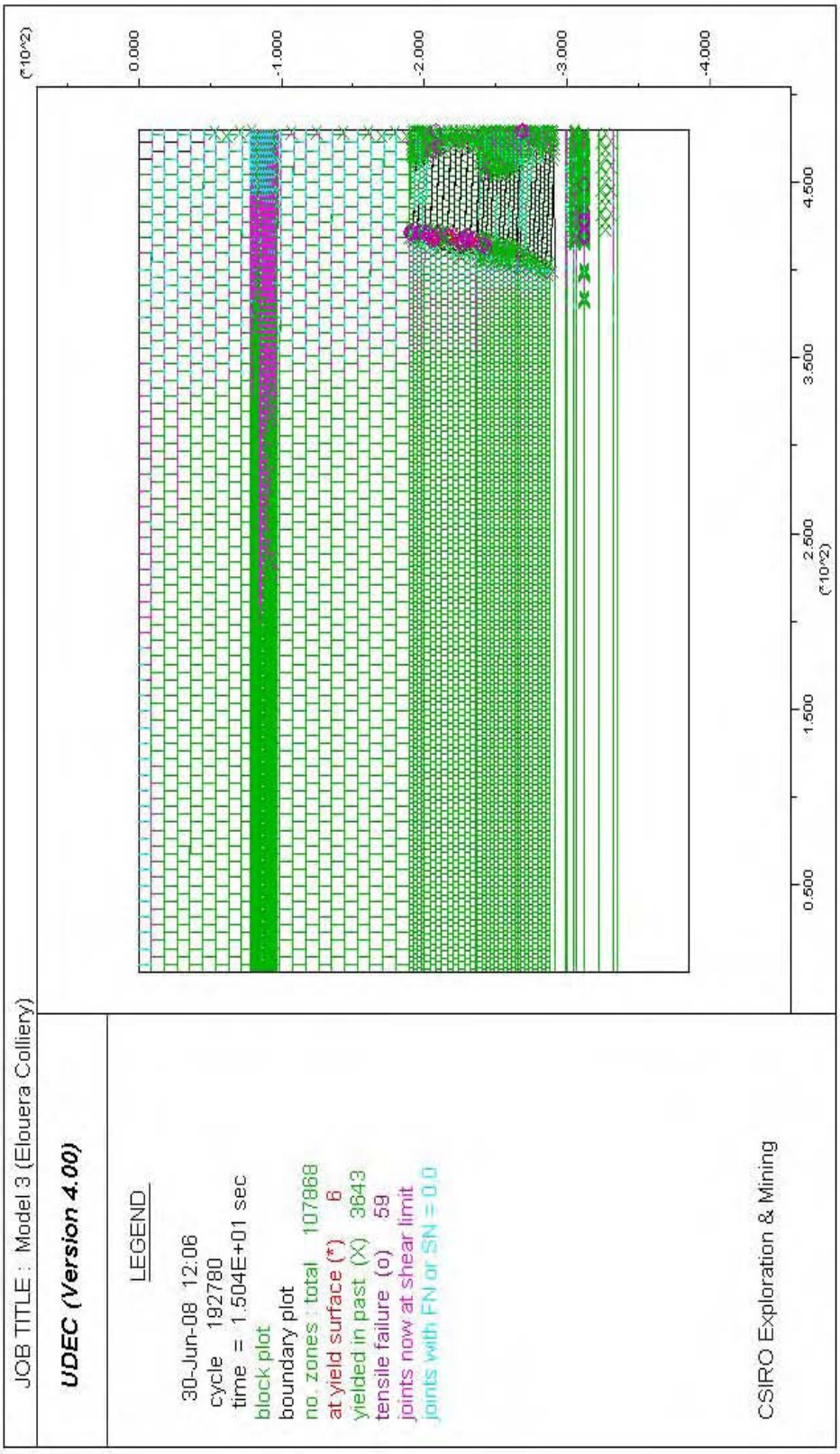

Fig. 5.34 – Yielded zones and joint slip in Model 3

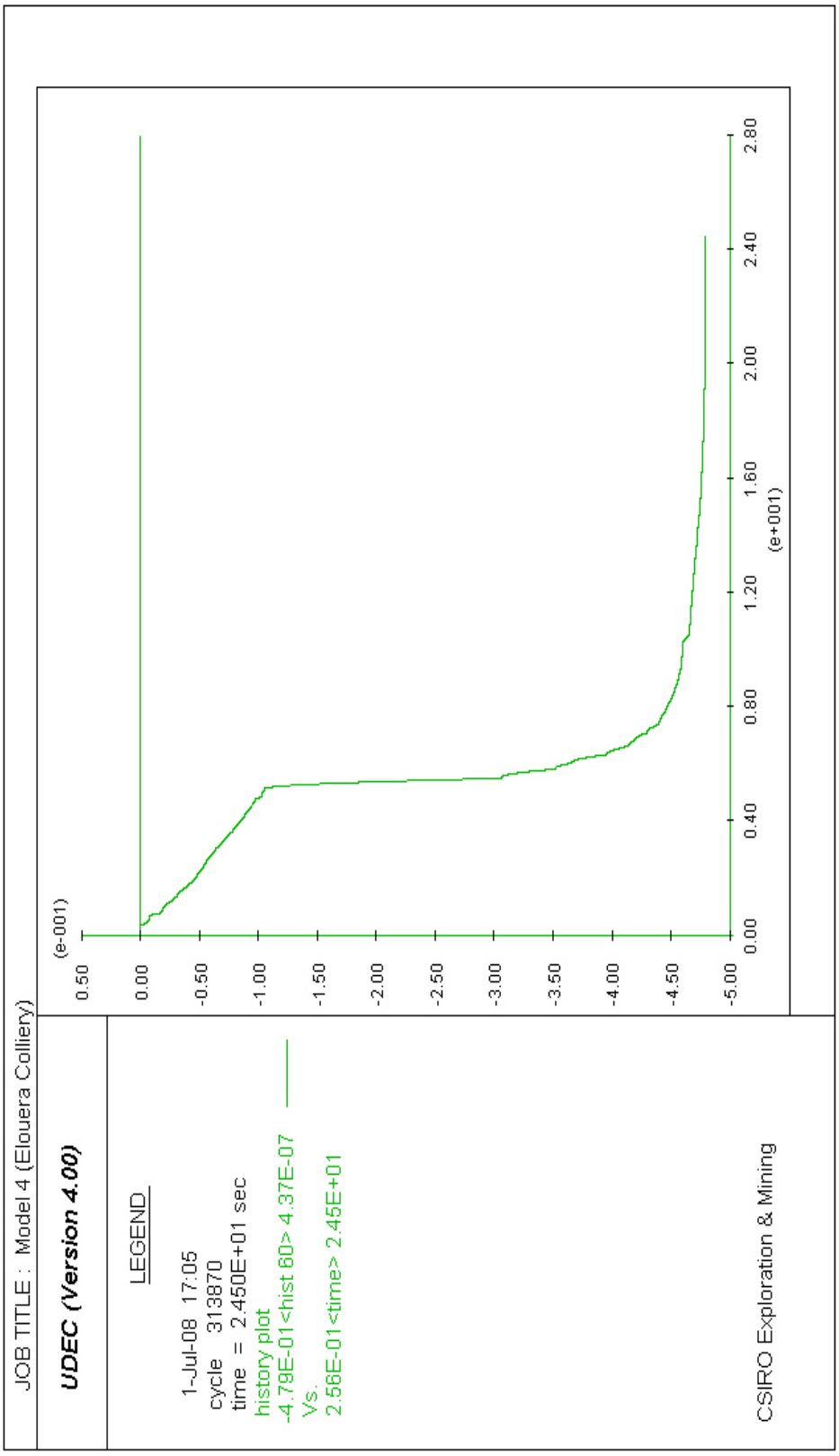

Fig. 5.35 – Development of maximum subsidence in Model 4

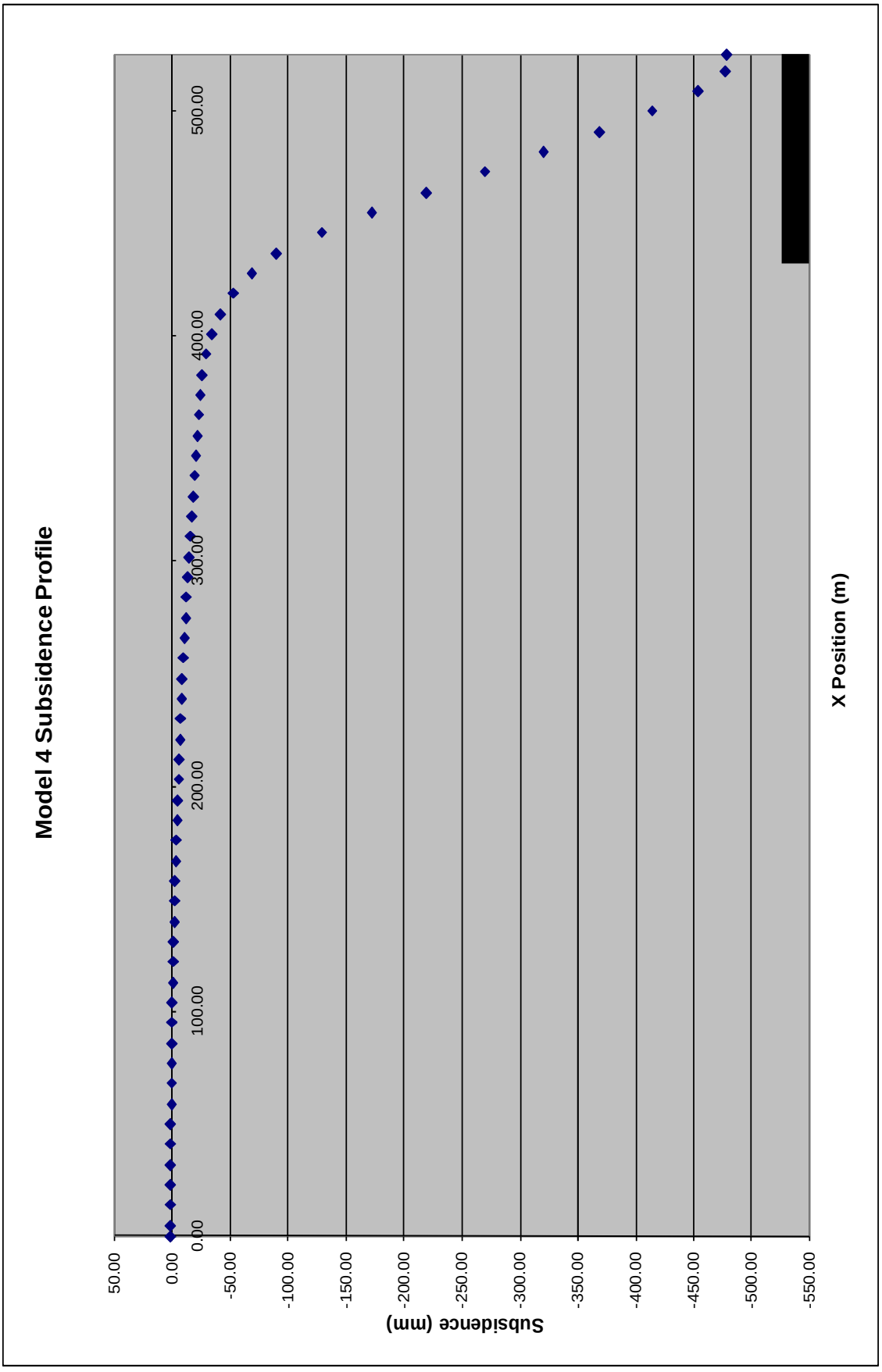

Fig. 5.36 – Subsidence profile for Model 4

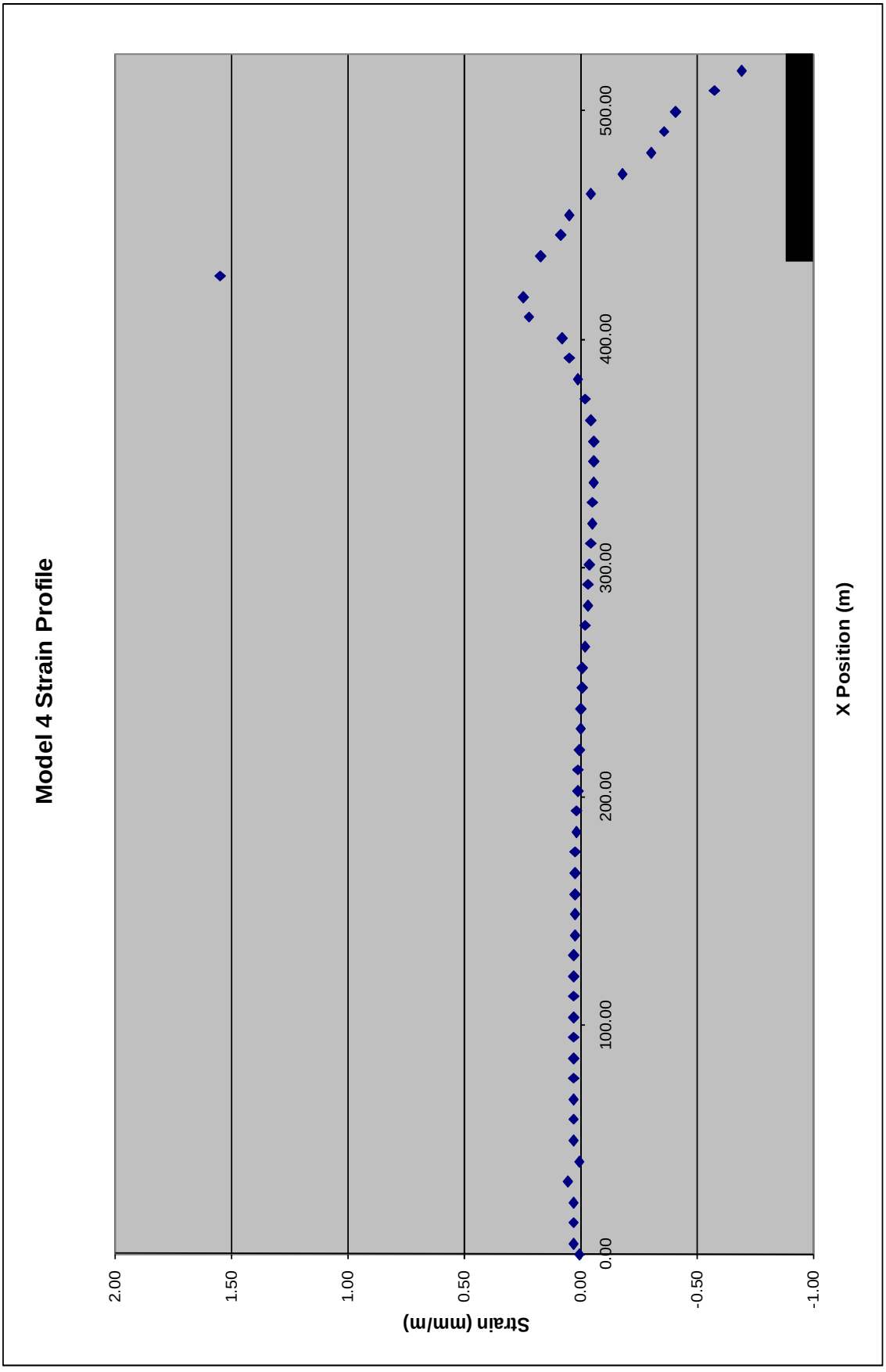

Fig. 5.37 – Strain profile for Model 4

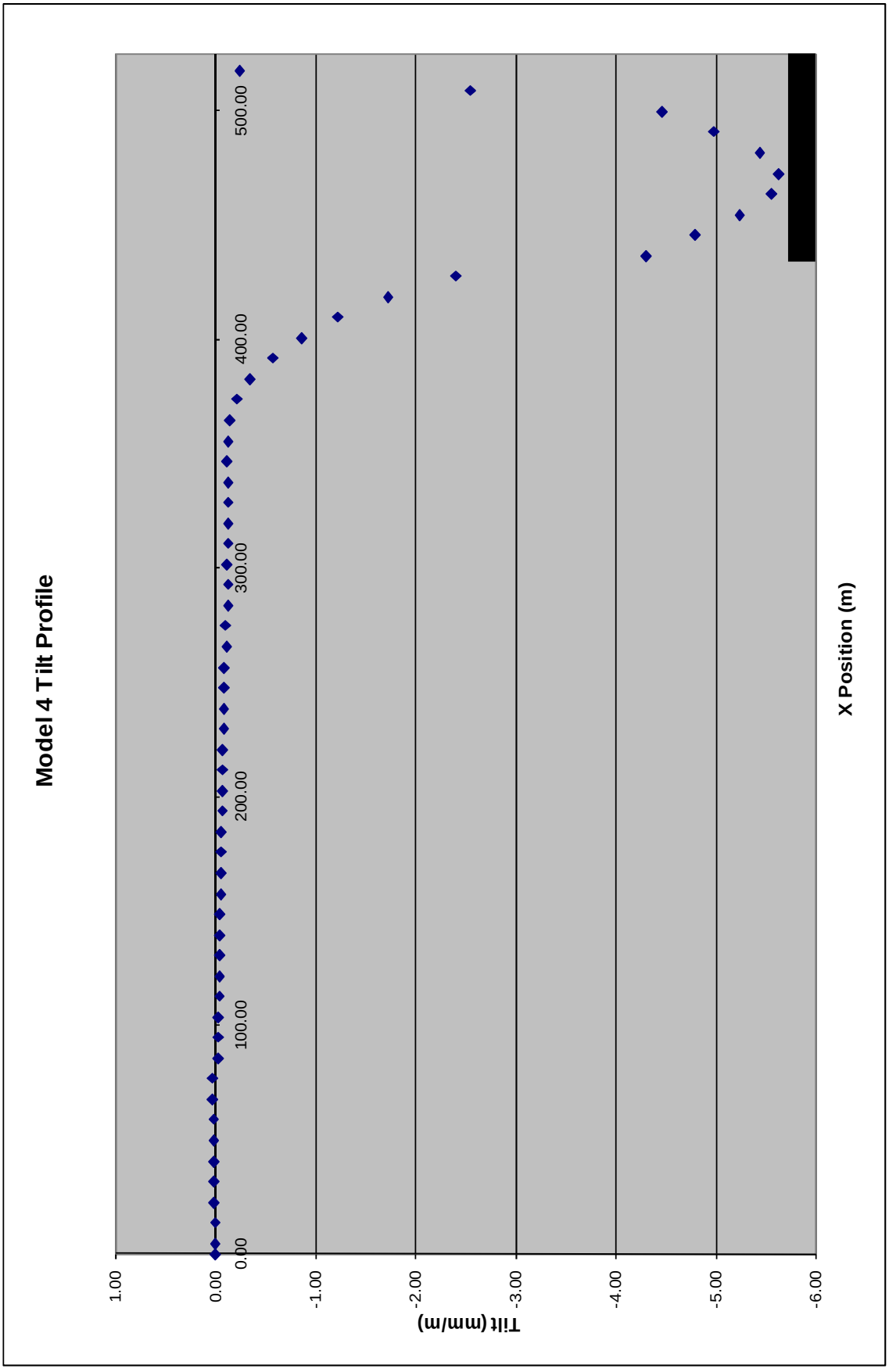

Fig. 5.38 – Tilt profile for Model 4

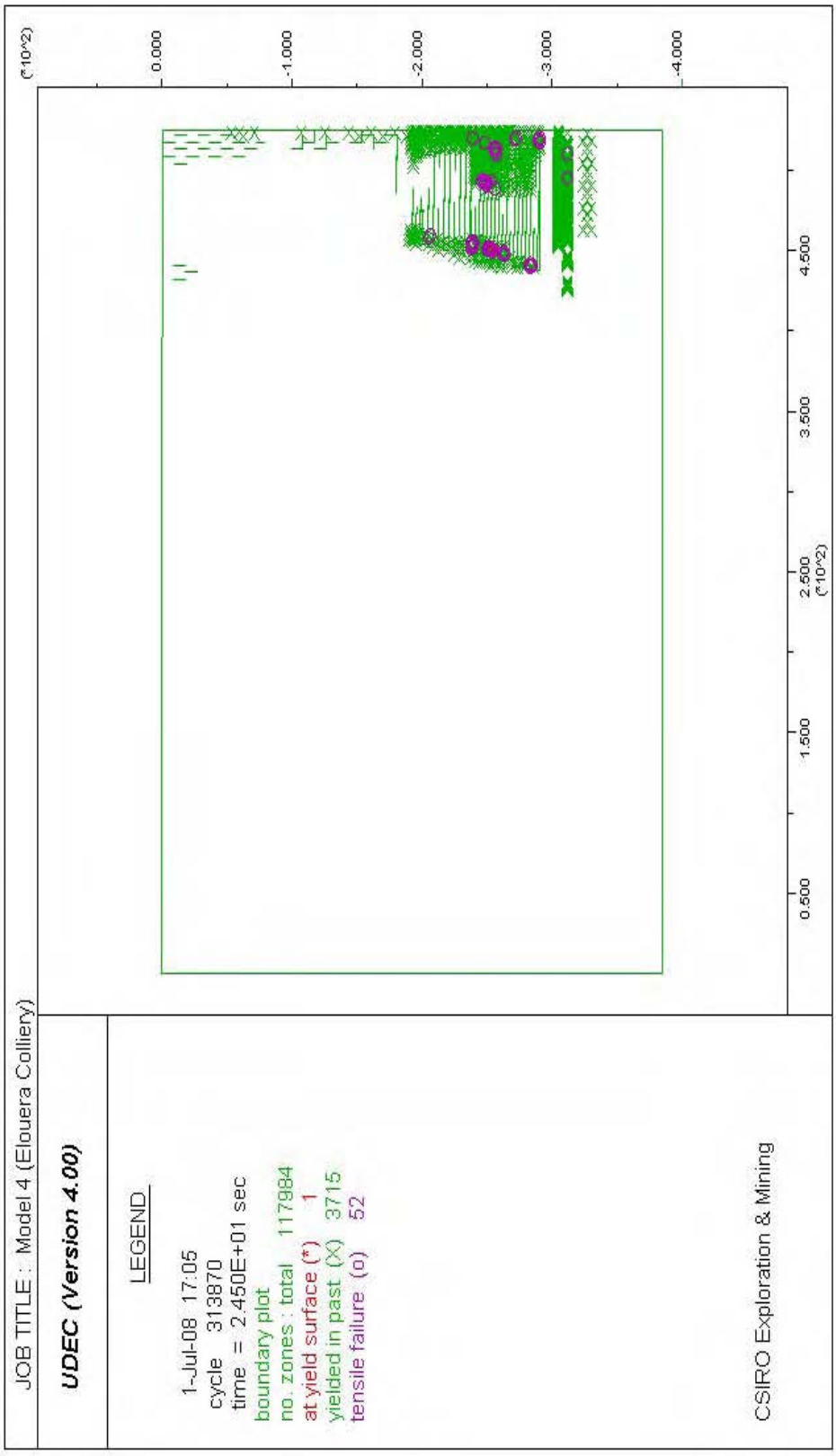

Fig. 5.39– Yielded zones and caving development in Model 4

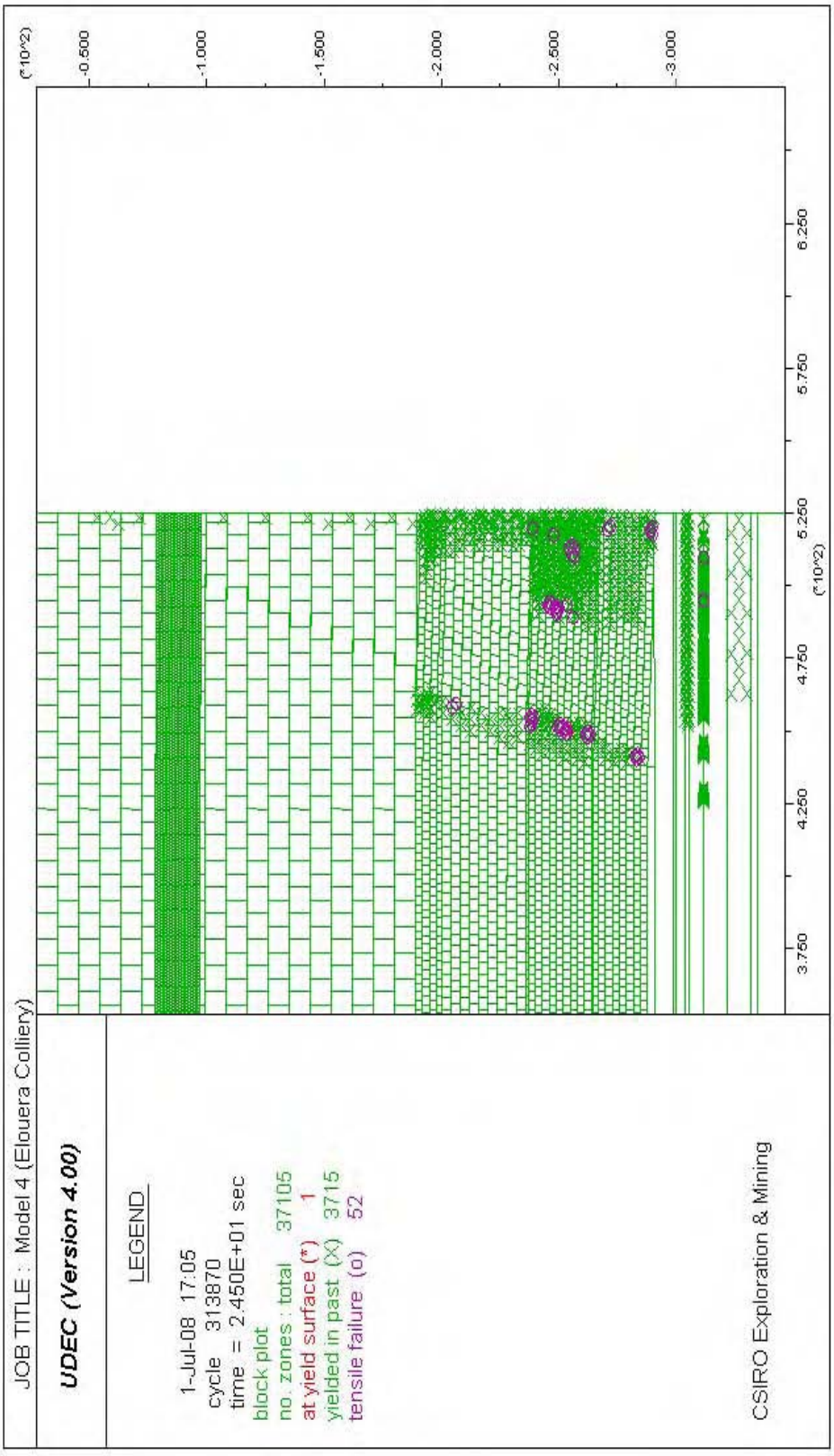

Fig. 5.40 – Detailed view of yielded zones in Model 4

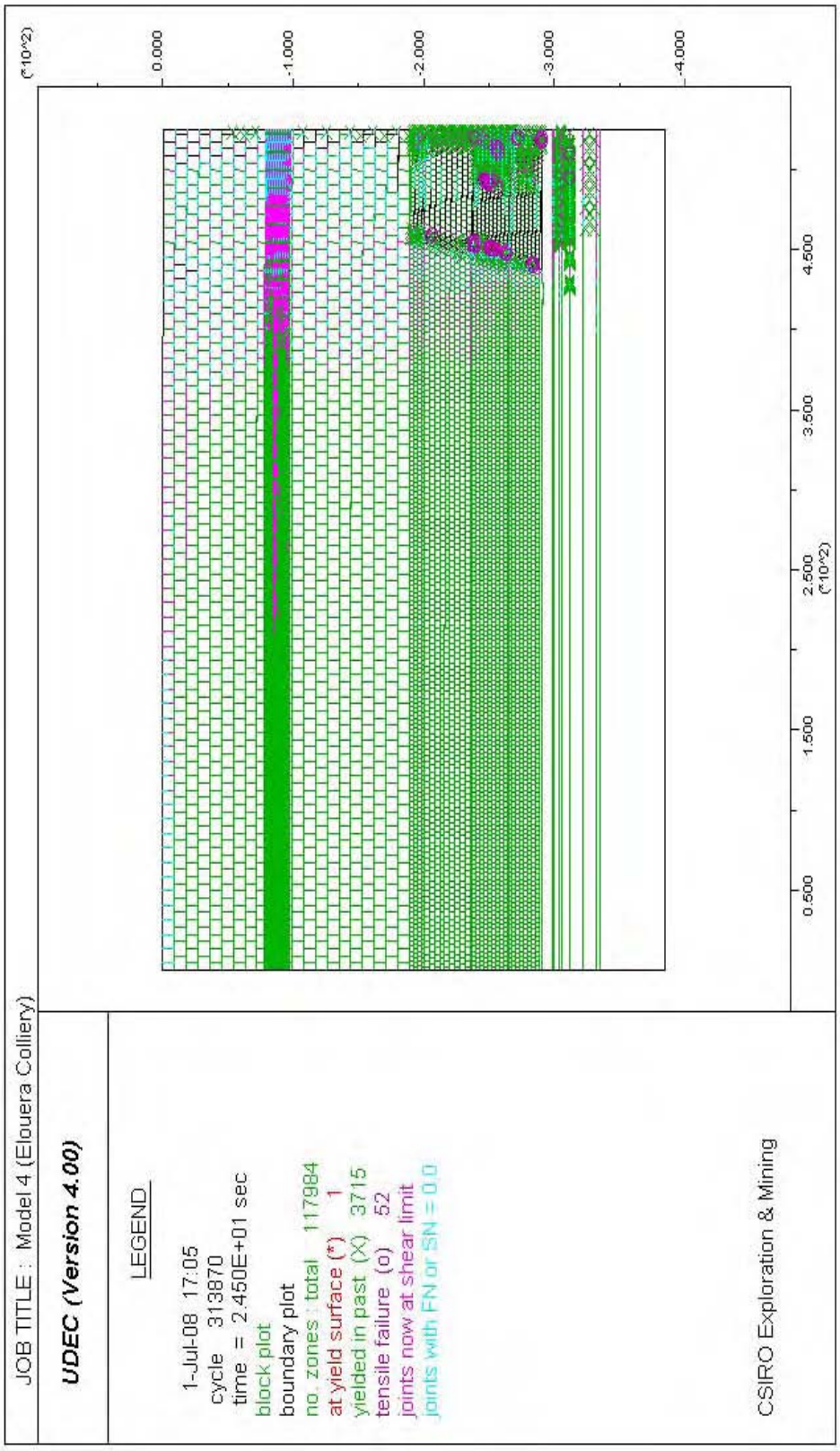

Fig. 5.41 – Yielded zones and joint slip in Model 4

The subsidence development plots (Figures 5.14, 5.21, 5.28 and 5.35) illustrate that the models had been cycled to equilibrium until the maximum developed subsidence stabilised and stopped increasing. This model state was paramount as the quality of the final results would have been compromised if this state was not reached.

It can be seen that the subsidence profiles (Figures 5.15, 5.22, 5.29 and 5.36), strain profiles (Figures 5.16, 5.23, 5.30 and 5.37) and tilt profiles (Figures 5.17, 5.24, 5.31 and 5.38) are generally in the expected theoretical shape. The subsidence profiles for all models indicate that the boundaries were at a sufficient distance from the longwall extractions. The 'noise' in the strain profiles for all models was also evident.

It can also be seen from Figures 5.18, 5.25, 5.32 and 5.39 that caving develops with accordance to the conceptual subsidence model for the Southern Coalfield (Chapter 2). Except for Model 1 where the longwall panel may have been too narrow to initiate substantial caving, it can be seen from Figures 5.19, 5.26, 5.33 and 5.40 that the goaf angle for Model 2 was between 11° to 25°, Model 3 was 14° to 25°, and Model 4 was 13° to 25°. This compared favourably with numerical modelling by CSIRO Exploration and Mining and Strata Control Technology (1999) of the caving in the Southern Coalfield that supported a goaf angle value of 12º.

Caving and cracking events are generally contained below the base of the Bulgo Sandstone. In Models 3 and 4, the cave zone penetrated through the base of the Bulgo Sandstone which suggested that the Bulgo Sandstone is the major control on subsidence up to W/H ratios of approximately 0.5 (Chapter 2). Once the Bulgo Sandstone fails, it is no longer the massive spanning unit that controls subsidence, resulting in a large increase in the subsidence factor. This trend is evident in the empirical prediction curve (see Figure 5.8) and was reflected by the subsidence factors of Model 3 and Model 4. It was also noticed that the caving of the goaf was not really a massive combination of block yield and rotations, but more a gradual settling and deflection of the roof strata. This would have resulted in substantially less bulking in the goaf, but does not seem to be an issue as far as subsidence predictions are concerned. The failure to produce bulking in the goaf was also noted by Coulthard (1995).

Figures 5.20, 5.27, 5.34 and 5.41 illustrate the yielded zones of each model, combined with joint slip. It can be seen that as W/H increases, so does the amount of joint slip in the vertical and horizontal direction. It was noted that joint slip was more prominent in rock units that had closely spaced joints. This can be seen in Figures 5.27, 5.34 and 5.41, where substantial joint slip is evident in the Newport Formation and Bald Hill Claystone.

From the results, it can be seen that the numerical models are satisfactorily verified by the empirical results when it comes to subsidence predictions and the prediction of the shape of the subsidence trough over single longwall panels.

5.13 SUMMARY

In this chapter, a set of UDEC numerical models was developed to simulate single panel longwall extractions. The process of creating the models, including the compilation of material/joint properties and the determination of the geometry for each individual model was discussed. It was emphasised that all the material/joint properties should be transparent and fully traceable to minimise the appearance of 'adjusting' certain parameters to fit a predefined outcome.

From the results, it was seen that the numerical models provided quite a good match to the empirical results, and the caving development evident in the numerical models also agreed with the caving characteristics discussed in Chapter 2 and supported the theory that the Bulgo Sandstone is the control on sub-critical subsidence. Overall, it was concluded that the numerical models were satisfactorily verified by the empirical results and a major outcome of this modelling was the creation of a tool that can be used for sensitivity studies to identify the key controlling parameters. The formation of numerical models that contain a river valley is the subject of the next chapter. These numerical models will share the basic characteristics as the models discussed in this chapter.

CHAPTER 6
SINGLE LONGWALL PANEL MODELS WITH RIVER VALLEY

6.1 INTRODUCTION

The previous chapter illustrated that UDEC is a valid tool for assessing subsidence for single longwall panel extractions in flat terrain. The objective of this chapter is to show that the mechanics of the proposed block movement model are feasible, i.e. to demonstrate block sliding and valley closure occurs with minimal upsidence when a translation plane exists at the base of the valley, and to demonstrate the occurrence of reduced valley closure and upsidence when the translation plane is below the base of the valley. The numerical models used in this chapter are quite simple and loosely based on Model 4 in Chapter 5. It must be noted that there is no comparison between the models in this chapter and the previous numerical models, as the aim of this chapter is to validate the block movement proposal, rather than create a series of prediction tools. Examples of the modelling scripts used can be found in Appendix C and Appendix D.

6.2 MODELLING STRATEGY

The mechanism of the block movement model was described in detail in Chapter 3. The key factor which governs the magnitude of valley closure and upsidence in the block movement model is the location of the translation plane and curvature/tilt. As proposed, if the translation plane is located at the base of the valley then the sides of the valley can slide on this plane, maximising valley closure and producing little upsidence. If the translation plane is located at a vertical distance below the base of the valley, then as the sides of the valleys move inwards, the horizontal beam formed by the positioning of the translation plane below the valley base is subjected to horizontal compressive stresses and negligible vertical stresses and is expected to bulge or buckle under compression, leading to increased upsidence. Following the discussion in Chapter 3, it was decided to place the translation plane one metre below the base of the valleys to maximise the potential for buckling and demonstrate the alternate block movement mechanism.

Previous explanations for valley closure and upsidence above unmined coal are attributed to redistribution of undefined horizontal stresses or movement along discontinuities, but do not take into account that the region above unmined coal is largely in the tensile or hogging phase of the subsidence profile, as illustrated in Chapter 3. The block movement model postulates that valley closure and upsidence above unmined coal and old longwall panels is a result of curvature/tilt driven en masse movement into the void created by a river valley.

In order to investigate the block movement theory with UDEC, it was decided to create a set of numerical models that were simple enough to produce results without excessive run times. With a set of reasonably simple models, validation of the block movement model with room for further enhancement was possible.

The river valley models had prescribed velocities applied to the bottom of the model (Bulgo Sandstone), in an effort to 'pull' the model down to try to recreate a subsidence profile on the surface. These displacements were based on the vertical displacement profile of the base of the Bulgo Sandstone in Model 4 from Chapter 5. It was expected that the developed subsidence profiles would not exactly match the profile from Model 4, due to the modelling of the upper 70 m of Hawkesbury Sandstone as solid blocks to represent valley closure as en masse movements, or due to the presence of a translation plane. This approach was taken simply to investigate the block movement model by reducing run times through the elimination of the modelling of the caving process.

6.3 INITIAL MODELS AND MESH DENSITY ANALYSIS

Before modelling of river valleys was able to commence, a set of initial test models was constructed and run with the purpose of investigating the impact of various assumptions and simplifications. It must be noted that the initial test models did not excavate and model valleys as the focus was on devising a process that would deform the base of the models in a manner that was consistent with Model 4.

The purpose of the initial modelling was:

- To create a methodology that would adequately replicate the vertical displacements of a chosen rock unit in Model 4 and eliminate the need to model the caving process,
- To investigate the effects of the removal of bedding and joints from the top 70 m of the Hawkesbury Sandstone, and
- To ensure that the chosen base of the river valley models did not impact on the subsequent model results.

The incorporation of these changes meant that it was not necessary to model the caving process (which was noted in Chapter 5 to be largely contained by the Bulgo Sandstone, and which also accounted for the majority of running time). The removal of bedding planes and joints in the top 70 m of the Hawkesbury Sandstone was performed to see if the observation of rigid body type movement (Holla & Barclay 2000) was present in the initial models.

In order to determine what rock units could be taken out of the model, the vertical displacements at the base of the Hawkesbury Sandstone, Newport Formation, Bald Hill Claystone and Bulgo Sandstone were compared to the vertical displacements at the surface. A graph of the vertical displacements for the above mentioned units is shown in Figure 6.1. It can be seen from Figure 6.1 that the vertical displacements at the base of the Bald Hill Claystone were slightly different to the vertical displacements at the surface, whilst the vertical displacements at the base of the Bulgo Sandstone were also slightly different except for those at the centre of the longwall panel. The displacements noted at the centre of the longwall panel in Figure 6.1 were most likely a result of bedding planes separating after yield in tension. The Bulgo Sandstone in Model 4 experienced some tensile cracking at its base and was sagging into the caved zone, hence the large increase in vertical displacement at the centre of the panel. It was considered making the Bald Hill Claystone the base of the new models, but there was a chance that any element failure may have encroached the areas of interest hence it was decided that the Bulgo Sandstone would form the base of the river valley models.

In order to replicate the vertical displacements at the base of the Bulgo Sandstone in the river valley models, a three metre thick beam was incorporated into the base of the Bulgo Sandstone by creating a bedding plane and assigning very high cohesion, friction angle and tensile strength to prevent detachment from the base of the Bulgo Sandstone. This beam had a vertical joint spacing of nine metres so it directly coincided with the vertical joint spacing of the Hawkesbury Sandstone, from which the vertical displacements were monitored. These vertical joints were also assigned very high strength parameters to prevent separation.

According to the UDEC User's Guide (Itasca 2000), displacements cannot be controlled directly in UDEC. To deform a boundary to a desired profile, it is necessary to prescribe the boundary's velocity for a given number of steps. For example, if the desired displacement at one point is D, a velocity, V, is applied for a time increment, T (i.e., $D = VT$), where $T = \Delta tN$, Δt is the timestep and N is the number of steps (or cycles). In practice, V should be kept small and N large, in order to minimise shocks to the system being modelled.

The process to pull down the base of the river valley models so the base of the model matched the base of the Bulgo Sandstone in Model 4 was as follows:

1. Fix the sides of the model and cycle for one step to obtain the time step,
2. Identify grid points at the base of the model to which velocities will be attached,
3. Define the maximum displacement for each previously identified grid point (as derived from the displacement profile for the Bulgo Sandstone in Model 4),
4. Calculate the y velocity for the identified grid points using $V = D/\Delta tN$,
5. Assign y velocities to grid points, and
6. Cycle model for N cycles.

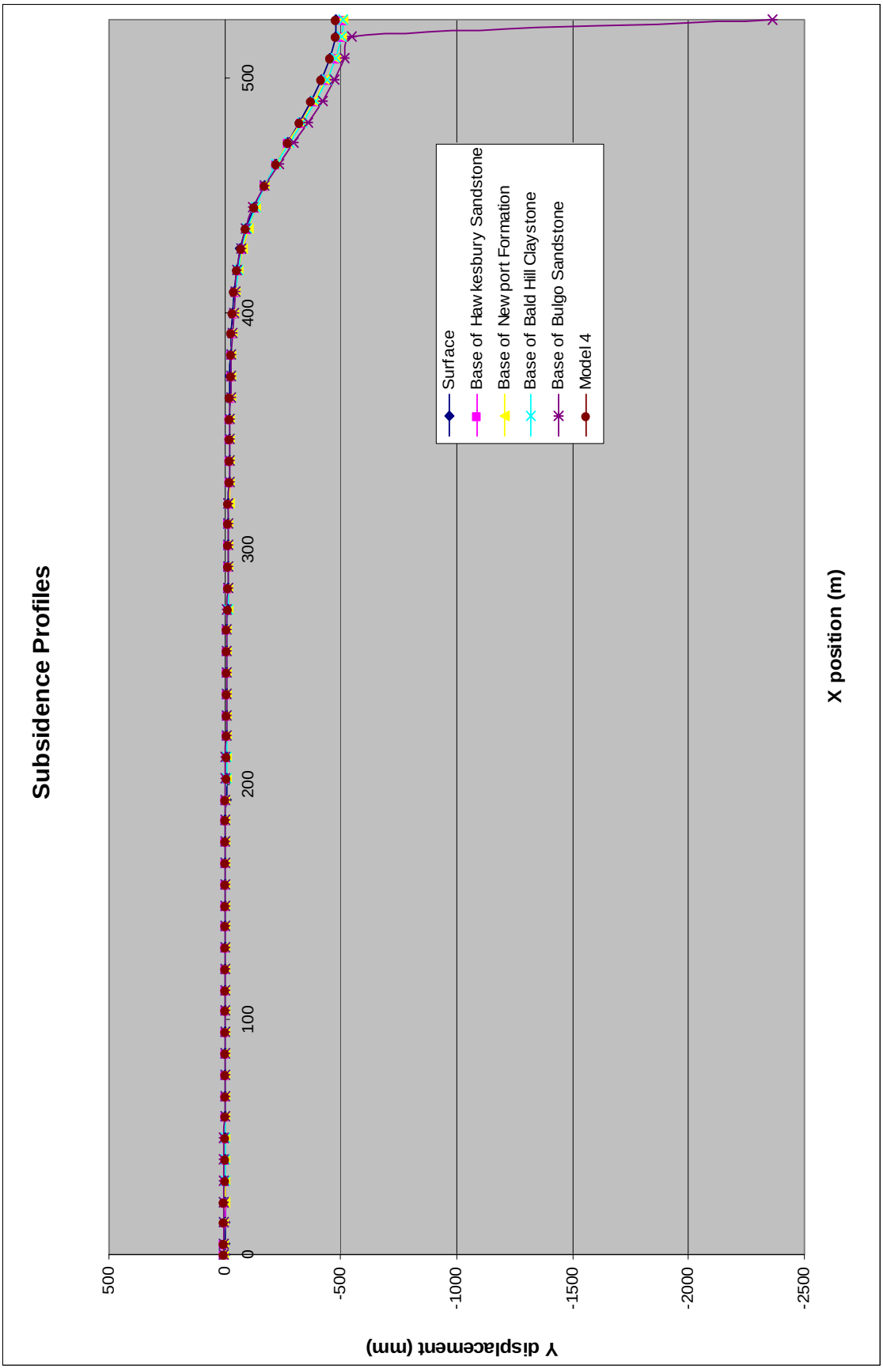

Fig. 6.1 – Y-displacements on the surface and at the base of various rock units

To identify the optimum number of steps (*N*), a series of initial models with the translation plane at the base of the valley was set up for different values of *N* (100, 1000, 10000, 20000, 30000, 40000, 50000 and 100000). The vertical displacements at the base of the Bulgo Sandstone was monitored for each of these models and compared with Model 4, and the subsidence profile on the surface was also compared to that of Model 4. Yielded zones were also noted to ensure that the base of the models was at a sufficient distance below the river valleys.

The geometry of the valleys is a typical representation of valleys in the Southern Coalfield. The valleys were 70 m deep and 50 m wide (CSIRO Petroleum 2002). For these simple numerical models, the valleys were assumed to have vertical sides and the rectangular geometry remained constant, no changes were made to the valley depth, valley width or slope of the valley sides. The valleys were modelled by creating a bedding plane at a depth of 70 m in the Hawkesbury Sandstone and creating vertical joints 50 m apart. The vertical joints were arranged so that the central valley was situated directly above the longwall centreline. For the models that contained the translation plane at the base of the valleys, the horizontal joints at the bottom of the blocks that formed the valleys were assigned the same strength parameters as the bedding planes in Chapter 5. For the models that contained the translation plane one metre below the valleys, the translation plane was assigned the same bedding plane properties as detailed in Chapter 5, whilst the horizontal joints at the base of the valleys were assigned very high strength parameters to eliminate the effect of those joints. The remaining material, joint and bedding plane properties remained the same as the models in Chapter 5, as did the constitutive models and in-situ stress regime (K = 2), in an effort to maintain consistency. Symmetry was not able to be used because of the presence of the valley.

The geometry of the initial models can be seen in Figure 6.2. It must be noted that no valleys were excavated at this stage since the purpose of these models was to determine the optimum number of cycles required to minimise model run times and provide consistent results. The width of the initial models was 1050 m and the depth was 189 m. Figure 6.3 illustrates the mesh (finite different zoning in the blocks) and it can be seen that it is the same as used in Model 4 (see Figure 5.1) and this has been kept constant in the initial river valley models only.

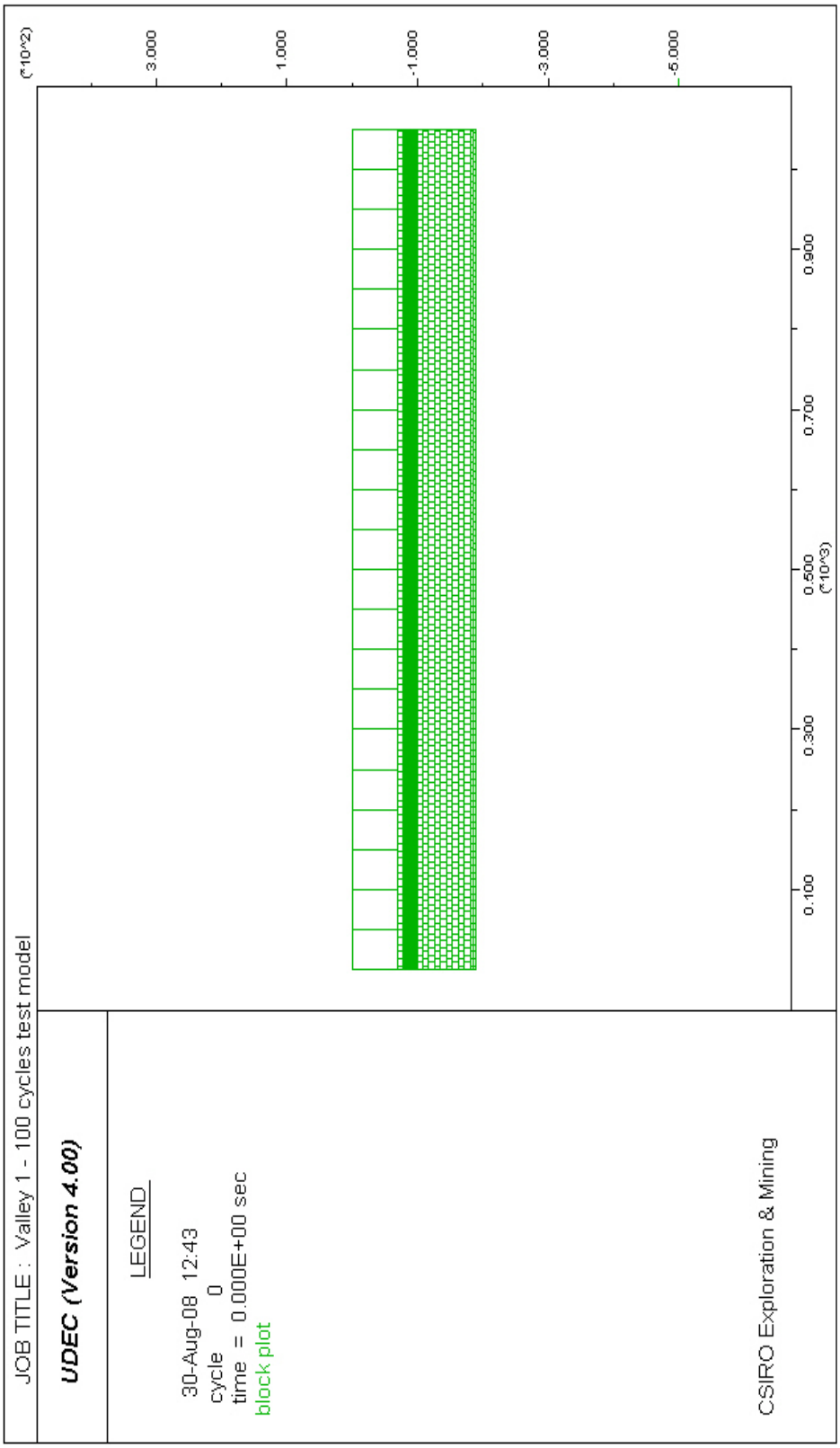

Fig. 6.2 – Geometry of initial river valley models

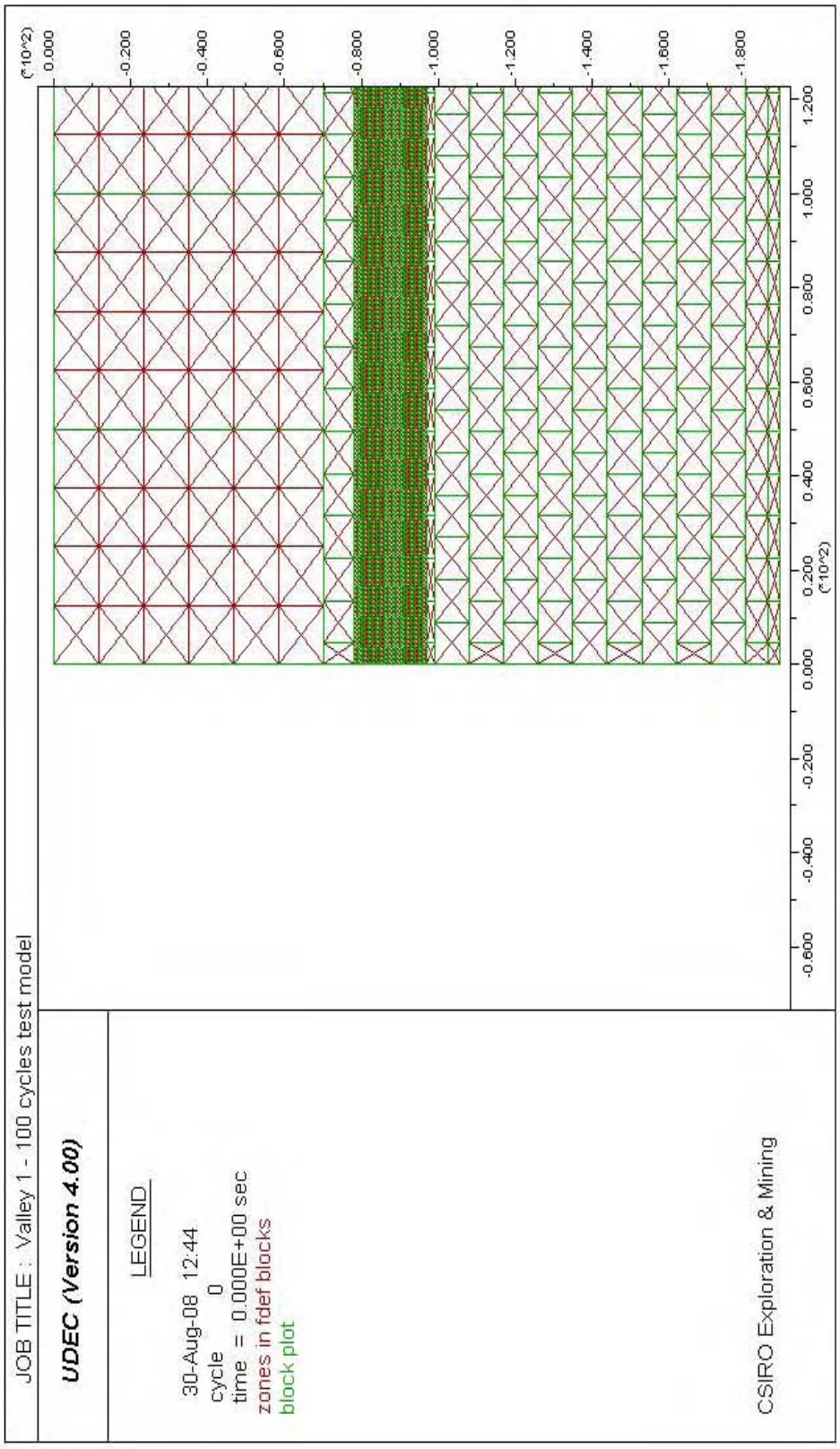

Fig. 6.3 – Finite different zoning used in valley models

The subsidence results from the initial river valley models are summarised in Table 6.1.

Table 6.1 – Subsidence results from initial river valley models

Model	Run time (minutes)	Maximum subsidence (mm)
100cycles	25	13
1000cycles	30	124
10000cycles	90	196
20000cycles	120	200
30000cycles	150	201
40000cycles	180	201
50000cycles	210	201
100000cycles	420	200

The displacements at the base of the models (base of Bulgo Sandstone) for the models in Table 6.1 are compared against Model 4 in Figure 6.4. The results from Table 6.1 are represented in Figure 6.5.

It can be seen from Figure 6.4 that the method of attaching y velocities to required points and cycling for *N* steps exactly replicated the required profile. From Figure 6.5, it can be seen that the resultant subsidence profiles did not match the profile from Model 4, with the maximum developed subsidence in the river valley models 42 % of the maximum developed subsidence in Model 4. This was expected due to the lack of bedding and joints in the upper 70 m of the Hawkesbury Sandstone.

It can be seen from Figure 6.5 that the maximum developed subsidence flattened out at approximately 200 mm. To ensure that any yielded zones did not impact on the area near the translation plane or the valleys, Figure 6.6 shows the yielded zones for N = 30,000 cycles. It can be seen that the yielded zones were restricted to the base of the model (in the beam attached to the base) and did not impact on the areas of interest. It was decided to use N = 30,000 cycles for the subsequent river valley models as it was a reasonable compromise between maximum developed subsidence (201 mm) and run time (150 minutes) and the model did not produce unwanted yielding in the areas of interest.

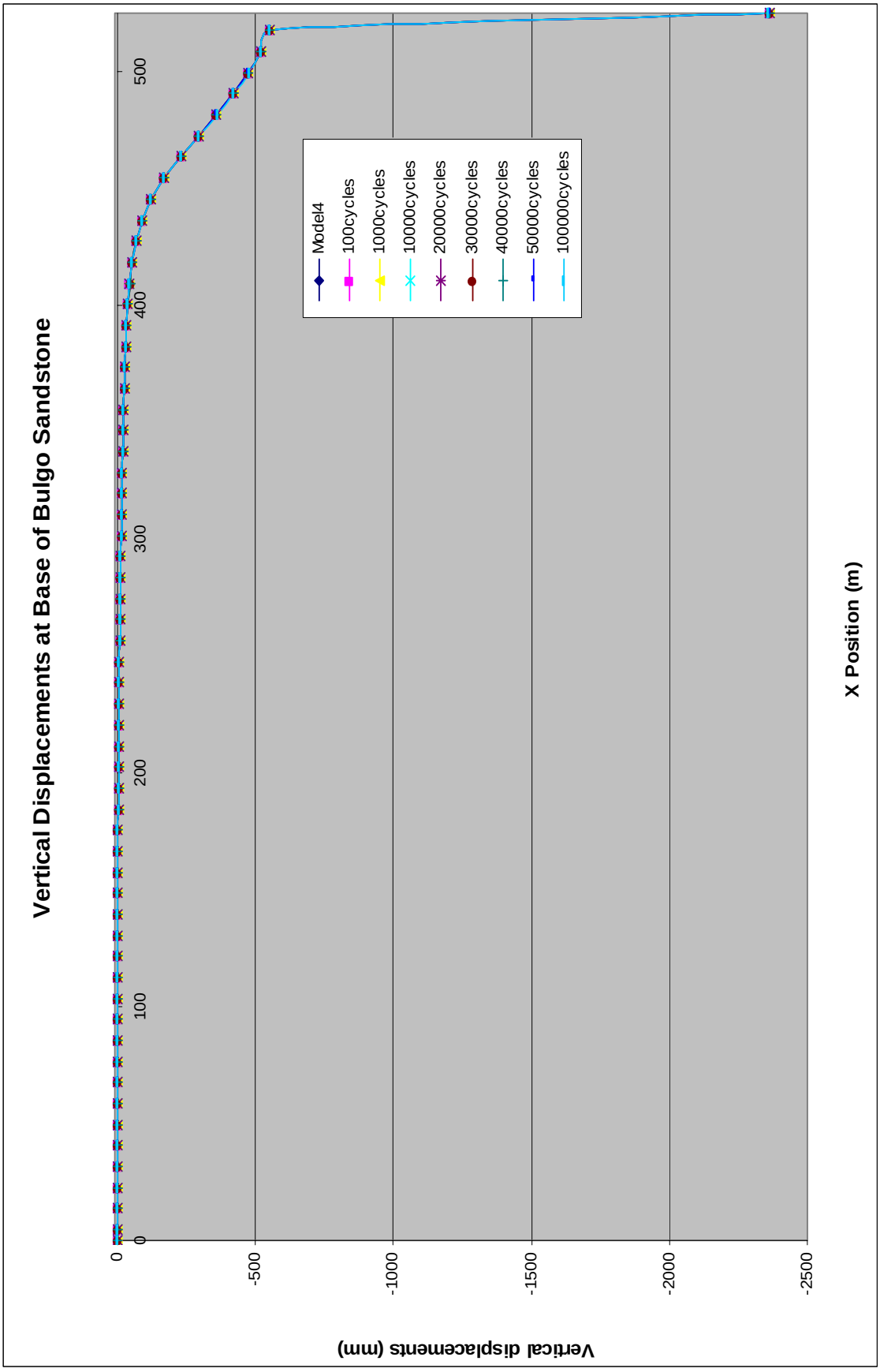

Fig. 6.4 – Vertical displacements at base of Bulgo Sandstone

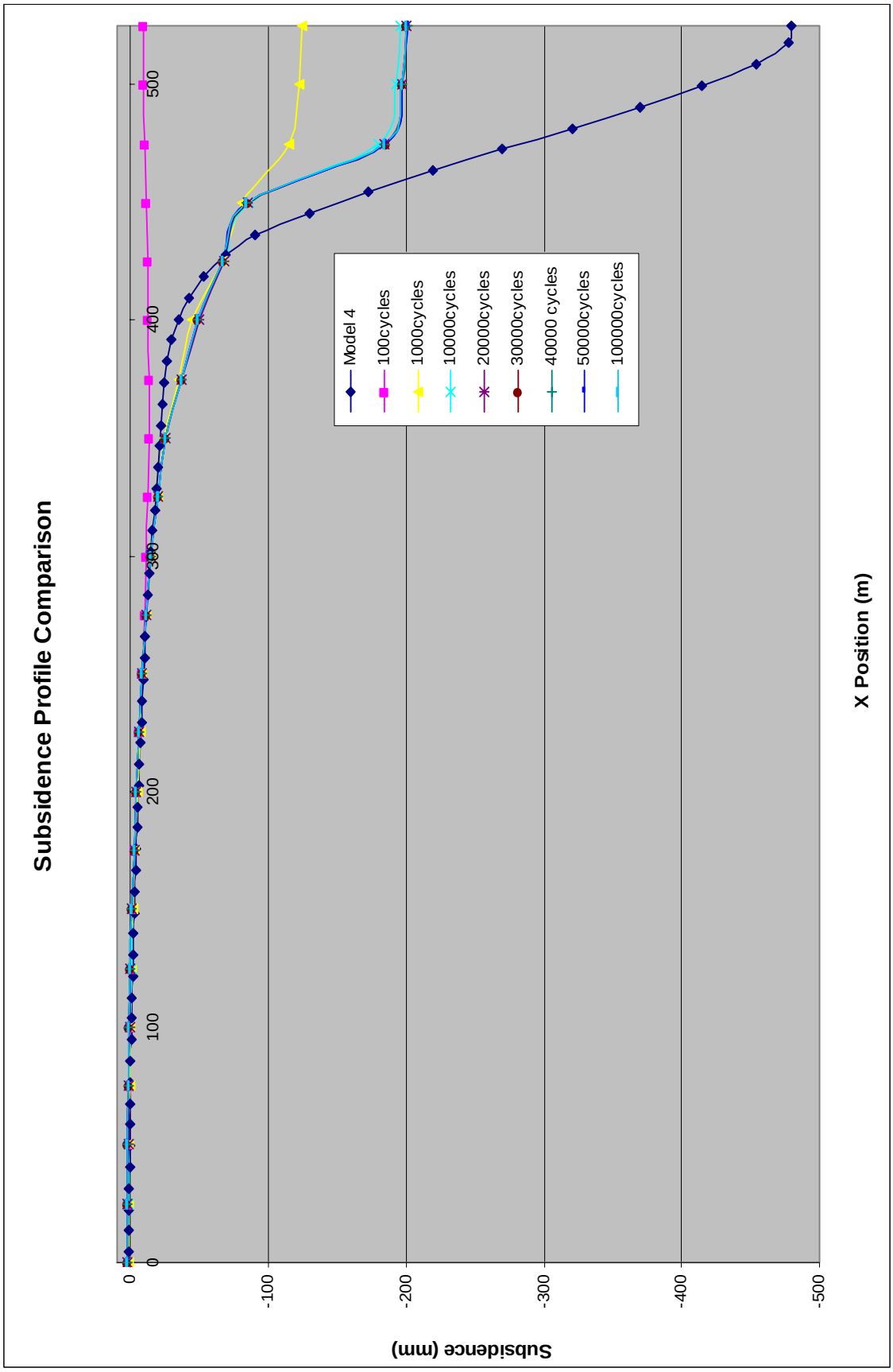

Fig. 6.5 – Subsidence profile comparison for varying cycles (N)

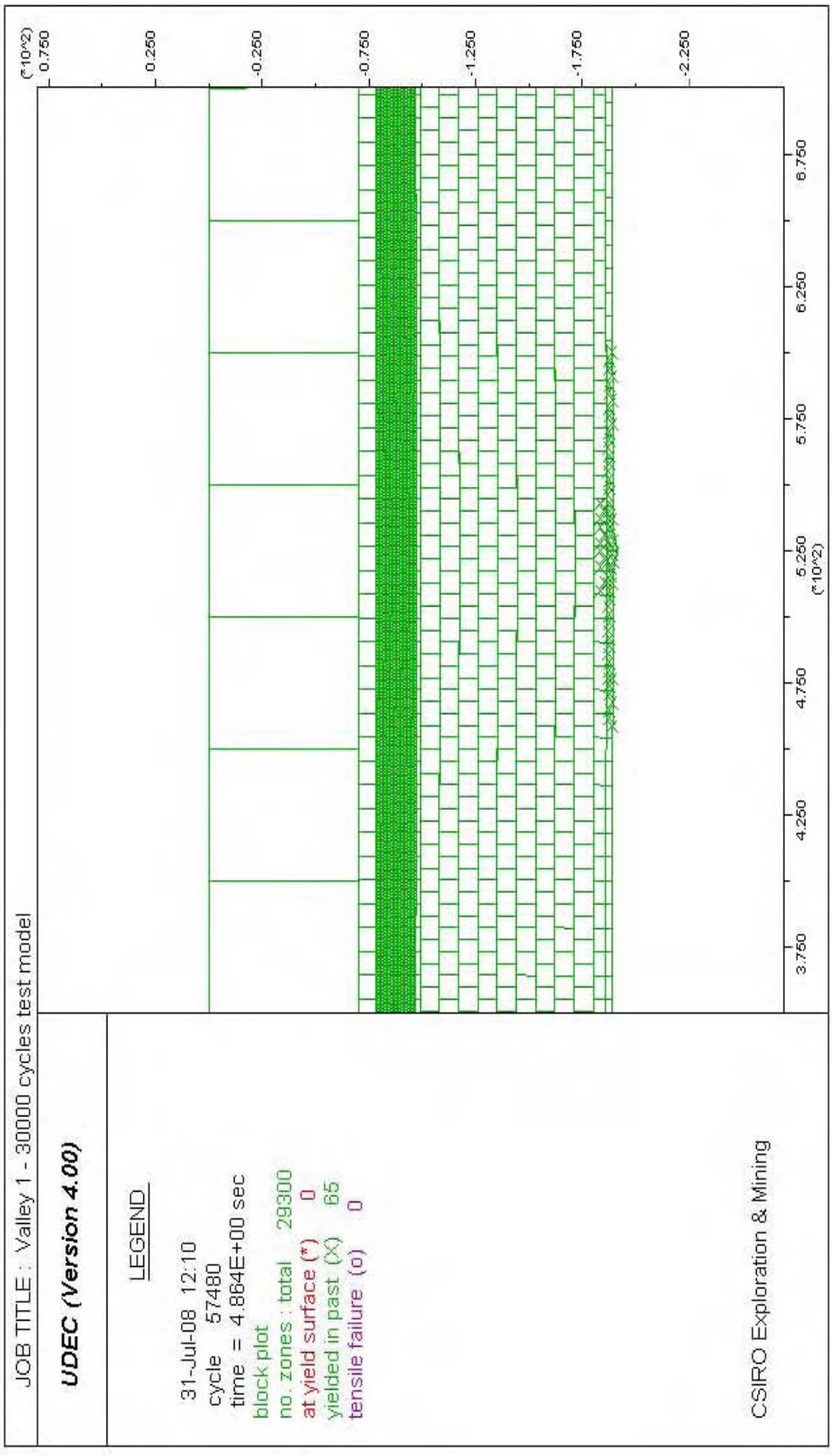

Fig. 6.6 – Yielded zones for N = 30,000 cycles

The next step was to examine the effect that bedding and joints in the upper 70 m of the Hawkesbury Sandstone had on the developed subsidence profile. Figure 6.7 is an illustration of a river valley models with bedding only, and Figure 6.8 is with bedding and joints. The maximum developed subsidence from these models is contained in Table 6.2. The subsidence profiles from the models in Figure 6.7 and Figure 6.8 are shown in Figure 6.9, along with the subsidence profile from Model 4.

Table 6.2 – Subsidence results with bedding and joints (N = 30,000)

Model	Maximum subsidence (mm)
Bedding	398
Bedding and joints	424
Model 4	479

It can be seen from Table 6.2 and Figure 6.9 that the addition of bedding planes and joints had a substantial impact on the maximum developed subsidence. As expected, the absence of bedding planes and joints in the upper 70 m of the Hawkesbury Sandstone served to reduce the development of subsidence due to the upper 70 m acting like solid blocks. It was anticipated that the inclusion of bedding and joints in a river valley model would result in the valley sides ‘leaning in’ in a staggered fashion. The addition of bedding planes resulted in the maximum subsidence being 83 % of that from Model 4, whilst the addition of bedding planes and joints resulted in the maximum subsidence being 88 % of that from Model 4. Compared to the models in Table 6.1, the addition of bedding planes and joints resulted in a 111 % increase in maximum subsidence.

Figure 6.10 and Figure 6.11 show the yielded zones in the bedding only and bedding and joints models respectively. It can be seen that the yielded zones were generally contained to the base of the Bulgo Sandstone, although there is one single yielded element in the side of a yet to be excavated river valley. This single yielded element was not considered to be of any significance.

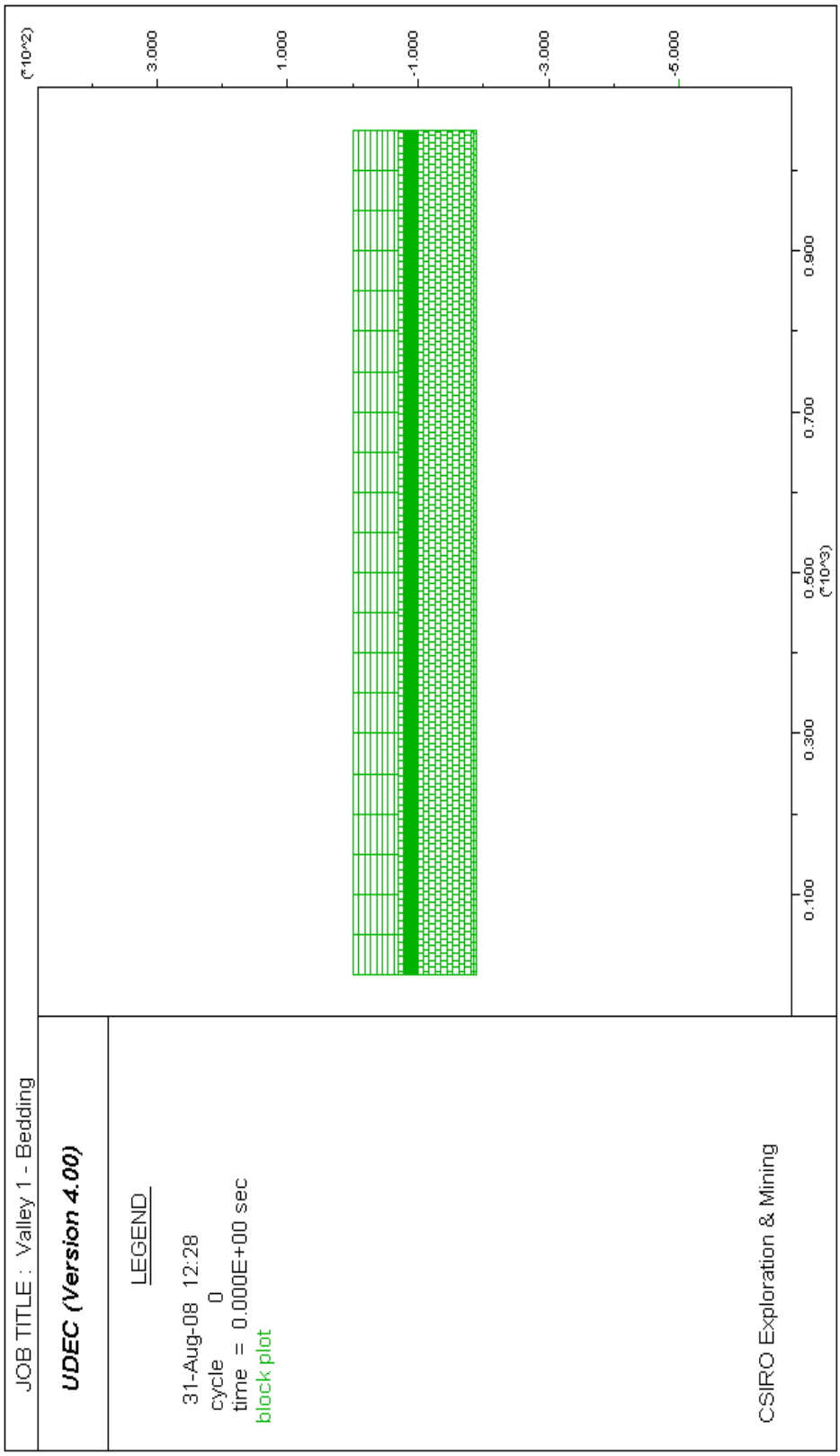

Fig. 6.7 – Model with bedding in upper 70 m of Hawkesbury Sandstone

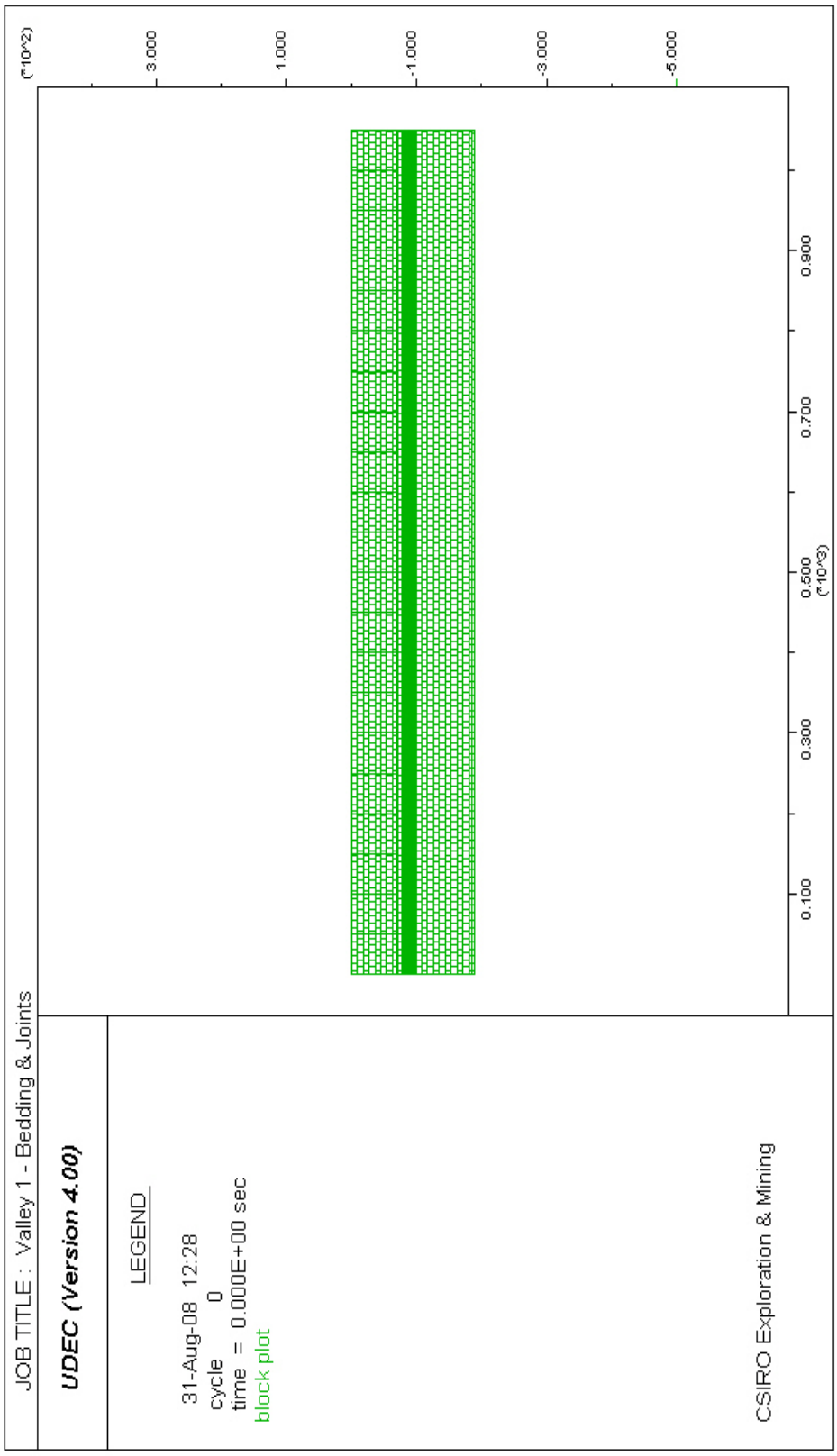

Fig. 6.8 – Model with bedding and joints in upper 70 m of Hawkesbury Sandstone

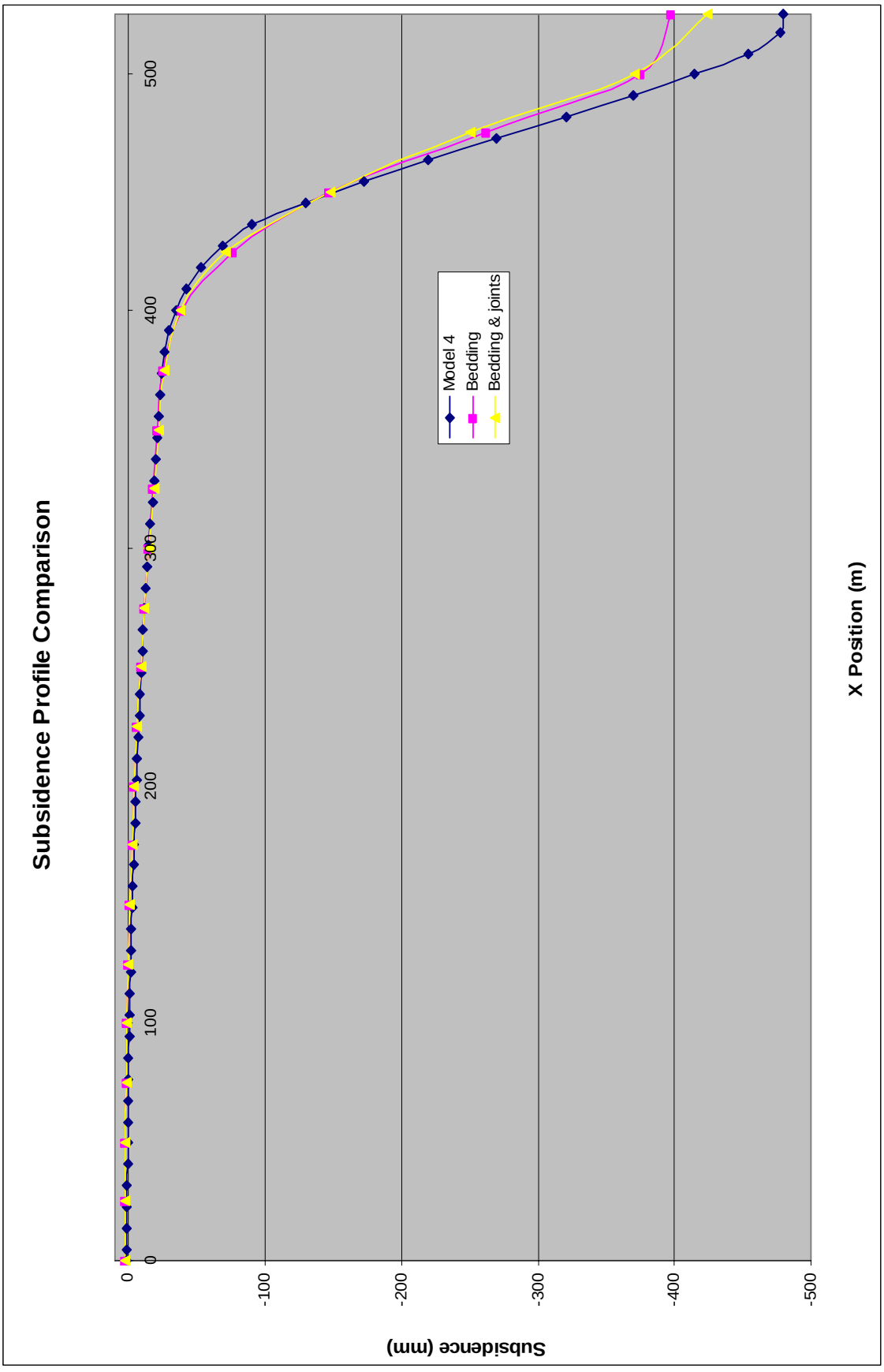

Fig. 6.9 – Subsidence profile comparison for bedding and joints

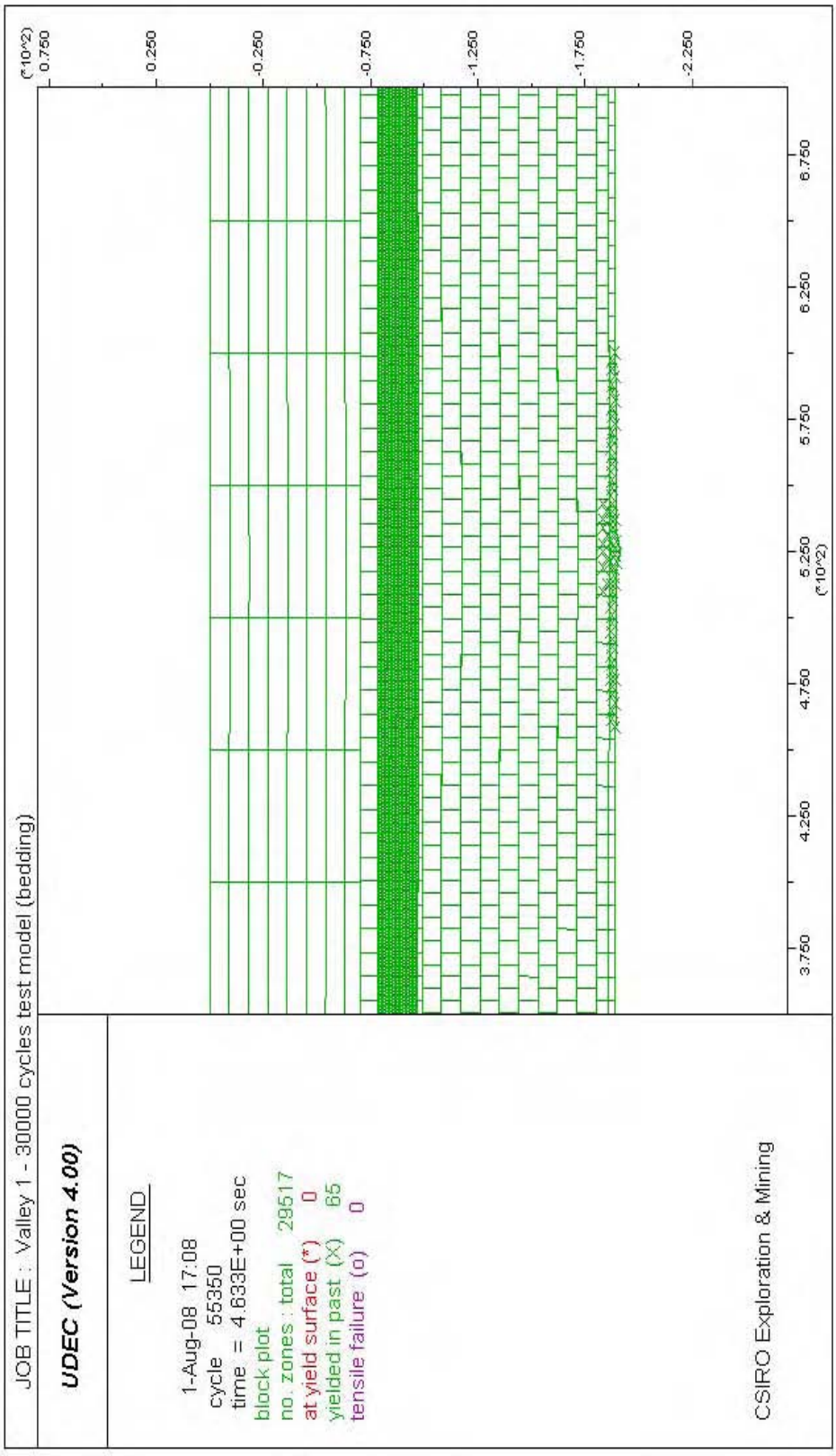

Fig. 6.10 – Yielded zones in a river valley model with bedding

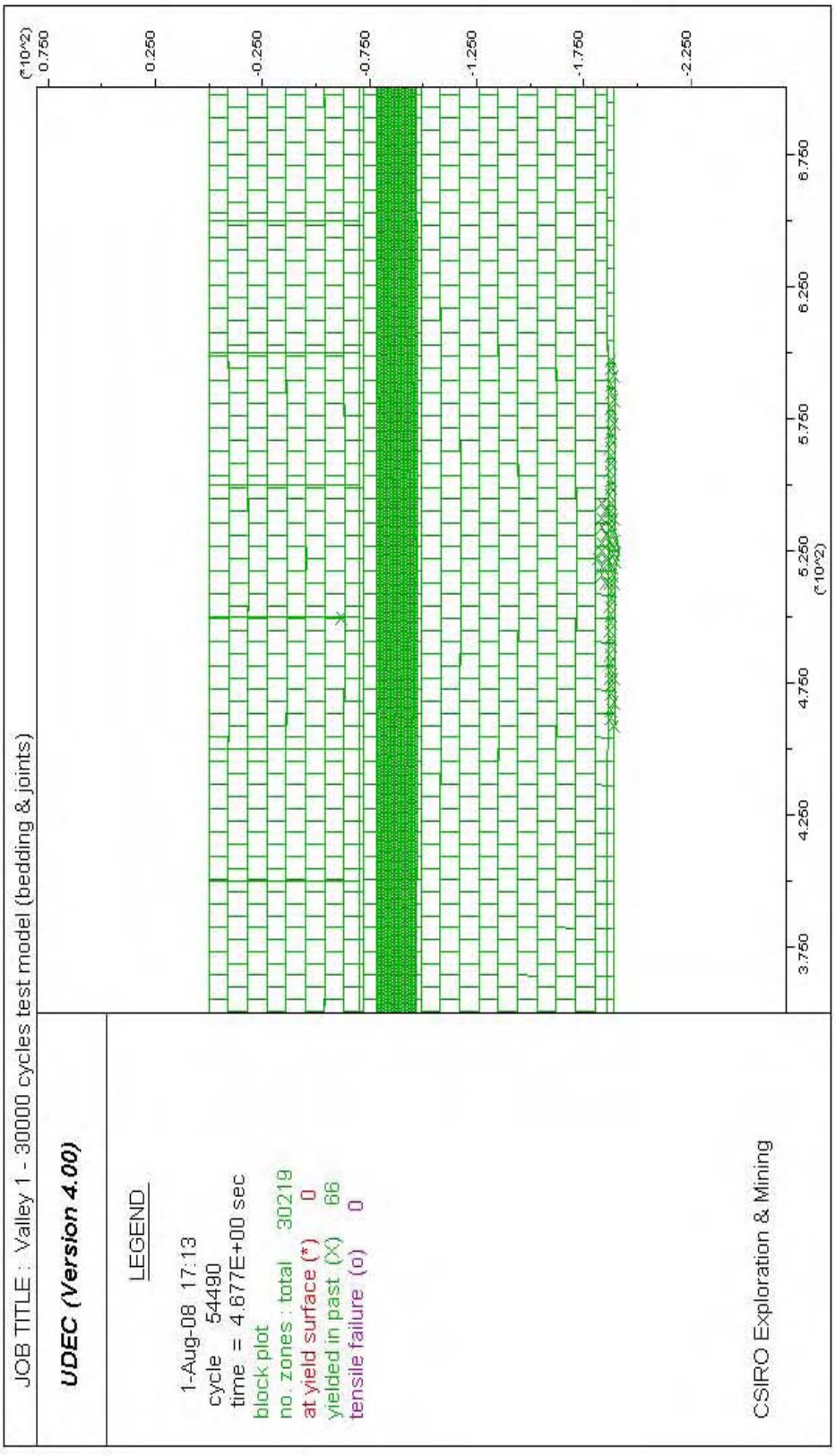

Fig. 6.11 – Yielded zones in a river valley model with bedding and joints

It was necessary to perform a mesh density analysis on the beam formed by the translation plane one metre below the base of the valley. Referring to Figure 6.3, it was likely that the mesh density used in the Hawkesbury Sandstone (*gen quad 12.70*) would not be fine enough to permit potential buckling of the beam and produce upsidence. Table 6.3 contains the details and results of the river valley models in the mesh density analysis.

Table 6.3 – Mesh density analysis results

Model	Mesh density in beam	Valley closure shoulder (mm)	Valley closure base (mm)	Subsidence at valley base (mm)
1	12.70	452	30	-335
2	6.35	692	50	-409
3	3.18	680	55	-410
4	1.59	712	60	-419
5	0.79	713	60	-419
6	0.40	711	60	10
7	0.20	708	60	57
8	0.10	703	50	25

It can be seen from Table 6.3 that as mesh density in the beam increased, the degree of buckling in the beam and valley closure increased. Model 7 produced the greatest amount of upward vertical movement. The upward movement in Model 8 decreased due to the buckling mode of the beam. Figure 6.12 and Figure 6.13 illustrate the exaggerated buckling in Model 7 and Model 8 respectively.

Fig. 6.12 – Beam buckling in Model 7

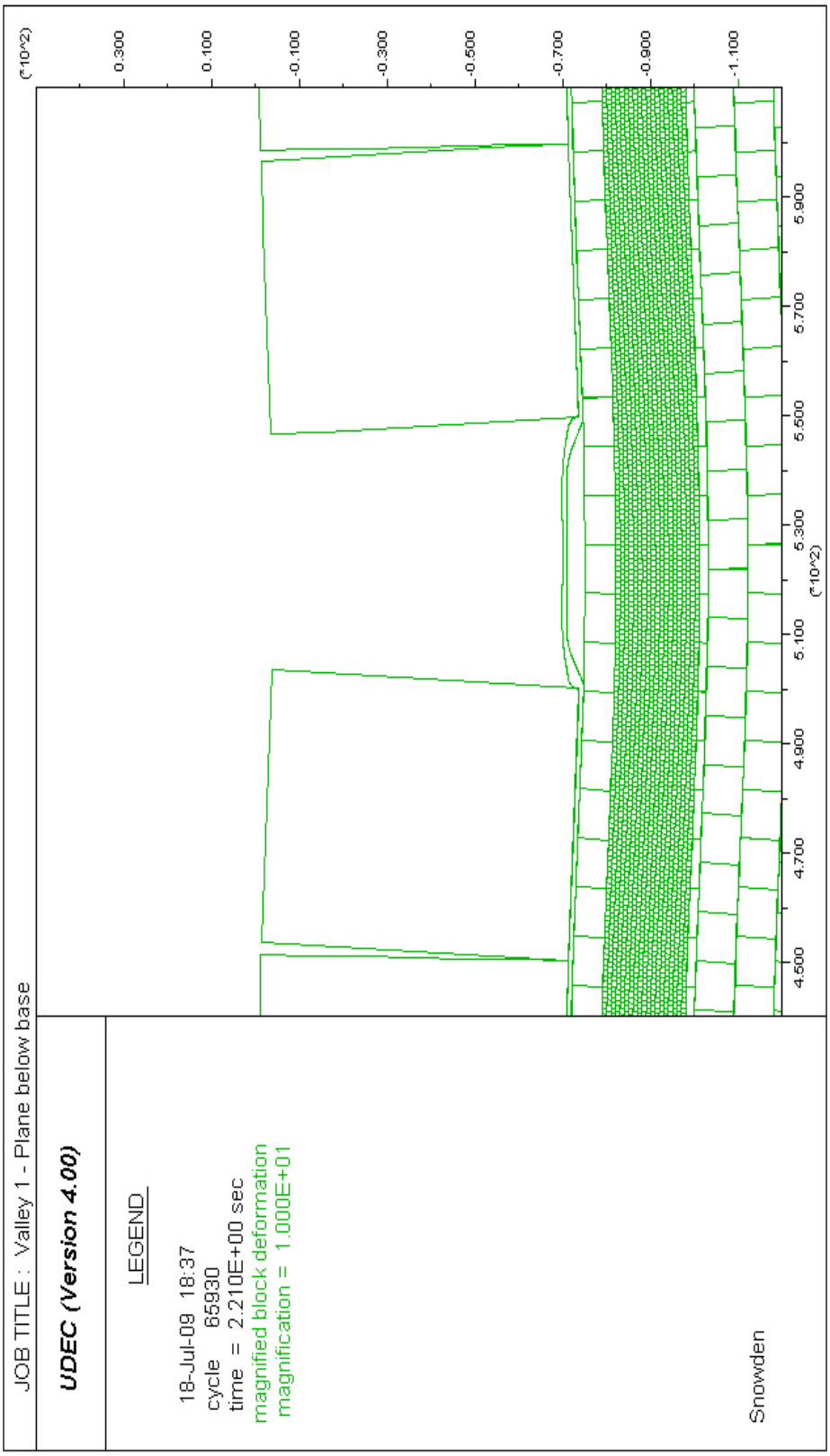

Fig. 6.13 – Beam buckling in Model 8

It was decided to use the mesh density in Model 7, as it produced the greatest amount of vertical upward movement in the valley and represented simple buckling.

It was concluded that the initial models successfully identified the appropriate number of cycles (N = 30,000) to be applied to the model by analysis of maximum developed subsidence and run times. The initial models also sufficiently demonstrated that the base of the models was at an acceptable distance from the base of the proposed river valleys, and the methodology of deforming the base of the models exactly replicated the Bulgo Sandstone profile in Model 4. The subsidence profiles from the initial models were considered sufficient enough to conduct an analysis with the river valley models. As stated previously, the sole purpose of the modelling was to investigate the block movement theory, and an attempt has been made to produce reasonable deformations in order to enable this.

6.4 RIVER VALLEY MODELS

Following on from the initial models and mesh density analysis, a total of fifty river valley models were created based on the following variations and characteristics:

- **No bedding and joints in upper 70 m of Hawkesbury Sandstone**
  - Translation plane at base
  - Translation plane below base
    - No joints in beam formed by translation plane
    - Joints in beam formed by translation plane

- **Bedding and joints in upper 70 m of Hawkesbury Sandstone**
  - Translation plane at base
  - Translation plane below base

There were five major parameters that were changed throughout the analysis. These were the position of the valley relative to the longwall centreline, the location of the translation plane, bedding and joints in the upper 70 m of the Hawkesbury Sandstone, and the addition of vertical joints in the beam formed when the translation plane was one metre below the base of the valleys.

Varying the position of the valley relative to the longwall panel allowed assessment of horizontal and vertical movements in the area above unmined coal (hogging phase). Moving the location of the translation plane from the base of the valleys to one metre below the valley base permitted examination of the proposed theory that valley closure is reduced when the translation plane is below the base of the valley. Adding bedding and joints in the upper 70 m of the Hawkesbury Sandstone was done to test the model against the rigid body observation by Holla and Barclay (2000). Adding joints to the beam formed by the translation plane beneath the base of the valley was done to ascertain if this had any effect on subsidence and valley closure.

The definition of upsidence given by Waddington Kay and Associates (2002) is “a reduction in the expected quantum of subsidence at a point, being the difference between the predicted or estimated subsidence and the vertical displacement actually measured”. Using this definition, it is possible to measure upsidence in an existing valley by comparing the difference in subsidence at the base of a valley when variations are performed on the model. It must be noted that the above definition is not conclusive. Upsidence could also be defined as direct upward movement in a river valley base as a result of base yield and buckling. In the models, it was decided to use the Waddington Kay and Associates definition to distinguish if it yielded conclusive results.

Figure 6.14 is a representative view of a typical valley model with no bedding or joints in the upper 70 m of the Hawkesbury Sandstone. In this figure, the valley centreline corresponds with the longwall centreline. In the river valley models, the location of the valley varied in the left hand side of the model.

Figure 6.15 is a close up view of a valley with no bedding or joints in the upper 70 m of the Hawkesbury Sandstone, with the translation plane at the base of the valley. Figure 6.16 is a close up view of a valley with no bedding or joints in the upper 70 m of the Hawkesbury Sandstone, with the translation plane one metre below the base of the valley. Figure 6.17 is a close up view of a valley with bedding planes and joints in the upper 70 m of the Hawkesbury Sandstone, with the translation plane at the base of the valley. Figure 6.18 is a close up view of a valley with bedding planes and joints in the upper 70 m of the Hawkesbury Sandstone, with the translation plane one metre below the base of the valley. Figure 6.19 is a close up view of a valley with no bedding and

joints in the upper 70 m of the Hawkesbury Sandstone, with the translation plane one metre below the base of the valley and with joints in the beam formed by the translation plane.

The modelling procedure for the river valley models was as follows:

1. Create geometry, assign properties, boundary conditions, in-situ stress regime and cycle to equilibrium,
2. Excavate required valley and cycle to equilibrium,
3. Reset velocities, displacements and boundary conditions,
4. Apply roller boundaries to the sides of the model,
5. Cycle for one step to obtain the time step,
6. Identify grid points at the base of the model to which velocities will be attached,
7. Define the maximum displacement for each previously identified grid point (as derived from the displacement profile for the Bulgo Sandstone in Model 4),
8. Calculate the y velocity for the identified grid points using $V = D/\Delta tN$,
9. Assign y velocities to grid points,
10. Cycle model for N (30,000) cycles to obtain required displacement at base,
11. Reset boundary conditions and place roller boundaries on each side of model, and
12. Cycle model for an additional 20,000 cycles to ensure final equilibrium is reached.

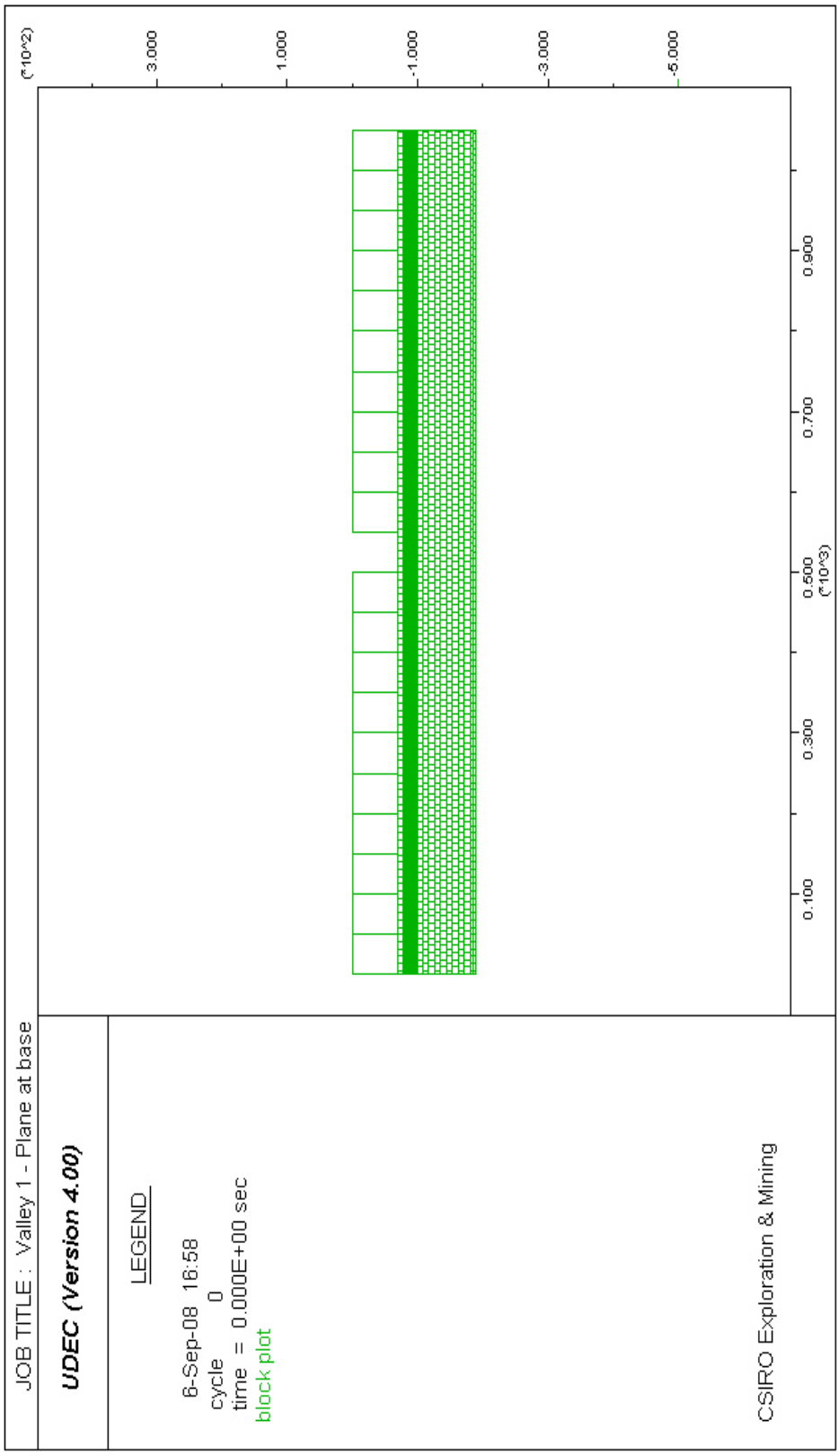

Fig. 6.14 – Typical river valley model

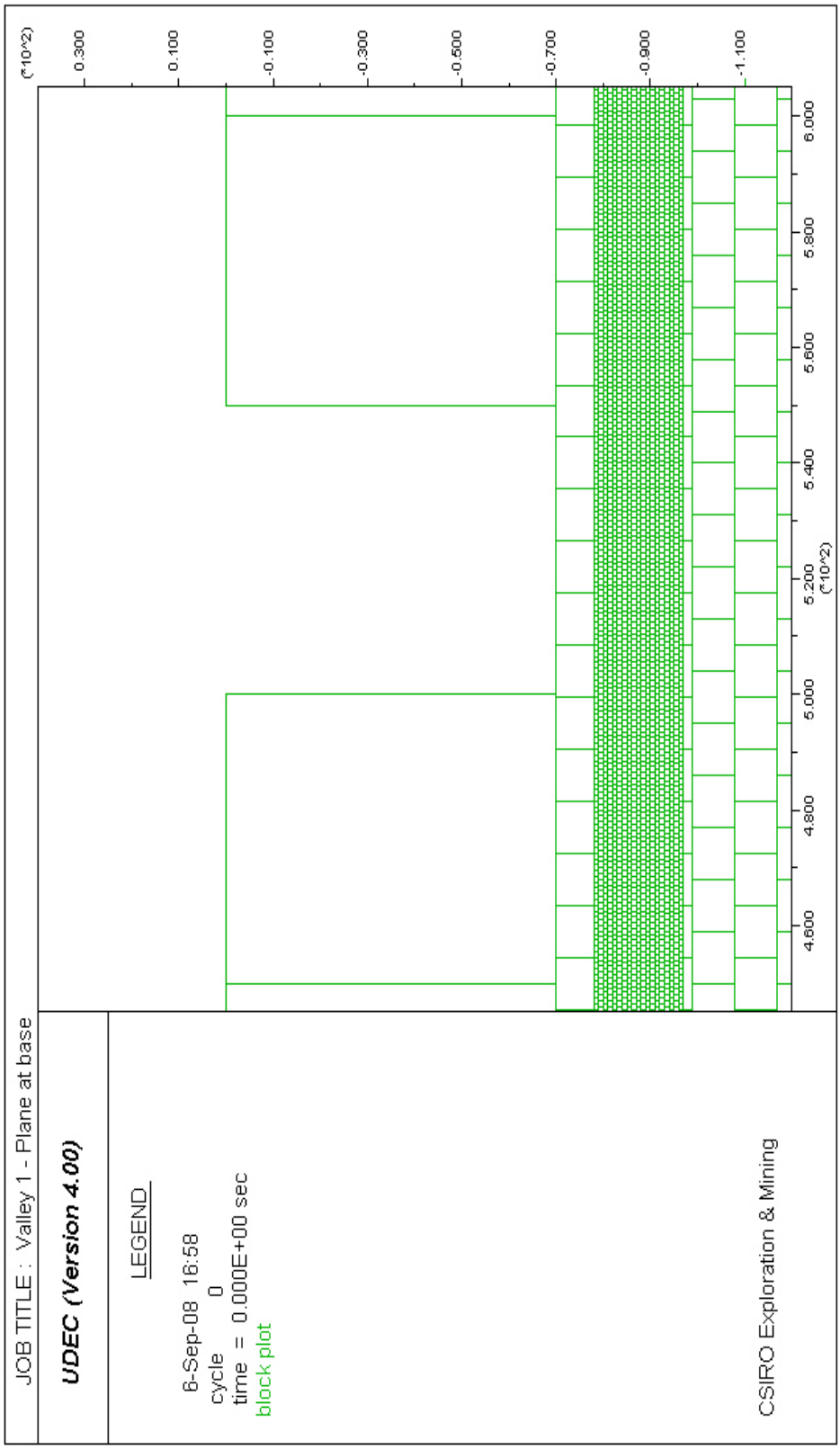

Fig. 6.15 – Translation plane at base of valley

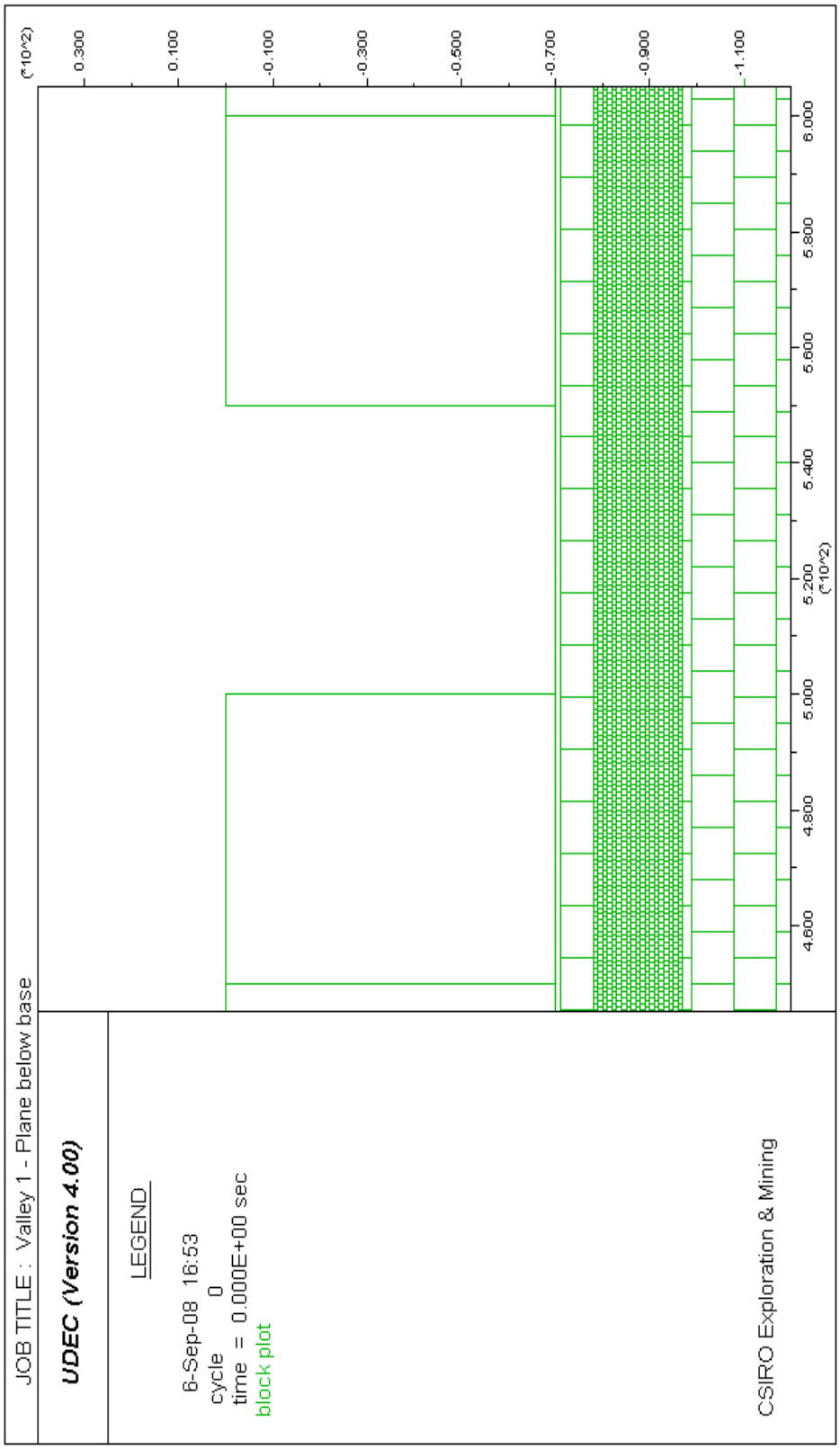

Fig. 6.16 – Translation plane below base of valley

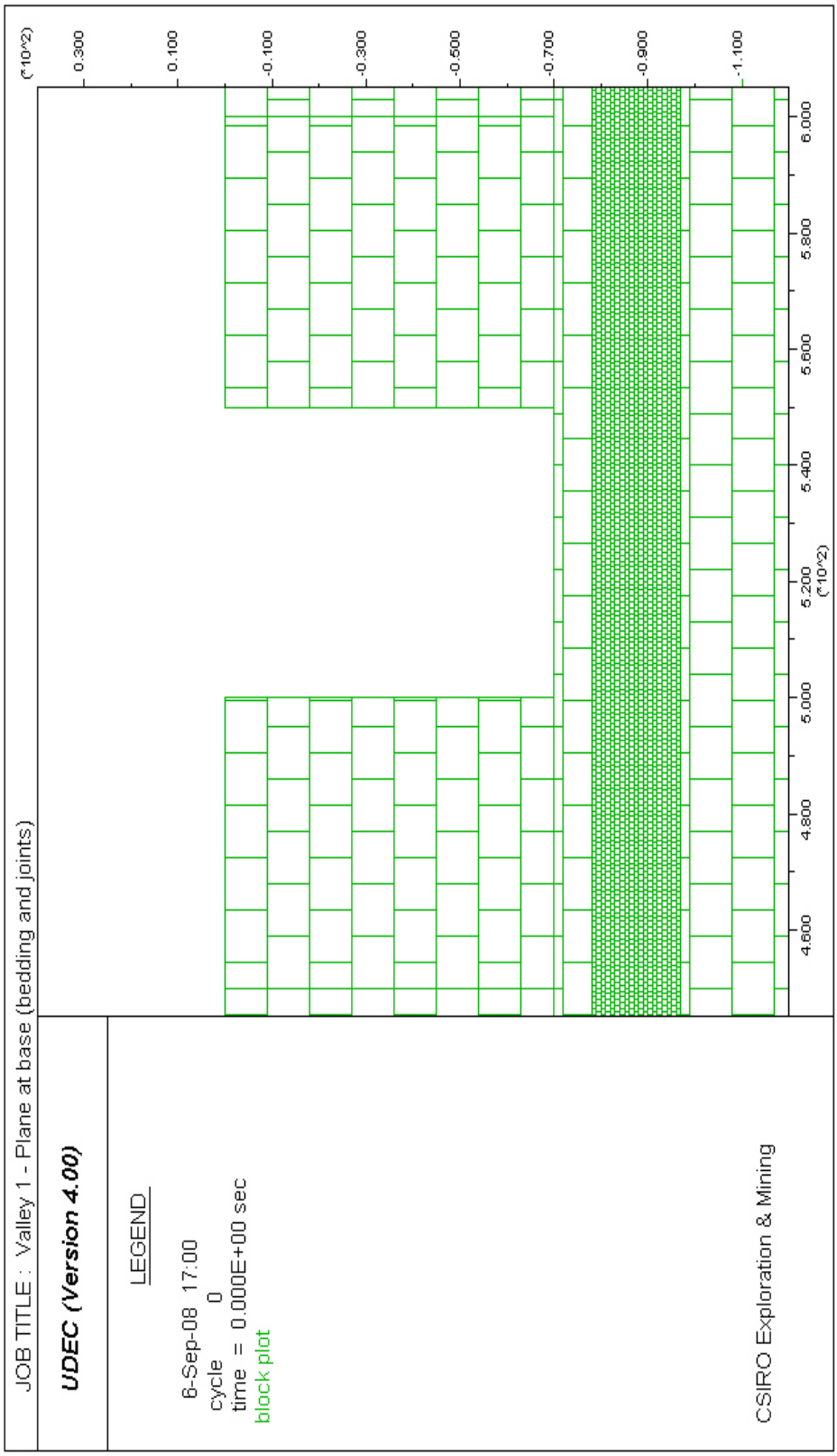

Fig. 6.17 – Translation plane at base of valley (bedding and joints)

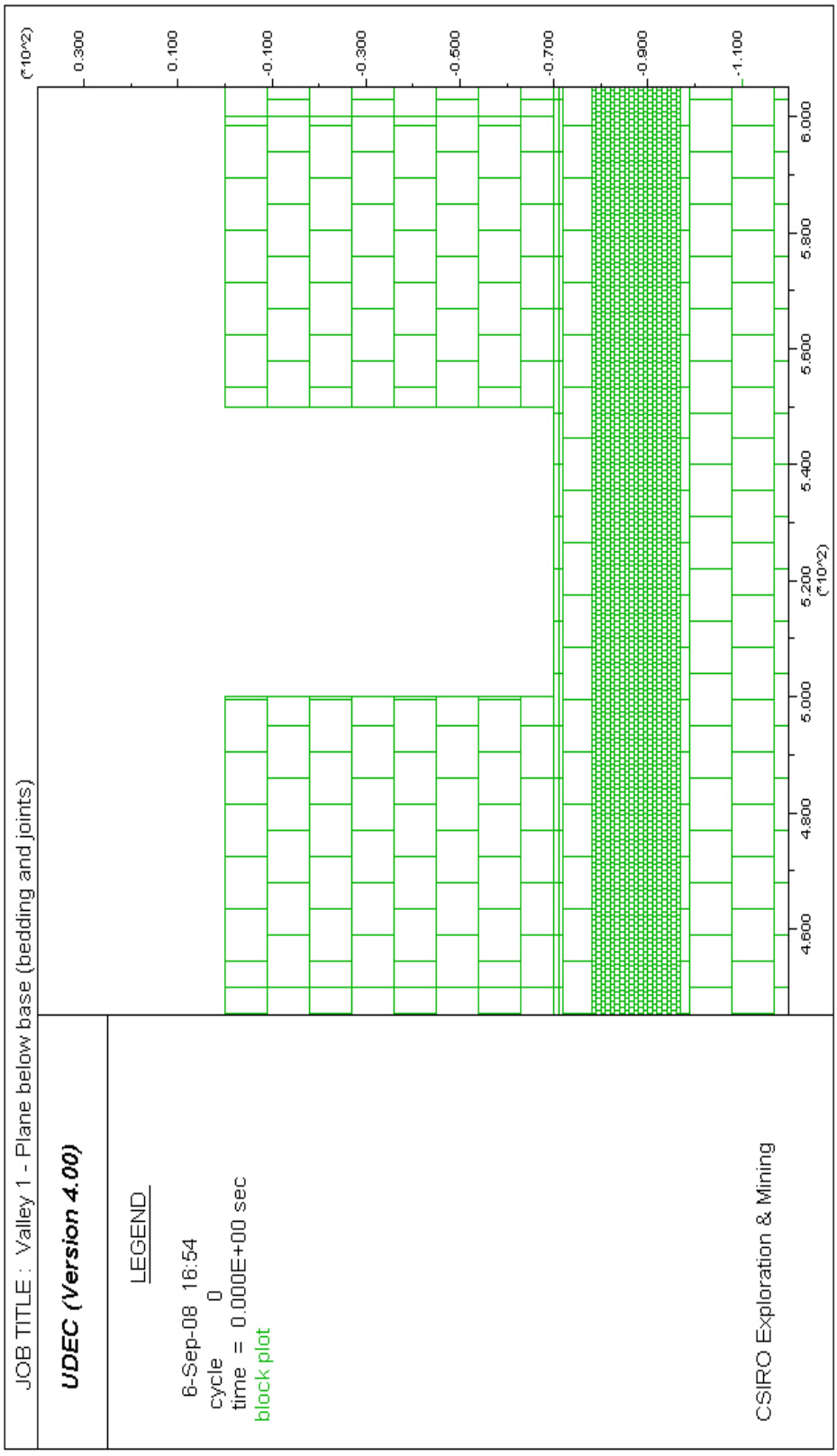

Fig. 6.18 – Translation plane below base of valley (bedding and joints)

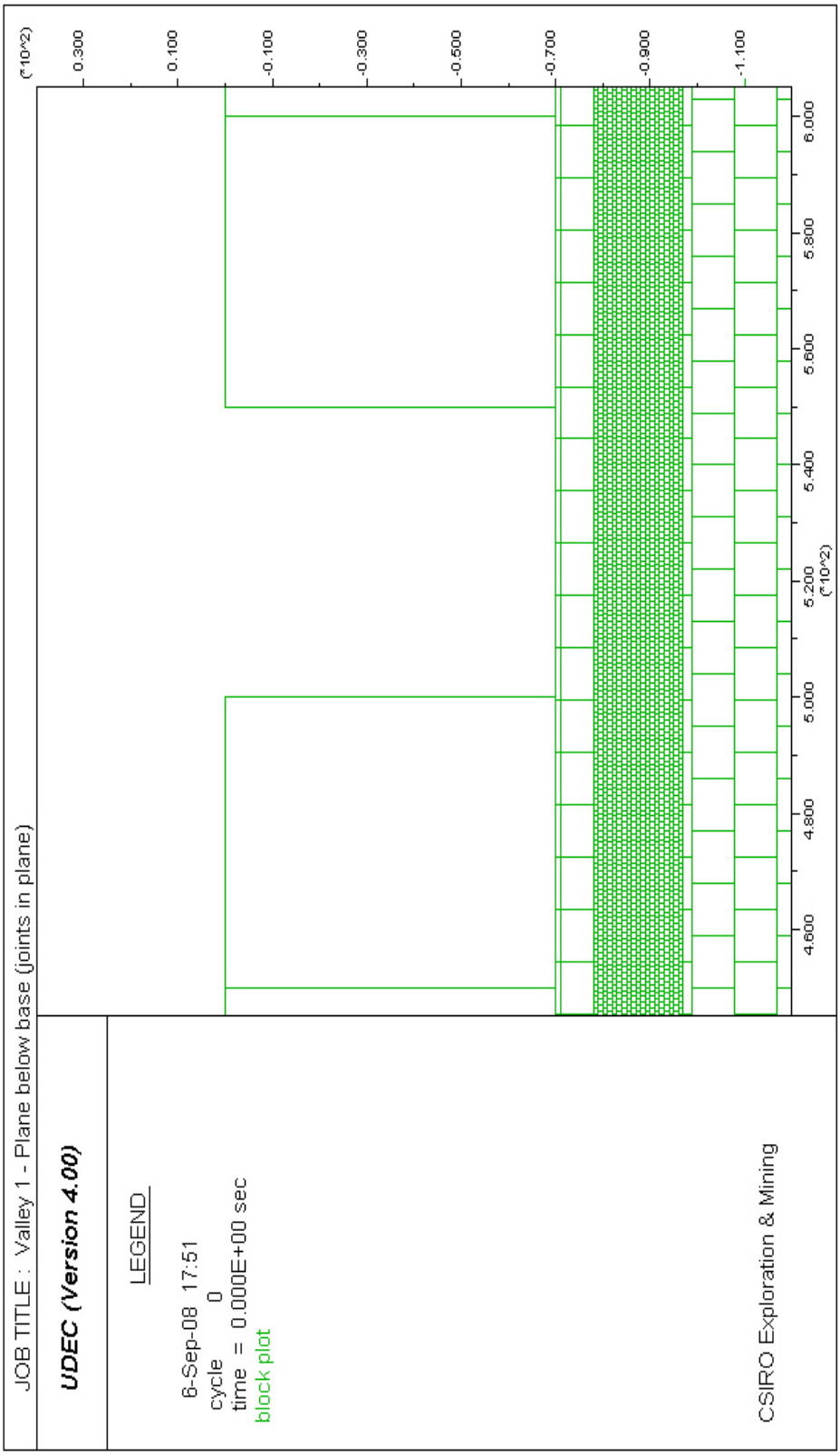

Fig. 6.19 – Translation plane below base of valley (joints in beam)

X-displacement history points were placed on the shoulders of each valley, along with y-displacement history points that were placed on the centre of the valley floor. These history points were monitored for each individual valley in question and the models were investigated to see whether they conformed to the expected behaviour i.e. increased valley closure and minimal valley base yield with a translation plane at the base of a valley, and decreased valley closure with increased valley base yield with the translation plane one metre below the valley floor.

6.5 RESULTS

The results from the valley models are shown in Tables 6.4 to 6.8. Figure 6.20 and Figure 6.21 are the subsidence profiles prior to valley excavation for the models (no bedding and joints in the upper 70 m of the Hawkesbury Sandstone, and bedding and joints in the upper 70 m of the Hawkesbury Sandstone). Figure 6.22 and Figure 6.23 are the corresponding tilt profiles. Figure 6.24 and Figure 6.29 illustrate the subsidence at the base of the valley as a function of distance from the longwall centreline. Figure 6.33 and Figure 6.34 illustrate the valley closure at the shoulders of the valleys as a function of distance from the longwall centreline. Figure 6.41 and Figure 6.42 illustrate the valley closure at the base of the valleys as a function of distance from the longwall centreline.

Table 6.4 – No bedding and joints in the upper 70 m of Hawkesbury Sandstone, translation plane at base

Valley	Valley centre to longwall centre (m)	Valley closure shoulder (mm)	Valley closure base (mm)	Subsidence at valley base (mm)
1	0	727	70	-423
2	50	413	195	-266
3	100	138	432	-71
4	150	72	175	-26
5	200	64	89	-18
6	250	46	58	-10
7	300	35	39	-5
8	350	22	28	-2
9	400	7	11	0
10	450	-3	0	2

Table 6.5 – No bedding and joints in the upper 70 m of Hawkesbury Sandstone, translation plane below base, no joints in beam

Valley	Valley centre to longwall centre (m)	Valley closure shoulder (mm)	Valley closure base (mm)	Subsidence at valley base (mm)
1	0	708	45	57
2	50	323	35	14
3	100	166	56	-12
4	150	25	66	-27
5	200	24	46	-17
6	250	27	33	-10
7	300	18	22	-5
8	350	8	10	-1
9	400	4	0	0
10	450	-2	0	2

Table 6.6 – No bedding and joints in the upper 70 m of Hawkesbury Sandstone, translation plane below base, joints in beam

Valley	Valley centre to longwall centre (m)	Valley closure shoulder (mm)	Valley closure base (mm)	Subsidence at valley base (mm)
1	0	701	60	50
2	50	331	45	12
3	100	171	60	-12
4	150	29	76	-27
5	200	30	54	-17
6	250	28	38	-9
7	300	20	22	-5
8	350	6	9	-2
9	400	0	3	1
10	450	-3	0	2

Table 6.7 – Bedding and joints in the upper 70 m of Hawkesbury Sandstone, translation plane at base

Valley	Valley centre to longwall centre (m)	Valley closure shoulder (mm)	Valley closure base (mm)	Subsidence at valley base (mm)
1	0	693	55	-415
2	50	349	128	-289
3	100	146	158	-57
4	150	111	96	-27
5	200	89	94	-18
6	250	72	77	-10
7	300	54	55	-5
8	350	31	32	-2
9	400	14	16	1
10	450	1	4	2

Table 6.8 – Bedding and joints in the upper 70 m of Hawkesbury Sandstone, translation plane below base

Valley	Valley centre to longwall centre (m)	Valley closure shoulder (mm)	Valley closure base (mm)	Subsidence at valley base (mm)
1	0	685	55	46
2	50	348	50	24
3	100	134	26	-21
4	150	104	33	-27
5	200	86	28	-18
6	250	67	15	-11
7	300	47	5	-6
8	350	32	4	-1
9	400	14	4	0
10	450	1	3	2

6.5.1 Subsidence without valley excavation

From Figure 6.20, it can be seen that when the translation plane was at the base of the valley and no bedding and joints were present in the upper 70m of Hawkesbury Sandstone, the maximum developed subsidence was 201 mm. This was to be expected as this model was the same as the model in Table 6.1 (N = 30,000).

When the translation plane was moved one metre below the base of the valley, it can be seen from Figure 6.20 that the maximum developed subsidence reduced to 198 mm. When joints were added to the beam formed by the translation plane, it can be seen from Figure 6.18 that the maximum developed subsidence increased to 199 mm.

When bedding and joints were added to the upper 70 m of Hawkesbury Sandstone and the translation plane was at the base of the valleys, it can be seen from Figure 6.21 that the maximum developed subsidence was 411 mm. When the translation plane was moved one metre below the valley base, it can be seen from Figure 6.21 that the maximum developed subsidence was 419 mm. The increase in maximum developed subsidence when bedding and joints were added to the upper 70 m of the Hawkesbury Sandstone was expected, due to the increased flexibility of the model afforded by the extra discontinuities.

The models prior to valley excavation show that the model results were consistent and did not vary substantially prior to valley excavation. This establishes a stable numerical modelling base when valleys are excavated. For example, when bedding and joints were not present in the upper 70 m of Hawkesbury Sandstone, the maximum variation in subsidence was in the order of 3 mm. When bedding and joints were present, the maximum variation was 8 mm.

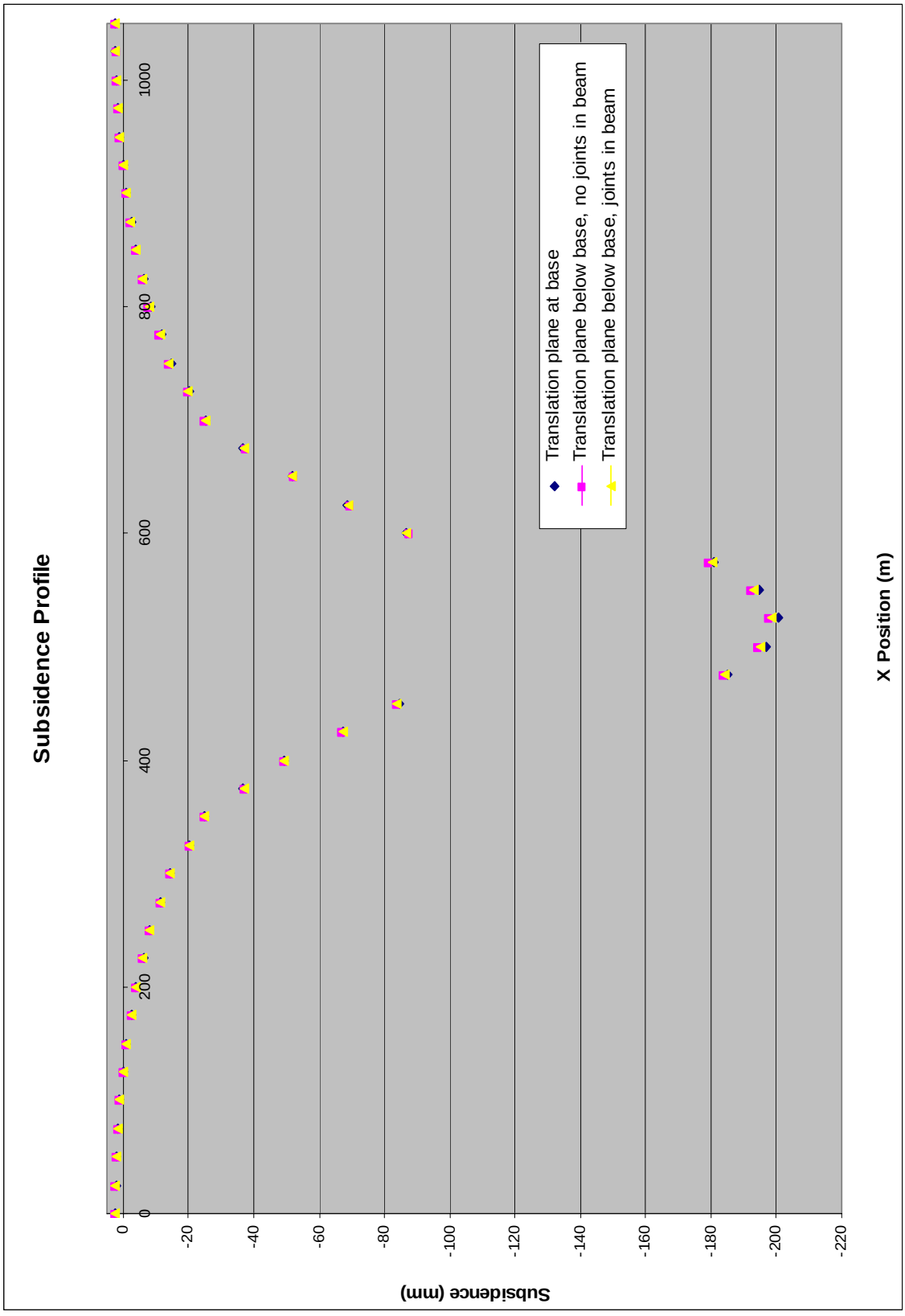

Fig. 6.20 – Subsidence prior to valley excavation (no bedding and joints in upper 70 m of Hawkesbury Sandstone)

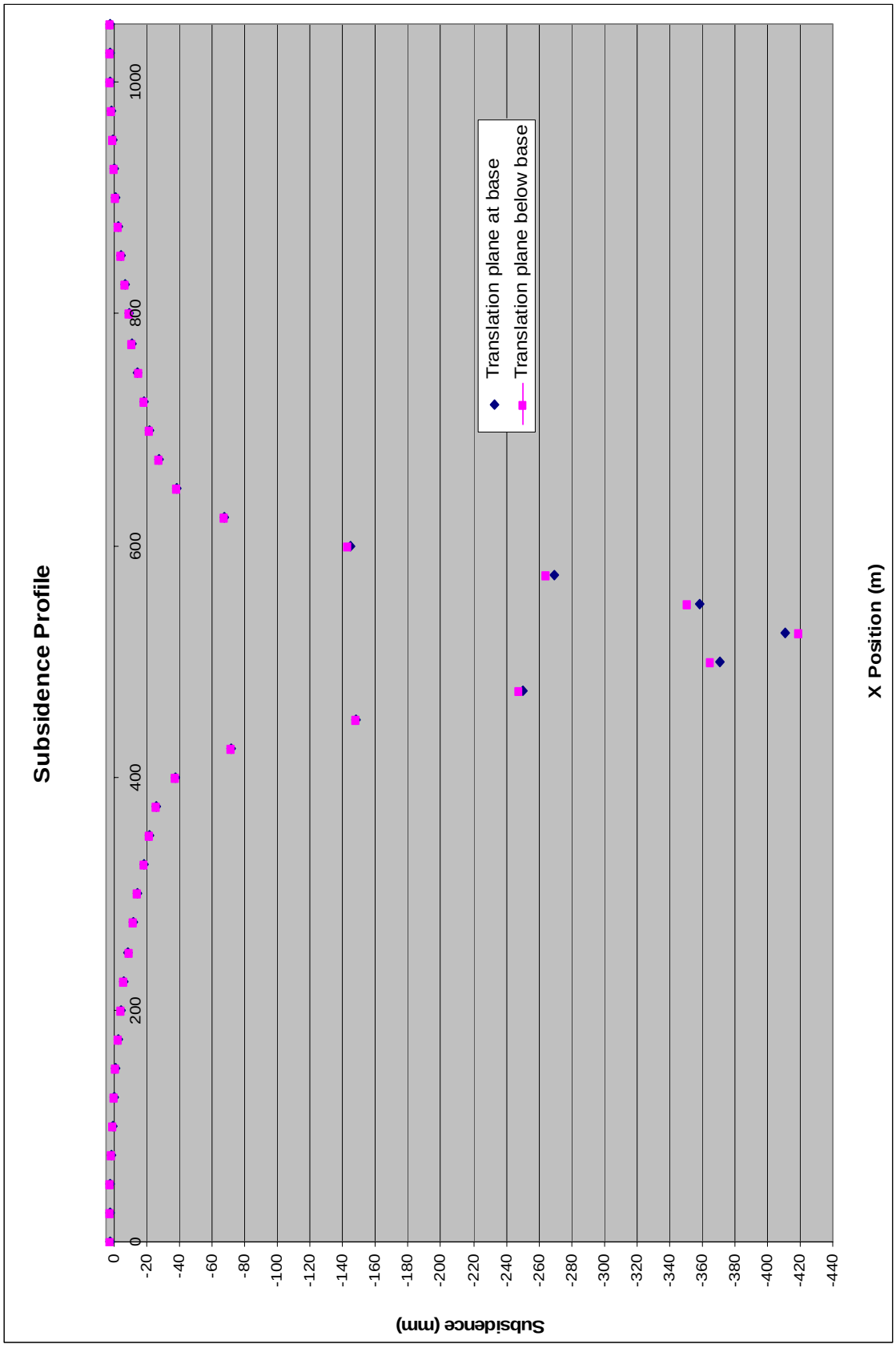

Fig. 6.21 – Subsidence prior to valley excavation (bedding and joints in upper 70 m of Hawkesbury Sandstone)

6.5.2 Tilt without valley excavation

It can be seen in Figure 6.22 when the translation plane was at the base of the valley; the average maximum tilt was 3.89 mm/m. The point of maximum tilt (or inflection point) was located 62.50 m from the longwall centreline. When the translation plane was moved one metre below the base of the valley (Figure 6.22), the average maximum tilt reduced to 3.83 mm/m, and the point of maximum tilt was also located 62.50 m from the longwall centreline. When joints were added to the beam formed by the translation plane, it can be seen from Figure 6.22 that the average tilt increased to 3.87 mm/m. The position of maximum tilt was also located 62.50 m from the longwall centreline.

When bedding and joints were added to the upper 70 m of the Hawkesbury Sandstone, it can be seen from Figure 6.23 that when the translation plane was at the base of the valley, the average maximum tilt was 4.90 mm/m. The point of maximum tilt was located 37.50 m from the longwall centreline. When the translation plane was moved one metre below the base of the valley (Figure 6.23), the average maximum tilt decreased to 4.77 mm/m, and the point of maximum tilt was also located 37.50 m from the longwall centreline.

The tilt results prior to valley excavation illustrate a stable numerical modelling platform, like the subsidence results prior to valley excavation. The difference in the magnitude of tilt and the location of the position of maximum tilt when bedding and joints were added to the upper 70 m of the Hawkesbury Sandstone can be attributed to the increased flexibility of the model, and the resulting increased subsidence and altered shape of the subsidence profile.

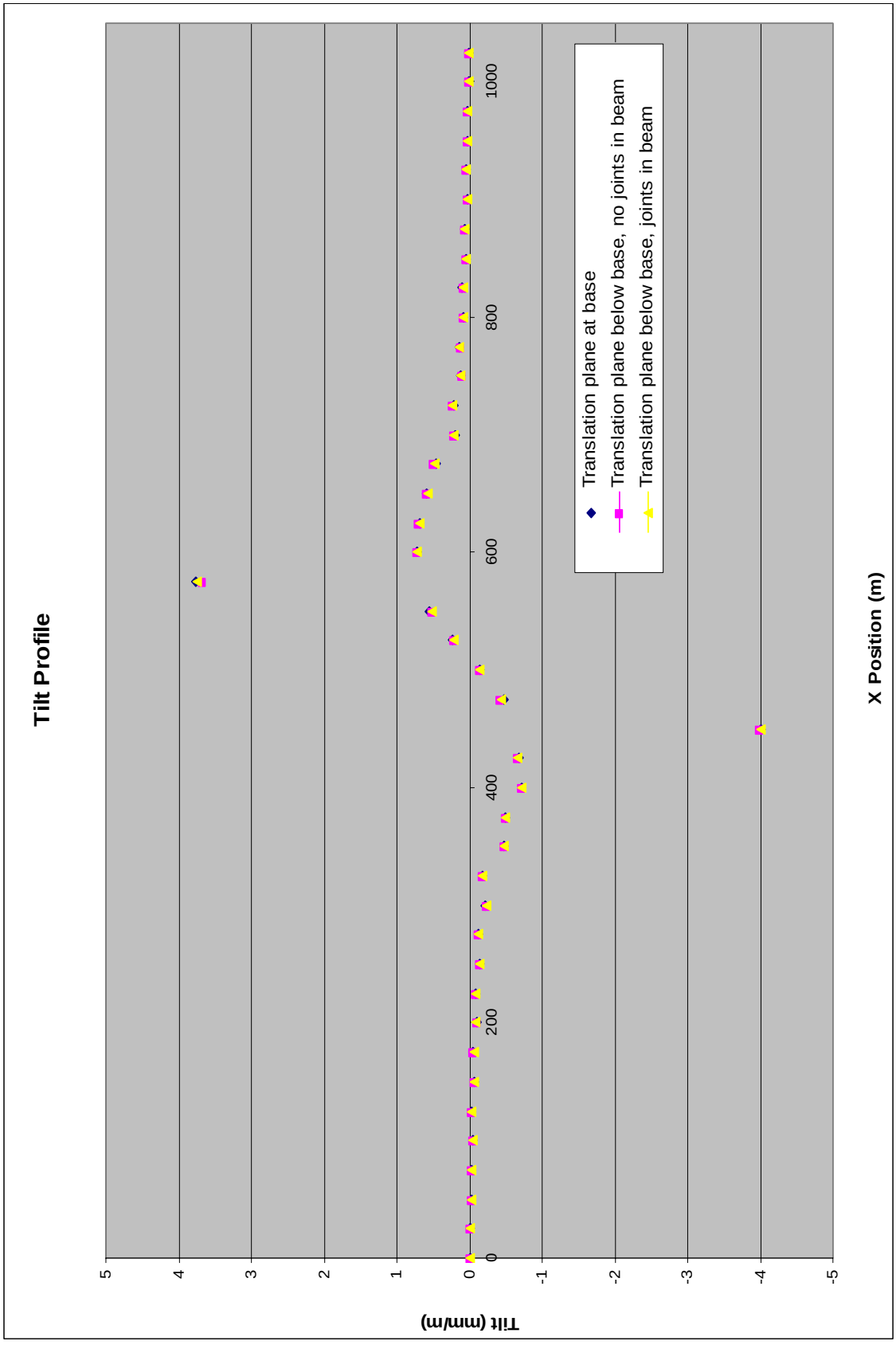

Fig. 6.22 – Tilt prior to valley excavation (no bedding and joints in upper 70 m of Hawkesbury Sandstone)

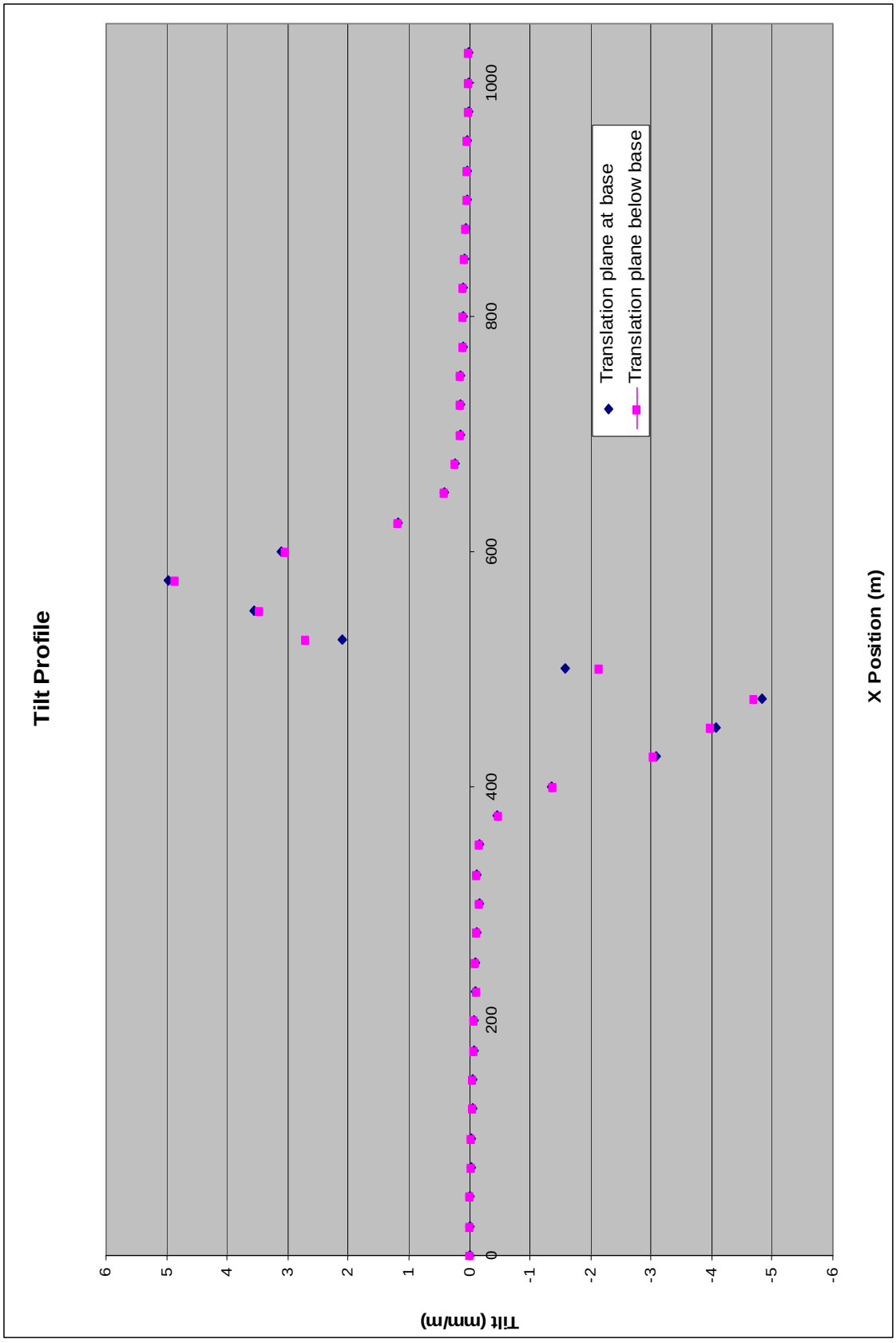

Fig. 6.23 – Tilt prior to valley excavation (bedding and joints in upper 70 m of Hawkesbury Sandstone)

6.5.3 Subsidence/upsidence at base of valleys

The subsidence results and the calculated upsidence are shown in Tables 6.9 to 6.11.

Table 6.9 – Upsidence between models in Table 6.4 and Table 6.5

Valley	Valley centre to longwall centre (m)	Subsidence (mm, Table 6.4)	Subsidence (mm, Table 6.5)	Upsidence (mm)
1	0	-423	57	480
2	50	-266	14	280
3	100	-71	-12	59
4	150	-26	-27	-1
5	200	-18	-17	1
6	250	-10	-10	0
7	300	-5	-5	0
8	350	-2	-1	1
9	400	0	0	0
10	450	2	2	0

Table 6.10 – Upsidence between models in Table 6.4 and Table 6.6

Valley	Valley centre to longwall centre (m)	Subsidence (mm, Table 6.4)	Subsidence (mm, Table 6.6)	Upsidence (mm)
1	0	-423	50	473
2	50	-266	12	278
3	100	-71	-12	59
4	150	-26	-27	-1
5	200	-18	-17	1
6	250	-10	-9	1
7	300	-5	-5	0
8	350	-2	-2	0
9	400	0	1	1
10	450	2	2	0

Table 6.11 – Upsidence between models in Table 6.7 and Table 6.8

Valley	Valley centre to longwall centre (m)	Subsidence (mm, Table 6.7)	Subsidence (mm, Table 6.8)	Upsidence (mm)
1	0	-415	46	461
2	50	-289	24	313
3	100	-57	-21	36
4	150	-27	-27	0
5	200	-18	-18	0
6	250	-10	-11	-1
7	300	-5	-6	-1
8	350	-2	-1	1
9	400	1	0	-1
10	450	2	2	0

When the upper 70 m of Hawkesbury Sandstone contained no bedding and joints, it can be seen from Table 6.9, Table 6.10 and Figure 6.24 that upsidence was produced when the translation plane was located below the base of the valley, but not when the location plane was located at the base of the valley.

From Table 6.9, it can be seen that moving the translation plane one metre below the base of the valleys and not adding any joints to the beam formed by the translation plane produced a maximum upsidence of 480 mm above the longwall centreline, 280 mm at 50 m from the longwall centreline, and 59 mm at 100 m from the longwall centreline.

Figures 6.25 to 6.27 are plots of the exaggerated block deformations when the centreline of the valley was at 0 m, 50 m and 100 m from the longwall centreline respectively, with the plane below the valley base and no bedding and joints in the upper 70 m of Hawkesbury Sandstone.

Given that the river valley models are based on Model 4 in Chapter 5, which has a longwall width of 175 m, it can be seen that upsidence occurred outside the goaf edge, and not solely above the longwall centreline.

From Table 6.10 and Figure 6.24, it can be seen that the addition of vertical joints in the beam formed by the translation plane produced very little difference in terms of subsidence and calculated upsidence. Figure 6.28 is a block deformation plot of a valley

above the longwall centreline, with joints in the beam formed by the translation plane. Shear displacements are also illustrated and it can be seen that no shear occurred in the vertical joints.

When bedding and joints were added to the upper 70 m of Hawkesbury Sandstone, it can be seen from Table 6.11 and Figure 6.29 that the subsidence and calculated upsidence was generally less outside the goaf edge. Figure 6.30 is a plot of block deformations and shear displacements outside the goaf edge (100 m from the longwall centreline), and it can be seen that as the rock mass was being forced into the free face provided by the valley, the increased shear displacements in the walls of the valley alleviated the horizontal stress concentration in the corner of the valley closest to the longwall centreline, which is illustrated in Figure 6.31 and Figure 6.32. It can be seen from Figure 6.31 and Figure 6.32 that when the model contained no bedding and joints in the upper 70 m of Hawkesbury Sandstone, a horizontal compressive stress of 85 MPa was concentrated in the corner of the valley, and when the model contained bedding and joints in the upper 70 m of Hawkesbury Sandstone, the concentration of compressive stress in the corner of the valley reduced to 27.5 MPa.

It can also be seen from Table 6.11 and Figure 6.29 that the amount of subsidence influenced upsidence. When bedding and joints were added to the upper 70 m of Hawkesbury Sandstone, it can be seen that the upsidence at 50 m from the longwall centreline (313 mm) was greater than the models with no bedding and joints in the upper 70 m of Hawkesbury Sandstone. Likewise, a greater amount of subsidence had occurred in this location. It was previously demonstrated in Figure 6.31 and Figure 6.32 that the addition of bedding and joints in the upper 70 m of Hawkesbury Sandstone served to reduce the concentration of compressive stress in the valley. This occurrence of upsidence which was greater than the upsidence produced by rigid block movements at the same location illustrates that horizontal compressive stress redistribution is not the primary mechanism behind upsidence, rather the subsidence profile with its associated tilts and curvatures are.

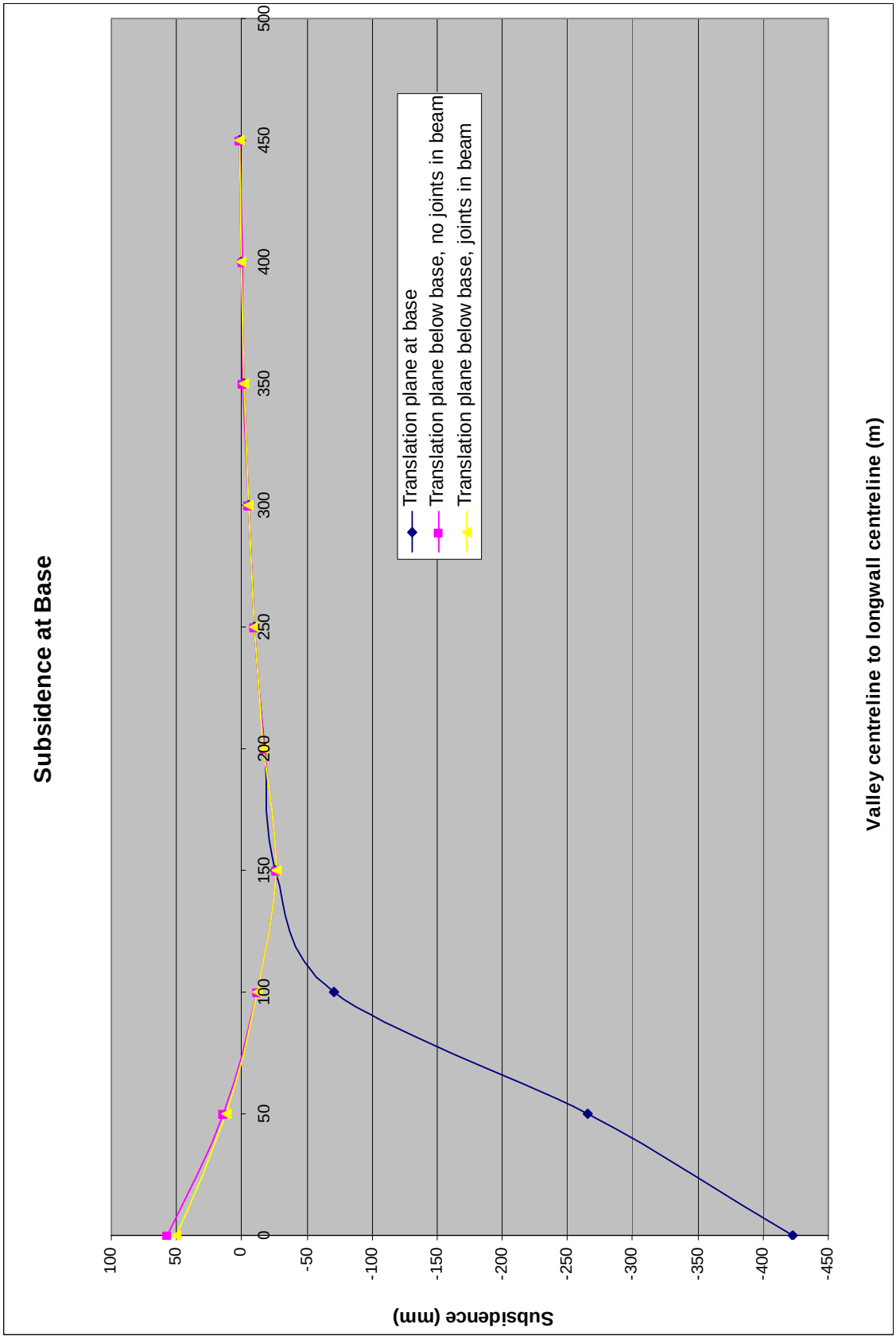

Fig. 6.24 – Subsidence at base (no bedding and joints in upper 70 m of Hawkesbury Sandstone)

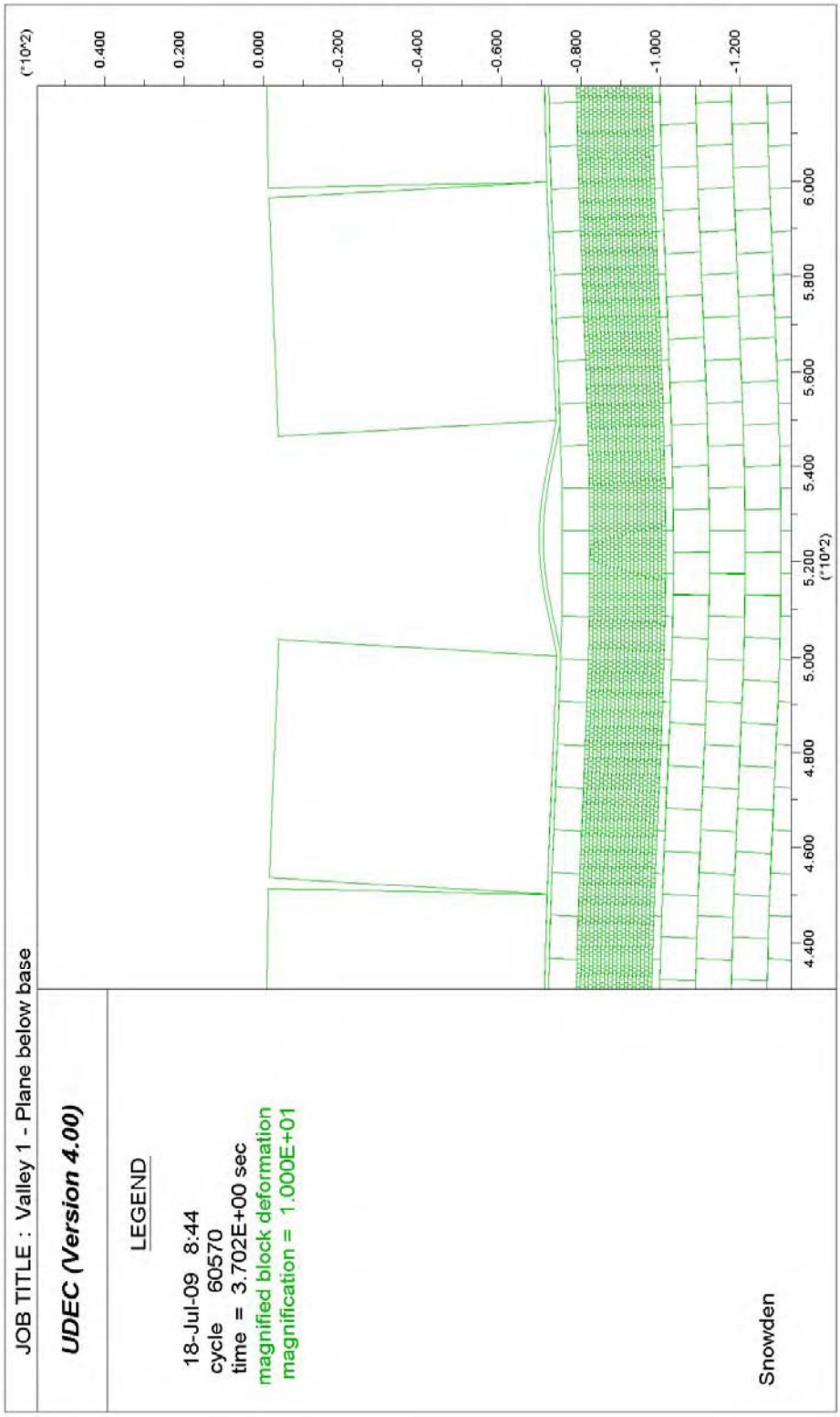

Fig. 6.25 – Exaggerated block deformations when valley is 0 m from longwall centreline (no bedding and joints in upper 70 m of Hawkesbury Sandstone)

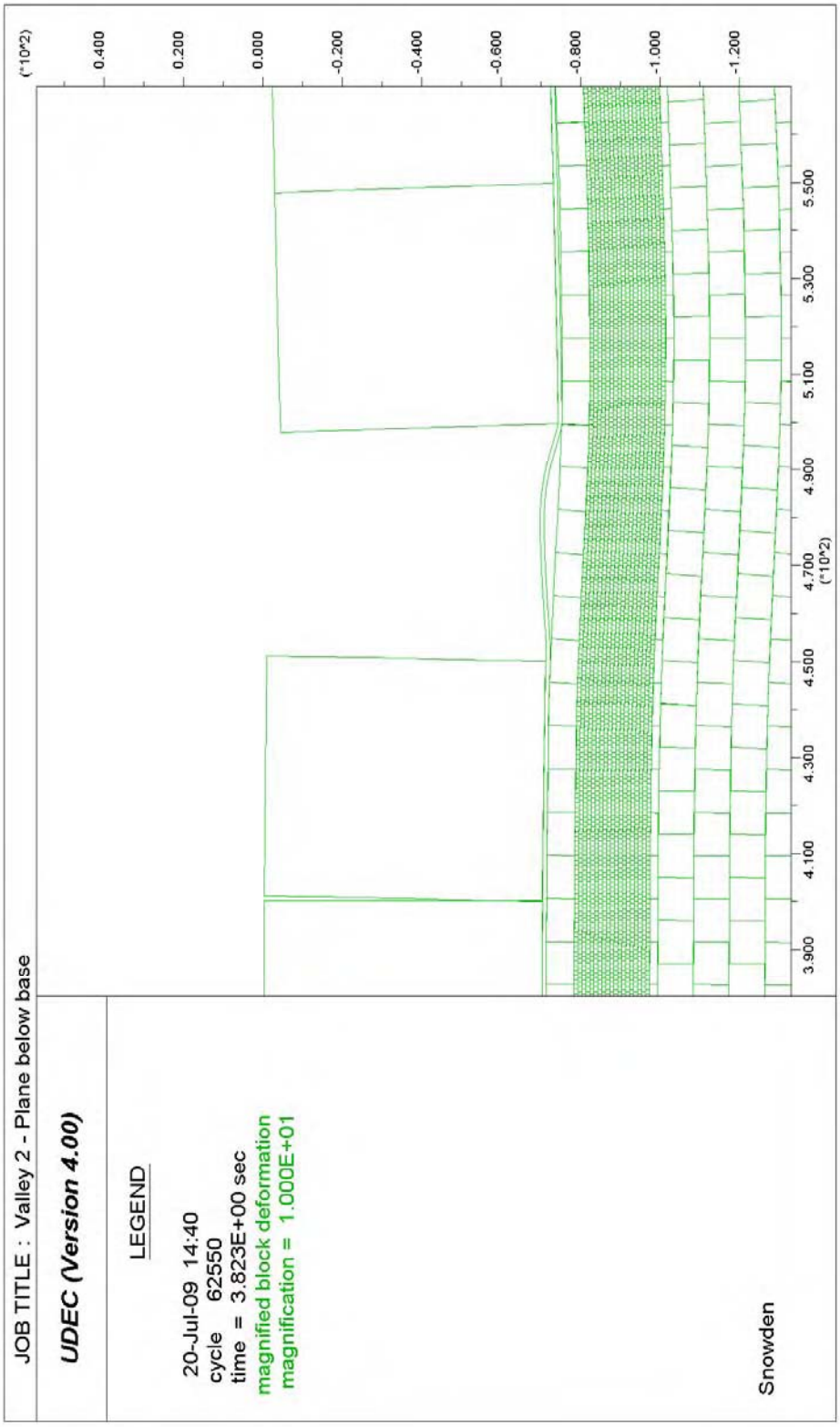

Fig. 6.26 – Exaggerated block deformations when valley is 50 m from longwall centreline (no bedding and joints in upper 70 m of Hawkesbury Sandstone)

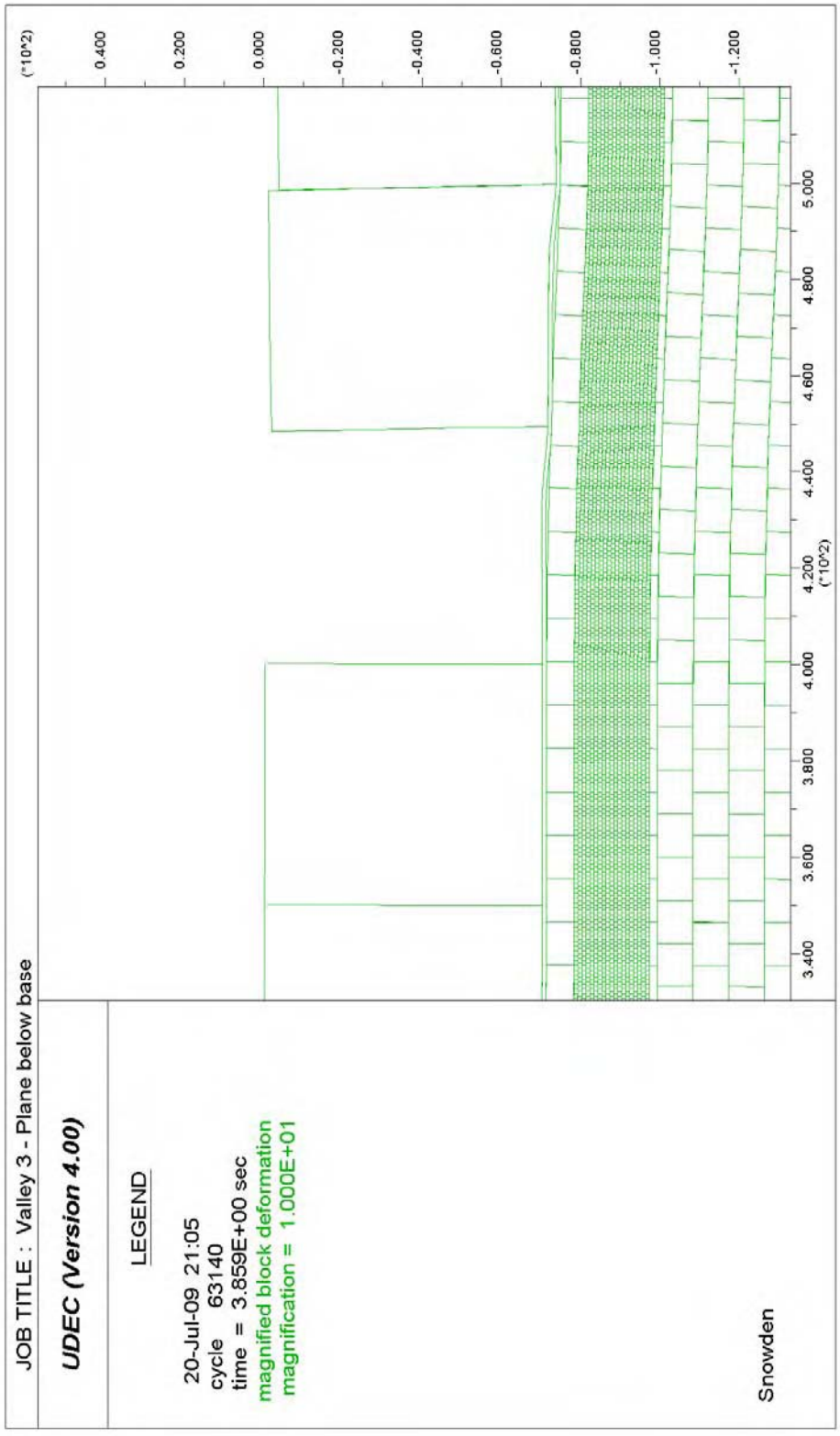

Fig. 6.27 – Exaggerated block deformations when valley is 100 m from longwall centreline (no bedding and joints in upper 70 m of Hawkesbury Sandstone)

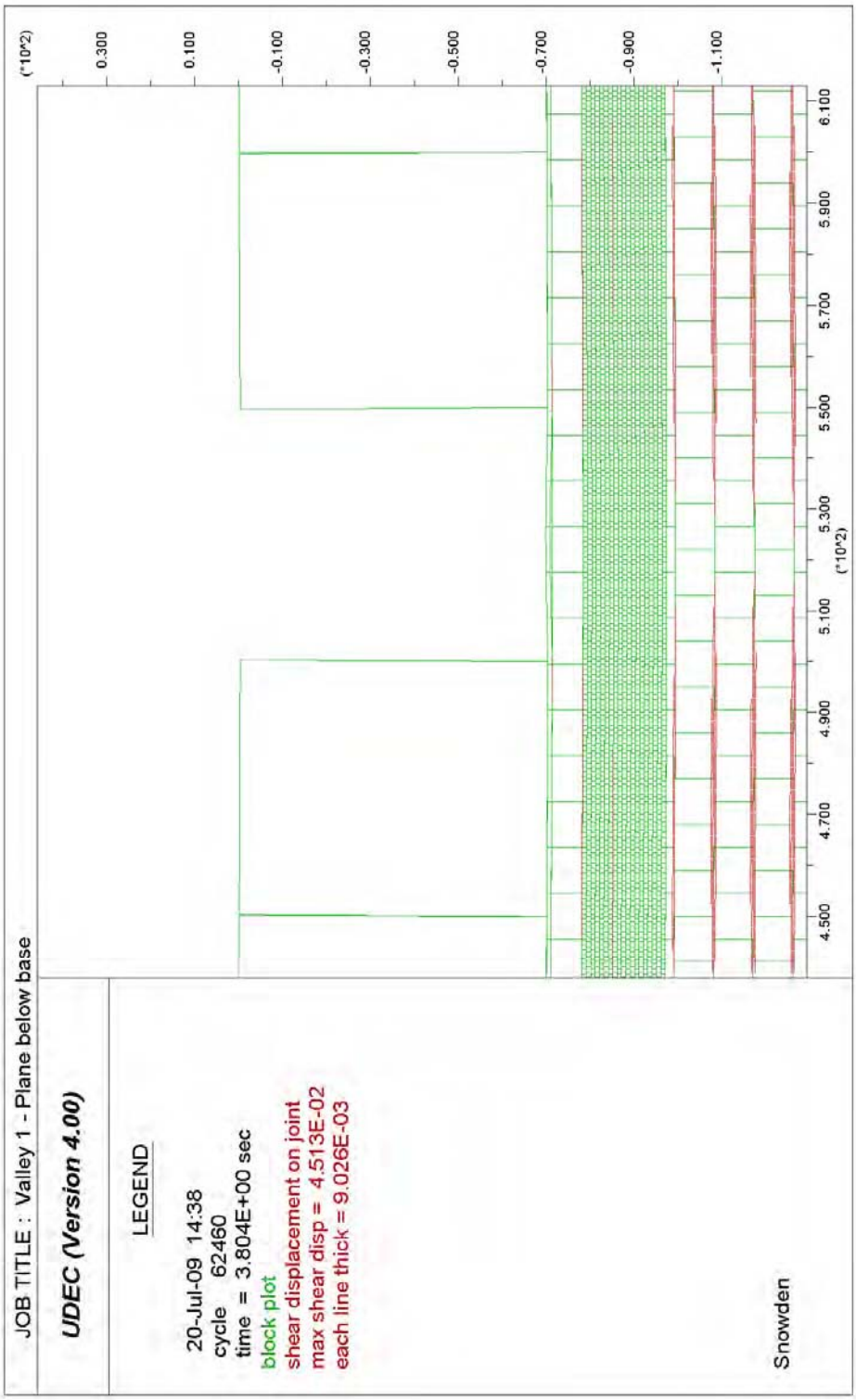

Fig. 6.28 – Block deformations and shear when valley is 0 m from longwall centreline (no bedding and joints in upper 70 m of Hawkesbury Sandstone, joints in beam)

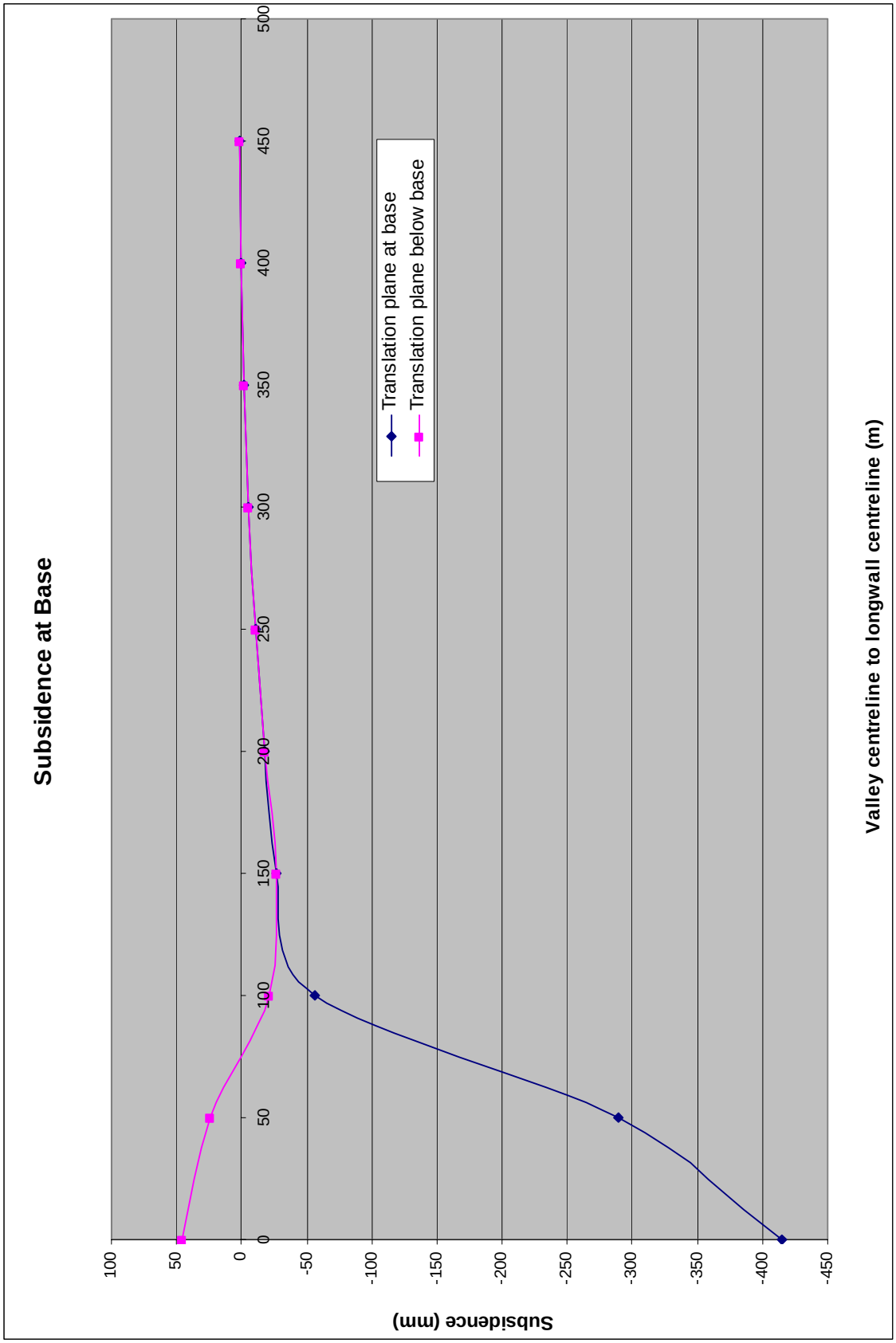

Fig. 6.29 – Subsidence at base (bedding and joints in upper 70 m of Hawkesbury Sandstone)

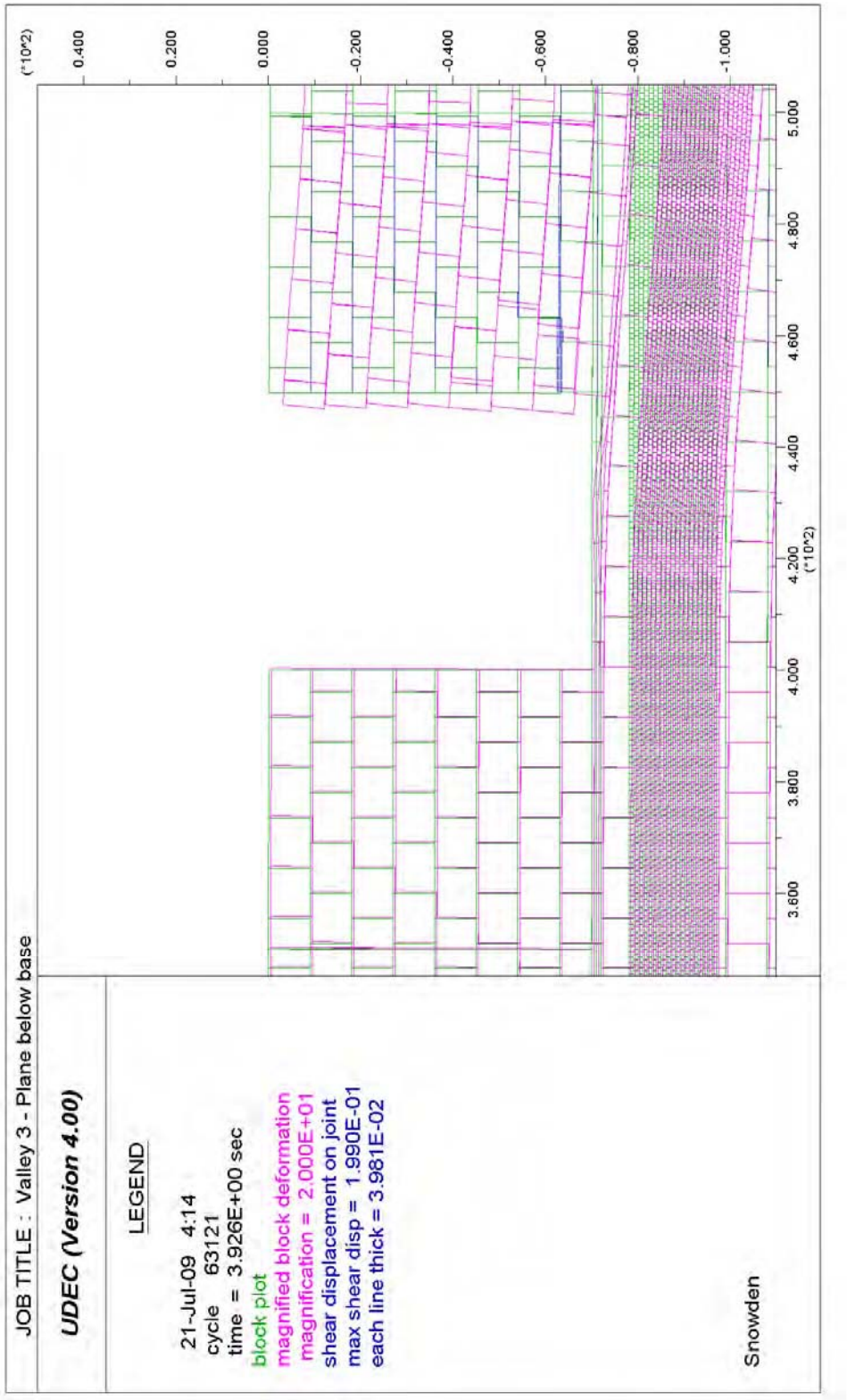

Fig. 6.30 – Block deformation and shear when valley is 100 m from longwall centreline (bedding and joints in upper 70 m of Hawkesbury Sandstone)

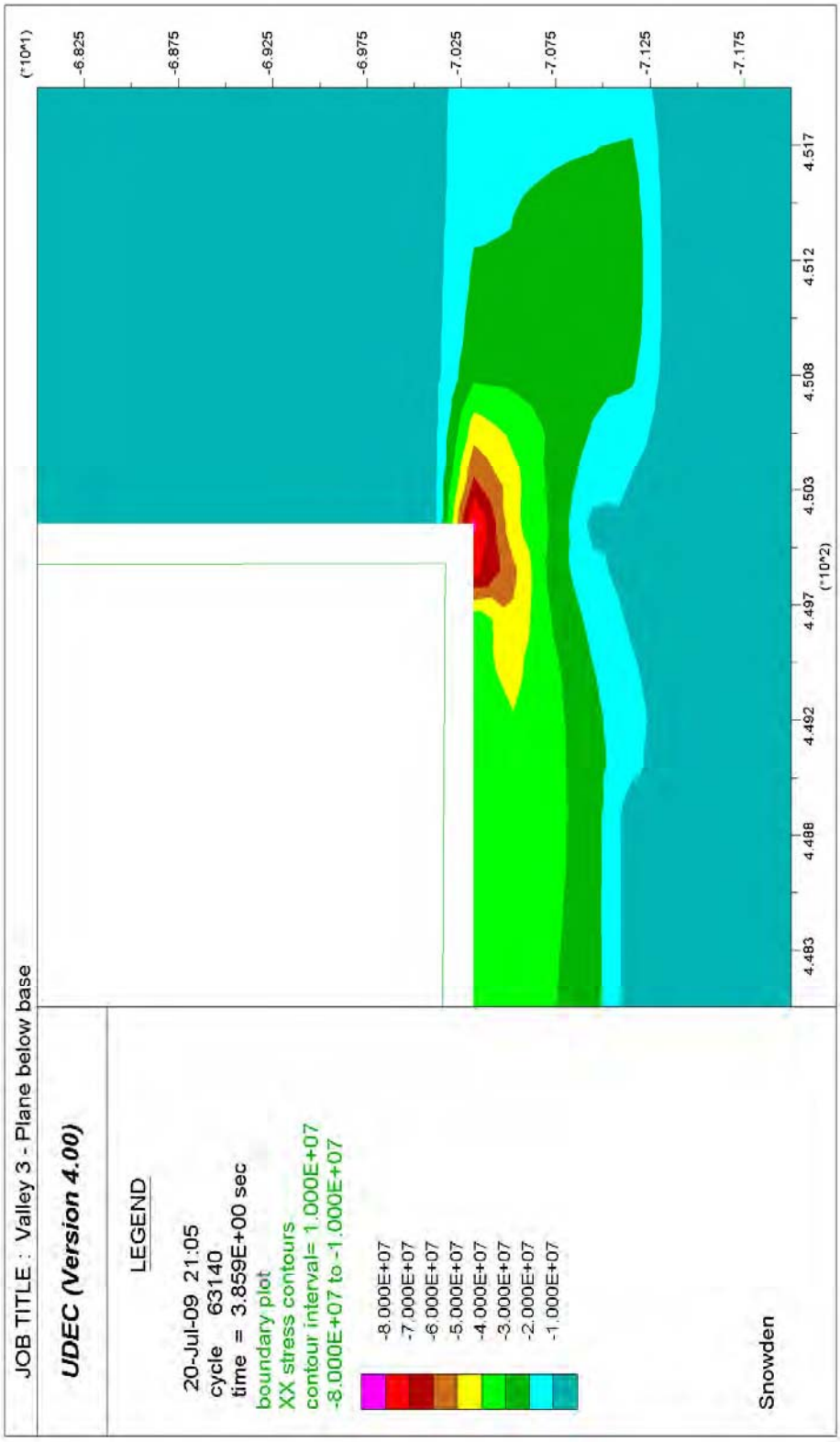

Fig. 6.31 – Horizontal stress when valley is 100 m from longwall centreline (no bedding and joints in upper 70 m of Hawkesbury Sandstone)

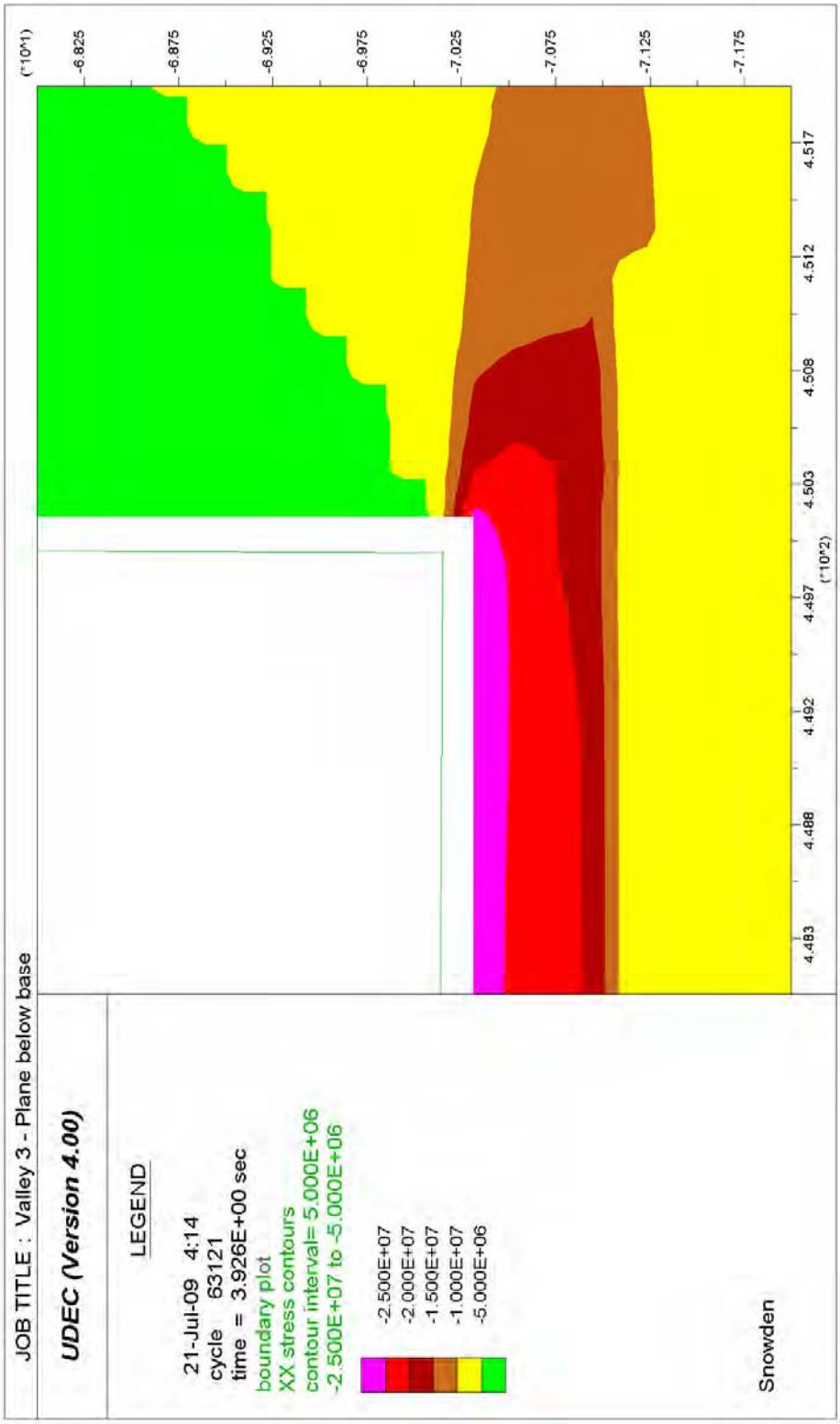

Fig. 6.32 – Horizontal stress when valley is 100 m from longwall centreline (bedding and joints in upper 70 m of Hawkesbury Sandstone)

6.5.4 Valley closure at shoulders

It can be seen from Figure 6.33 and Figure 6.34 that the general trend in closure was for the maximum to be above the centre of the longwall panel, and reducing as the distance from the longwall centreline increased. When valleys are represented as blocks sliding on a plane, the closure at the valley shoulders is a function of the geometry of the subsidence profile, hence the greatest closure above the longwall centreline. This is illustrated in Figure 6.35.

When the upper 70 m of the Hawkesbury Sandstone contained no bedding or joints, it can be seen from Figure 6.33 that the most valley closure was produced when the translation plane was at the base of the valley. When the translation plane was moved underneath the base of the valley by one metre, and there were no joints in the beam formed by the translation plane, valley closure at the shoulders was reduced by an average of 37 %. The greatest reduction as a percentage of original closure occurred at the point 150 m away from the longwall centreline, where a 65 % reduction in closure occurred.

In Figure 6.33, the closure occurring when the translation plane was beneath the base of the valley exceeded the closure when the translation plane was at the base of the valley when the valley was 100 m from the longwall centreline. An examination of the block movements in both of these cases revealed that when the beam was beneath the base of the valley, it was buckling not only at the valley base, but also adjacent to the valley. This resulted in the block adjacent to the valley being tilted towards the valley which produced the greater valley closure. This is illustrated in Figure 6.36 and Figure 6.37.

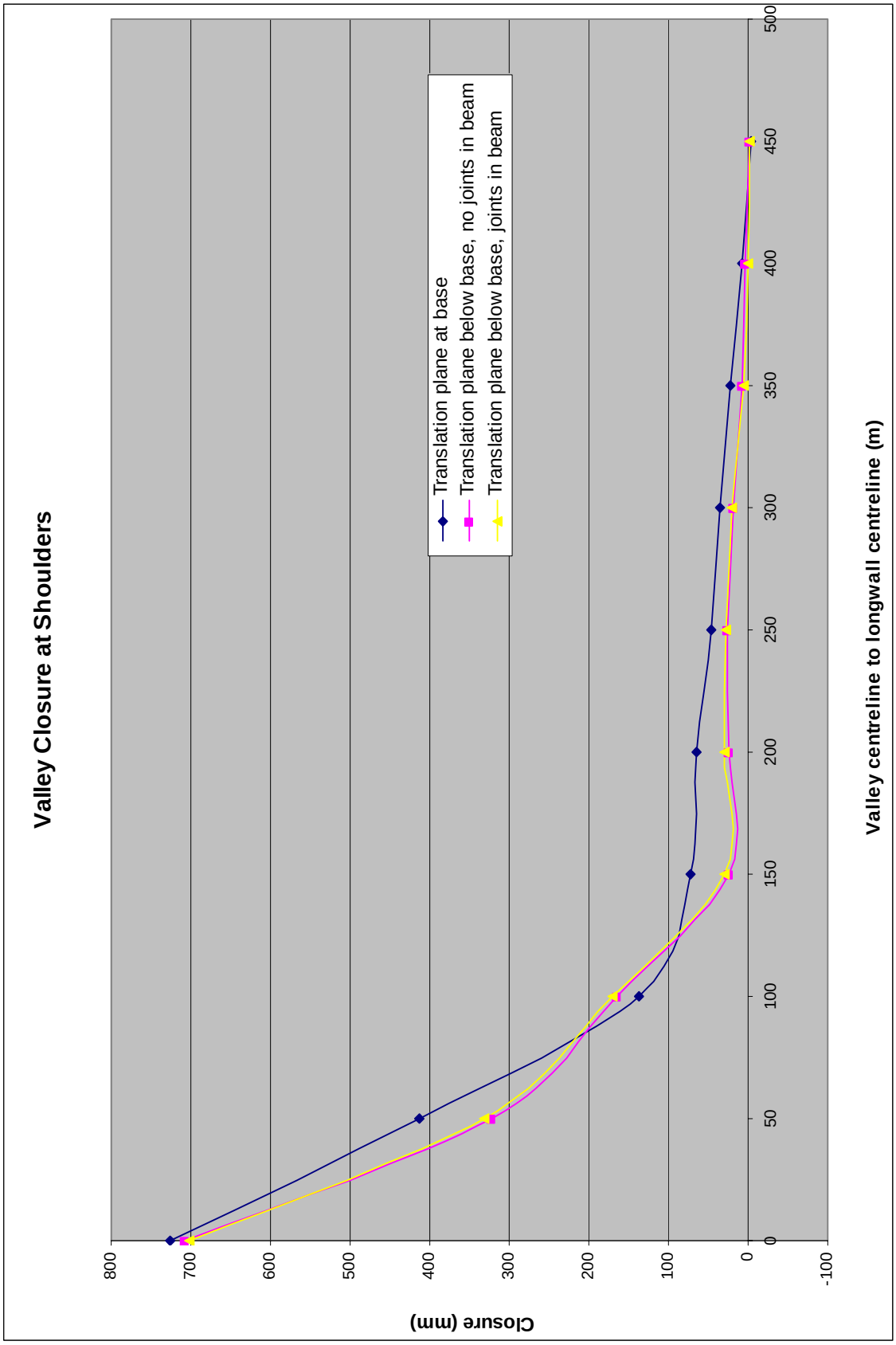

Fig. 6.33 – Valley closure at shoulders (no bedding and joints in upper 70 m of Hawkesbury Sandstone)

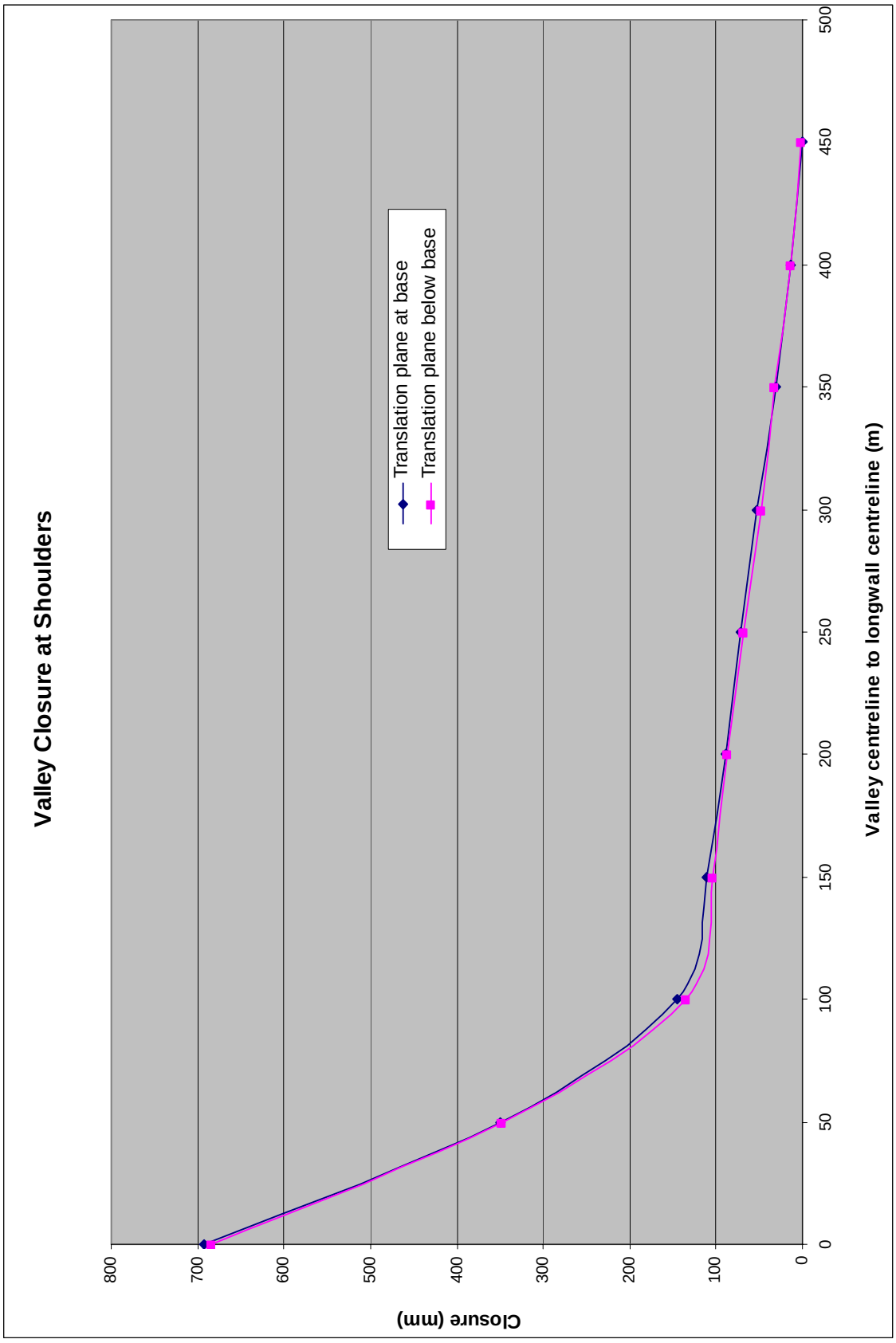

Fig. 6.34 – Valley closure at shoulders (bedding and joints in upper 70 m of Hawkesbury Sandstone)

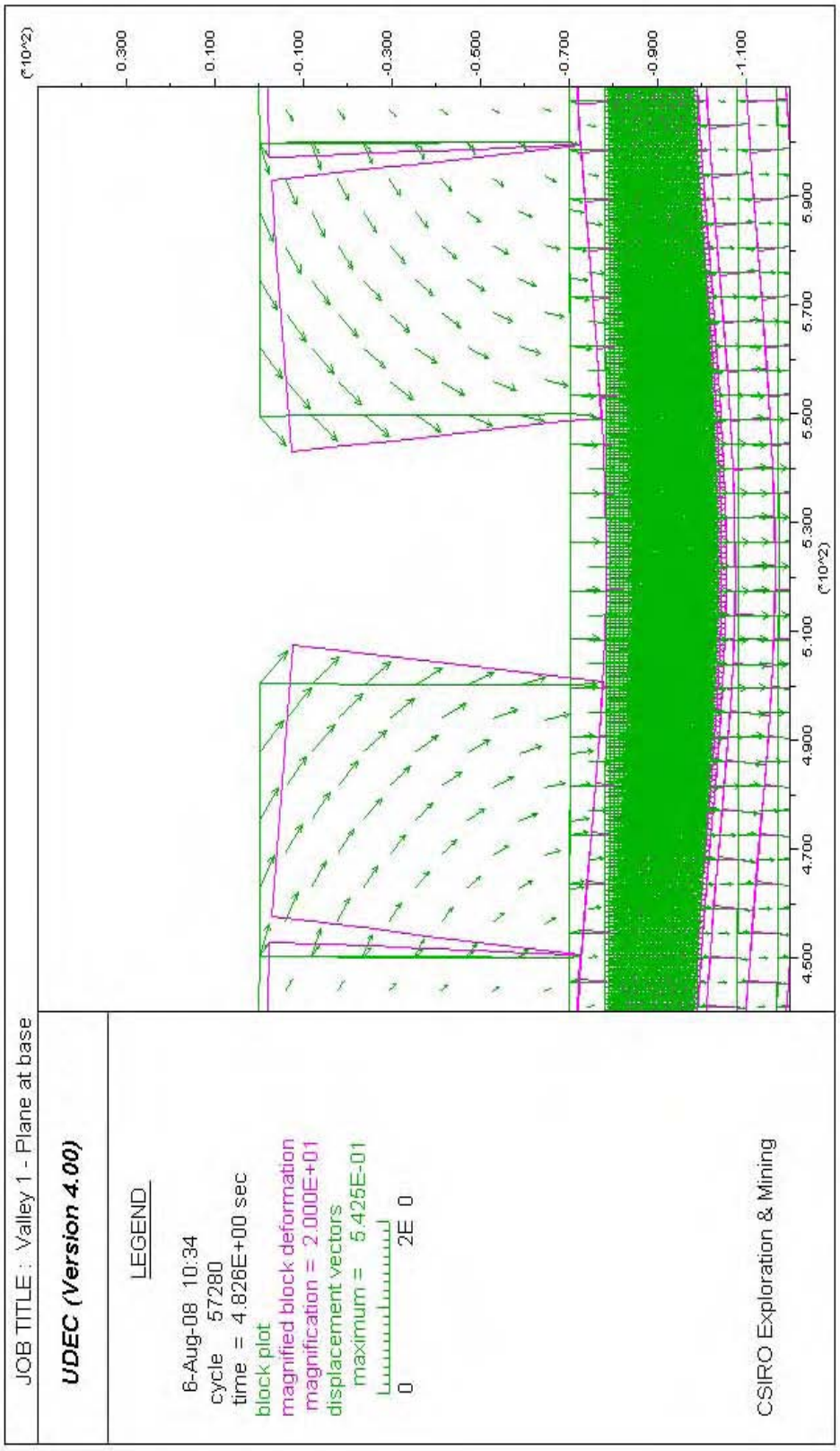

Fig. 6.35 – Exaggerated displacements above longwall centreline, plane at base

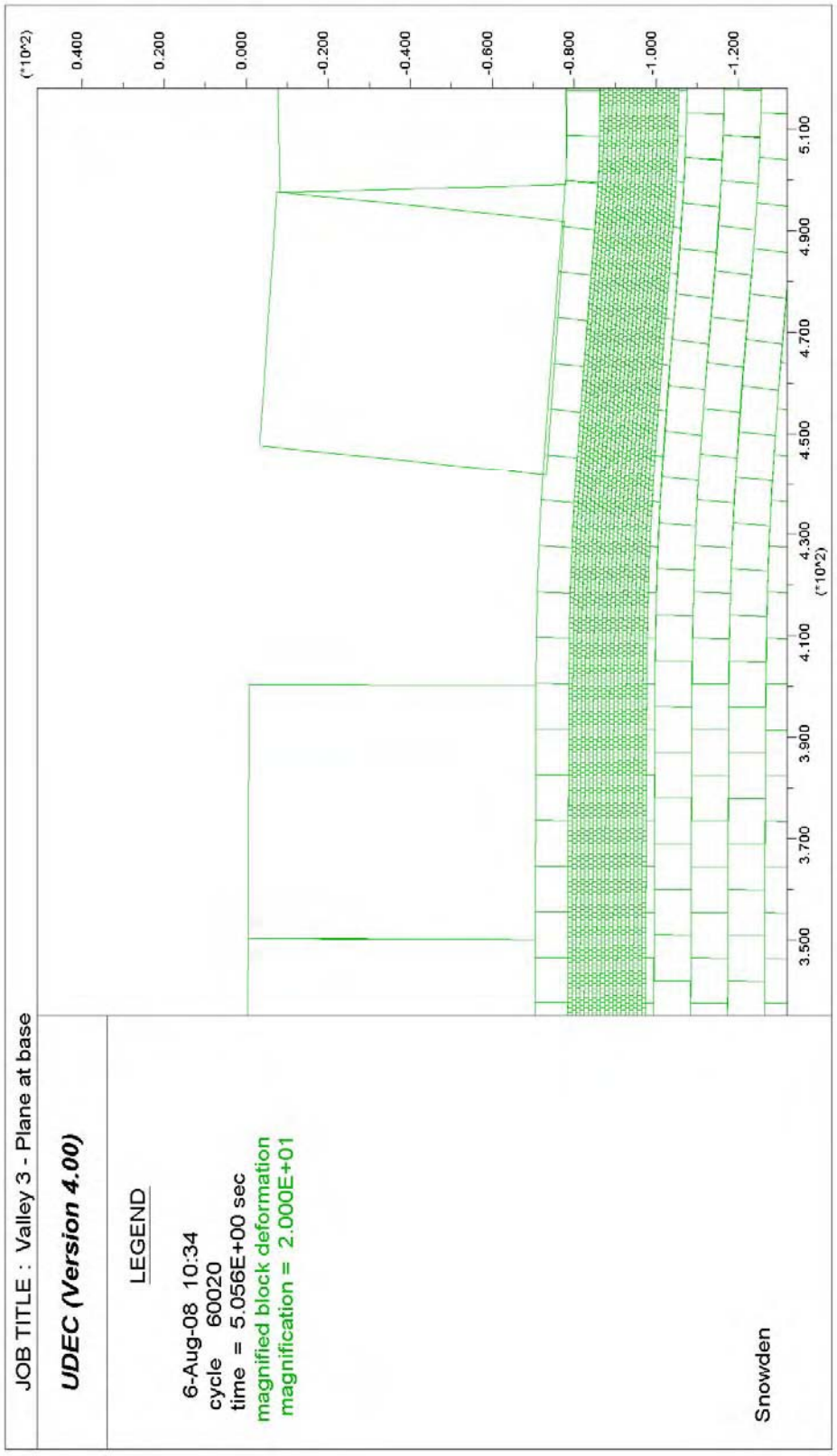

Fig. 6.36 – Exaggerated displacements, plane at base

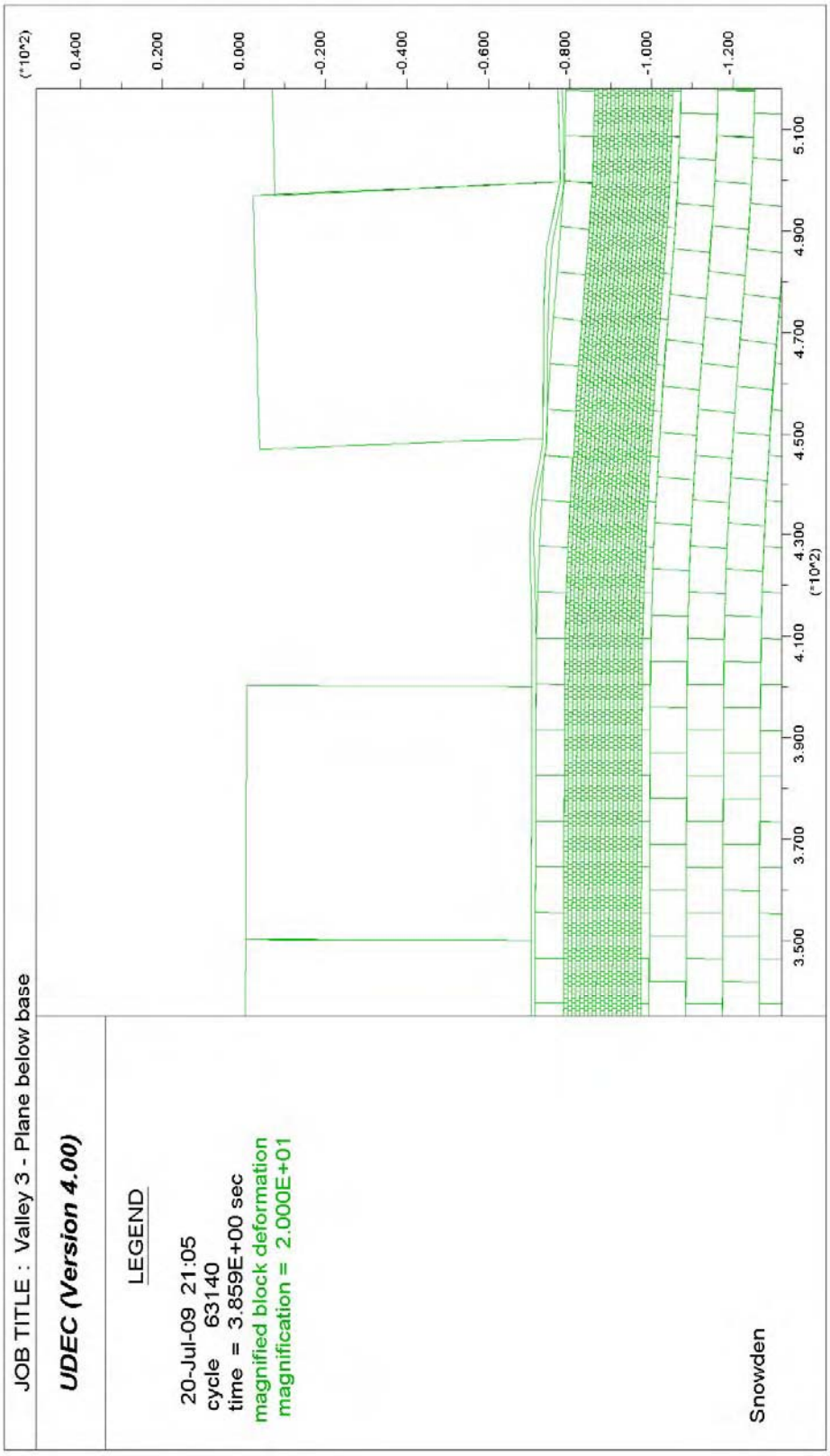

Fig. 6.37 – Exaggerated displacements, plane below base

When joints were added to the beam formed by the translation plane, it can be seen from Figure 6.33 that the magnitude of closure was generally the same compared to the models with no joints in the beam. This was to be expected, as the presence of joints in the beam formed by the translation plane did not increase the maximum developed subsidence substantially, compared to when the joints were absent.

It can be seen from Tables 6.4 to 6.6 that closure at the shoulders was negative around 450 m from the longwall centreline. This was a result of the modelling procedure, where the sides of the models were fixed, so the last valley actually opened up as the subsidence profile formed (Figure 6.38). In some instances valley closure was still positive, but the magnitude of closure involved is in the order of millimetres and as such, was ignored in this analysis.

When the upper 70 m of the Hawkesbury Sandstone contained bedding and joints, it can be seen from Figure 6.34 there was very little difference in closure at the valley shoulders between the translation plane at the base of the valleys, and the translation plane below the base of the valleys. Accordingly, there were no instances of yield in the valley bases in the models where the translation plane was at the base of the valleys, due to slip along bedding in the upper 70 m of Hawkesbury Sandstone resulting in the valley walls being pushed into the valley in a staggered pattern and releasing any build up of horizontal stresses (Figure 6.30). As such, this lends support to the observation by Holla and Barclay (2000) that rigid block type movements occur out in the field.

Figure 6.39 is an illustration of the tensile areas around a valley that was 350 m from the longwall centreline. Figure 6.40 is an illustration of valley closure in the same valley when the translation plane was at the base of the valley – this figure confirms that valley closure in the tensile portion of the subsidence profile is a result of blocks being pushed into the void created by the valley.

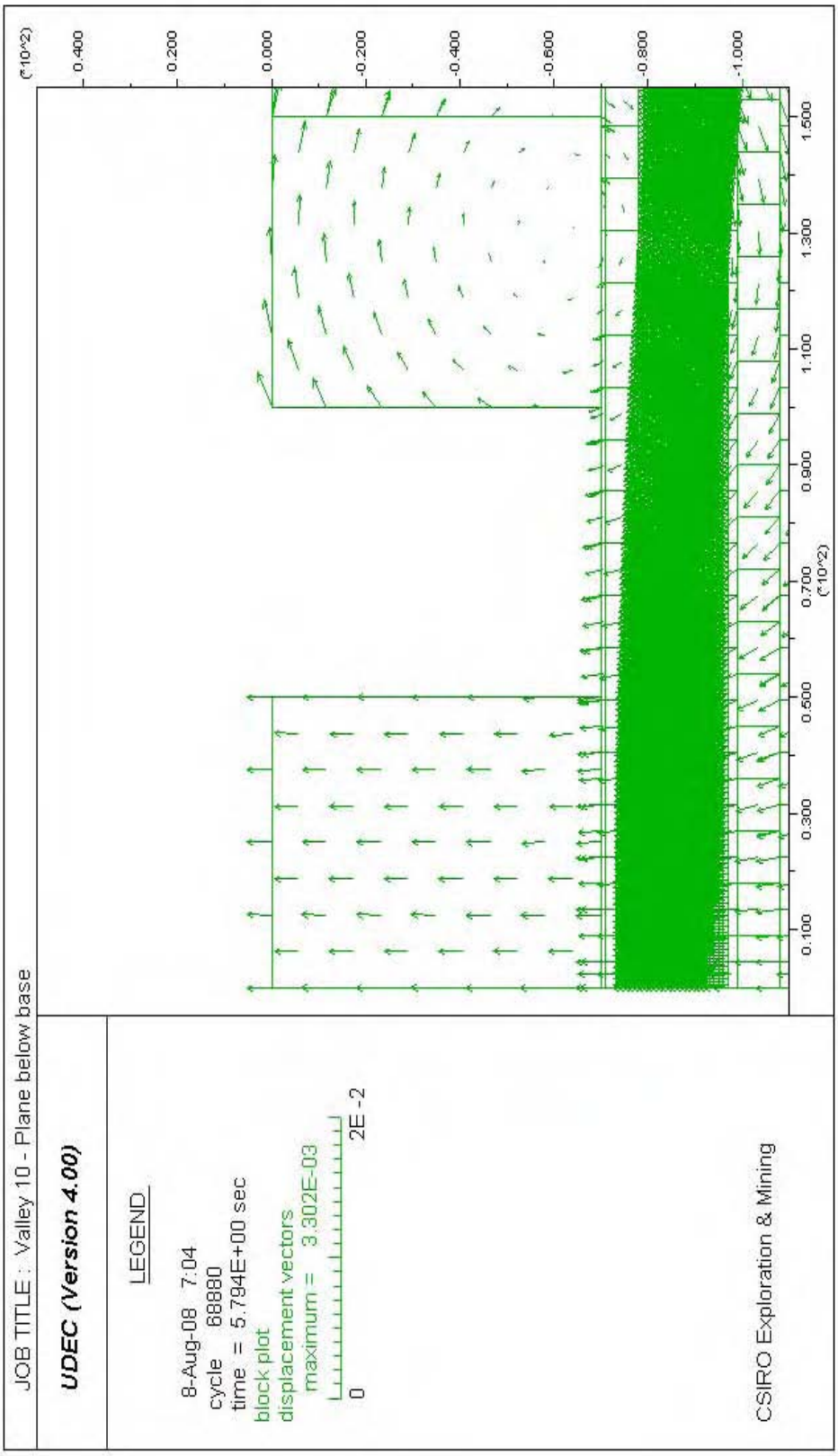

Fig. 6.38 – Example of negative valley closure due to boundary conditions

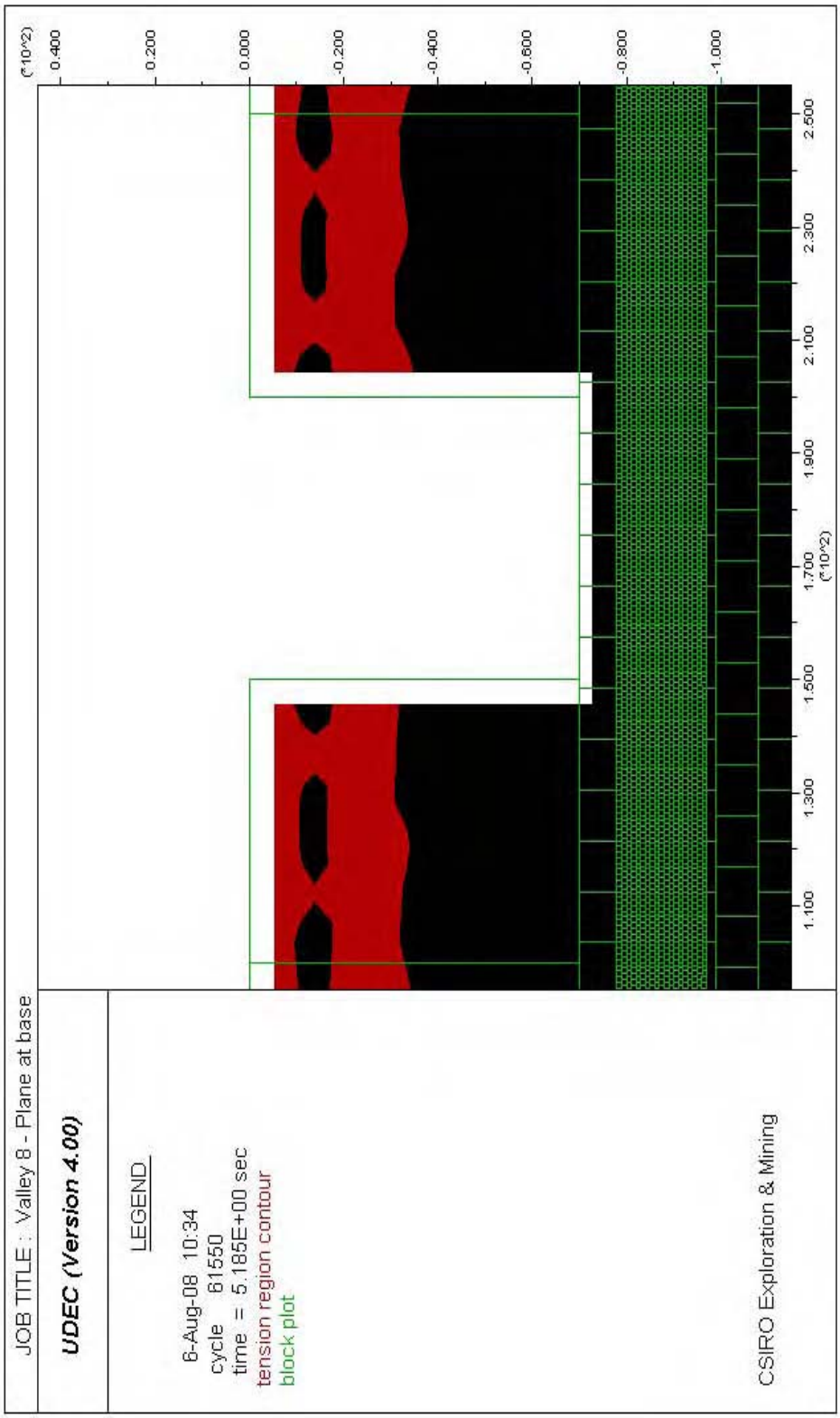

Fig. 6.39 – Tensile areas around valley located 350 m from longwall centreline, plane at base

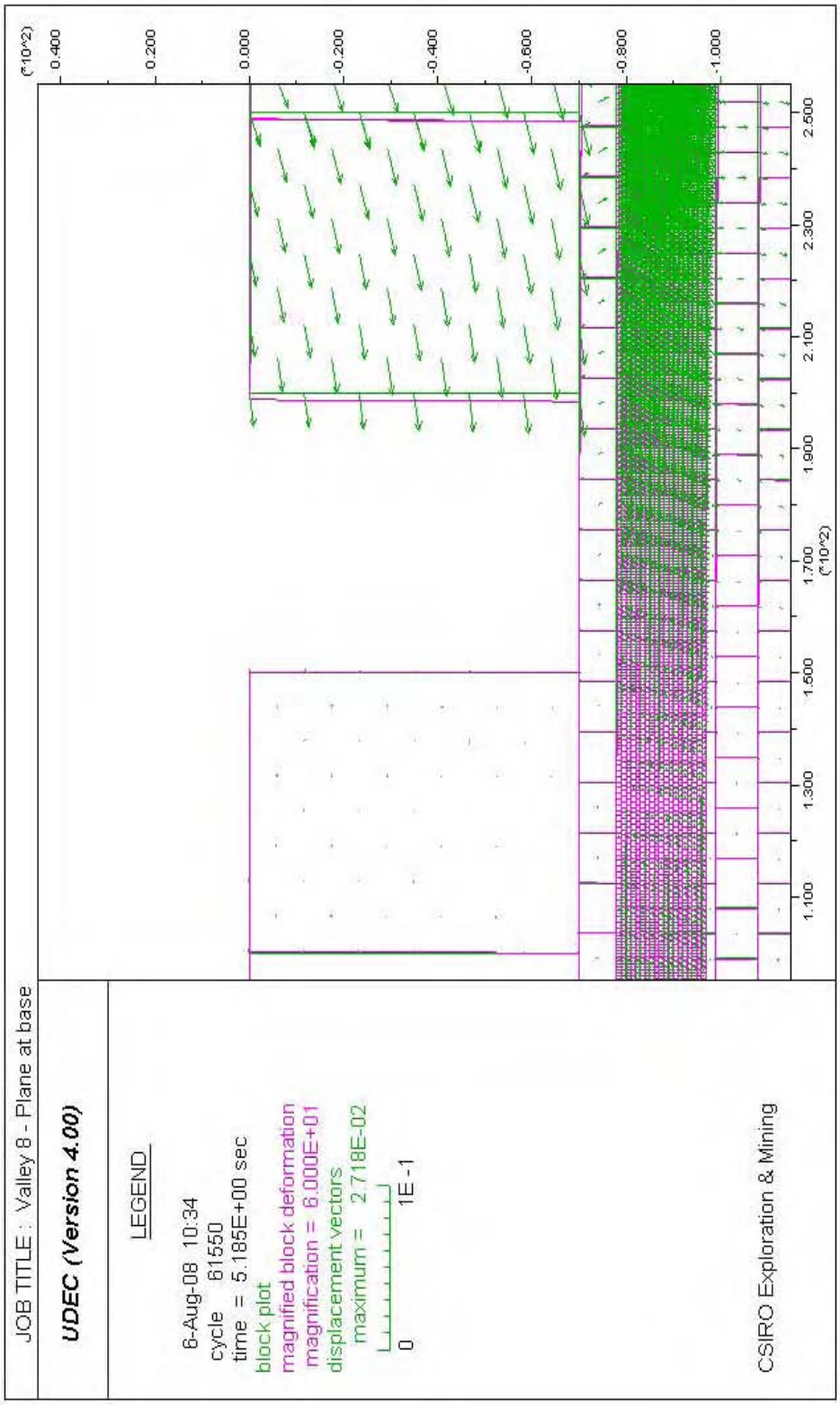

Fig. 6.40 – Valley closure when translation plane is at the base of the valley, 350 m from longwall centreline

6.5.5 Valley closure at base

Following on from valley closure at the shoulders, it can be seen from Figure 6.41 and Figure 6.42 that the development of valley closure at the base had the same characteristics as valley closure at the shoulders.

These characteristics were:

1. Closure is maximum when the translation plane was at the base of the valleys,
2. Closure is minimum when the translation plane was below the base of the valleys, and
3. Adding joints to the beam formed by the translation plane made minimal difference.

It can be seen from Figure 6.41 and Figure 6.42 that when no bedding and joints were added to the upper 70 m of Hawkesbury Sandstone, closure at the base peaked at 100 m from the longwall centreline when the translation plane was at the base of the valleys, and 150 m from the longwall centreline when the translation plane was below the base of the valleys. When bedding and joints were added to the upper 70 m of Hawkesbury Sandstone, the closure at the base peaked at 100 m from the longwall centreline when the translation plane was at the base of the valleys, and 0 m when the translation plane was below the valleys.

As with valley closure at the shoulders, Figure 6.41 and Figure 6.42 illustrate that valley closure at the base occurred in the tensile portion of the subsidence profile when the translation plane was at the base of the valley.

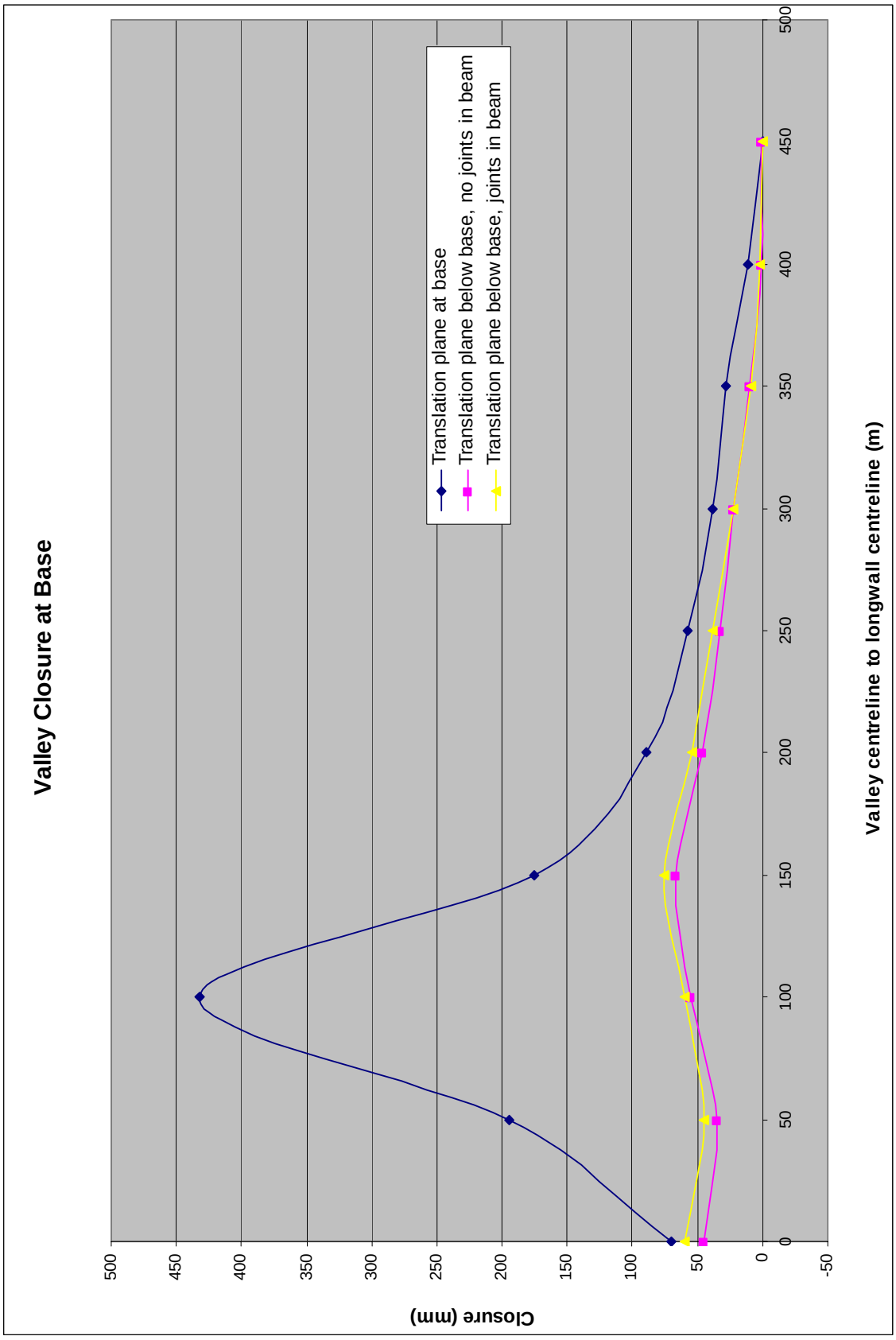

Fig. 6.41 – Valley closure at base (no bedding and joints in upper 70 m of Hawkesbury Sandstone)

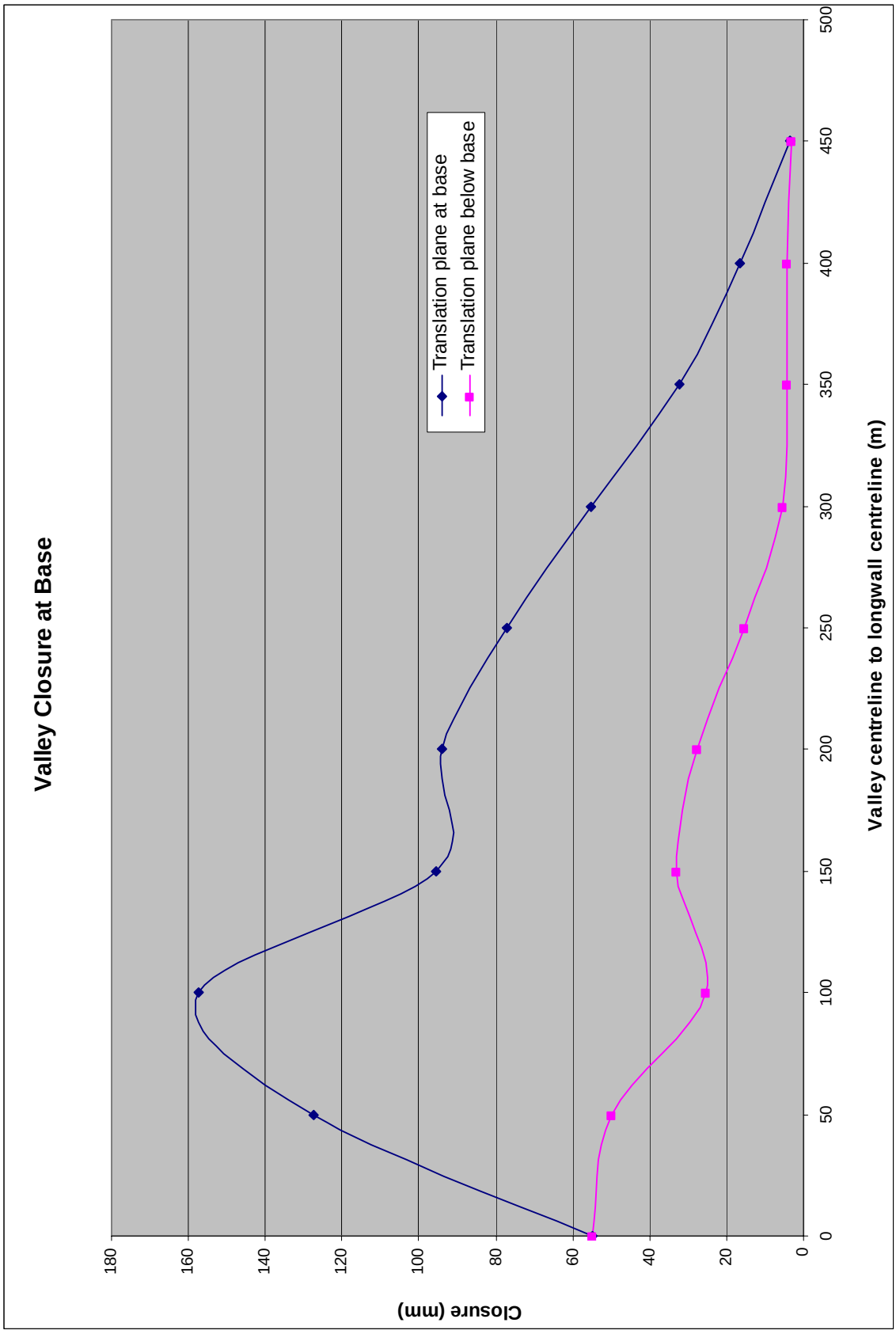

Fig. 6.42 – Valley closure at base (bedding and joints in upper 70 m of Hawkesbury Sandstone)

6.5.6 Valley base yield

The river valley models were examined for cases where yielded elements were present in the base of the valleys.

The models that contained bedding and joints in the upper 70 m of the Hawkesbury Sandstone did not contain any cases of yield in the valley bases when the translation plane was at the base of the valleys. This was expected because the extra bedding and joints in the walls of the valleys served to relieve any build up of horizontal stresses by sliding out. When the translation plane was below the base of the valleys, upsidence and beam buckling occurred, and the beam formed by the translation plane yielded when the valley was above the longwall centreline, and gradually tapered off at 50 m from the longwall centreline. Figure 6.43 is a plot of yield when the valley was directly above the longwall centreline, and Figure 6.44 is a plot of yield when the valley was 50 m from the longwall centreline.

The models that did not have any bedding and joints in the upper 70 m of the Hawkesbury Sandstone exhibited yield in the valley bases, and this occurred only when the translation plane was moved one metre below the base of the valleys. When the beam formed by the translation plane contained no joints, the yield occurred in valleys located directly above the longwall centreline, and out to 100 m from the longwall centreline. When the beam formed by the translation plane contained joints, yield occurred in valleys also up to 100 m longwall centreline. Figure 6.45 is a plot of yield when the valley was directly above the longwall centreline, and Figure 6.46 is a plot of yield when the valley was 100 m from the longwall centreline.

The increased occurrence of yield in the models without bedding and joints in the upper 70 m of Hawkesbury Sandstone implied that greater valley base yield occurred when the sides of the valleys were represented as rigid blocks, and this was supported by the rigid block movements observed by Holla and Barclay (2000).

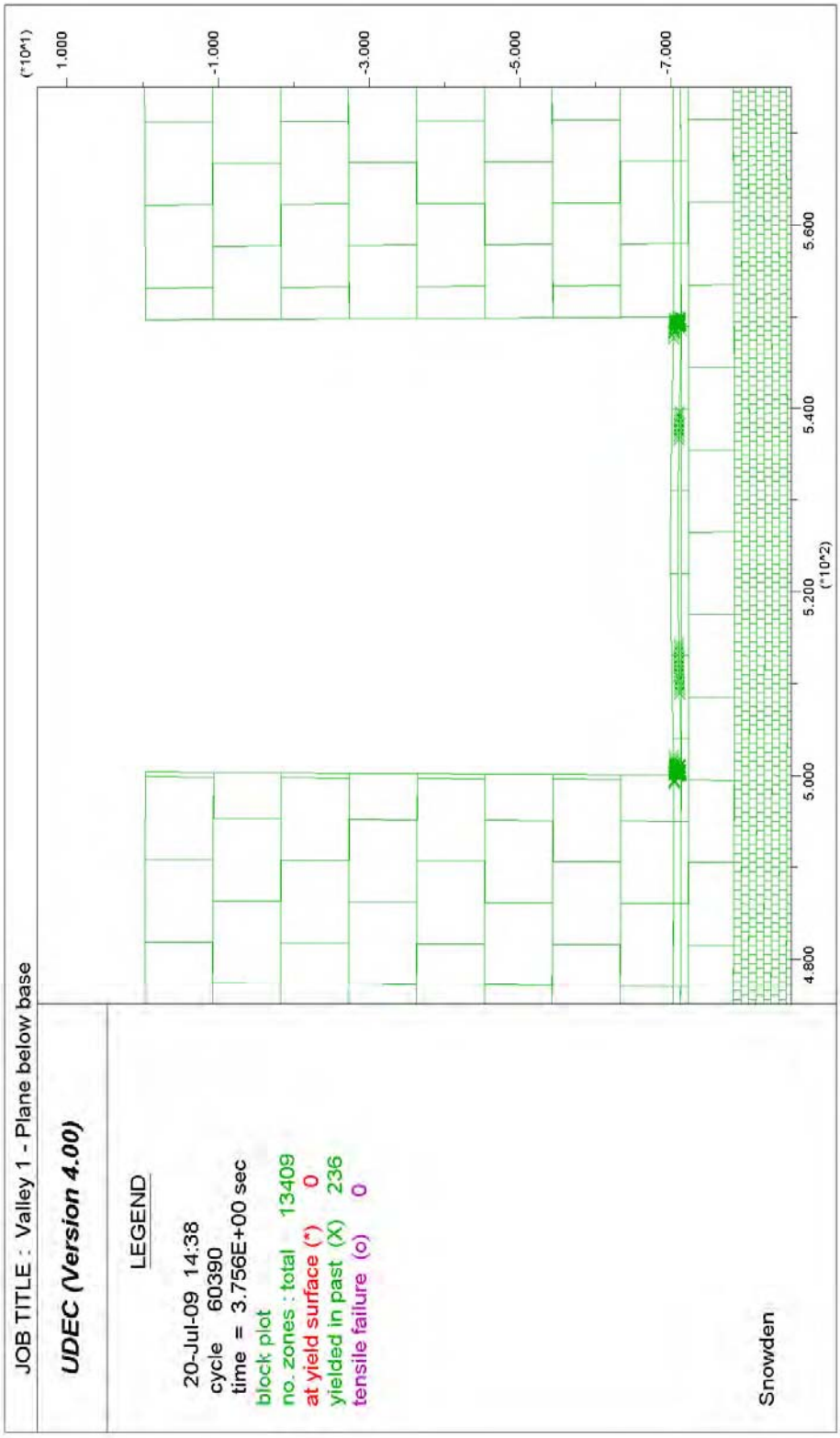

Fig. 6.43 – Yield in model when valley is 0 m from longwall centreline (plane below base, bedding and joints in upper 70 m of Hawkesbury Sandstone)

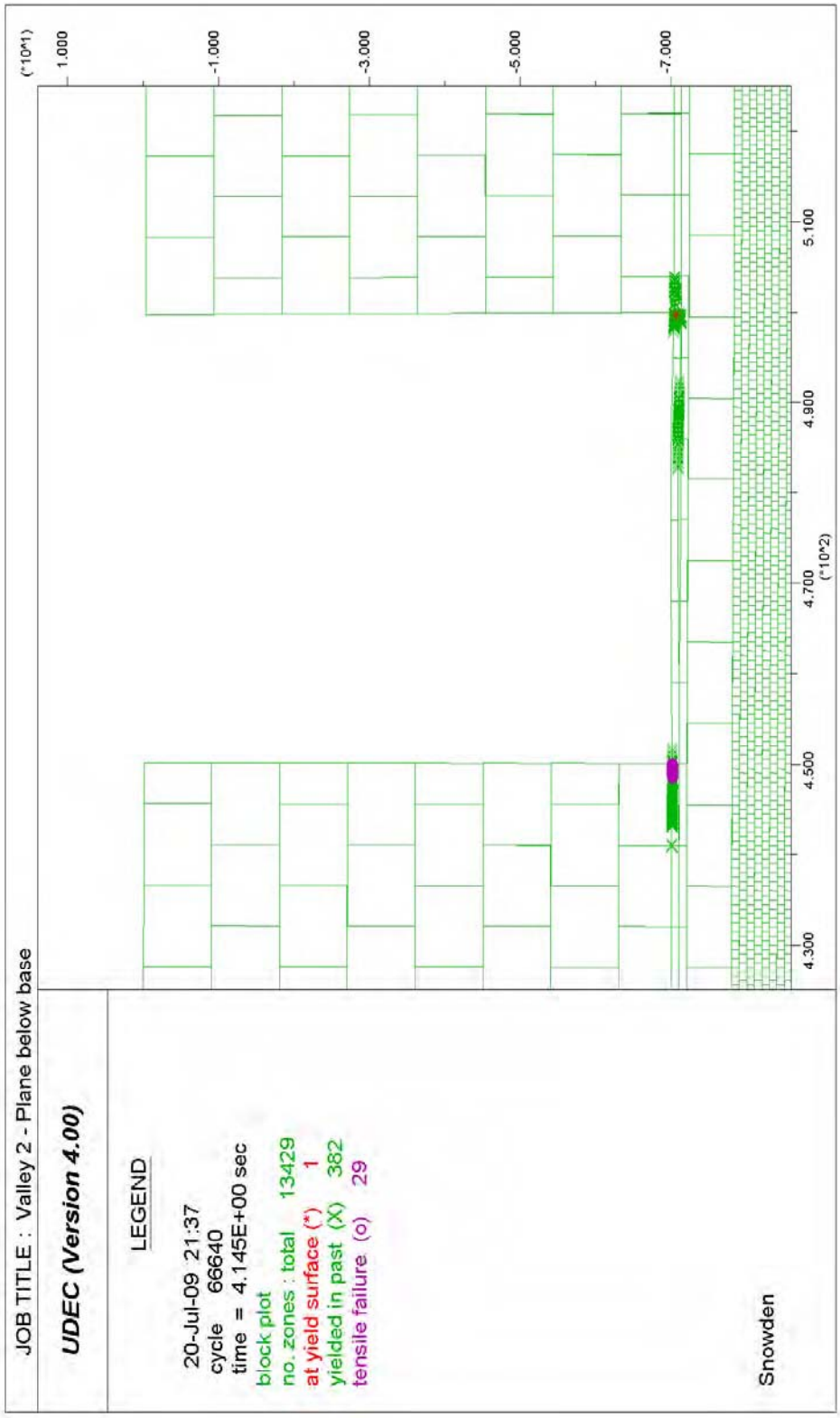

Fig. 6.44 – Yield in model when valley is 50 m from longwall centreline (plane below base, bedding and joints in upper 70 m of Hawkesbury Sandstone)

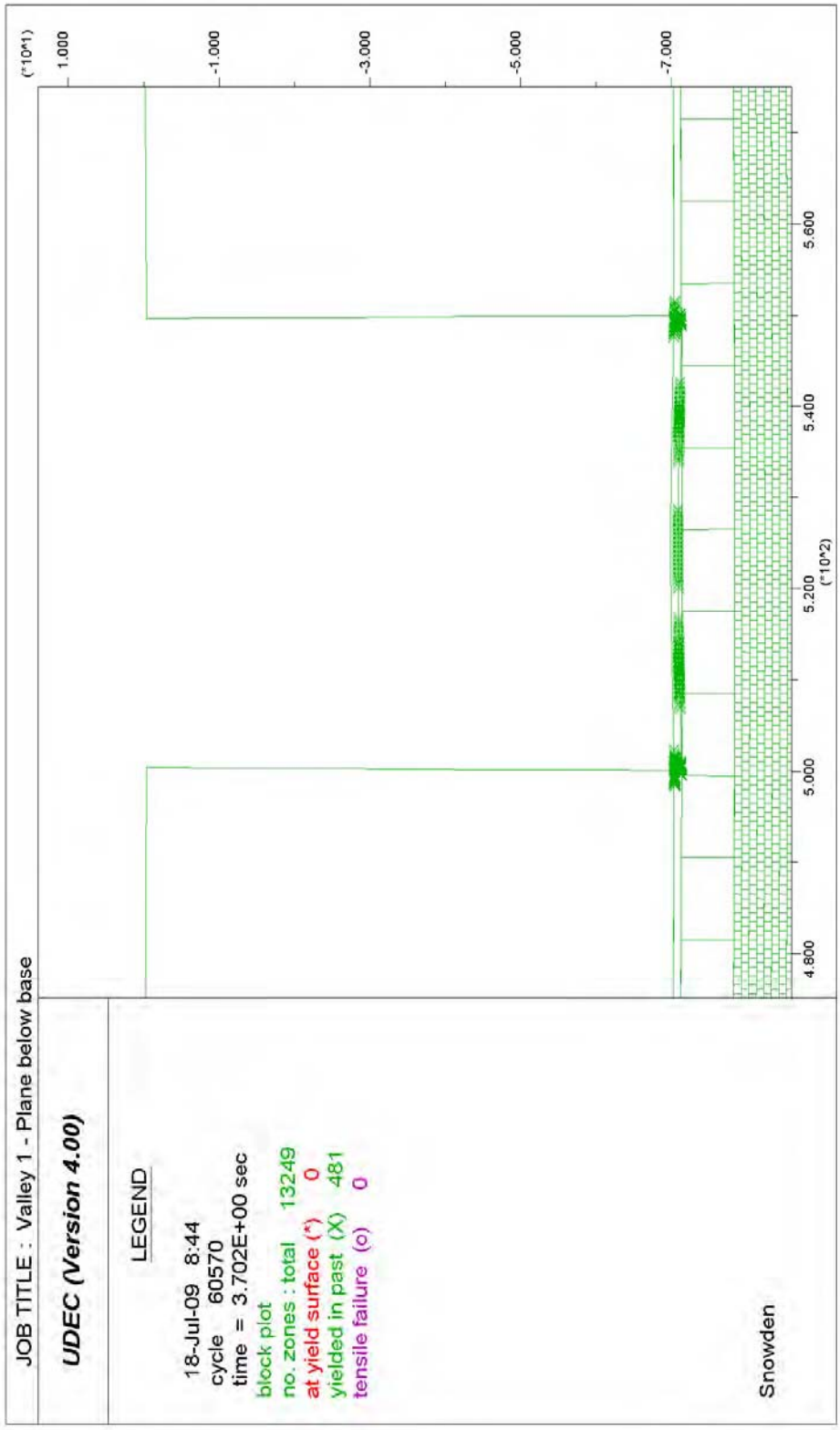

Fig. 6.45 – Yield in model when valley is 0 m from longwall centreline (plane below base, no bedding and joints in upper 70 m of Hawkesbury Sandstone)

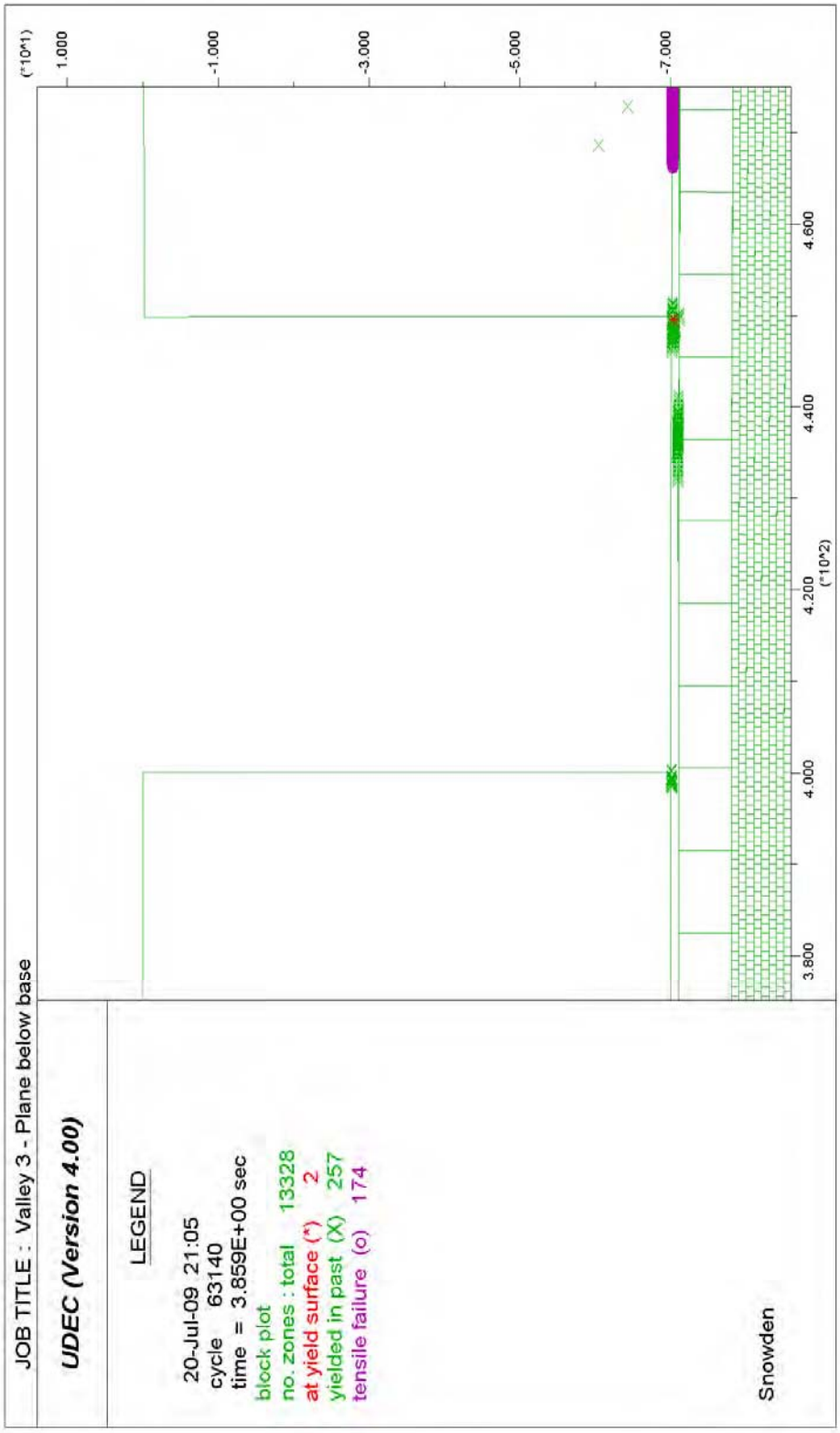

Fig. 6.46 – Yield in model when valley is 100 m from longwall centreline (plane below base, no bedding and joints in upper 70 m of Hawkesbury Sandstone)

6.6 COMPARISON TO EMPIRICAL DATA

The results from the models with no valley excavation indicated that average tilts ranged from 3.89 mm/m to 4.90 mm/m, both being close to the average tilt of 4 mm/m noted by Holla and Barclay (2000).

The closure results in Tables 6.4 to 6.8 are plotted (in red) against the empirical data plots produced by Waddington Kay and Associates (2002) in Figures 6.47 to 6.56 respectively. The upsidence results in Tables 6.9 to 6.11 are plotted (in red) against empirical data in Figures 6.57 to 6.59 respectively. It must be noted that not all values in the above mentioned tables were able to be plotted, either because they exceeded the maximum values on the empirical plots or they were negative (explained as boundary effects earlier).

It can be seen from Figures 6.47 to 6.59 that there are observed data points (in blue) and adjusted data points in the Waddington Kay and Associates database. From Figures 6.47 to 6.59 it is encouraging to note that the shoulder closure and upsidence results from the river valley models mostly fall within the adjusted upper bound curve and closely mirror the observed data points, instead of the adjusted data points. This suggests that the shoulder closure and upsidence patterns produced by the models replicated the trend observed in the empirical data.

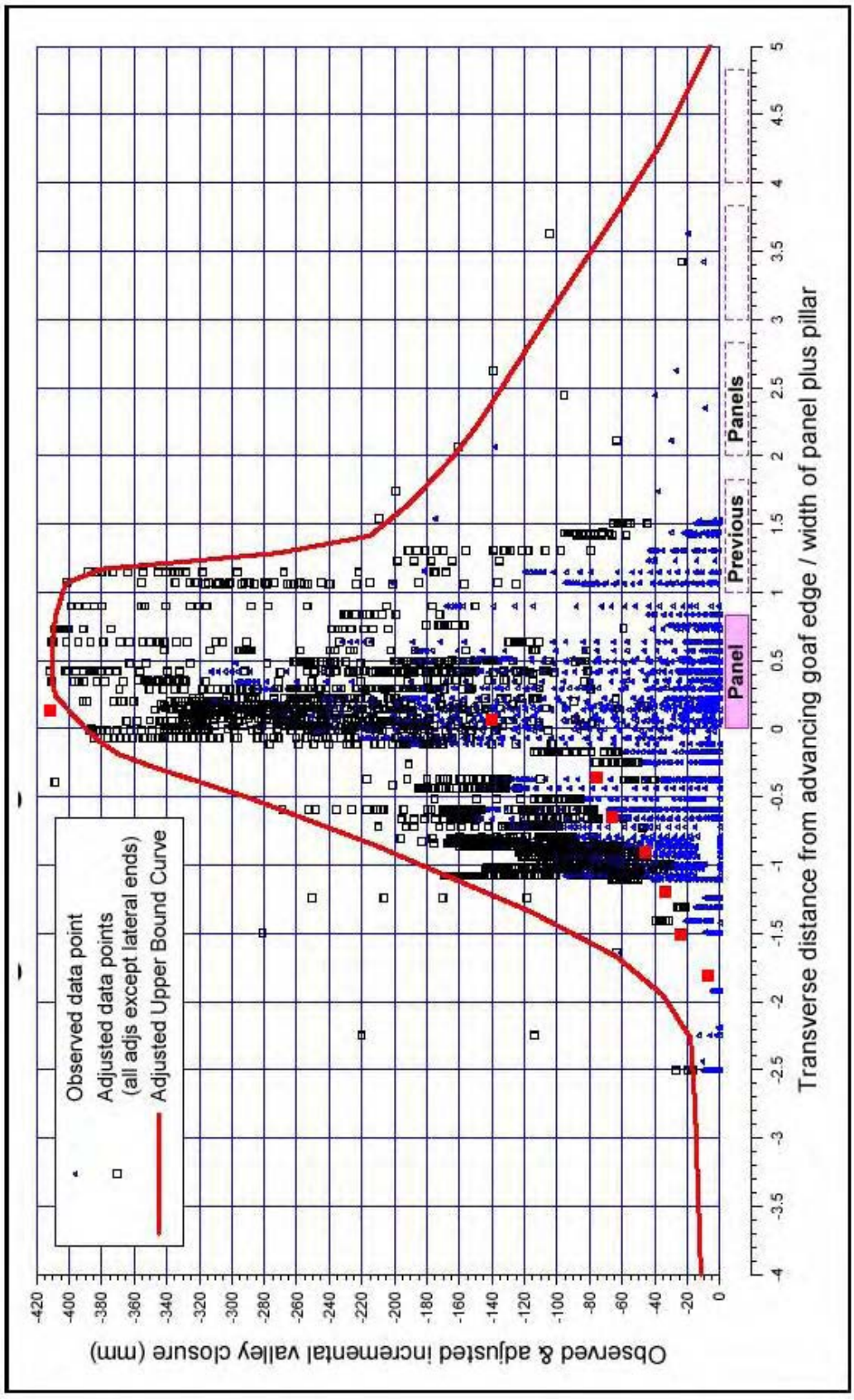

Fig. 6.47 – Closure at shoulders, no bedding and joints in upper 70 m of Hawkesbury Sandstone, translation plane at base

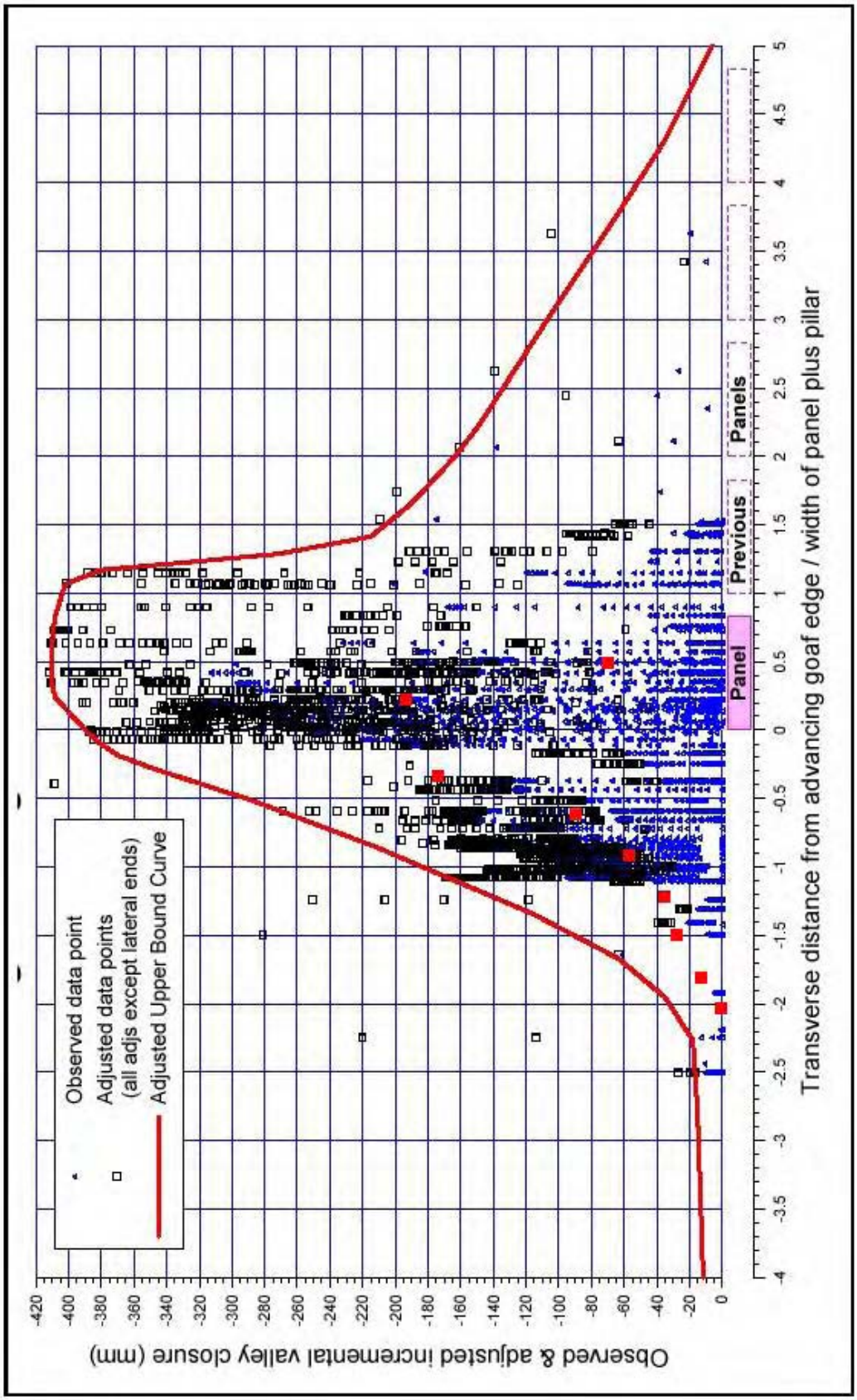

Fig. 6.48 – Closure at base, no bedding and joints in upper 70 m of Hawkesbury Sandstone, translation plane at base

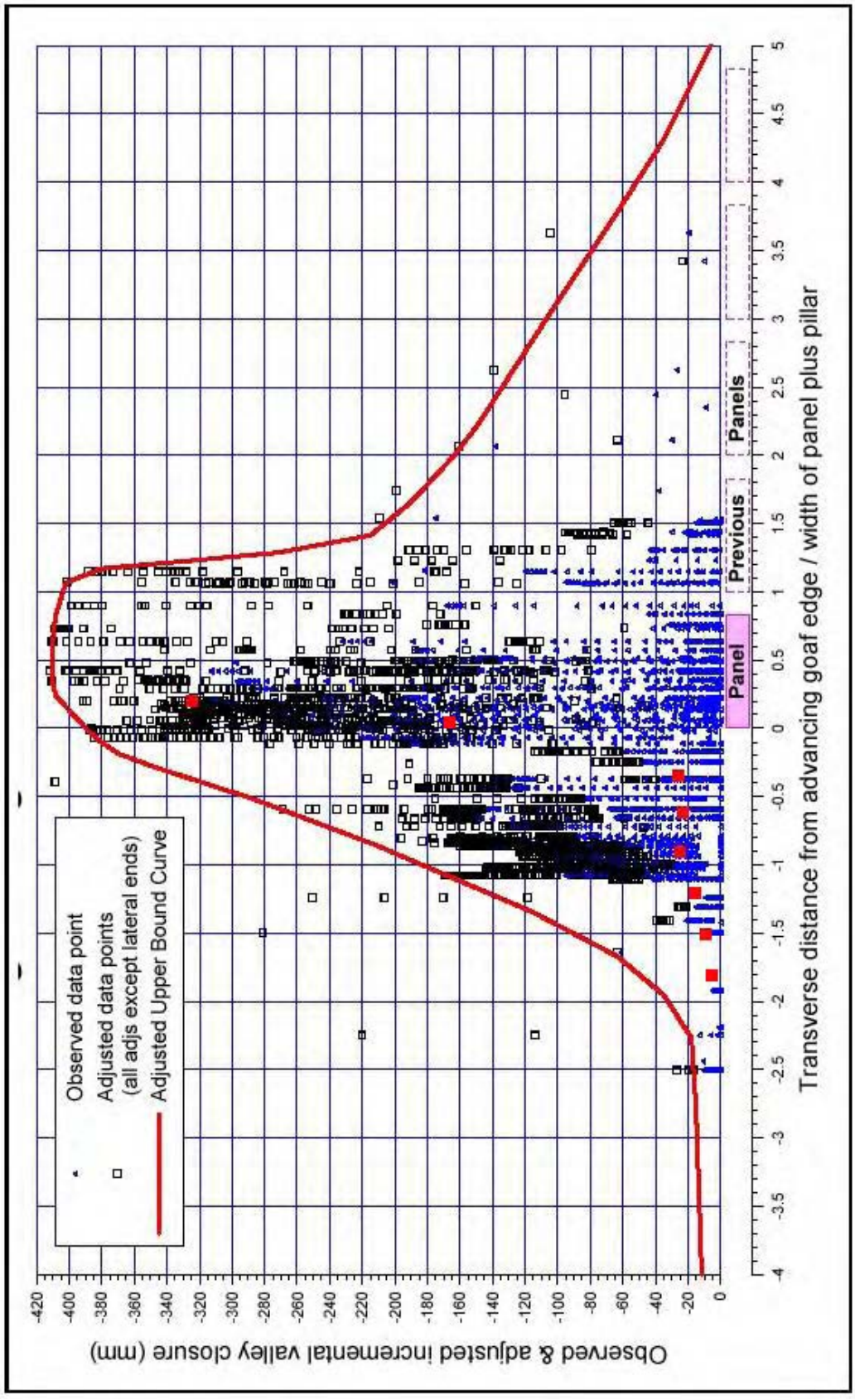

Fig. 6.49 – Closure at shoulders, no bedding and joints in upper 70 m of Hawkesbury Sandstone, translation plane below base, no joints in beam

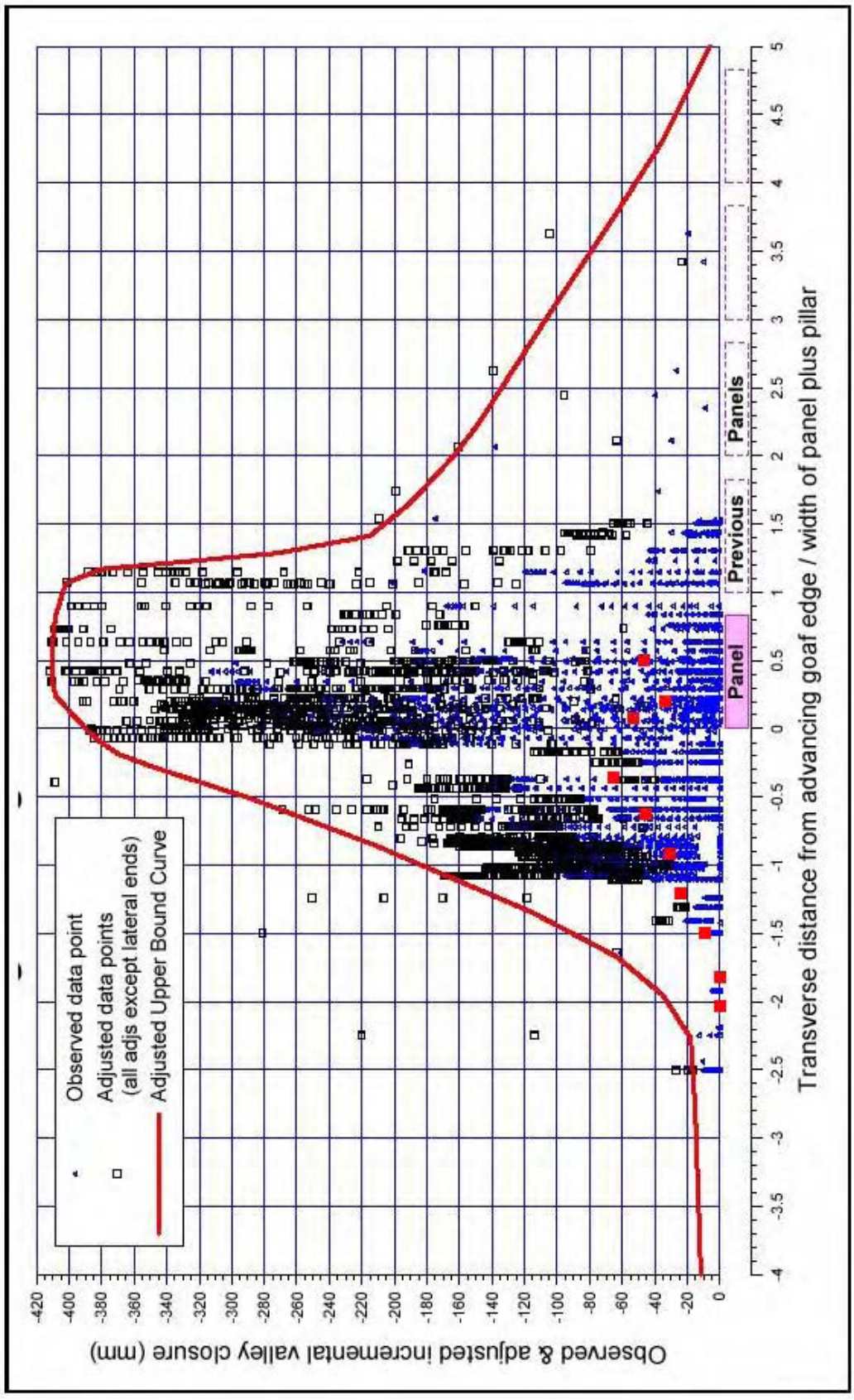

Fig. 6.50 – Closure at base, no bedding and joints in upper 70 m of Hawkesbury Sandstone, translation plane below base, no joints in beam

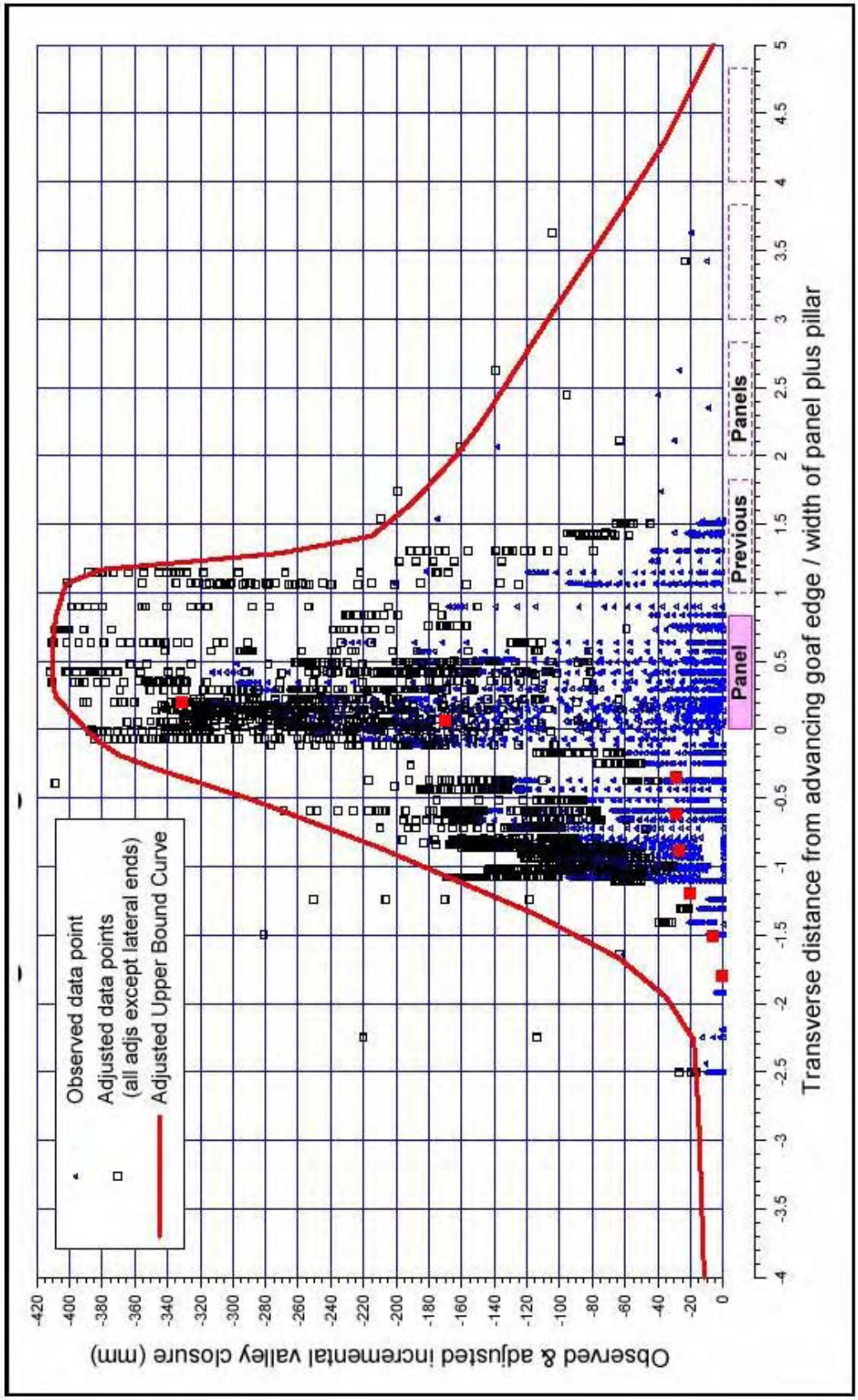

Fig. 6.51 – Closure at shoulders, no bedding and joints in upper 70 m of Hawkesbury Sandstone, translation plane below base, joints in beam

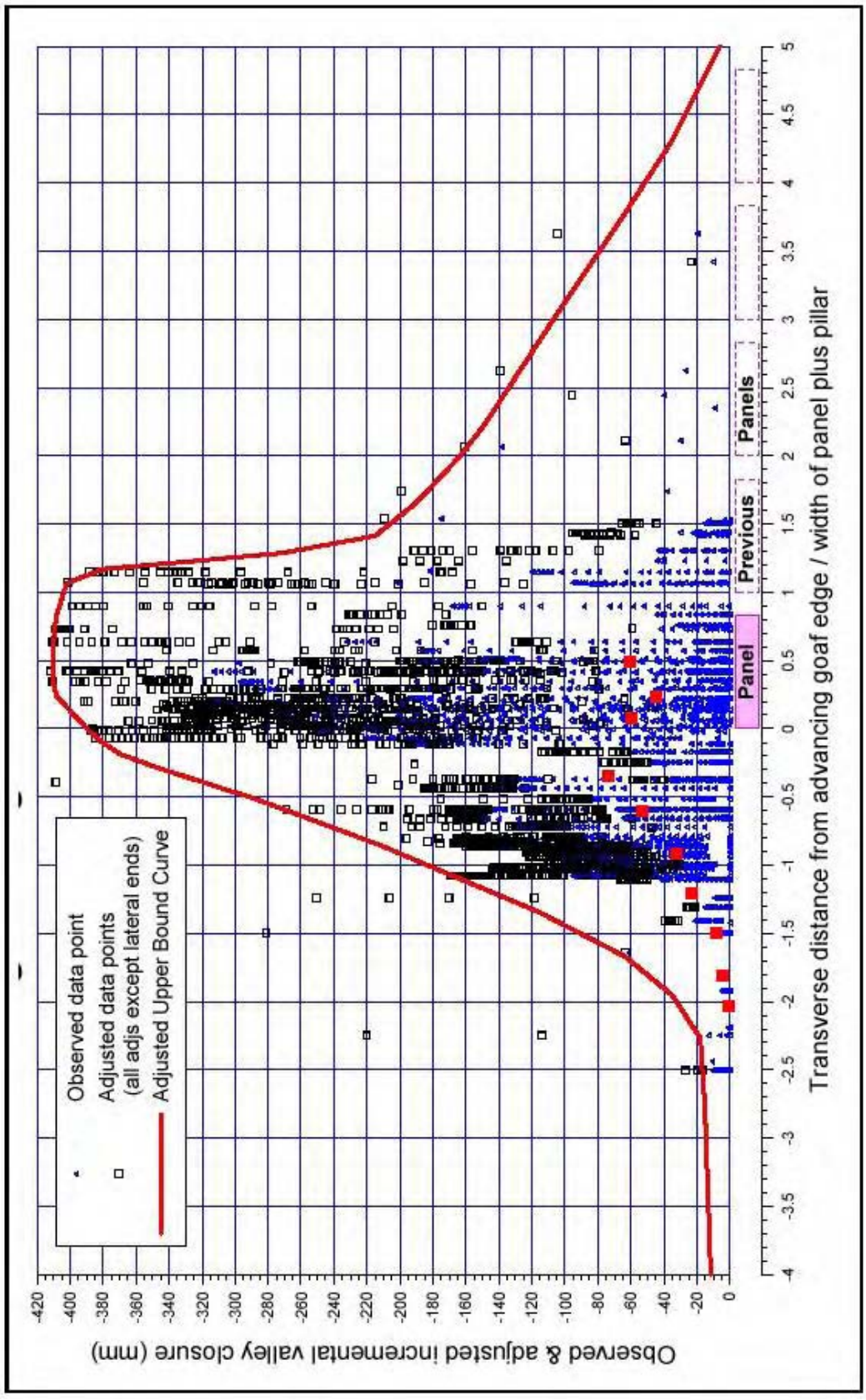

Fig. 6.52 – Closure at base, no bedding and joints in upper 70 m of Hawkesbury Sandstone, translation plane below base, joints in beam

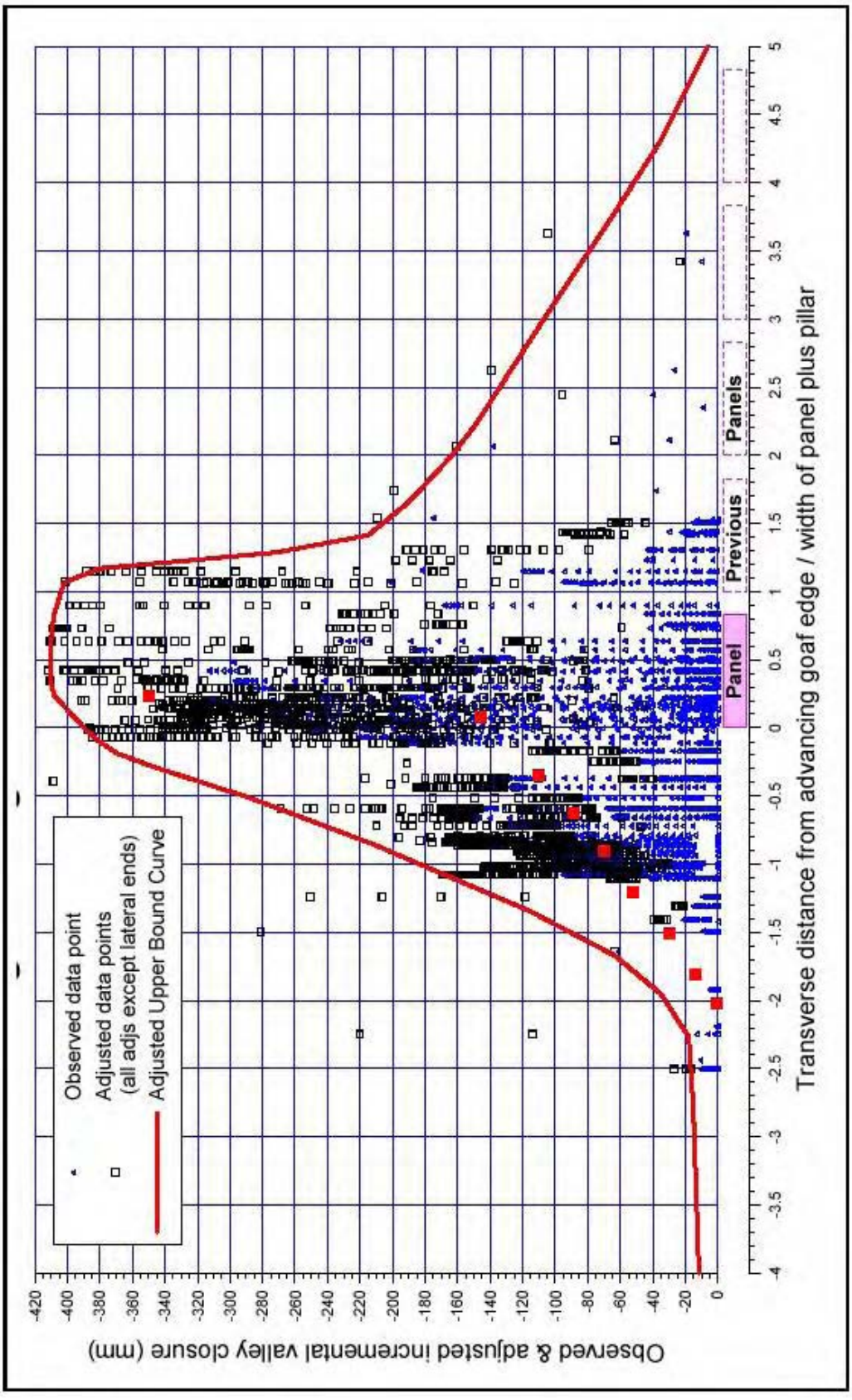

Fig. 6.53 – Closure at shoulders, bedding and joints in upper 70 m of Hawkesbury Sandstone, translation plane at base

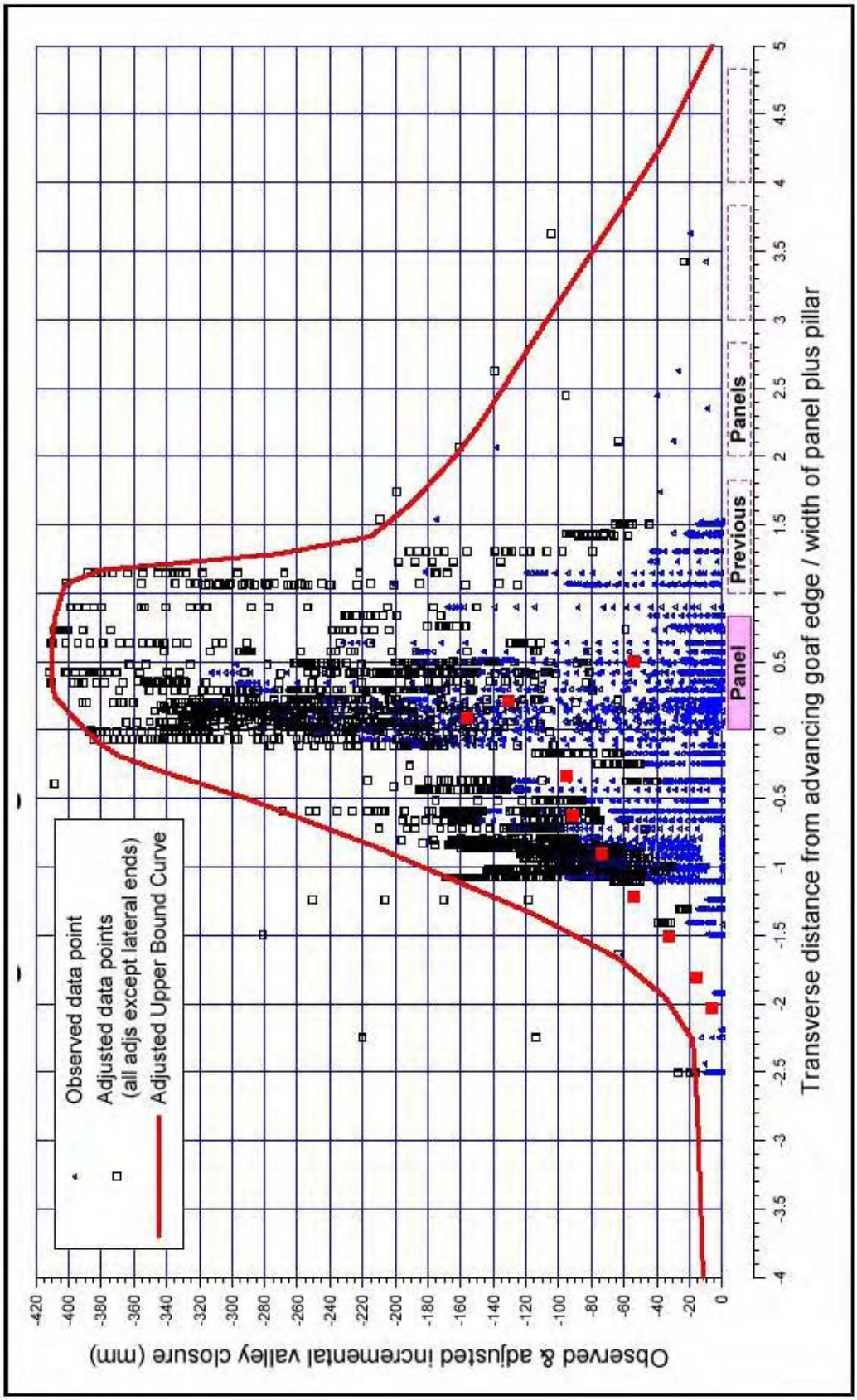

Fig. 6.54 – Closure at base, bedding and joints in upper 70 m of Hawkesbury Sandstone, translation plane at base

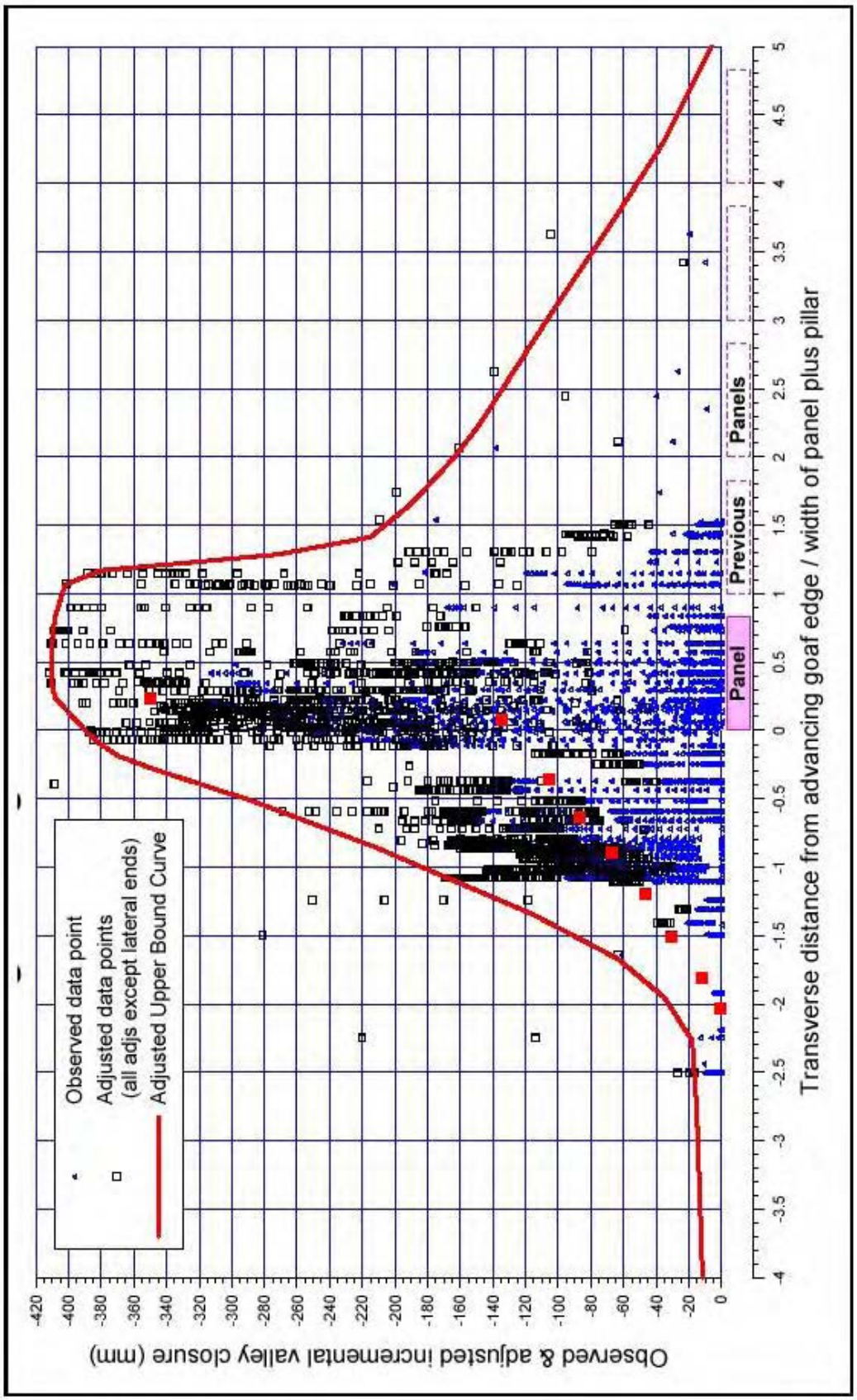

Fig. 6.55 – Closure at shoulders, bedding and joints in upper 70 m of Hawkesbury Sandstone, translation plane below base

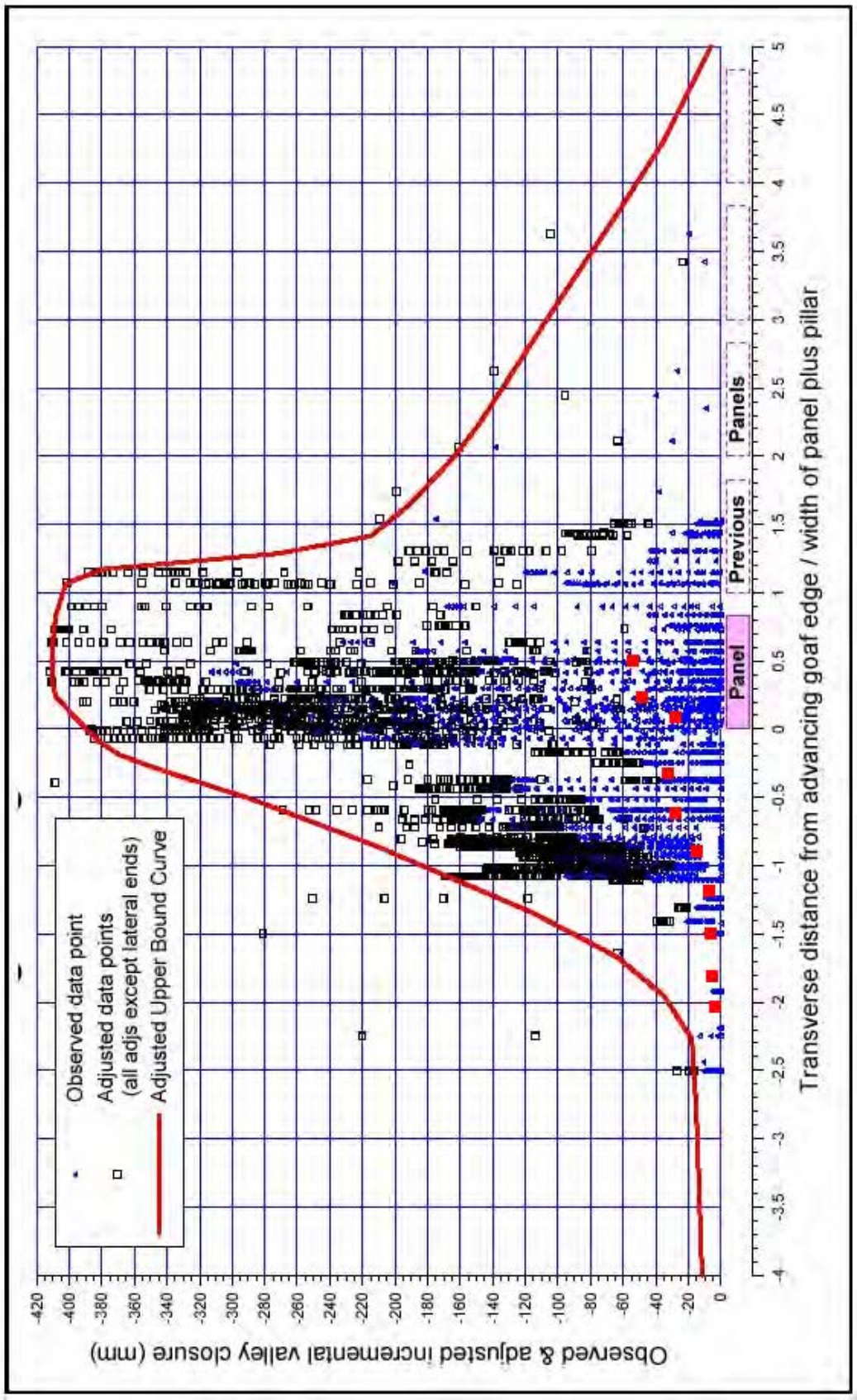

Fig. 6.56 – Closure at base, bedding and joints in upper 70 m of Hawkesbury Sandstone, translation plane below base

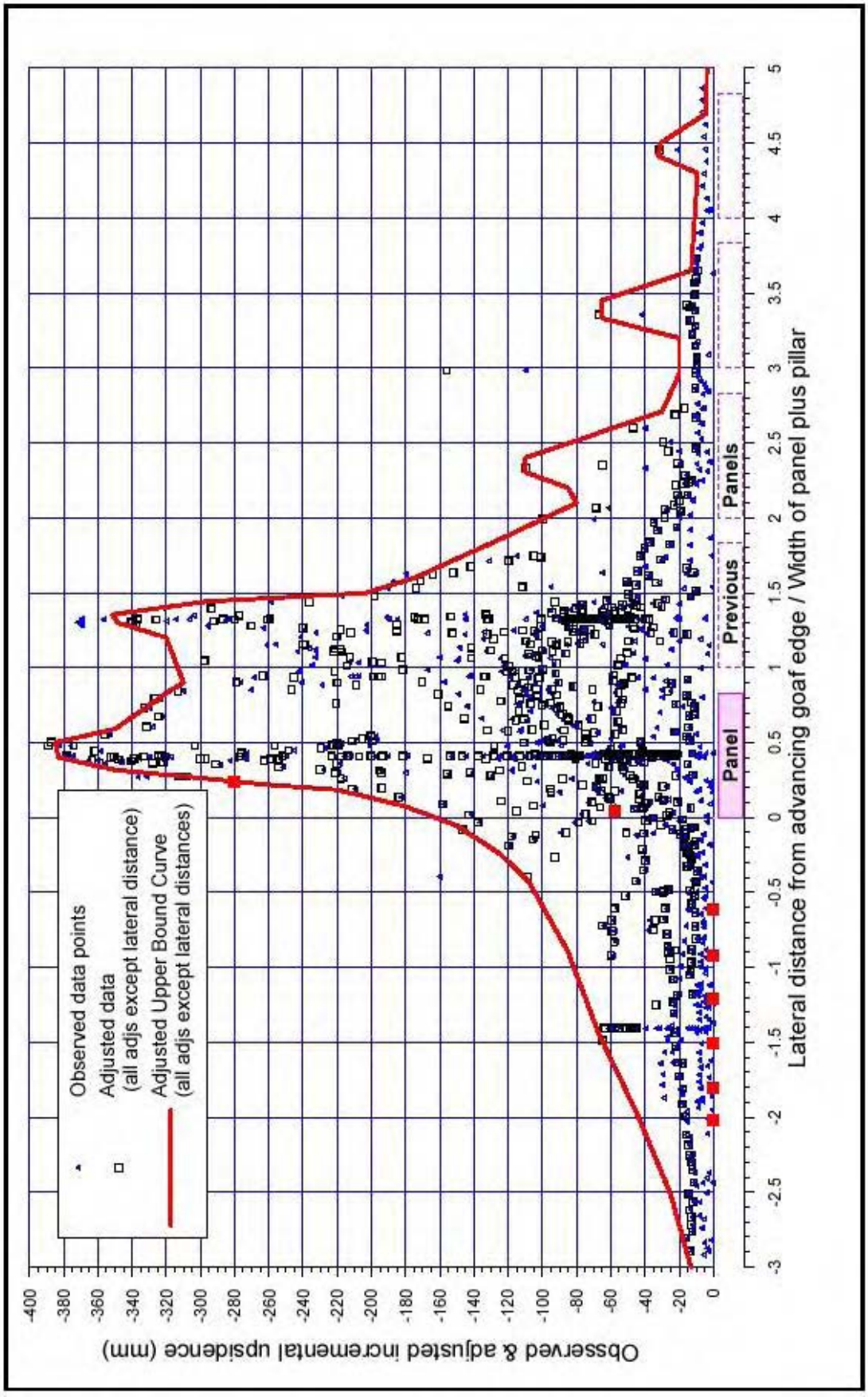

Fig. 6.57 – Upsidence at base (from Table 6.9)

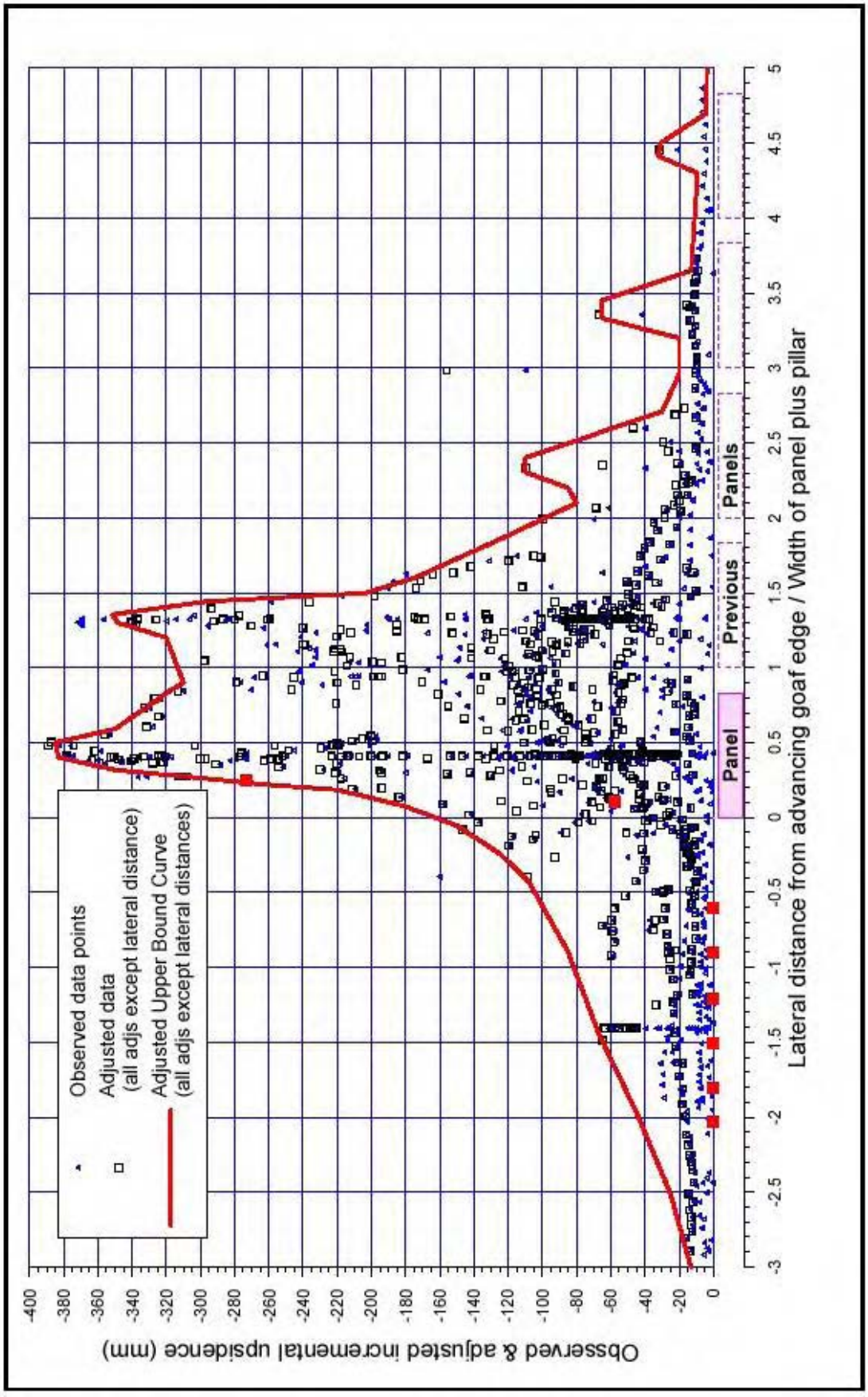

Fig. 6.58 – Upsidence at base (from Table 6.10)

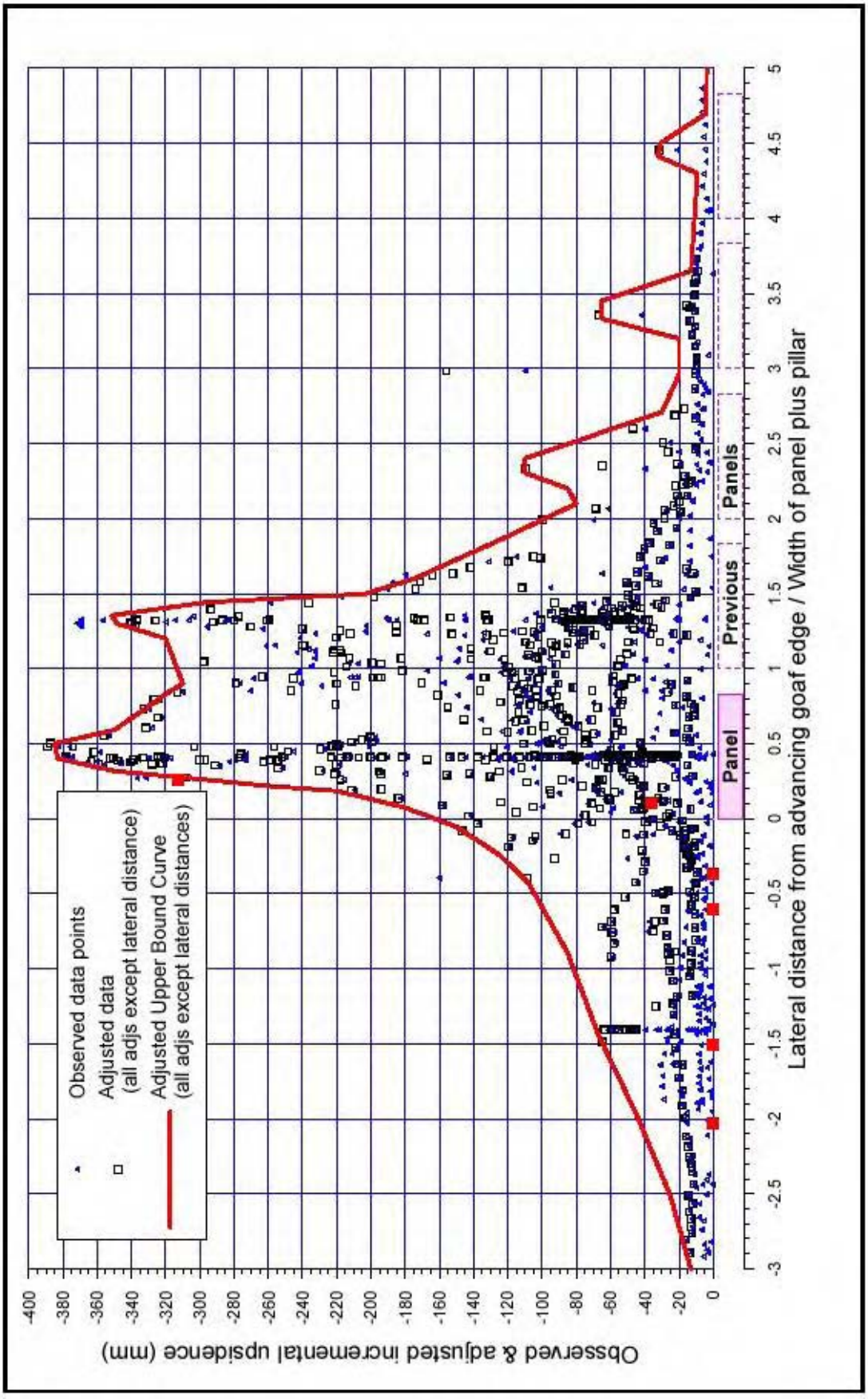

Fig. 6.59 – Upsidence at base (from Table 6.11)

6.7 PARAMETRIC STUDY

A parametric study was performed to examine the effect of the translation plane friction angle and cohesion. Twenty five models were created that varied the friction angle from 20° to 40° and the cohesion from 2 MPa to 10 MPa. These models were based on the river valley model that contained the valley centre 150 m from the longwall centreline (Valley 4, see Table 6.4). The purpose of this parametric study was to gain an insight into joint conditions (friction and cohesion) required to limit movement. Table 6.12 lists the additional models and the results.

Table 6.12 – Additional models for parametric study and results

Model	Joint Friction Angle (°)	Joint Cohesion (MPa)	Closure Top (mm)	Closure Bottom (mm)
1	20	2	74	177
2	20	4	76	177
3	20	6	65	157
4	20	8	9	18
5	20	10	9	17
6	25	2	73	177
7	25	4	76	157
8	25	6	9	17
9	25	8	9	17
10	25	10	9	17
11	30	2	73	177
12	30	4	77	177
13	30	6	9	17
14	30	8	9	17
15	30	10	9	17
16	35	2	75	177
17	35	4	76	177
18	35	6	9	17
19	35	8	9	17
20	35	10	9	16
21	40	2	77	177
22	40	4	9	17
23	40	6	9	17
24	40	8	9	17
25	40	10	9	17

The results in Table 6.12 can be seen in Figures 6.60 to 6.63.

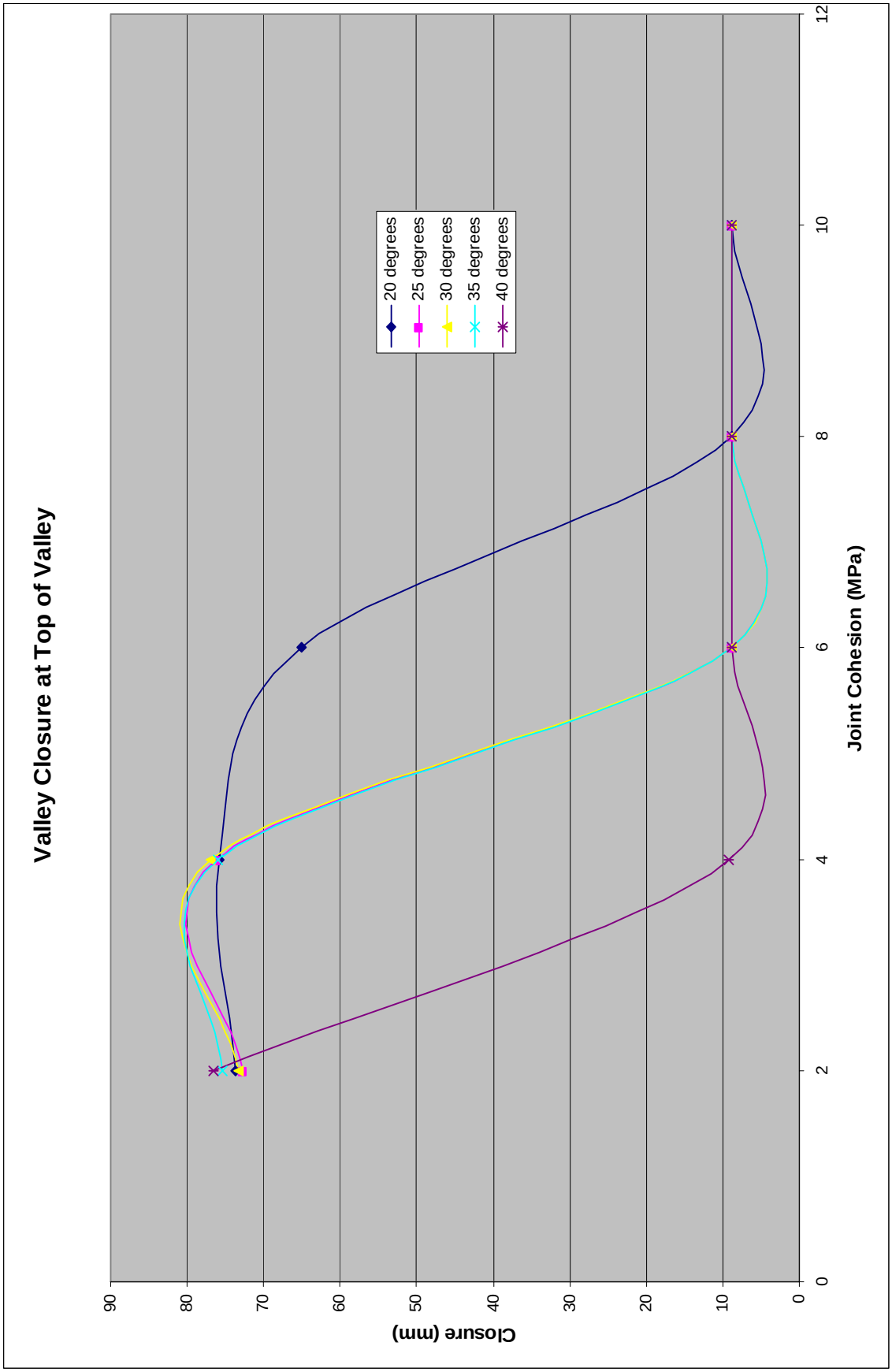

Fig. 6.60 – Valley closure at top of valley as a function of joint friction angle

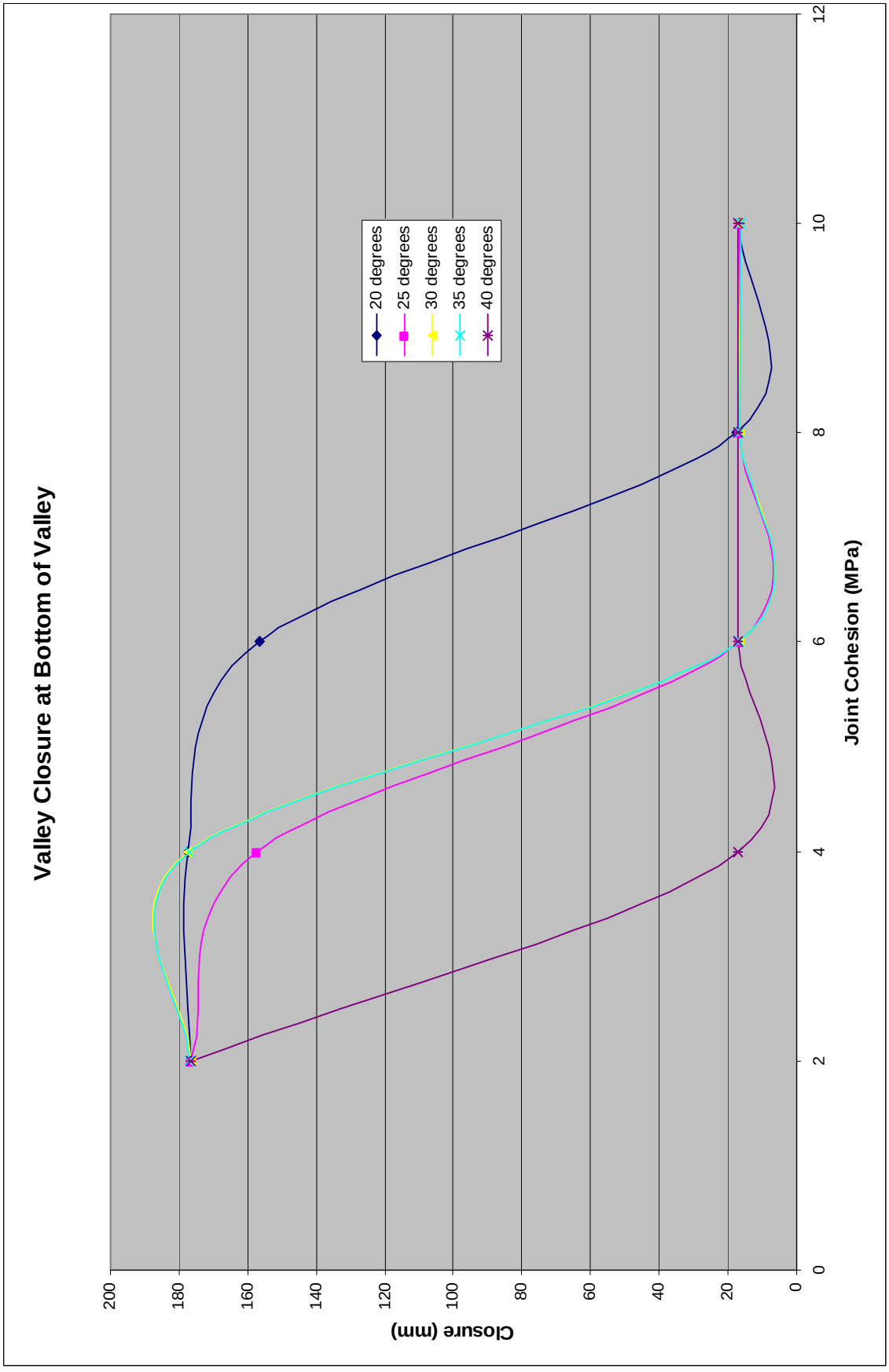

Fig. 6.61 – Valley closure at bottom of valley as a function of joint friction angle

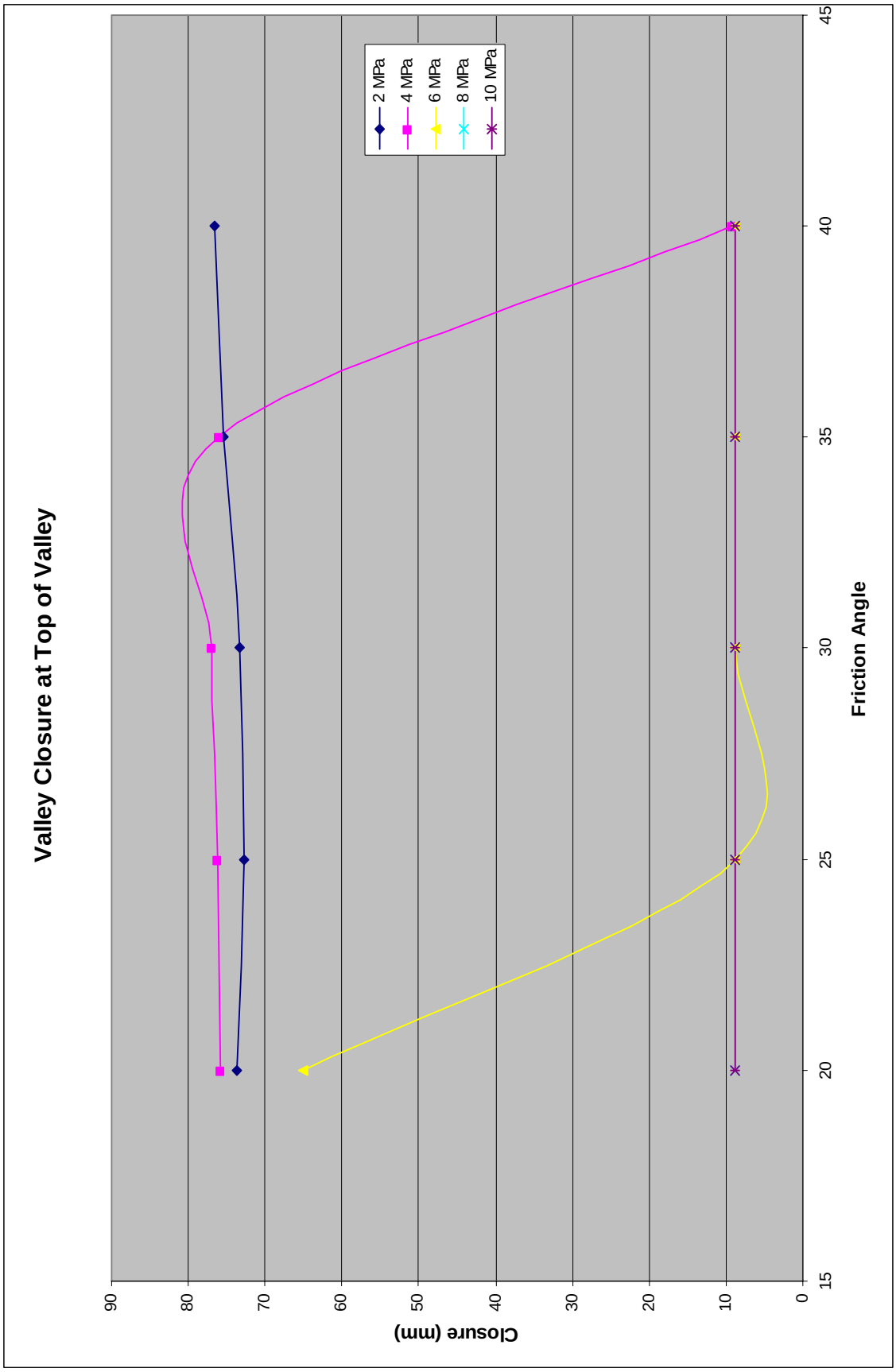

Fig. 6.62 – Valley closure at top of valley as a function of joint cohesion

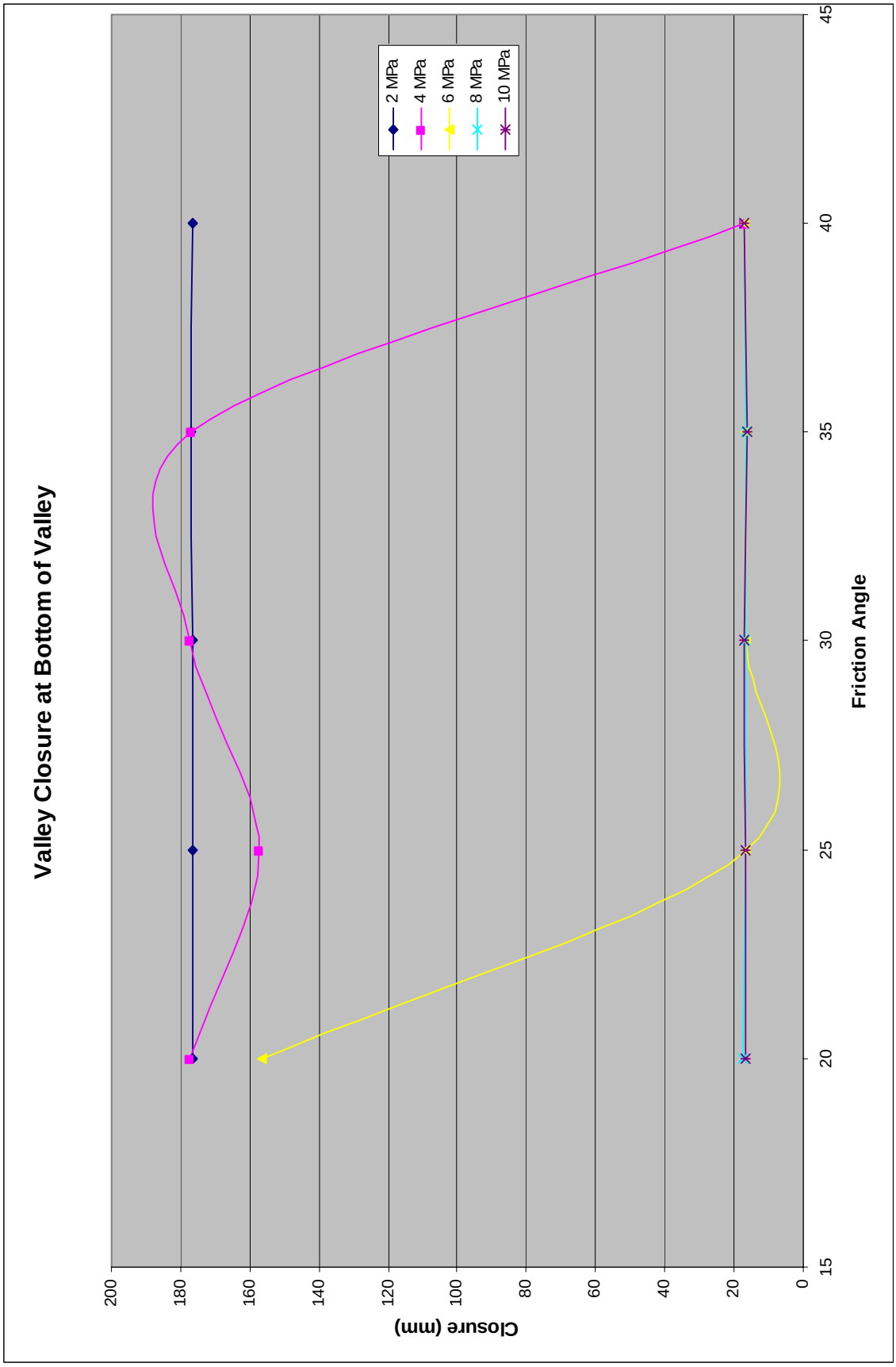

Fig. 6.63 – Valley closure at bottom of valley as a function of joint cohesion

It can be seen from Figure 6.60 that as joint cohesion increased, valley closure decreased. In all cases of joint friction angle, valley closure stabilised at 9 mm. When the joint friction angle was 20°, the required joint cohesion to stabilise the closure was 8 MPa. When the joint friction angle was 25°, 30° and 35°, the required joint cohesion was 6 MPa. When the joint friction angle was 40°, the required joint cohesion was 4 MPa. This was logical as it was expected that as joint friction angle increased, valley closure would decrease, and likewise with joint cohesion (which was evident by the decreasing amount of joint cohesion required to bring the closure down to the minimum level as joint friction angle increased). The same behaviour is evident in Figure 6.61.

When the results are plotted as a function of joint cohesion, it can be seen from Figure 6.62 and Figure 6.63 that when the joint cohesion is 2 MPa, the closure does not reduce to a minimum level throughout the range of joint friction angles. A joint cohesion of 4 MPa appeared to be the threshold at which the valley closure reduced dramatically as joint friction angle increased, in this case 35°. As expected, as the joint cohesion increased above 4 MPa, there was a reduction in the joint friction angle needed to bring the valley closure to a minimum.

6.8 COMPARISON TO BLOCK KINEMATICS

It was discussed earlier in Chapter 3 that inward closure of the valley wall that is furthest from the longwall panel, or the total valley closure of a valley directly above a longwall panel could potentially be calculated by Equation 3.12, which essentially related valley closure and tilt.

The inward shoulder closure of the valley walls furthest from the longwall panel was calculated using Equation 3.12 and the results are in Table 6.13 and Figure 6.64. The calculations have been performed on the models that have the translation plane at the base of the valleys and no bedding and joints in the upper 70 m of Hawkesbury Sandstone.

The valley closure at the shoulders for the valleys directly over the longwall centreline was also calculated using Equation 3.12 and the results are in Table 6.14.

Table 6.13 – Valley wall closure comparison

Valley	Valley centre to longwall centre (m)	Analytical valley wall closure (mm)	UDEC valley wall closure (mm)
1	0	381	375
2	50	104	133
3	100	14	20
4	150	9	14
5	200	7	9
6	250	4	6
7	300	3	4
8	350	0	2
9	400	1	1
10	450	0	0

Table 6.14 – Valley closure comparison

Model	Analytical valley closure (mm)	UDEC valley closure (mm)
Translation plane at base	736	727
Translation plane below base, no joints in beam	724	708
Translation plane below base, joints in beam	719	701

It can be seen from Table 6.13 and Figure 6.64 that Equation 3.12 calculated valley wall closure quite well. It can also be seen from Table 6.14 that Equation 3.12 calculated total valley closure for valleys directly above the longwall centreline to within 2 % of the values produced by UDEC.

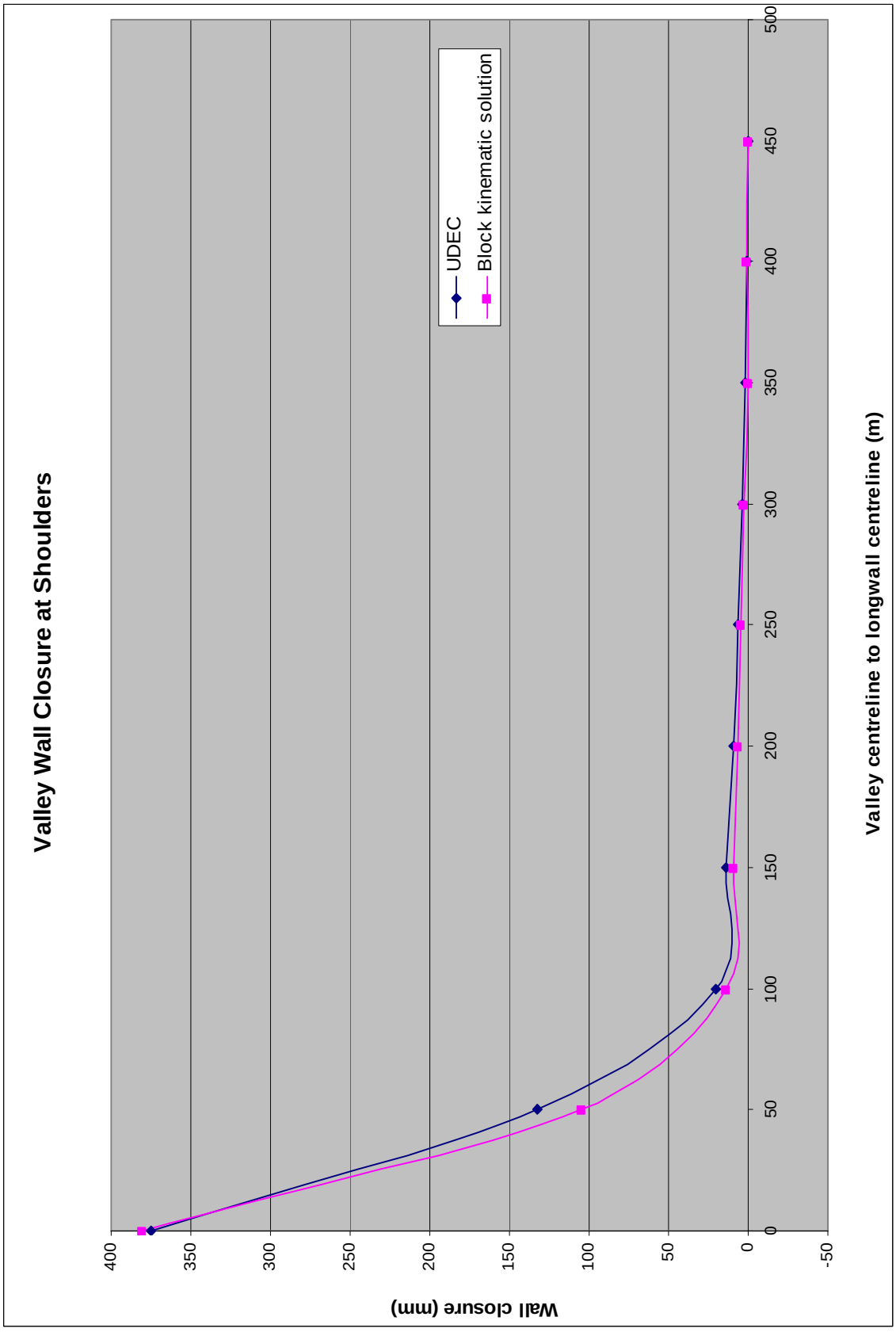

Fig. 6.64 – Comparison of valley wall closure at shoulders between the UDEC models and the block kinematic solution

6.9 SUMMARY

A series of simplified models that represented each potential river valley as a block was constructed to test the alternative block movement theory. Two major cases (with variations) were considered, the first where a translation plane existed at the base of the valley and the second, where a translation plane existed one metre below the base of the valley. The variations included adding bedding and joints in the upper 70 m of the Hawkesbury Sandstone and adding vertical joints in the beam formed by the translation plane one metre below the base of the valley. It was proposed that for the first case, valley closure would be maximised whilst upsidence and valley base yield would be minimised. For the second case, it was proposed that valley closure would decrease and upsidence and valley base yield would increase due to the effect of the translation plane.

From the results it was seen that the models conformed to the proposed block movement explanation. When the translation plane was located at the base of the valley, the blocks closest to the longwall panel slid along the plane away from the longwall panel and the blocks in the left hand side of the valley moved towards the longwall panel as a function of the geometry of the subsidence profile (see Figure 6.35 and Figure 6.40), maximising valley closure and minimising valley base yield. When the translation plane was located one metre below the base of the valley, the blocks exhibited similar behaviour but produced lesser valley closure whilst at the same time increasing the occurrence of upsidence (see Figures 6.25 to 6.27), and valley base yield as a result of the horizontal stress build up due to the lack of a sliding surface at the base of the valleys (see Figures 6.43 to 6.46). The term yield instead of failure has been used in the discussion of results as the UDEC models are quite simple.

The results from the numerical models were plotted against the empirical curves and it was seen that most of the model data points were contained below the empirical upper-bound curve and most of the model data points were situated within the observed empirical data points (see Figures 6.47 to 6.59). This was fitting as the model data points were not adjusted at all. This further supported the block movement theory, as the models were based on the block movement theory and also conformed to observed field behaviour (Holla & Barclay 2000).

The parametric study revealed that the magnitudes of closure at the top and bottom of the valleys were quite sensitive to the range of joint cohesion (2 MPa, 4 MPa, 6 MPa, 8 MPa and 10 MPa) and joint friction angle (20°, 25°, 30°, 35° and 40°) modelled. The parametric study also provided clues as to what the threshold values for joint friction angle and joint cohesion was needed to drastically reduce closure at the top and bottom of the valleys (see Figures 6.60 to 6.63). This concept could prove useful when considering which method to use to strengthen the valley base prior to mining.

The model results were also compared to the block kinematics discussed in Chapter 3. Using Equation 3.12, valley wall closure and total valley closure above the longwall centreline was calculated and compared to the model results (see Table 6.13, Table 6.14 and Figure 6.64). The trends were captured quite well and could be the subject of further refinement and investigation in the future.

In summary, the river valley models have successfully demonstrated the mechanism behind the proposed block movement model, i.e. block sliding and valley closure occurs with minimal upsidence when a translation plane exists at the base of the valley, and increased upsidence and reduced valley closure occur when the translation plane is below the base of the valley (see Figures 6.24, 6.29, 6.33, 6.34, 6.41 and 6.42). Furthermore, the river valley models demonstrated that tilt dependant valley closure was occurring at a distance several hundred metres away from the longwall centreline (in the hogging or tensile portion of the subsidence profile), by virtue of blocks being pushed into the void created by the valley (see Figures 6.36, 6.37 and 6.40). The end result is a demonstrated mechanism that produces closure and identifies what can cause the onset of upsidence. More importantly, it suggests that quantifying closure may be possible.

CHAPTER 7
APPLICATION OF VOUSSOIR BEAM AND PLATE BUCKLING THEORY

7.1 INTRODUCTION

Independent checks on aspects of the numerical models that were introduced in Chapter 5 and Chapter 6 are the subject of consideration in this chapter. Voussoir beam theory will be applied to the models developed in Chapter 5 to corroborate the ability of the models in simulating the deflection of the Bulgo Sandstone, and plate buckling theory will be applied to the models developed in Chapter 6 to corroborate the ability of the models in predicting valley base yield.

7.2 APPLICATION OF VOUSSOIR BEAM THEORY

A basic derivation and how to use voussoir beam theory from Sofianos (1996), Sofianos and Kapenis (1998) and Nomikos, Sofianos and Tsoutrelis (2002) can be found in Appendix E. This theory has been used to calculate the theoretical deflection of the Bulgo Sandstone in Models 1 to 4.

The results from Models 1 to 4 (Chapter 5) indicated that the Bulgo Sandstone was the massive spanning unit in the overburden and the majority of the caving was confined below the base of the massive unit. This was the case for Model 2, whilst failure extended into the Bulgo Sandstone in Models 3 and 4. It was noted that caving was not sufficient enough to produce any measurable goaf angle in Model 1, therefore this model could not be analysed with the voussoir beam method. The geometry of the cave zone was defined by a goaf angle of 11° to 25° for Model 2, 14° to 25° for Model 3 and 13° to 25° for Model 4.

In order to perform an analysis, the following parameters must be known:

- Longwall panel width (m),
- Cover depth (m),
- Hawkesbury Sandstone thickness (m),
- Newport Formation thickness (m),
- Bald Hill Claystone thickness (m),
- Bald Hill Claystone density (kg/m^3),
- Bulgo Sandstone thickness (m),
- Bulgo Sandstone density (kg/m^3),
- Bulgo Sandstone Young's Modulus (MPa),
- Cave zone height (m), and
- Goaf angle (°).

See Figure 2.1 for a definition on caving height and goaf angle.

It is important to note that the analysis is actually performed on the base of the Bulgo Sandstone as defined by the bedding plane spacing and extent of failure into the spanning unit, and using the notion that thinner bedded layers load thicker bedded layers (Obert & Duvall 1967), it is only the Bald Hill Claystone that acts as a surcharge on the Bulgo Sandstone (see Table 5.5).

For example, if the Bulgo Sandstone is 92 m thick with a bedding plane spacing of 9 m, the Bald Hill Claystone 12 m thick and the cave zone penetrates 64 m into the Bulgo Sandstone, the analysis would be performed on the bottom 9 m of unbroken Bulgo Sandstone with that layer being loaded by a surcharge of 31 m. The area and weight of the surcharge was defined by the goaf angle and the weighted average density of the surcharge. Using the procedure described in Appendix E, a simple spreadsheet was set up to calculate the deflection of the Bulgo Sandstone for each model geometry. It was found that the calculated deflections were highly sensitive to the goaf angle value. However, there was agreement within the confines of the simple model for the goaf angle. Table 7.1 contains the analytical and numerical deflection of the Bulgo Sandstone.

Table 7.1 – Analytical and numerical deflection of the Bulgo Sandstone

Model	UDEC Deflection (mm)	UDEC Goaf Angle (°)	Back-Calculated Goaf Angle (°)
2	275	11 – 25	20.0
3	345	14 – 25	11.6
4	506	13 – 25	12.5

7.3 APPLICATION OF PLATE BUCKLING THEORY

The UDEC models in Chapter 6 produced behaviour that may indicate the onset of yield in the base of the valleys of the type shown in Chapter 3. For the models that contained the translation plane below the base of the valley, with no joints in the beam formed by the translation plane, the maximum average horizontal stress immediately below the sides of the valleys ranged from 18 MPa to 65 MPa.

Hoek and Brown (1980) provided a comprehensive overview of plate buckling theory, and stated that the axial stress at which a plate will buckle is given by (Equation 7.1):

$$\sigma_\alpha = \frac{\pi^2 E}{12q^2(l/t)^2} \qquad [7.1]$$

Where,

σ_α = Axial stress required for buckling (MPa)
E = Elastic or Young's Modulus (MPa)
q = A constant (0.5 for both ends clamped)
l = Length of plate (m)
t = Thickness of plate (m)

Equation 7.1 can be rearranged so that the critical thickness of a plate can be determined if the axial stress is already known (Equation 7.2):

$$t = \frac{l}{\sqrt{\pi^2 E/\sigma_\alpha(12q^2)}} \qquad [7.2]$$

Figure 7.1 illustrates the critical thickness for beams given an average horizontal stress for different valley widths.

It can be seen from Figure 7.1 that when the values of maximum average horizontal stresses in the river valley models (18 MPa – 65 MPa) are applied to this graph, the calculated thickness of the beam that would buckle for a 50 m wide valley is in the order of 1 m to 1.9 m. This is corroborated by the author's recollection of buckling in a similar geographical location where buckled slabs were usually 0.5 m to 1 m thick, and rarely exceeded 2 m in thickness. Simple buckling (Figure 7.2) and low angle shear (Figure 3.6) were common features in the field.

7.4 SUMMARY

Two analytical solutions were introduced and applied to the river valley numerical models in an attempt to further test the credibility of the numerical models. This was undertaken to provide a possible means of analysing a complex problem with simple analytical tools and to assess whether there was any merit in using any of the solutions in the future. It was seen that the numerical models complied with both analytical solutions. Voussoir beam theory back-calculated goaf angles that were in general agreement with the goaf angles produced by UDEC, and the plate buckling solution (along with the author's recollection of buckling events) suggested that the horizontal stresses produced by the UDEC modelling is in the vicinity of what is required to buckle the valley floor for the valley geometry modelled. The critical thickness of the slabs calculated by the plate buckling analogue corresponds to field observations.

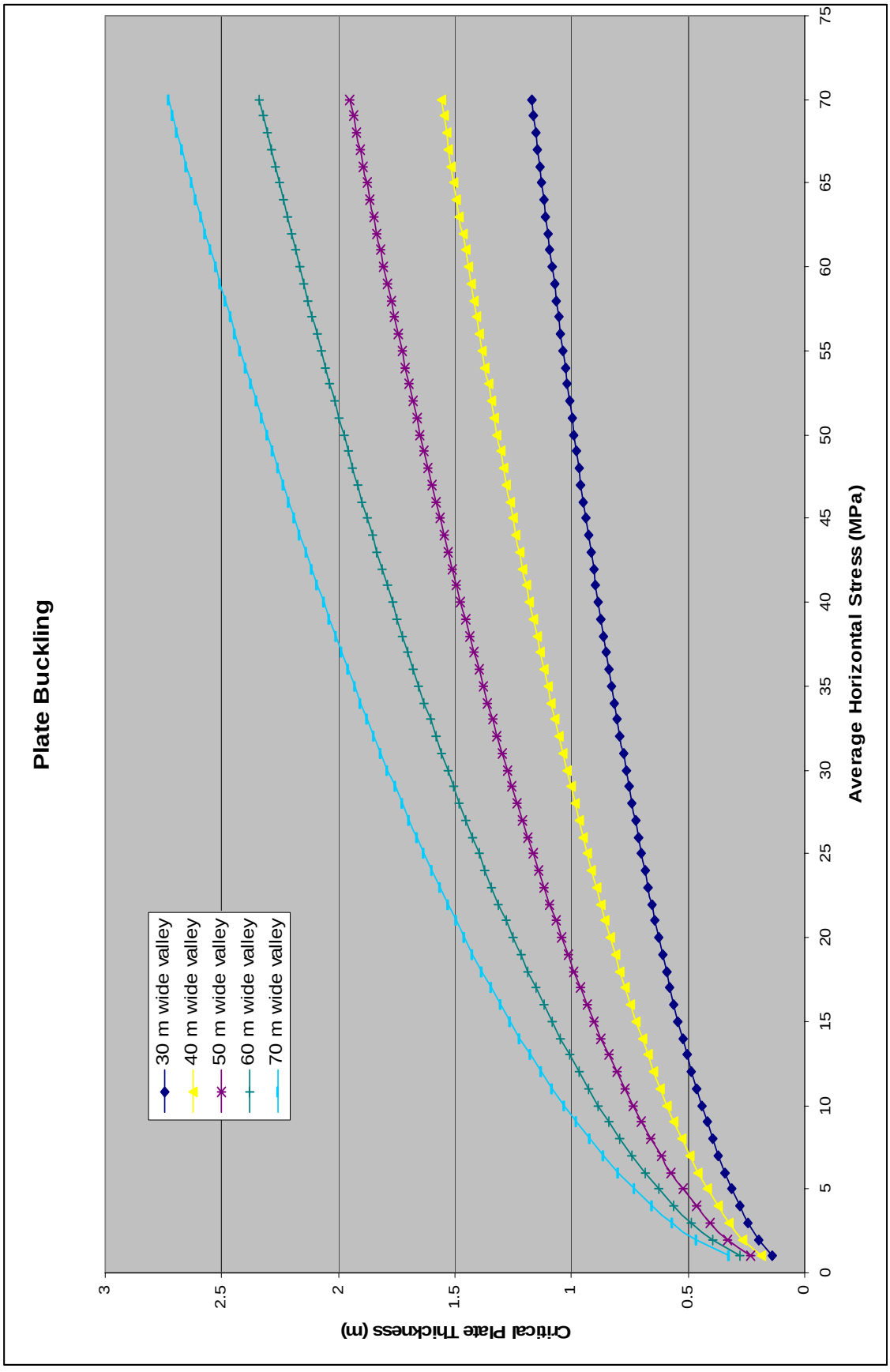

Fig. 7.1 – Critical plate thickness for buckling

Fig. 7.2 – Simple buckling in the field

CHAPTER 8
SUMMARY, CONCLUSIONS AND RECOMMENDATIONS

8.1 SUMMARY

This thesis aimed to investigate the mechanisms behind valley closure and upsidence over unmined coal and old longwall panels using UDEC. In order to achieve this, the choice of UDEC had to be justified and verified with the New South Wales Department of Primary Industries empirical method of subsidence prediction (Holla & Barclay 2000), the empirical method developed by Waddington Kay and Associates (2002) for valley closure and upsidence, and two analytical solutions.

One alternative explanation for valley closure and upsidence above unmined coal was proposed and successfully investigated with UDEC.

This research has been driven by the need for understanding why valley closure and upsidence occur above unmined coal, a phenomenon which can have far reaching consequences in terms of surface damage and the possibility of forced sterilisation of coal.

This project is a successful demonstration of the principles of using numerical, empirical and analytical techniques to investigate a complex problem.

8.1.1 Review of problem

A review of valley closure and upsidence was undertaken and it was found that very little literature exists on this topic. The most comprehensive review to date had been performed by Waddington Kay & Associates (2002) and in this reference, a conceptual model was proposed that suggested valley closure and upsidence is a result of some undefined horizontal compressive stresses. It was speculated that this conceptual model may be valid for river valleys that are directly undermined by longwall panels. The

suggestion by Waddington Kay and Associates that upsidence is directly related to valley closure was challenged.

The field data in Waddington Kay and Associates (2002) illustrated that valley closure and upsidence was occurring above both unmined coal and old longwall panels (Figure 3.8 and Figure 3.12), thereby raising questions about the wide application of this horizontal compressive stress model, especially in areas above unmined coal that are theoretically in tension and over old longwall panels which would have been relieved of high horizontal compressive stresses during the extraction process.

Therefore, the questions that were raised about the horizontal compressive stress model were:

1. Why does valley closure and upsidence occur in the tensile or hogging portion of the subsidence profile above unmined coal?
2. Why does valley closure and upsidence occur over old longwall panels?

8.1.2 The block movement model

To address the short-comings of the horizontal compressive stress model detailed in Waddington Kay and Associates (2002) and to provide answers to the questions posed above, an alternative model of block movements was proposed (Chapter 3).

The block movement model proposed that an incised ground surface is comprised of an assemblage of blocks such that the valley incisions can be represented by the absence of blocks. When the ground surface sags due to the extraction of a longwall panel, the horizontal shortening of the ground surface above the longwall panel results in the blocks being forced into the free face provided by the valley (Figure 3.17), whether it be over unmined coal or old longwall panels.

This model assumed that the blocks had a surface to slide along, termed the translation plane. If the translation plane existed at the bottom of the valley, then it was proposed that valley closure would dominate over upsidence due to the dissipation in horizontal stress provided by the translation plane. If the translation plane existed at a distance

below the bottom of the valley, then it was proposed that valley closure would be reduced and upsidence increased.

The kinematics of a particle moving along a curved surface was described and it was pointed out that an adaptation to blocks moving along a curved surface was possible but needed further investigation. It was deduced that the kinematics related horizontal movement of the blocks to valley depth and curvature (Equation 3.12).

8.1.3 Numerical modelling

The numerical modelling was undertaken in accordance to the guidelines set out in Hudson, Stephansson and Andersson (2005). This was done to ensure that the modelling process was fully traceable and transparent.

A review of recent references that dealt with UDEC, FLAC and similar software in mining or underground applications was undertaken. It was found that whilst UDEC seemed to be a more logical choice for modelling discontinuous rock masses, there was a trend of using FLAC and creating custom constitutive models and calibrating material properties. This approach is acceptable when a predictive model is required for a localised area, but does not lend itself to a true predictor status. It was decided that UDEC was the most appropriate software to use for this project because it did not require the creation of a custom constitutive model or the excessive calibration of material properties to replicate the effects of jointing.

The single longwall panel numerical models were created so they could be verified with the empirical method. The geometry of the models and the model parameters were derived from the literature. The models were designed to be transparent, and all the model parameters and assumptions were fully traceable. It was also decided to make the models as simple as possible to decrease the number of assumptions that had to be made, as the more complex a numerical model is, the more uncertainty is built in. The models were designed to predict maximum subsidence, goaf edge subsidence, strain, tilt and inflection point location.

When the models were analysed, it was seen that a goaf angle does exist and that the caving was largely contained below the Bulgo Sandstone. This was in good agreement with the factors identified in the literature survey on mine subsidence. When the results were compared to the empirical curves (see Figures 5.8 to 5.13), it was seen that the numerical predictions were in good agreement with the empirical curves. The only parameter where the numerical predictions showed some limitations was the strain predictions. This was attributed to the small levels of strain predicted and the inability of the numerical model to predict strain of such small magnitude.

After the success of the single longwall panel models, a series of models were created to simulate river valley response to mining in order to test if the proposed block movement theory in Chapter 3 was plausible. Instead of creating a full scale model that encompassed everything between the longwall and the surface, it was decided to scale the model down by replicating the surface profile with a sequence of vertical displacements that were applied to the new base of the model.

The new base of the model was determined by analysing the vertical displacements of the surface, the Bald Hill Claystone and the Bulgo Sandstone. It was found that the vertical displacement of the Bald Hill Claystone differed little from the surface vertical displacements. When the Bald Hill Claystone was used as the base of the model, the chance of yielded elements occurring in the vicinity of the river valley was too great to ignore. As a result of this the Bulgo Sandstone was used as the base of the models, thereby restricting yielded elements to those directly related to valley base yield, and not those that were a by-product of the modelling procedure. All material and joint properties remained the same as in the single longwall panel models to maintain consistency.

Two types of models were developed. The first type incorporated a translation plane at the base of the valleys and the second type incorporated a translation plane located one metre below the base of the valleys. The purpose of this was to test the proposed block movement theory in Chapter 3. It was noted that there was some uncertainty with the exact definition of upsidence, and it was decided that for the purpose of the modelling, upsidence was defined as the difference in upsidence between models with the translation plane at the base of the valleys, and the models with the translation plane

below the base of the valleys. Several variations were included in the numerical modelling, including adding bedding and joints in the upper 70 m of the Hawkesbury Sandstone, and adding joints to the beam formed by the translation plane.

The models behaved according to the proposed block movement theory and compared well to the empirical and field observations (see Figures 6.20 to 6.59). The modelling also demonstrated that tilt/curvature was the primary driver of valley closure and upsidence, and was not controlled by a redistribution of horizontal stresses as widely thought. A parametric study was conducted on the translation plane cohesion and friction angle (see Figures 6.60 to 6.63), and it was found that it was possible to quantify a joint cohesion and friction angle that was required to limit movement along the translation plane.

The key objective of the numerical modelling was to demonstrate the block movement model, a goal that has been achieved.

8.1.4 Application of analytical solutions

In an attempt to further the credibility of the numerical models, it was decided to apply the voussoir beam solution to the single longwall panel models and the plate buckling solution to the river valley models to see if the models corresponded with proven analytical solutions. From the results it was seen that the voussoir beam solution back calculated the goaf angle satisfactorily (see Table 7.1) and the plate buckling solution corroborated with field observations (see Figure 7.1 and Figure 7.2). Both types of models agreed well with the analytical solutions, even though the analytical solutions were derived for elastic material.

8.2 CONCLUSIONS

The following conclusions were drawn from this research project:

- UDEC was suitable for use in mine subsidence related problems. This was illustrated by the excellent match to the empirical curves used for validation purposes. As UDEC is a Distinct Element code, the inclusion of joints

automatically accounted for the reduction in rock mass strength, therefore eliminating the need to modify or calibrate material properties derived by laboratory testing. This is keeping in accordance with the transparent and fully traceable principle.

- The block movement model was a feasible explanation for valley closure above unmined coal and old longwall panels. The numerical modelling demonstrated that the forces generated were sufficient to induce movement in the hogging portion of the subsidence profile by forcing blocks in an outward direction into the void provided by the valley. In addition, the kinematics was relatively simple and explained the relationship between block movement, valley depth and tilt/curvature.
- The block movement model was capable of indicating the onset of valley base yield. This was extensively demonstrated in the numerical modelling.
- The block movement model also introduced a number of implications. Block rotations on a curved surface may induce surface cracking that extends to the depth of the adjacent block, in any case much deeper than might be expected. The depth of this surface cracking coupled with bedding plane dilation may have adverse effects on horizontal permeability as well. It may be possible to control the magnitude of upsidence or valley closure by reinforcing the valley base in critical situations.
- The block movement model demonstrated that it was possible to predict valley closure and the onset of valley base yield using block kinematics and the plate buckling solution. Further refinement is needed to replace numerical models with analytical solutions; nevertheless the basic principles are sound.

8.3 LIMITATIONS OF THE STUDY

Modelling longwall caving, subsequent subsidence and river valley response is complex and required simplifications and assumptions. The modelling work was limited by the following conditions:

- No three dimensional modelling was undertaken. Given the amount of unknown assumptions that would have had to be made, limiting the modelling to two dimensions was prudent.

- The difficulty in replication pillar deformation restricted the modelling to single panel longwalls.
- Some material properties from the geotechnical characterisation (MacGregor & Conquest 2005) were missing and had to be evaluated using the Mohr-Coulomb failure criteria and various guides.
- Joint properties were not available and had to be assumed.
- Vertical joint spacing was impossible to determine from core samples and was assumed to be the same as bedding plane spacing.
- Reproducing bulking in the goaf was difficult. Again, time constraints prevented additional models being created with more random sub-vertical joint orientations to try and increase bulking.
- No field data was provided in order to verify models, the empirical method was used for verification instead and this in itself was not ideal due to the data scatter evident in the empirical curves.

8.4 RECOMMENDATIONS

This project achieved its objectives and it also highlighted areas that would benefit from future research. These areas are:

- The application of UDEC as a greenfields subsidence prediction tool in sub-critical mining environments. This project has demonstrated that UDEC is capable of predicting subsidence for single isolated panels provided that the material properties are known.
- The establishment of a geotechnical database containing typical rock mass and joint properties for the rock units in the Southern Coalfield. Compiling the data needed for the numerical modelling was one of the most time consuming processes in the entire project.
- It would be advantageous to model a wider range of longwall panel geometries to try and cover the majority of the empirical prediction curve. For this to occur, bulking needs to be replicated in the goaf to correctly model the large increase in subsidence evident when W/H ratios exceed approximately 0.5.
- In order to model multiple longwall panel layouts, further investigation into the mechanics and numerical modelling of pillar deformation should be undertaken.

- Valley closure could theoretically be evaluated using block kinematics. Further research needs to be carried out to derive expressions to calculate the forces exerted by one block to another, and therefore displacement as the blocks undergo rotation due to the development of the subsidence trough.

LIST OF REFERENCES

1. Alehossein, H & Carter, J P 1990, 'On the implicit and explicit inclusion of joints in the analysis of rock masses', in Rossmanith, H P (ed.), *Proceedings of the International Conference on Mechanics of Jointed and Faulted Rock*, 18th – 20th April 1990, Institute of Mechanics, Technical University of Vienna, Balkema, Rotterdam, pp. 487 – 494.

2. Alejano, L R, Ramirez-Oyanguren, P & Taboada, J 1999, 'FDM predictive methodology for subsidence due to flat and inclined coal seam mining', *International Journal of Rock Mechanics and Mining Sciences*, vol. 36, issue 4, June 1999, pp. 475 – 491.

3. Australian Mining Engineering Consultants 2000, 'The influence of subsidence cracking on longwall extraction beneath water courses, aquifers, open cut voids and spoil piles', ACARP Research Project No. C5016, *Australian Coal Association Research Program, Brisbane, Queensland, Australia*.

4. Badelow, F, Best, R, Bertuzzi, R & Maconochie, D 2005, 'Modelling of defect and rock bolt behaviour in geotechnical numerical analysis for Lane Cove Tunnel', *Proceedings Geotechnical Aspects of Tunnelling for Infrastructure Projects, Mini-Symposium*, 12th October 2005, Milsons Point, Australia, 9 p.

5. Barton, N 1976, 'The shear strength of rock and rock joints', *International Journal of Rock Mechanics and Mining Sciences and Geomechanics Abstracts*, vol. 13, issue 9, September 1976, pp. 255 – 279.

6. Bhasin, R & Høeg, K 1998, 'Parametric study for a large cavern in jointed rock using a distinct element model (UDEC-BB)', *International Journal of Rock Mechanics and Mining Sciences*, vol. 35, issue 1, January 1998, pp. 17 – 29.

7. BHP Billiton 2005, *BHP Sustainability Report 2005 – Community Case Studies – Integrated Mine Planning in the Illawarra*, BHP Billiton, Melbourne, Victoria, viewed 12 January 2007, <http://hsecreport.bhpbilliton.com/2005/repository/community/caseStudies/caseStudies23.asp>.

8. Bowman, H N 1974, 'Geology of the Wollongong, Kiama and Robertson 1:50,000 Sheets', *Geological Survey of New South Wales, Sydney*.

9. Brady, B H & Brown, E T 2006, *Rock Mechanics for Underground Mining*, 3rd edn, Springer, pp. 130 – 138.

10. Brady, B H, Hsiung, S H, Chowdhury, A H & Philip, J 1990, 'Verification studies on the UDEC computational model of jointed rock', in Rossmanith, H P (ed.), *Proceedings of the International Conference on Mechanics of Jointed and Faulted Rock*, 18th – 20th April 1990, Institute of Mechanics, Technical University of Vienna, Balkema, Rotterdam, pp. 551 – 558.

11. Chan, K F, Kotze, G P & Stone, P C 2005, 'Geotechnical modelling of station caverns for the Epping to Chatswood rail line project', *Proceedings Geotechnical Aspects of Tunnelling for Infrastructure Projects, Mini-Symposium*, 12th October 2005, Milsons Point, Australia, 15 p.

12. Choi, S K & Coulthard, M A 1990, 'Modelling of jointed rock masses using the distinct element method', in Rossmanith, H P (ed.), *Proceedings of the International Conference on Mechanics of Jointed and Faulted Rock*, 18th – 20th April 1990, Institute of Mechanics, Technical University of Vienna, Balkema, Rotterdam, pp. 471 – 477.

13. Colwell Geotechnical Services 1998, 'Chain pillar design (calibration of ALPS)', ACARP Research Project No. C6036, *Australian Coal Association Research Program, Brisbane, Queensland, Australia*.

14. Coulthard, M A 1995, 'Distinct element modelling of mining-induced subsidence – a case study', in Myer, L R et al. (eds.), *Proceedings of the Conference on Fractured and Jointed Rock Masses*, 3rd – 5th June 1992, Lake Tahoe, California, USA, Balkema, Rotterdam, pp. 725 – 732.

15. Coulthard, M A & Dutton, A J 1988, 'Numerical modelling of subsidence induced by underground coal mining' in Cundall P A, Sterling R L & Starfield, A M (eds.), *Proceedings of the 29th U.S. Symposium: Key Questions in Rock Mechanics*, 13th – 15th June 1988, University of Minnesota, Minneapolis, Balkema, Rotterdam, pp. 529 – 536.

16. CSIRO Exploration & Mining & Strata Control Technology 1999, 'Ground behaviour about longwall faces and its effect on mining', ACARP Research Project No. C5017, *Australian Coal Association Research Program, Brisbane, Queensland, Australia*.

17. CSIRO Petroleum 2002, 'Numerical Modelling Studies', in Waddington Kay & Associates, '*Research into the impacts of mine subsidence on the strata and hydrology of river valleys and development of management guidelines for undermining cliffs, gorges and river systems*', ACARP Research Project No. C9067, *Australian Coal Association Research Program, Brisbane, Queensland, Australia*.

18. Cundall, P A 1971, 'A computer model for simulating progressive large-scale movements in blocky rock systems', *Proceedings of the Symposium of the International Society for Rock Mechanics, Nancy, France, 1971*, vol. 1, Paper No. II-8.

19. Gale, W J 2005, 'Application of computer modelling in the understanding of caving and induced hydraulic conductivity about longwall panels', *Proceedings of the Coal2005 6th Australasian Coal Operators' Conference*, 26th – 28th April 2005, Brisbane, Australia, pp. 11 – 15.

20. Ghobadi, M H 1994, 'Engineering geologic factors influencing the stability of slopes in the Northern Illawarra region', PhD thesis, University of Wollongong, Australia.

21. Hanlon, F N 1953, 'Southern Coalfield, geology of the Stanwell Park – Coledale area', Technical Report No. 1, *Department of Mines, New South Wales*, pp. 20 – 35.

22. Hibbeler, RC 1997, *Engineering Mechanics – Dynamics*, SI edn, Prentice Hall, pp. 47 – 49.

23. Hoek, E 2000, *Rock Engineering Course Notes*, Evert Hoek Consulting Engineer Inc., viewed 7 March 2007, <http://www.rocscience.com/hoek/PracticalRockEngineering.asp>.

24. Hoek, E & Brown, ET 1980, *Underground Excavations in Rock*, The Institute of Mining and Metallurgy, p. 235.

25. Holla, L 1985, *Mining Subsidence in New South Wales – Surface Subsidence Prediction in the Southern Coalfield*, New South Wales Department of Mineral Resources, Sydney, p. 8.

26. Holla, L & Armstrong, M 1986, 'Measurement of sub-surface strata movement by multi-wire borehole instrumentation', *The AusIMM Bulletin & Proceedings*, The Australasian Institute of Mining and Metallurgy, Parkville, Victoria, vol. 291, no. 7, October 1986, pp. 65 – 72.

27. Holla, L & Barclay, E 2000, *Mine Subsidence in the Southern Coalfield, NSW, Australia*, New South Wales Department of Mineral Resources, pp. 1 – 16.

28. Hudson, J A, Stephansson, O & Andersson, J 2005, 'Guidance on numerical modelling of thermo-hydro-mechanical coupled processes for performance assessment of radioactive waste repositories', *International Journal of Rock Mechanics and Mining Sciences*, vol. 42, issues 5 – 6, July – September 1999, pp. 850 – 870.

29. Itasca 2000, *UDEC User's Guide Version 3.1*, Itasca Consulting Group, Inc: Minneapolis, Minnesota, USA.

30. Johansson, E, Reikkola, R & Lorig, L 1988, 'Design analysis of multiple parallel caverns using explicit finite difference methods' in Cundall P A, Sterling R L & Starfield, A M (eds.), *Proceedings of the 29th U.S. Symposium: Key Questions in Rock Mechanics*, 13th – 15th June 1988, University of Minnesota, Minneapolis, Balkema, Rotterdam, pp. 325 – 333.

31. Jones, B G & Rust, B R 1983, 'Massive sandstone facies in the Hawkesbury Sandstone, a Triassic fluvial deposit near Sydney, Australia', *Journal of Sedimentary Research*, vol. 53, no. 4, December 1983, pp. 1249 – 1259.

32. Kapp, W A 1984, 'Mine subsidence and strata control in the Newcastle District of the Northern Coalfield New South Wales', PhD thesis, University of Wollongong, Australia.

33. Kratzsch, H 1983, *Mining Subsidence Engineering*, Springer – Verlag, p. 41, 153.

34. MacGregor, S & Conquest, G 2005, 'Geotechnical characterization and borehole completion logs for surface boreholes: Endeavour 3 (WCC DDH29), Endeavour 4 (WCC DDH 30) and Endeavour 5 (WCC DDH 31)', Report No. BHPC2843, *SCT Operations Pty. Ltd.*

35. Mandl, G 2005, *Rock Joints – The Mechanical Genesis*, Springer – Verlag, Germany, pp. 55 – 97.

36. McNally, G H 1996, 'Estimation of the geomechanical properties of coal measures rocks for numerical modelling', in McNally, G M & Ward, C R (eds.), *Proceedings of the Symposium on Geology in Longwall Mining*, 12th – 13th November 1996, University of New South Wales, pp. 63 – 72.

37. Mills, K W 2002, 'In situ measurements and installation of monitoring instruments at WRS1', Report No. MET2367, *Strata Control Technology Operations Pty. Ltd.*, pp. 6 – 16.

38. Mills, K W & Huuskes, W 2004, 'The effects of mining subsidence on rockbars in the Waratah Rivulet at Metropolitan Colliery', *Proceedings of the 6th Triennial Conference on Subsidence Management Issues*, Mine Subsidence Technological Society, Newcastle, Australia, pp. 47 – 64.

39. Mineral Policy Institute 2005, *RIVERS SOS: BHP Billiton and others urged to commit to mine a safe distance from precious water resources*, Mineral Policy Institute, Erskineville, New South Wales, viewed 12 January 2007, <http://www.mpi.org.au/companies/bhpb/river_sos/>.

40. National Coal Board 1975, *Subsidence Engineers' Handbook*, 2nd edn, National Coal Board Mining Department, UK, 111 p.

41. Nemcik, J A 2003, 'Floor failure mechanisms at underground longwall face', PhD thesis, University of Wollongong, Australia.

42. Nomikos, P P, Sofianos, A I & Tsoutrelis, C E 2002, 'Structural response of vertically multi-jointed roof rock beams', *International Journal of Rock Mechanics and Mining Sciences*, vol. 39, issue 1, January 2002, pp. 79 – 94.

43. NSW Department of Planning 2008, 'Impacts of underground coal mining on natural features in the Southern Coalfield – Strategic Review', *NSW Department of Planning, Sydney*.

44. NSW Planning Assessment Commission 2009, 'The Metropolitan Coal Project – Report Review', *NSW Planning Assessment Commission, Sydney*.

45. Obert, L & Duvall, W I 1967, *Rock Mechanics and the Design of Structures in Rock*, John Wiley and Sons, Inc., pp. 518 – 522.

46. O'Connor, K M & Dowding, C H 1990, 'Monitoring and simulation of mining-induced subsidence', in Rossmanith, H P (ed.), *Proceedings of the International Conference on Mechanics of Jointed and Faulted Rock*, 18th – 20th April 1990, Institute of Mechanics, Technical University of Vienna, Balkema, Rotterdam, pp. 781 – 787.

47. Packham, G H (ed.) 1969, *The Geology of New South Wales*, The Geological Society of Australia Incorporated, Sydney, pp. 370 – 375.

48. Pells, P J N 1985, 'Engineering properties of rocks in the Narrabeen Group', in P J N Pells (ed.), *Engineering Geology of the Sydney Region*, Balkema, Rotterdam, pp. 205 – 211.

49. Pells, P J N 1993, 'The 1993 E.H Davies Memorial lecture, rock mechanics and engineering geology in the design of underground works', *Australian Geomechanics Society*, pp. 3.1 – 3.33.

50. Peng, S S 1992, *Surface Subsidence Engineering*, Society for Mining, Metallurgy, and Exploration, Inc. (AIME), Braun-Brumfield, Inc., pp. 1 – 20.

51. Price, N J 1966, *Fault and Joint Development in Brittle and Semi-Brittle Rock*, Permagon Press Ltd., London, pp. 144 – 147.

52. Reynolds, R G 1977, 'Coal mining under stored waters (stored waters inquiry report)', *New South Wales Government, Sydney*.

53. Seedsman, R W 2004, 'Back analysis of sub-critical subsidence events in the Newcastle Coalfield using voussoir beam concepts', *Proceedings of the 6th Triennial Conference on Subsidence Management Issues*, Mine Subsidence Technological Society, Newcastle, Australia, pp. 65 – 74.

54. Selley, R C 2000, *Applied Sedimentology*, 2nd edn, Academic Press, California, p. 142.

55. Sitharam, T G & Madhavi Latha, G 2002, 'Simulation of excavations in jointed rock masses using a practical equivalent continuum approach', *International Journal of Rock Mechanics and Mining Sciences*, vol. 39, issue 4, June 2002, pp. 517 – 525.

56. Sofianos, A I 1996, 'Analysis and design of an underground hard rock voussoir beam roof', *International Journal of Rock Mechanics and Mining Sciences*, vol. 33, issue 2, February 1996, pp. 153 – 166.

57. Sofianos, A I & Kapenis, A P 1998, 'Numerical evaluation of the response in bending of an underground hard rock voussoir beam roof', *International Journal of Rock Mechanics and Mining Sciences*, vol. 35, issue 8, December 1998, pp. 1071 – 1086.

58. Tucker, M E 2003, *Sedimentary Rocks in the Field*, 3rd edn, John Wiley & Sons Ltd, England, pp. 88 – 94.

59. Waddington, A A & Kay, D R 1995, 'The Incremental Profile Method for prediction of subsidence, tilt, curvature and strain over a series of longwalls', *Proceedings of the 3rd Triennial Conference on Mine Subsidence*, Mine Subsidence Technological Society, Newcastle, Australia, pp. 189 – 198.

60. Waddington, A A & Kay, D R 2001, 'Closure and uplift in creeks, valleys and gorges due to mine subsidence', *Proceedings of the 5th Triennial Conference on Coal Mine Subsidence Current Practice and Issues*, Mine Subsidence Technological Society, Newcastle, Australia, pp. 49 – 61.

61. Waddington Kay & Associates 2002, 'Research into the impacts of mine subsidence on the strata and hydrology of river valleys and development of management guidelines for undermining cliffs, gorges and river systems', ACARP Research Project No. C9067, *Australian Coal Association Research Program, Brisbane, Queensland, Australia*.

62. Waddington Kay & Associates, CSIRO Petroleum Division & University of New South Wales 2002, 'Management information handbook on the undermining of cliffs, gorges and river systems – projects C8005 and C9067', *Australian Coal Association Research Program, Brisbane, Queensland, Australia*.

63. Whittaker, B N & Reddish, D J 1989, *Subsidence – Occurrence, Prediction and Control*, Elsevier Science Publishers B V, pp. 15 – 113.

64. Williams, W A & Gray, P A 1980, 'The nature and properties of coal and coal measure strata', in Hargraves, A J (ed.), *Proceedings of Support in Coal Mines, The Aus. I.M.M., Illawarra Branch Roof Support Colloquium*, September 1980, The Australasian Institute of Mining and Metallurgy, Parkville, Victoria, Australia, pp. 1 – 12.

APPENDIX A
NUMERICAL MODELLING AUDITS

A.1 PART 1 OF THE SOFT AUDIT: 'ROBUSTNESS QUESTIONS'

1. What is the purpose of the modelling?

To investigate the mechanics of valley closure and upsidence using the block movement theory.

2. In what way is this work different to previous similar modelling work?

To the best of the author's knowledge, modelling valley closure and upsidence using block movements has never been attempted before.

3. What is the scale of the rock mass being modelled?

Large scale models with dimensions measured in the order of several hundred metres.

4. What is the basic modelling geometry?

For the isolated single panel models, the geometry encompasses everything from below the longwall up to the surface. For the river valley models, only the first few rock strata was modelled, with the replication of the subsidence profile being achieved by 'pulling down' the base of the models. The width of all models was defined by the distance at which a full subsidence profile could be developed.

5. **Has it been necessary to divide the rock mass into separate rock mass domains? (Rock mass domain: a region of the rock mass in which the rock properties are statistically similar, but different to the properties of the surrounding rock in other structural domains)**

   Yes, in the isolated single panel models there were 19 separate rock mass domains representing the different strata units. In the river valley models there were four separate rock mass domains.

6. **Are the intact rock properties being specifically incorporated?**

   Yes.

7. **How are the fracture properties being incorporated?**

   The fracture properties are incorporated by way of the numerical modelling code's nature. The numerical code used (UDEC) is a Distinct Element code. Tools like ubiquitous joints were not used at all.

8. **Are features of the structural geology of the rock mass being incorporated?**

   Yes. Bedding plane spacing, sub-vertical joint spacing and sub-vertical joint dip are incorporated. The strata units were assumed to be perfectly horizontal.

9. **Are the rock mass properties being input directly (as opposed to being a result of the input intact rock and fracture properties)?**

   No. The intact properties for the blocks together with the presence of joints in the model were assumed to produce realistic rock mass strength.

10. **How have the rock mass properties been estimated?**

    The majority of the intact rock properties were estimated by laboratory triaxial testing. The material properties that were missing were obtained from the literature,

and if partial material properties were available the remainder were estimated using the Mohr-Coulomb failure criterion. The presence of joints was expected to result in a realistic rock mass strength.

11. Is a constitutive law required for the rock mass? If so, how was it established?

The rock mass was assumed to conform to the Mohr-Coulomb constitutive law given that some material properties were estimated using this constitutive law.

12. Has the rock mass been modelled as a CHILE material? (CHILE: Continuous, homogenous, isotropic, linearly elastic.) What has been done to account for the DIANE aspects of the rock reality (DIANE: Discontinuous, inhomogeneous, anisotropic, not elastic)

DIANE. The numerical code automatically accounts for the DIANE aspects of the rock reality.

13. How have the stress boundary conditions been established?

Stress boundary conditions were not used. An in-situ stress regime with fixed boundaries was utilised instead.

14. Does the model include any failure criteria. If so, which one(s)?

The rock mass is governed by the Mohr-Coulomb plasticity failure criterion. The joints are governed by the Joint Area Contact model which is a Coulomb slip model with residual strength.

15. Is the rock being modelled as a continuum, discontinuum, or combination of the two?

Discontinuum.

16. What are the hydrogeological conditions in the model?

Hydrogeological conditions were not incorporated.

17. How have the hydrological boundary conditions been established?

Hydrogeological boundary conditions were not incorporated.

18. Are effective stresses being used?

No.

19. How are the thermal properties being incorporated?

Thermal properties were not incorporated.

20. How are the THM components being included in the modelling: as uncoupled components, pairwise coupled components, fully coupled components?

Only the mechanical components are being modelled.

21. Are there any special boundary conditions, loading conditions, or rock mass features in the modelling?

There are no special boundary conditions or rock mass features in the modelling. The loading conditions consist of the establishment of an in-situ stress regime.

22. Has physical rock testing been used to obtain any parameters in the modelling?

Yes.

23. Has there been any study of potential adverse interactions that could lead to positive feedbacks and hence instabilities – in the rock mass and in the modelling?

Yes. In the isolated single panel models there was some concern that the instantaneous extraction of the longwall could shock the model. Different damping mechanisms for these models were tried, including a quasi-elastic sub stage, but the final results were very similar. In the river valley models, it was necessary to experiment and find what the most suitable velocity displacement profile could be applied to the base of the models to avoid premature rock mass failure but still maximise developed subsidence.

24. Have all the potential failure mechanisms been identified?

Yes. Cave zones, bedding plane dilation, vertical cracks and spanning rock beams have been identified in the literature and observed in the numerical models.

25. Have modelling sensitivity studies been undertaken?

Yes. Basic sensitivity analysis on mesh density, joint friction angle and joint cohesion has been performed on the river valley models.

26. Have modelling protocols been used?

Yes.

27. How will the modelling methods and results be presented?

The modelling results are presented as a series of tables and graphs.

28. Can the modelling be verified/validated? – in this study and in principle?

Yes, the modelling has been verified by empirical techniques. The analytical techniques produced good matches but cannot be used as verification tools as they are designed to work on much simpler systems.

29. Are there any features of the model or modelling work not covered by the points above?

No.

A.2 PART 2 OF THE SOFT AUDIT: SPECIFYING THE COMPONENTS AND FEATURES OF THE MODELLING

1. THE MODELLING OBJECTIVE

1.1. Has the modelling objective been clearly established?

Yes, the modelling objective has been clearly established. The main objective was to investigate if the proposed block movement model is feasible for the tilts and curvatures generated in the Southern Coalfield. For this to occur, the models must conform to observed subsidence behaviour in the Southern Coalfield.

1.2. How will it be known when the modelling work is completed?

The modelling work, in keeping with the objectives of this thesis, is complete.

2. CONCEPTUALISATION OF THE PROCESSES BEING MODELLED

2.1. What rock mass systems are being considered?

The rock mass includes 19 different rock types.

2.2. What are the main physical processes being modelled?

The main physical processes being modelled in the isolated single panel models are the extraction of the longwall, the subsequent formation of the cave zone and the resulting deformation on the ground surface. The main physical processes being modelled in the river valley models are the replication of the surface subsidence profile by 'pulling down' the base of the model and the resulting valley closure and upsidence.

3. SPECIFICATION OF THE MODELLING CONTENT

3.1. Is the model 1D, 2D, 3D or some combination?

The model is 2D.

3.2. Is a continuum or a discontinuum being modelled?

A discontinuum is being modelled.

3.3. Specification of the boundary conditions.

The isolated single panel models have their boundaries fixed in the x and y-directions at the sides and base of the models. The top of the models is a free surface. The river valley models have their sides fixed in the x and y directions whilst the base is only fixed in the x direction. A velocity displacement profile is applied at the base of the models to replicate the surface subsidence profile. The top of the models is a free surface.

3.4. Specification of the initial conditions.

The initial conditions consist of implementing gravity and an in-situ stress regime. This is done for both the isolated single panel models and the river valley models. The models are then cycled to equilibrium to obtain the initial conditions.

3.5. How is the final condition established?

For the isolated single panel models, the final condition is established after the longwall is excavated and the model is allowed to cycle until the subsidence reaches a maximum value and remains constant. For the river valley models, the final condition is established when maximum developed subsidence on the surface reaches a prescribed value, and the models are cycled for an additional period of time to ensure final equilibrium.

4. MODELLING SOLUTION REQUIREMENTS

4.1. What is the required model output?

For the isolated single panel models, the required model output includes the x and y movement on the surface, the deflection of the Bulgo Sandstone and the visual indication of a goaf angle. For the river valley models, the required model output includes the x-displacements of the valley shoulders, the x-displacements of the valley base, y-displacements of the valley centres, horizontal stresses beneath the sides of the valley, and a visual indication of valley base yield, translation plane slip and buckling.

4.2. Does the model output match the modelling objectives?

Yes. The outputs listed for the isolated single panel models are used to calculate maximum developed subsidence, goaf edge subsidence, strains, tilt, inflection point location and goaf angle. These parameters are necessary for verification with empirical and analytical techniques. The outputs listed for the river valley models are used to determine whether rock blocks are rotating, calculate valley closure and upsidence, and valley base yield. These parameters are necessary for verification with analytical techniques.

5. MODELLING SOLUTION TECHNIQUE

5.1. In principle, how is the model output to be obtained: one code, one set of data, one run? – or a suite of numerical experiments?

The model output is obtained by a suite of numerical experiments. The isolated single panel models were designed to cover a portion of mining geometries in the Southern Coalfield and the river valley models were designed to test river valley response in relation to its transverse distance from a longwall and its vertical distance from a translation plane.

5.2. Are any quality control checks in place? Checking the input data have been entered correctly, validation against known solutions, independent duplication of runs?

Yes. Each script was carefully checked numerous times for errors as the models were run in a batch and any errors would not have been detected until the models had finished running, in some cases this took two weeks. The isolated single panel models and river valley models were verified with empirical and analytical data.

6. NUMERICAL CODE UTILISED

6.1. Which numerical code is to be used?

UDEC – Universal Distinct Element Code.

6.2. Why is that code being used?

UDEC is being used because of its ability to model discontinuous rock masses. This is paramount as the rock masses being modelled are blocky with well defined discontinuities.

6.3. Where did the code originate from?

The code has its origins in Cundall (1971) and is intended for analysis of rock engineering projects where potential modes of failure are directly related to the presence of discontinuous features.

6.4. How has the code been validated?

The code has been validated by the numerous simulations that are performed and verified by analytical techniques. These simulations are available in the UDEC User's Guide (Itasca 2000).

7. SUPPORTING MODEL DATA AND DATA INPUT METHOD

7.1. Listing of type and justification of boundary conditions.

For all models, the surface did not contain any boundary conditions as it represented the ground surface which is naturally free of conditions. In all models, the left hand and right hand sides of the models were fixed in the x and y-directions. This decision was made after it was found that the in-situ stresses at the side boundaries were not affected by the longwall excavation. In the isolated single panel models, the base was fixed in the y-direction so the entire model would not move downwards en masse. In the river valley models, the base was subjected to a displacement boundary in order to replicate the subsidence profile observed in the isolated single panel models. This was also done to drastically reduce the modelling time required.

7.2. Listing of input data with source of the data and justification.

Model geometries

- Holla and Barclay (2000).

Material properties

- CSIRO Petroleum (2002),
- MacGregor and Conquest (2005),
- McNally (1996),
- Pells (1993), and
- Williams and Gray (1980).

Bedding plane/sub-vertical joint spacing, properties and assumptions

- Author's field visits,
- Badelow et al. (2005),
- Barton (1976),
- Chan, Kotze and Stone (2005),
- Coulthard (1995),
- Ghobadi (1994),
- Itasca (2000),
- Mandl (2005),
- Pells (1993),
- Price (1966),
- Selley (2003), and
- Tucker (2003).

In-situ stress

- CSIRO Petroleum (2002).

Mesh generation

- Coulthard (1995).

It can be seen that all the input data is fully traceable and comes from reputable sources. Any assumptions are clearly stated.

7.3. Do the data have to be adjusted before being input?

No. Transparency and traceability were the main objectives of the input data.

8. MODEL SENSITIVITY ANALYSIS

8.1. How does the model output depend on the input parameter values?

The model is very geometrically dependent as there is a wide variation in results for the isolated single panel models. Although not tested, it is expected that differences in material/joint properties and spacings would also have a significant effect on the model output. In the river valley models, an increase in the translation plane joint cohesion and friction angle reduced the magnitude of valley closure.

8.2. Is a sensitivity analysis being conducted? If so, what type of analysis? Processes, mechanisms, parameters, boundary conditions, couplings etc.

Yes, a basic sensitivity analysis was performed on the river valley models by varying the joint friction angle and joint cohesion of the translation plane.

8.3. How are the results of the sensitivity analysis to be summarised?

Table format and graphs.

9. PRESENTATION OF MODELLING RESULTS

9.1. Is it possible to demonstrate that the numerical code is operating correctly?

Yes. The verification carried out is evidence of this.

9.2. Is it possible to show that the supporting data are reasonable assumptions for a rock mass?

Yes, the verification also proves this point, as does the sources cited.

9.3. How are the modelling results to be presented?

The modelling results are presented as figures, tables and graphs. For the verification purposes, the modelling results are overlain onto empirical graphs.

9.4. Does the presentation of the modelling results link with the modelling objective?

Yes. Ultimately it was able to be shown by graphs, tables and visual representations of the models that valley closure and upsidence was caused by block movements.

10. SOURCES OF ERRORS

10.1. Have you already corrected any errors?

Yes. Any errors evident at the time of model execution have been corrected.

10.2. List the sources of potentially significant errors.

- Typographical mistakes,
- Incorrect material and joint properties,
- Incorrect in-situ stress regime, and
- Boundaries too close to excavation.

10.3. Do any of the potentially significant errors invalidate the modelling objective, concept and conclusions?

Yes they would because it could mean that the subsidence parameters are not being correctly simulated, simulated sub-surface deformations are not in accordance with the literature and observed behaviour, which has implications for individual block movements and hence the concept of the block movement model.

11. MODELLING ADEQUACY

11.1. Do all the previous questions indicate that in principle the model is adequate for the purpose?

Yes.

11.2. If not, list the problem areas

Not applicable.

11.3. What corrective action is required?

Not applicable.

11.4. Does the soft audit have to be repeated after corrective action has been taken?

No.

A.3 DEVELOPING FROM THE SOFT AUDIT TO THE HARD AUDIT

The process of developing a soft audit to a hard audit involves the same subjects and questions as the soft audit but including detailed justifications to the questions. The procedure for developing a soft audit to hard audit can be seen in Figure A.1.

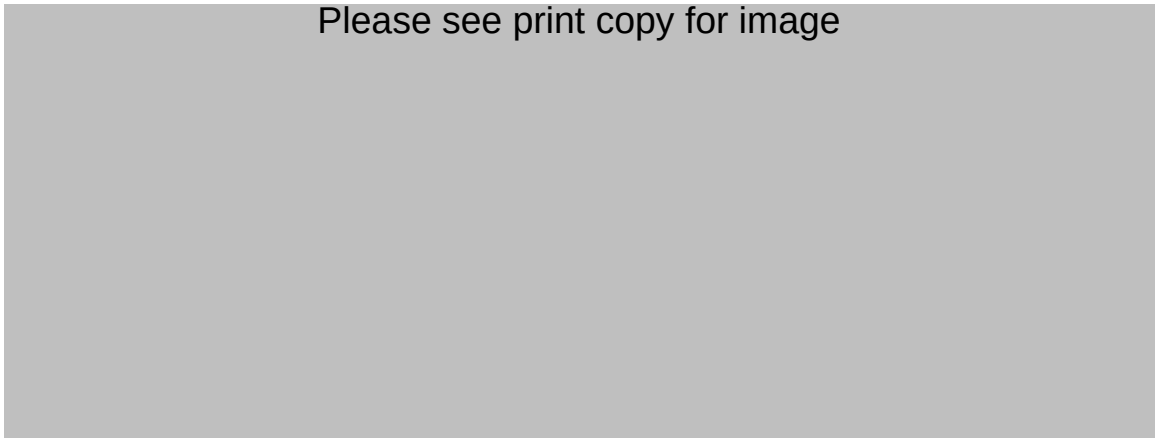

Fig. A.1 – The procedure for developing from the soft audit to the hard audit (Hudson, Stephansson & Andersson 2005)

It can be seen in Section A.2 that the justifications have been included to the answers of the soft audit and the final answer is that the modelling is adequate for the purposes stated.

APPENDIX B

SINGLE LONGWALL PANEL MODEL WITH NO RIVER VALLEY

```
; Model based on Metropolitan Colliery
; Using symmetry
; Depth of cover = 413 m
; Longwall width = 105 m
; Extracted thickness = 2.7 m
; W/h ratio = 0.25
; Model dimensions: 815 m x 509.8 m

ti
Model 1 (Metropolitan Colliery)

; Creating model geometry

ro = 0.01
se ov = 0.2

bl 0,-509.8 0,0 815,0 815,-509.8
cr 0,-88    815,-88             ; Hawkesbury Sandstone (88 m thick)
cr 0,-108   815,-108            ; Newport Formation (20 m thick)
cr 0,-142   815,-142            ; Bald Hill Claystone (34 m thick)
cr 0,-287   815,-287            ; Bulgo Sandstone (145 m thick)
cr 0,-327   815,-327            ; Stanwell Park Claystone (40 m thick)
cr 0,-377   815,-377            ; Scarborough Sandstone (50 m thick)
cr 0,-393   815,-393            ; Wombarra Shale (16 m thick)
cr 0,-413   815,-413            ; Coal Cliff Sandstone (20 m thick)
cr 0,-415.7 815,-415.7          ; Bulli Seam (2.7 m thick)
cr 0,-423.7 815,-423.7          ; Loddon Sandstone (8 m thick)
cr 0,-424.7 815,-424.7          ; Balgownie Seam (1 m thick)
cr 0,-428.7 815,-428.7          ; Lawrence Sandstone (4 m thick)
cr 0,-430.7 815,-430.7          ; Cape Horn Seam (2 m thick)
cr 0,-436.7 815,-436.7          ; UN2 (6 m thick)
cr 0,-436.8 815,-436.8          ; Hargraves Coal Member (0.1 m thick)
cr 0,-446.8 815,-446.8          ; UN3 (10 m thick)
cr 0,-456.8 815,-456.8          ; Wongawilli Seam (10 m thick)
```

```
cr 0,-459.8 815,-459.8          ; Kembla Sandstone (3 m thick)
cr 0,-509.8 815,-509.8          ; Coal Measures (50 m thick)

; Defining longwall

cr 762.5,-413 762.5,-415.7
cr 815,-413 815,-415.7

; Defining discontinuities

jr 0,-88 0,0 815,0 815,-88         ; Hawkesbury Sandstone
js 0,0 815,0 0,0 9,0
js 90,0 9,0 9,0 9,0
js 90,0 9,0 9,0 9,0 4.5 -9

jr 0,-108 0,-88 815,-88 815,-108   ; Newport Formation
js 0,0 815,0 0,0 1,0
js 90,0 1,0 1,0 1,0
js 90,0 1,0 1,0 1,0 0.5,-89

jr 0,-142 0,-108 815,-108 815,-142 ; Bald Hill Claystone
js 0,0 815,0 0,0 1,0
js 90,0 1,0 1,0 1,0
js 90,0 1,0 1,0 1,0 0.5,-109

jr 0,-287 0,-142 815,-142 815,-287 ; Bulgo Sandstone
js 0,0 815,0 0,0 9,0
js 90,0 9,0 9,0 9,0
js 90,0 9,0 9,0 9,0 4.5,-153

jr 0,-327 0,-287 815,-287 815,-327 ; Stanwell Park Claystone
js 0,0 815,0 0,0 3,0
js 90,0 3,0 3,0 3,0
js 90,0 3,0 3,0 3,0 1.5,-291

jr 0,-377 0,-327 815,-327 815,-377 ; Scarborough Sandstone
js 0,0 815,0 0,0 4,0
js 90,0 4,0 4,0 4,0
js 90,0 4,0 4,0 4,0 2,-332
```

```
jr 0,-393 0,-377 815,-377 815,-393 ; Wombarra Shale
js 0,0 815,0 0,0 3,0
js 90,0 3,0 3,0 3,0
js 90,0 3,0 3,0 3,0 1.5,-381

jr 0,-413 0,-393 815,-393 815,-413 ; Coal Cliff Sandstone
js 0,0 815,0 0,0 3,0
js 90,0 3,0 3,0 3,0
js 90,0 3,0 3,0 3,0 1.5,-399

; Generating zones for deformable blocks

ge q 12.7 ra 0 815    -88      0 ; Hawkesbury Sandstone
ge q 1.4  ra 0 815   -108    -88 ; Newport Formation
ge q 1.4  ra 0 815   -142   -108 ; Bald Hill Claystone
ge q 12.7 ra 0 815   -287   -142 ; Bulgo Sandstone
ge q 4.2  ra 0 815   -327   -287 ; Stanwell Park Claystone
ge q 5.7  ra 0 815   -377   -327 ; Scarborough Sandstone
ge q 4.2  ra 0 815   -393   -377 ; Wombarra Shale
ge q 4.2  ra 0 815   -413   -393 ; Coal Cliff Sandstone
ge q 3.5  ra 0 815 -415.7   -413 ; Bulli Seam
ge q 11.3 ra 0 815 -423.7 -415.7 ; Loddon Sandstone
ge q 1.4  ra 0 815 -424.7 -423.7 ; Balgownie Seam
ge q 5.7  ra 0 815 -428.7 -424.7 ; Lawrence Sandstone
ge q 2.8  ra 0 815 -430.7 -428.7 ; Cape Horn Seam
ge q 8.5  ra 0 815 -436.7 -430.7 ; UN2
ge q 0.1  ra 0 815 -436.8 -436.7 ; Hargraves Coal Member
ge q 14.1 ra 0 815 -446.8 -436.8 ; UN3
ge q 14.1 ra 0 815 -456.8 -446.8 ; Wongawilli Seam
ge q 4.2  ra 0 815 -459.8 -456.8 ; Kembla Sandstone
ge q 4.2  ra 0 815 -509.8 -459.8 ; Coal Measures

sa model1_ini1.sav

; Defining material properties

pro m 1  de = 2397 b = 11.47e9 sh = 5.65e9 coh = 9.70e6  fr = 37.25 &
         ten = 3.58e6 ; Hawkesbury Sandstone

pro m 2  de = 2290 b = 7.77e9  sh = 4.66e9 coh = 8.85e6  fr = 35.00 &
         ten = 3.40e6 ; Newport Formation
```

```
pro m 3  de = 2719 b = 14.12e9 sh = 4.72e9 coh = 10.60e6 fr = 27.80 &
         ten = 2.90e6 ; Bald Hill Claystone

pro m 4  de = 2527 b = 12.60e9 sh = 7.91e9  coh = 17.72e6 fr = 35.40 &
         ten = 6.55e6 ; Bulgo Sandstone

pro m 5  de = 2693 b = 13.22e9 sh = 7.63e9  coh = 14.57e6 fr = 27.80 &
         ten =4 .83e6 ; Stanwell Park Claystone

pro m 6  de = 2514 b = 16.16e9 sh = 10.80e9 coh = 13.25e6 fr = 40.35 &
         ten = 7.18e6 ; Scarborough Sandstone

pro m 7  de = 2643 b = 24.81e9 sh = 7.24e9  coh = 14.51e6 fr = 27.80 &
         ten = 4.81e6 ; Wombarra Shale

pro m 8  de = 2600 b = 17.07e9 sh = 11.44e9 coh = 19.40e6 fr = 33.30 &
         ten = 7.87e6 ; Coal Cliff Sandstone

pro m 9  de = 1500 b = 2.33e9  sh = 1.08e9  coh = 6.37e6  fr = 25.00 &
         ten = 0.84e6 ; Bulli Seam

pro m 10 de = 2539 b = 16.76e9 sh = 6.51e9  coh = 17.10e6 fr = 28.90 &
         ten = 5.65e6 ; Loddon Sandstone

pro m 11 de = 1500 b = 2.33e9  sh = 1.08e9  coh = 6.37e6  fr = 25.00 &
         ten = 0.84e6 ; Balgownie Seam

pro m 12 de = 2539 b = 16.76e9 sh = 6.51e9  coh = 17.10e6 fr = 28.90 &
         ten = 5.65e6 ; Lawrence Sandstone

pro m 13 de = 1500 b = 1.67e9  sh = 0.77e9  coh = 2.87e6  fr = 25.00 &
         ten = 0.70e6 ; Cape Horn Seam

pro m 14 de = 2560 b = 8.99e9  sh = 5.39e9  coh = 19.89e6 fr = 28.90 &
         ten = 6.74e6 ; UN2

pro m 15 de = 1500 b = 2.33e9  sh = 1.08e9  coh = 6.37e6  fr = 25.00 &
         ten = 0.84e6 ; Hargraves Coal Member

pro m 16 de = 2620 b = 8.67e9  sh = 5.20e9  coh = 19.18e6 fr = 28.90 &
         ten = 6.50e6 ; UN3
```

```
pro m 17 de = 1500 b = 1.67e9  sh = 0.77e9  coh = 2.87e6  fr = 25.00 &
         ten =0 .70e6 ; Wongawilli Seam

pro m 18 de = 2569 b = 13.79e9 sh = 7.12e9  coh = 18.02e6 fr = 28.90 &
         ten = 6.11e6 ; Kembla Sandstone

pro m 19 de = 2092 b = 8.11e9  sh = 3.83e9  coh = 12.20e6 fr = 27.17 &
         ten = 3.75e6 ; Coal Measures

; Assigning material properties

ch cons 3

ch m 1  ra 0 815    -88      0 ; Hawkesbury Sandstone
ch m 2  ra 0 815   -108    -88 ; Newport Formation
ch m 3  ra 0 815   -142   -108 ; Bald Hill Claystone
ch m 4  ra 0 815   -287   -142 ; Bulgo Sandstone
ch m 5  ra 0 815   -327   -287 ; Stanwell Park Claystone
ch m 6  ra 0 815   -377   -327 ; Scarborough Sandstone
ch m 7  ra 0 815   -393   -377 ; Wombarra Shale
ch m 8  ra 0 815   -413   -393 ; Coal Cliff Sandstone
ch m 9  ra 0 815 -415.7   -413 ; Bulli Seam
ch m 10 ra 0 815 -423.7 -415.7 ; Loddon Sandstone
ch m 11 ra 0 815 -424.7 -423.7 ; Balgownie Seam
ch m 12 ra 0 815 -428.7 -424.7 ; Lawrence Sandstone
ch m 13 ra 0 815 -430.7 -428.7 ; Cape Horn Seam
ch m 14 ra 0 815 -436.7 -430.7 ; UN2
ch m 15 ra 0 815 -436.8 -436.7 ; Hargraves Coal Member
ch m 16 ra 0 815 -446.8 -436.8 ; UN3
ch m 17 ra 0 815 -456.8 -446.8 ; Wongawilli Seam
ch m 18 ra 0 815 -459.8 -456.8 ; Kembla Sandstone
ch m 19 ra 0 815 -509.8 -459.8 ; Coal Measures

; Defining bedding plane properties

pro jm = 1 jkn = 21e9   jks   = 2.1e9  & ; Hawkesbury Sandstone
           jf  = 25     jrf   = 15     &
           jc  = 0.29e6 jresc = 0
```

```
pro jm = 2 jkn = 140e9  jks   = 14e9   & ; Newport Formation
           jf  = 25     jrf   = 15     &
           jc  = 0.29e6 jresc = 0

pro jm = 3 jkn = 204e9  jks   = 20.4e9 & ; Bald Hill Claystone
           jf  = 25     jrf   = 15     &
           jc  = 0.29e6 jresc = 0

pro jm = 4 jkn = 26e9   jks   = 2.6e9  & ; Bulgo Sandstone
           jf  = 25     jrf   = 15     &
           jc  = 0.29e6 jresc = 0

pro jm = 5 jkn = 78e9   jks   = 7.8e9  & ; Stanwell Park Claystone
           jfc = 25     jrf   = 15     &
           jc  = 0.29e6 jresc = 0

pro jm = 6 jkn = 76e9   jks   = 7.6e9  & ; Scarborough Sandstone
           jf  = 25     jrf   = 15     &
           jc  = 0.29e6 jresc = 0

pro jm = 7 jkn = 115e9  jks   = 11.5e9 & ; Wombarra Shale
           jf  = 25     jrf   = 15     &
           jc  = 0.29e6 jresc = 0

pro jm = 8 jkn = 400e9  jks   = 40e9   & ; Coal Cliff Sandstone
           jf  = 25     jrf   = 15     &
           jc  = 0.29e6 jresc = 0

pro jm = 9 jkn = 400e9  jks   = 40e9   & ; Sub Bulli
           jf  = 25     jrf   = 15     &
           jc  = 0.29e6 jresc = 0

; Assigning bedding plane properties

ch jc = 5 ra 0 815 -509.8 0 ang -1 1
se jc = 5

ch jm 1 ra 0 815  -88    0 ang -1 1 ; Hawkesbury Sandstone
ch jm 2 ra 0 815 -108  -88 ang -1 1 ; Newport Formation
ch jm 3 ra 0 815 -142 -108 ang -1 1 ; Bald Hill Claystone
ch jm 4 ra 0 815 -287 -142 ang -1 1 ; Bulgo Sandstone
```

```
ch jm 5 ra 0 815 -327 -287 ang -1 1   ; Stanwell Park Claystone
ch jm 6 ra 0 815 -377 -327 ang -1 1   ; Scarborough Sandstone
ch jm 7 ra 0 815 -393 -377 ang -1 1   ; Wombarra Shale
ch jm 8 ra 0 815 -413 -393 ang -1 1   ; Coal Cliff Sandstone
ch jm 9 ra 0 815 -509.8 -413 ang -1 1 ; Sub Bulli

; Defining vertical joint properties

pro jm = 10 jkn = 21e9   jks   = 2.1e9  & ; Hawkesbury Sandstone
            jf  = 19     jrf   = 15     &
            jc  = 0.86e6 jresc = 0

pro jm = 11 jkn = 140e9  jks   = 14e9   & ; Newport Formation
            jf  = 19     jrf   = 15     &
            jc  = 0.86e6 jresc = 0

pro jm = 12 jkn = 204e9  jks   = 20.4e9 & ; Bald Hill Claystone
            jf  = 19     jrf   = 15     &
            jc  = 0.86e6 jresc = 0

pro jm = 13 jkn = 26e9   jks   = 2.6e9  & ; Bulgo Sandstone
            jf  = 19     jrf   = 15     &
            jc  = 0.86e6 jresc = 0

pro jm = 14 jkn = 78e9   jks   = 7.8e9  & ; Stanwell Park Claystone
            jf  = 19     jrf   = 15     &
            jc  = 0.86e6 jresc = 0

pro jm = 15 jkn = 76e9   jks   = 7.6e9  & ; Scarborough Sandstone
            jf  = 19     jrf   = 15     &
            jc  = 0.86e6 jresc = 0

pro jm = 16 jkn = 115e9  jks   = 11.5e9 & ; Wombarra Shale
            jf  = 19     jrf   = 15     &
            jc  = 0.86e6 jresc = 0

pro jm = 17 jkn = 400e9  jks   = 40e9   & ; Coal Cliff Sandstone
            jf  = 19     jrf   = 15     &
            jc  = 0.86e6 jresc = 0
```

```
pro jm = 18 jkn = 400e9  jks   = 40e9   & ; Sub Bulli
            jf  = 19     jrf   = 15     &
            jc  = 0.86e6 jresc = 0

; Assigning vertical joint properties

ch jc = 5 ra 0 815 -509.8 0 ang 89 91
se jc = 5

ch jm 10 ra 0 815    -88    0 ang 89 91 ; Hawkesbury Sandstone
ch jm 11 ra 0 815   -108  -88 ang 89 91 ; Newport Formation
ch jm 12 ra 0 815   -142 -108 ang 89 91 ; Bald Hill Claystone
ch jm 13 ra 0 815   -287 -142 ang 89 91 ; Bulgo Sandstone
ch jm 14 ra 0 815   -327 -287 ang 89 91 ; Stanwell Park Claystone
ch jm 15 ra 0 815   -377 -327 ang 89 91 ; Scarborough Sandstone
ch jm 16 ra 0 815   -393 -377 ang 89 91 ; Wombarra Shale
ch jm 17 ra 0 815   -413 -393 ang 89 91 ; Coal Cliff Sandstone
ch jm 18 ra 0 815 -509.8 -413 ang 89 91 ; Sub Bulli

; Defining gravity

se gr 0 -9.81

; Defining boundary conditions

bo xv 0 ra -0.1 0.1 -509.8 0
bo xv 0 ra 814.9 815.1 -509.8,0
bo yv 0 ra 0 815 -509.9 -509.7

; Defining initial stress conditions

in st 0 0 0 yg 4.82e4 0 2.41e4 szz 0 zg 0 4.82e4 ra 0 815 -509.8 0

da a

so

sa model1_ini2.sav
```

```
; Initialising displacements

rese vel
rese di

; Defining histories
; Y-displacements

hi yd     0 0 ;1
hi yd   4.5 0 ;2
hi yd  13.5 0 ;3
hi yd  22.5 0 ;4
hi yd  31.5 0 ;5
hi yd  40.5 0 ;6
hi yd  49.5 0 ;7
hi yd  58.5 0 ;8
hi yd  67.5 0 ;9
hi yd  76.5 0 ;10
hi yd  85.5 0 ;11
hi yd  94.5 0 ;12
hi yd 103.5 0 ;13
hi yd 112.5 0 ;14
hi yd 121.5 0 ;15
hi yd 130.5 0 ;16
hi yd 139.5 0 ;17
hi yd 148.5 0 ;18
hi yd 157.5 0 ;19
hi yd 166.5 0 ;20
hi yd 175.5 0 ;21
hi yd 184.5 0 ;22
hi yd 193.5 0 ;23
hi yd 202.5 0 ;24
hi yd 211.5 0 ;25
hi yd 220.5 0 ;26
hi yd 229.5 0 ;27
hi yd 238.5 0 ;28
hi yd 247.5 0 ;29
hi yd 256.5 0 ;30
hi yd 265.5 0 ;31
hi yd 274.5 0 ;32
hi yd 283.5 0 ;33
```

```
hi yd 292.5 0 ;34
hi yd 301.5 0 ;35
hi yd 310.5 0 ;36
hi yd 319.5 0 ;37
hi yd 328.5 0 ;38
hi yd 337.5 0 ;39
hi yd 346.5 0 ;40
hi yd 355.5 0 ;41
hi yd 364.5 0 ;42
hi yd 373.5 0 ;43
hi yd 382.5 0 ;44
hi yd 391.5 0 ;45
hi yd 400.5 0 ;46
hi yd 409.5 0 ;47
hi yd 418.5 0 ;48
hi yd 427.5 0 ;49
hi yd 436.5 0 ;50
hi yd 445.5 0 ;51
hi yd 454.5 0 ;52
hi yd 463.5 0 ;53
hi yd 472.5 0 ;54
hi yd 481.5 0 ;55
hi yd 490.5 0 ;56
hi yd 499.5 0 ;57
hi yd 508.5 0 ;58
hi yd 517.5 0 ;59
hi yd 526.5 0 ;60
hi yd 535.5 0 ;61
hi yd 544.5 0 ;62
hi yd 553.5 0 ;63
hi yd 562.5 0 ;64
hi yd 571.5 0 ;65
hi yd 580.5 0 ;66
hi yd 589.5 0 ;67
hi yd 598.5 0 ;68
hi yd 607.5 0 ;69
hi yd 616.5 0 ;70
hi yd 625.5 0 ;71
hi yd 634.5 0 ;72
hi yd 643.5 0 ;73
hi yd 652.5 0 ;74
```

```
hi yd 661.5 0 ;75
hi yd 670.5 0 ;76
hi yd 679.5 0 ;77
hi yd 688.5 0 ;78
hi yd 697.5 0 ;79
hi yd 706.5 0 ;80
hi yd 715.5 0 ;81
hi yd 724.5 0 ;82
hi yd 733.5 0 ;83
hi yd 742.5 0 ;84
hi yd 751.5 0 ;85
hi yd 760.5 0 ;86
hi yd 769.5 0 ;87
hi yd 778.5 0 ;88
hi yd 787.5 0 ;89
hi yd 796.5 0 ;90
hi yd 805.5 0 ;91
hi yd 814.5 0 ;92
hi yd 815.0 0 ;93

; X-displacements

hi xd     0 0 ;94
hi xd   4.5 0 ;95
hi xd  13.5 0 ;96
hi xd  22.5 0 ;97
hi xd  31.5 0 ;98
hi xd  40.5 0 ;99
hi xd  49.5 0 ;100
hi xd  58.5 0 ;101
hi xd  67.5 0 ;102
hi xd  76.5 0 ;103
hi xd  85.5 0 ;104
hi xd  94.5 0 ;105
hi xd 103.5 0 ;106
hi xd 112.5 0 ;107
hi xd 121.5 0 ;108
hi xd 130.5 0 ;109
hi xd 139.5 0 ;110
hi xd 148.5 0 ;111
hi xd 157.5 0 ;112
```

```
hi xd 166.5 0 ;113
hi xd 175.5 0 ;114
hi xd 184.5 0 ;115
hi xd 193.5 0 ;116
hi xd 202.5 0 ;117
hi xd 211.5 0 ;118
hi xd 220.5 0 ;119
hi xd 229.5 0 ;120
hi xd 238.5 0 ;121
hi xd 247.5 0 ;122
hi xd 256.5 0 ;123
hi xd 265.5 0 ;124
hi xd 274.5 0 ;125
hi xd 283.5 0 ;126
hi xd 292.5 0 ;127
hi xd 301.5 0 ;128
hi xd 310.5 0 ;129
hi xd 319.5 0 ;130
hi xd 328.5 0 ;131
hi xd 337.5 0 ;132
hi xd 346.5 0 ;133
hi xd 355.5 0 ;134
hi xd 364.5 0 ;135
hi xd 373.5 0 ;136
hi xd 382.5 0 ;137
hi xd 391.5 0 ;138
hi xd 400.5 0 ;139
hi xd 409.5 0 ;140
hi xd 418.5 0 ;141
hi xd 427.5 0 ;142
hi xd 436.5 0 ;143
hi xd 445.5 0 ;144
hi xd 454.5 0 ;145
hi xd 463.5 0 ;146
hi xd 472.5 0 ;147
hi xd 481.5 0 ;148
hi xd 490.5 0 ;149
hi xd 499.5 0 ;150
hi xd 508.5 0 ;151
hi xd 517.5 0 ;152
hi xd 526.5 0 ;153
```

```
hi xd 535.5 0 ;154
hi xd 544.5 0 ;155
hi xd 553.5 0 ;156
hi xd 562.5 0 ;157
hi xd 571.5 0 ;158
hi xd 580.5 0 ;159
hi xd 589.5 0 ;160
hi xd 598.5 0 ;161
hi xd 607.5 0 ;162
hi xd 616.5 0 ;163
hi xd 625.5 0 ;164
hi xd 634.5 0 ;165
hi xd 643.5 0 ;166
hi xd 652.5 0 ;167
hi xd 661.5 0 ;168
hi xd 670.5 0 ;169
hi xd 679.5 0 ;170
hi xd 688.5 0 ;171
hi xd 697.5 0 ;172
hi xd 706.5 0 ;173
hi xd 715.5 0 ;174
hi xd 724.5 0 ;175
hi xd 733.5 0 ;176
hi xd 742.5 0 ;177
hi xd 751.5 0 ;178
hi xd 760.5 0 ;179
hi xd 769.5 0 ;180
hi xd 778.5 0 ;181
hi xd 787.5 0 ;182
hi xd 796.5 0 ;183
hi xd 805.5 0 ;184
hi xd 814.5 0 ;185
hi xd 815.0 0 ;186
hi u          ;187

; Extracting longwall - instantaneous extraction

de b 4098

da a
```

```
; Solving for equilibrium

so rat 1e-5 ste 1000000000

sa model1_final.sav
```

APPENDIX C

RIVER VALLEY MODEL WITH PLANE AT BASE

```
ti
Valley 1

; Creating model geometry

ro = 0.01
set ov = 0.2

bl 0,-189 0,0 1050,0 1050,-189
cr 0,-78   1050,-78    ; Hawkesbury Sandstone (78 m thick)
cr 0,-85   1050,-85    ; Newport Formation (7 m thick)
cr 0,-97   1050,-97    ; Bald Hill Claystone (9 m thick)
cr 0,-186  1050,-186   ; Bulgo Sandstone (89 m thick + 3 m thick beam)

; Generating vertical cracks for beam at base of Bald Hill Claystone

jr 0,-189 0,-186 525,-186 525,-189
js 90,0 3,0 0,0 9,0 13.5,-189
cr 525,-189 525,-186
cr 532.5,-189 532.5,-186

jr 532.5,-189 532.5,-186 1050,-186 1050,-189
js 90,0 3,0 0,0 9,0 1045.5,-189

; Generating pre-defined cracks for valleys (70 m deep x 50 m wide)

cr 0,-70    1050,-70
cr 500,-70  500,0
cr 450,-70  450,0
cr 400,-70  400,0
cr 350,-70  350,0
cr 300,-70  300,0
cr 250,-70  250,0
cr 200,-70  200,0
cr 150,-70  150,0
cr 100,-70  100,0
```

```
cr 50,-70   50,0
cr 550,-70  550,0
cr 600,-70  600,0
cr 650,-70  650,0
cr 700,-70  700,0
cr 750,-70  750,0
cr 800,-70  800,0
cr 850,-70  850,0
cr 900,-70  900,0
cr 950,-70  950,0
cr 1000,-70 1000,0

; Defining discontinuities

jr 0,-78 0,-70 1050,-70 1050,-78            ; Hawkesbury Sandstone
js 90,0 9,0 9,0 9,0 4.5 -78

jr 0,-85 0,-78 1050,-78 1050,-85            ; Newport Formation
js 0,0 1050,0 0,0 1,0
js 90,0 1,0 1,0 1,0
js 90,0 1,0 1,0 1,0 0.5,-79

jr 0,-97 0,-85 1050,-85 1050,-97            ; Bald Hill Claystone
js 0,0 1050,0 0,0 1,0
js 90,0 1,0 1,0 1,0
js 90,0 1,0 1,0 1,0 0.5,-87

jr 0,-186 0,-97 1050,-97 1050,-186          ; Bulgo Sandstone
js 0,0 525,0 0,0 9,0
js 90,0 9,0 9,0 9,0
js 90,0 9,0 9,0 9,0 4.5,-117
jr 0,-189 0,-186 525,-186 525,-189
js 90,0 3,0 0,0 9,0 13.5,-189
cr 525,-189 525,-186
cr 532.5,-189 532.5,-186
jr 532.5,-189 532.5,-186 1050,-186 1050,-189
js 90,0 3,0 0,0 9,0 1045.5,-189
```

```
; Generating zones for deformable blocks

ge q 12.7 ra 0 1050 -78    0 ; Hawkesbury Sandstone
ge q 1.4  ra 0 1050 -85  -78 ; Newport Formation
ge q 1.4  ra 0 1050 -97  -85 ; Bald Hill Claystone
ge q 12.7 ra 0 1050 -189 -97 ; Bulgo Sandstone

; Defining material properties

pro m 1  de = 2397 b = 11.47e9 sh = 5.65e9 coh = 9.70e6  fr= 37.25 &
ten = 3.58e6 ; Hawkesbury Sandstone

pro m 2  de = 2290 b = 7.77e9  sh = 4.66e9 coh = 8.85e6  fr= 35.00 &
ten = 3.40e6 ; Newport Formation

pro m 3  de = 2719 b = 14.12e9 sh = 4.72e9 coh = 10.60e6 fr= 27.80 &
ten = 2.90e6 ; Bald Hill Claystone

pro m 4  de = 2527 b = 12.60e9 sh = 7.91e9 coh = 17.72e6 fr= 35.40 &
ten = 6.55e6 ; Bulgo Sandstone

; Assigning material properties

ch cons 3

ch m 1  ra 0 1050 -78 0    ; Hawkesbury Sandstone
ch m 2  ra 0 1050 -85 -78  ; Newport Formation
ch m 3  ra 0 1050 -97 -85  ; Bald Hill Claystone
ch m 4  ra 0 1050 -189 -97 ; Bulgo Sandstone

; Defining bedding plane properties

pro jm = 1 jkn = 21e9   jks   = 2.1e9  & ; Hawkesbury Sandstone
           jf  = 25     jrf   = 15     &
           jc  = 0.29e6 jresc = 0

pro jm = 2 jkn = 140e9  jks   = 14.0e9 & ; Newport Formation
           jf  = 25     jrf   = 15     &
           jc  = 0.29e6 jresc = 0
```

```
pro jm = 3 jkn = 204e9  jks   = 20.4e9 & ; Bald Hill Claystone
           jf  = 25     jrf   = 15     &
           jc  = 0.29e6 jresc = 0

pro jm = 4 jkn = 26e9   jks   = 2.6e9  & ; Bulgo Sandstone
           jf  = 25     jrf   = 15     &
           jc  = 0.29e6 jresc = 0

pro jm = 5 jkn = 204e9 jks   = 20.4e9 & ; Beam
           jf  = 89    jrf   = 89     &
           jc  = 1e10  jresc = 1e10   &
           jt  = 1e10  jrt   = 1e10

; Assigning bedding plane properties

ch jc = 5 ra 0 1050 -189 0 ang -1 1
se jc = 5

ch jm 1 ra 0 1050 -78 0     ang -1 1 ; Hawkesbury Sandstone
ch jm 2 ra 0 1050 -85 -78   ang -1 1 ; Newport Formation
ch jm 3 ra 0 1050 -97 -85   ang -1 1 ; Bald Hill Claystone
ch jm 4 ra 0 1050 -186 -97  ang -1 1 ; Bulgo Sandstone
ch jm 5 ra 0 1050 -189 -186 ang -1 1 ; Beam

; Vertical joint properties

pro jm = 6  jkn = 21e9  jks    = 2.1e9  & ; Hawkesbury Sandstone
            jf  = 19     jrf   = 15     &
            jc  = 0.86e6 jresc = 0

pro jm = 7  jkn = 140e9  jks   = 14.0e9 & ; Newport Formation
            jf  = 19     jrf   = 15     &
            jc  = 0.86e6 jresc = 0

pro jm = 8  jkn = 204e9  jks   = 20.4e9 & ; Bald Hill Claystone
            jf  = 19     jrf   = 15     &
            jc  = 0.86e6 jresc = 0

pro jm = 9  jkn = 26e9   jks   = 2.6e9 & ; Bulgo Sandstone;
            jf  = 19     jrf   = 15    &
            jc  = 0.86e6 jresc = 0
```

```
pro jm = 10 jkn = 204e9 jks   = 20.4e9 & ; Beam
            jf  = 89    jrf   = 89     &
            jc  = 1e10  jresc = 1e10   &
            jt  = 1e10  jrt   = 1e10

; Assigning vertical joint properties

ch jc = 5 ra 0 1050 -189 0 ang 89 91
se jc = 5

ch jm 6  ra 0 1050 -186    0  ang 89 91 ; Hawkesbury Sandstone
ch jm 7  ra 0 1050 -85   -78  ang 89 91 ; Newport Formation
ch jm 8  ra 0 1050 -97   -85  ang 89 91 ; Bald Hill Claystone
ch jm 9  ra 0 1050 -186  -97  ang 89 91 ; Bulgo Sandstone
ch jm 10 ra 0 1050 -189 -186  ang 89 91 ; Beam

; Defining gravity

se gr 0 -9.81

; Defining boundary conditions

bo yv 0 ra 0 1050 -189.1 -188.9
bo xv 0 ra -0.1 0.1 -189.1 0.1
bo xv 0 ra 1049.9 1050.1 -189.1 0.1

; Defining initial stress conditions

in st 0 0 0 yg 4.77e4 0 2.39e4 szz 0 zg 0 4.77e4 ra 0 1050 -189 0

sa valley1_ini1.sav

; Cycle to equilibrium

da a

so
```

```
; Removing valley and cycle to equilibrium

de ra 500 550 -70 0

da a

so

; Removing boundary conditions at base and attaching pre-determined y-displacements

rese vel
rese di

bo yfr
bo xfr
bo xv 0 ra -0.1 0.1 -189.1 0.1
bo xv 0 ra 1049.9 1050.1 -189.1 0.1

; Histories

; X Displacements (valley closure)
; Top of valley

hi xd 50  0 ;1
hi xd 100 0 ;2
hi xd 150 0 ;3
hi xd 200 0 ;4
hi xd 250 0 ;5
hi xd 300 0 ;6
hi xd 350 0 ;7
hi xd 400 0 ;8
hi xd 450 0 ;9
hi xd 500 0 ;10
hi xd 550 0 ;11

; Y Displacements (subsidence)

hi yd 0  0 ;12
hi yd 25 0 ;13
hi yd 50 0 ;14
```

```
hi yd 75   0 ;15
hi yd 100  0 ;16
hi yd 125  0 ;17
hi yd 150  0 ;18
hi yd 175  0 ;19
hi yd 200  0 ;20
hi yd 225  0 ;21
hi yd 250  0 ;22
hi yd 275  0 ;23
hi yd 300  0 ;24
hi yd 325  0 ;25
hi yd 350  0 ;26
hi yd 375  0 ;27
hi yd 400  0 ;28
hi yd 425  0 ;29
hi yd 450  0 ;30
hi yd 475  0 ;31
hi yd 500  0 ;32
hi yd 525  0 ;33
hi yd 550  0 ;34
hi yd 575  0 ;35
hi yd 600  0 ;36
hi yd 625  0 ;37
hi yd 650  0 ;38
hi yd 675  0 ;39
hi yd 700  0 ;40
hi yd 725  0 ;41
hi yd 750  0 ;42
hi yd 775  0 ;43
hi yd 800  0 ;44
hi yd 825  0 ;45
hi yd 850  0 ;46
hi yd 875  0 ;47
hi yd 900  0 ;48
hi yd 925  0 ;49
hi yd 950  0 ;50
hi yd 975  0 ;51
hi yd 1000 0 ;52
hi yd 1025 0 ;53
hi yd 1050 0 ;54
```

```
; Y displacements (base)

hi yd 0     -189 ;55
hi yd 4.5   -189 ;56
hi yd 13.5  -189 ;57
hi yd 22.5  -189 ;58
hi yd 31.5  -189 ;59
hi yd 40.5  -189 ;60
hi yd 49.5  -189 ;61
hi yd 58.5  -189 ;62
hi yd 67.5  -189 ;63
hi yd 76.5  -189 ;64
hi yd 85.5  -189 ;65
hi yd 94.5  -189 ;66
hi yd 103.5 -189 ;67
hi yd 112.5 -189 ;68
hi yd 121.5 -189 ;69
hi yd 130.5 -189 ;70
hi yd 139.5 -189 ;71
hi yd 148.5 -189 ;72
hi yd 157.5 -189 ;73
hi yd 166.5 -189 ;74
hi yd 175.5 -189 ;75
hi yd 184.5 -189 ;76
hi yd 193.5 -189 ;77
hi yd 202.5 -189 ;78
hi yd 211.5 -189 ;79
hi yd 220.5 -189 ;80
hi yd 229.5 -189 ;81
hi yd 238.5 -189 ;82
hi yd 247.5 -189 ;83
hi yd 256.5 -189 ;84
hi yd 265.5 -189 ;85
hi yd 274.5 -189 ;86
hi yd 283.5 -189 ;87
hi yd 292.5 -189 ;88
hi yd 301.5 -189 ;89
hi yd 310.5 -189 ;90
hi yd 319.5 -189 ;91
hi yd 328.5 -189 ;92
hi yd 337.5 -189 ;93
```

```
hi yd 346.5 -189 ;94
hi yd 355.5 -189 ;95
hi yd 364.5 -189 ;96
hi yd 373.5 -189 ;97
hi yd 382.5 -189 ;98
hi yd 391.5 -189 ;99
hi yd 400.5 -189 ;100
hi yd 409.5 -189 ;101
hi yd 418.5 -189 ;102
hi yd 427.5 -189 ;103
hi yd 436.5 -189 ;104
hi yd 445.5 -189 ;105
hi yd 454.5 -189 ;106
hi yd 463.5 -189 ;107
hi yd 472.5 -189 ;108
hi yd 481.5 -189 ;109
hi yd 490.5 -189 ;110
hi yd 499.5 -189 ;111
hi yd 508.5 -189 ;112
hi yd 517.5 -189 ;113
hi yd 525.0 -189 ;114

; Creating y-velocities at base and final solving routine

def valleysolve

; Step 1 to obtain time step

command
cyc 1
end_command

; Identifying gridpoints at base to which velocities will be attached

gri_chk1 = gp_near(0.0,-189)
gri_chk2 = gp_near(4.5,-189)
gri_chk3 = gp_near(13.5,-189)
gri_chk4 = gp_near(22.5,-189)
gri_chk5 = gp_near(31.5,-189)
gri_chk6 = gp_near(40.5,-189)
gri_chk7 = gp_near(49.5,-189)
```

```
gri_chk8  = gp_near(58.5,-189)
gri_chk9  = gp_near(67.5,-189)
gri_chk10 = gp_near(76.5,-189)
gri_chk11 = gp_near(85.5,-189)
gri_chk12 = gp_near(94.5,-189)
gri_chk13 = gp_near(103.5,-189)
gri_chk14 = gp_near(112.5,-189)
gri_chk15 = gp_near(121.5,-189)
gri_chk16 = gp_near(130.5,-189)
gri_chk17 = gp_near(139.5,-189)
gri_chk18 = gp_near(148.5,-189)
gri_chk19 = gp_near(157.5,-189)
gri_chk20 = gp_near(166.5,-189)
gri_chk21 = gp_near(175.5,-189)
gri_chk22 = gp_near(184.5,-189)
gri_chk23 = gp_near(193.5,-189)
gri_chk24 = gp_near(202.5,-189)
gri_chk25 = gp_near(211.5,-189)
gri_chk26 = gp_near(220.5,-189)
gri_chk27 = gp_near(229.5,-189)
gri_chk28 = gp_near(238.5,-189)
gri_chk29 = gp_near(247.5,-189)
gri_chk30 = gp_near(256.5,-189)
gri_chk31 = gp_near(265.5,-189)
gri_chk32 = gp_near(274.5,-189)
gri_chk33 = gp_near(283.5,-189)
gri_chk34 = gp_near(292.5,-189)
gri_chk35 = gp_near(301.5,-189)
gri_chk36 = gp_near(310.5,-189)
gri_chk37 = gp_near(319.5,-189)
gri_chk38 = gp_near(328.5,-189)
gri_chk39 = gp_near(337.5,-189)
gri_chk40 = gp_near(346.5,-189)
gri_chk41 = gp_near(355.5,-189)
gri_chk42 = gp_near(364.5,-189)
gri_chk43 = gp_near(373.5,-189)
gri_chk44 = gp_near(382.5,-189)
gri_chk45 = gp_near(391.5,-189)
gri_chk46 = gp_near(400.5,-189)
gri_chk47 = gp_near(409.5,-189)
gri_chk48 = gp_near(418.5,-189)
```

```
gri_chk49 = gp_near(427.5,-189)
gri_chk50 = gp_near(436.5,-189)
gri_chk51 = gp_near(445.5,-189)
gri_chk52 = gp_near(454.5,-189)
gri_chk53 = gp_near(463.5,-189)
gri_chk54 = gp_near(472.5,-189)
gri_chk55 = gp_near(481.5,-189)
gri_chk56 = gp_near(490.5,-189)
gri_chk57 = gp_near(499.5,-189)
gri_chk58 = gp_near(508.5,-189)
gri_chk59 = gp_near(517.5,-189)
gri_chk60 = gp_near(525.0,-189)
gri_chk61 = gp_near(532.5,-189)
gri_chk62 = gp_near(541.5,-189)
gri_chk63 = gp_near(550.5,-189)
gri_chk64 = gp_near(559.5,-189)
gri_chk65 = gp_near(568.5,-189)
gri_chk66 = gp_near(577.5,-189)
gri_chk67 = gp_near(586.5,-189)
gri_chk68 = gp_near(595.5,-189)
gri_chk69 = gp_near(604.5,-189)
gri_chk70 = gp_near(613.5,-189)
gri_chk71 = gp_near(622.5,-189)
gri_chk72 = gp_near(631.5,-189)
gri_chk73 = gp_near(640.5,-189)
gri_chk74 = gp_near(649.5,-189)
gri_chk75 = gp_near(658.5,-189)
gri_chk76 = gp_near(667.5,-189)
gri_chk77 = gp_near(676.5,-189)
gri_chk78 = gp_near(685.5,-189)
gri_chk79 = gp_near(694.5,-189)
gri_chk80 = gp_near(703.5,-189)
gri_chk81 = gp_near(712.5,-189)
gri_chk82 = gp_near(721.5,-189)
gri_chk83 = gp_near(730.5,-189)
gri_chk84 = gp_near(739.5,-189)
gri_chk85 = gp_near(748.5,-189)
gri_chk86 = gp_near(757.5,-189)
gri_chk87 = gp_near(766.5,-189)
gri_chk88 = gp_near(775.5,-189)
gri_chk89 = gp_near(784.5,-189)
```

```
gri_chk90  = gp_near(793.5,-189)
gri_chk91  = gp_near(802.5,-189)
gri_chk92  = gp_near(811.5,-189)
gri_chk93  = gp_near(820.5,-189)
gri_chk94  = gp_near(829.5,-189)
gri_chk95  = gp_near(838.5,-189)
gri_chk96  = gp_near(847.5,-189)
gri_chk97  = gp_near(856.5,-189)
gri_chk98  = gp_near(865.5,-189)
gri_chk99  = gp_near(874.5,-189)
gri_chk100 = gp_near(883.5,-189)
gri_chk101 = gp_near(892.5,-189)
gri_chk102 = gp_near(901.5,-189)
gri_chk103 = gp_near(910.5,-189)
gri_chk104 = gp_near(919.5,-189)
gri_chk105 = gp_near(928.5,-189)
gri_chk106 = gp_near(937.5,-189)
gri_chk107 = gp_near(946.5,-189)
gri_chk108 = gp_near(955.5,-189)
gri_chk109 = gp_near(964.5,-189)
gri_chk110 = gp_near(973.5,-189)
gri_chk111 = gp_near(982.5,-189)
gri_chk112 = gp_near(991.5,-189)
gri_chk113 = gp_near(1000.5,-189)
gri_chk114 = gp_near(1009.5,-189)
gri_chk115 = gp_near(1018.5,-189)
gri_chk116 = gp_near(1027.5,-189)
gri_chk117 = gp_near(1036.5,-189)
gri_chk118 = gp_near(1045.5,-189)
gri_chk119 = gp_near(1050.0,-189)

; Defining y-displacements from Model 4

max_disp1 = 1.398e-03
max_disp2 = 1.394e-03
max_disp3 = 1.372e-03
max_disp4 = 1.331e-03
max_disp5 = 1.270e-03
max_disp6 = 1.188e-03
max_disp7 = 1.086e-03
max_disp8 = 9.621e-04
```

```
max_disp9  =  8.172e-04
max_disp10 =  6.505e-04
max_disp11 =  4.614e-04
max_disp12 =  2.494e-04
max_disp13 =  1.411e-05
max_disp14 = -2.455e-04
max_disp15 = -5.299e-04
max_disp16 = -8.401e-04
max_disp17 = -1.177e-03
max_disp18 = -1.542e-03
max_disp19 = -1.937e-03
max_disp20 = -2.362e-03
max_disp21 = -2.820e-03
max_disp22 = -3.313e-03
max_disp23 = -3.843e-03
max_disp24 = -4.413e-03
max_disp25 = -5.027e-03
max_disp26 = -5.686e-03
max_disp27 = -6.396e-03
max_disp28 = -7.159e-03
max_disp29 = -7.980e-03
max_disp30 = -8.861e-03
max_disp31 = -9.804e-03
max_disp32 = -1.081e-02
max_disp33 = -1.190e-02
max_disp34 = -1.306e-02
max_disp35 = -1.430e-02
max_disp36 = -1.562e-02
max_disp37 = -1.703e-02
max_disp38 = -1.854e-02
max_disp39 = -2.014e-02
max_disp40 = -2.185e-02
max_disp41 = -2.367e-02
max_disp42 = -2.563e-02
max_disp43 = -2.778e-02
max_disp44 = -3.024e-02
max_disp45 = -3.344e-02
max_disp46 = -3.810e-02
max_disp47 = -4.513e-02
max_disp48 = -5.516e-02
max_disp49 = -6.945e-02
```

```
max_disp50 = -9.050e-02
max_disp51 = -1.225e-01
max_disp52 = -1.700e-01
max_disp53 = -2.312e-01
max_disp54 = -2.952e-01
max_disp55 = -3.600e-01
max_disp56 = -4.214e-01
max_disp57 = -4.754e-01
max_disp58 = -5.190e-01
max_disp59 = -5.502e-01
max_disp60 = -2.362e+00
max_disp61 = -5.502e-01
max_disp62 = -5.190e-01
max_disp63 = -4.754e-01
max_disp64 = -4.214e-01
max_disp65 = -3.600e-01
max_disp66 = -2.952e-01
max_disp67 = -2.312e-01
max_disp68 = -1.700e-01
max_disp69 = -1.225e-01
max_disp70 = -9.050e-02
max_disp71 = -6.945e-02
max_disp72 = -5.516e-02
max_disp73 = -4.513e-02
max_disp74 = -3.810e-02
max_disp75 = -3.344e-02
max_disp76 = -3.024e-02
max_disp77 = -2.778e-02
max_disp78 = -2.563e-02
max_disp79 = -2.367e-02
max_disp80 = -2.185e-02
max_disp81 = -2.014e-02
max_disp82 = -1.854e-02
max_disp83 = -1.703e-02
max_disp84 = -1.562e-02
max_disp85 = -1.430e-02
max_disp86 = -1.306e-02
max_disp87 = -1.190e-02
max_disp88 = -1.081e-02
max_disp89 = -9.804e-03
max_disp90 = -8.861e-03
```

```
max_disp91  = -7.980e-03
max_disp92  = -7.159e-03
max_disp93  = -6.396e-03
max_disp94  = -5.686e-03
max_disp95  = -5.027e-03
max_disp96  = -4.413e-03
max_disp97  = -3.843e-03
max_disp98  = -3.313e-03
max_disp99  = -2.820e-03
max_disp100 = -2.362e-03
max_disp101 = -1.937e-03
max_disp102 = -1.542e-03
max_disp103 = -1.177e-03
max_disp104 = -8.401e-04
max_disp105 = -5.299e-04
max_disp106 = -2.455e-04
max_disp107 =  1.411e-05
max_disp108 =  2.494e-04
max_disp109 =  4.614e-04
max_disp110 =  6.505e-04
max_disp111 =  8.172e-04
max_disp112 =  9.621e-04
max_disp113 =  1.086e-03
max_disp114 =  1.188e-03
max_disp115 =  1.270e-03
max_disp116 =  1.331e-03
max_disp117 =  1.372e-03
max_disp118 =  1.394e-03
max_disp119 =  1.398e-03

; Converting y-displacement into y-velocity via timestep and number of
cycles and assigning to corresponding gridpoints

gp_yvel(gri_chk1) = max_disp1/(30000*tdel)
gp_yvel(gri_chk2) = max_disp2/(30000*tdel)
gp_yvel(gri_chk3) = max_disp3/(30000*tdel)
gp_yvel(gri_chk4) = max_disp4/(30000*tdel)
gp_yvel(gri_chk5) = max_disp5/(30000*tdel)
gp_yvel(gri_chk6) = max_disp6/(30000*tdel)
gp_yvel(gri_chk7) = max_disp7/(30000*tdel)
gp_yvel(gri_chk8) = max_disp8/(30000*tdel)
```

```
gp_yvel(gri_chk9)  = max_disp9/(30000*tdel)
gp_yvel(gri_chk10) = max_disp10/(30000*tdel)
gp_yvel(gri_chk11) = max_disp11/(30000*tdel)
gp_yvel(gri_chk12) = max_disp12/(30000*tdel)
gp_yvel(gri_chk13) = max_disp13/(30000*tdel)
gp_yvel(gri_chk14) = max_disp14/(30000*tdel)
gp_yvel(gri_chk15) = max_disp15/(30000*tdel)
gp_yvel(gri_chk16) = max_disp16/(30000*tdel)
gp_yvel(gri_chk17) = max_disp17/(30000*tdel)
gp_yvel(gri_chk18) = max_disp18/(30000*tdel)
gp_yvel(gri_chk19) = max_disp19/(30000*tdel)
gp_yvel(gri_chk20) = max_disp20/(30000*tdel)
gp_yvel(gri_chk21) = max_disp21/(30000*tdel)
gp_yvel(gri_chk22) = max_disp22/(30000*tdel)
gp_yvel(gri_chk23) = max_disp23/(30000*tdel)
gp_yvel(gri_chk24) = max_disp24/(30000*tdel)
gp_yvel(gri_chk25) = max_disp25/(30000*tdel)
gp_yvel(gri_chk26) = max_disp26/(30000*tdel)
gp_yvel(gri_chk27) = max_disp27/(30000*tdel)
gp_yvel(gri_chk28) = max_disp28/(30000*tdel)
gp_yvel(gri_chk29) = max_disp29/(30000*tdel)
gp_yvel(gri_chk30) = max_disp30/(30000*tdel)
gp_yvel(gri_chk31) = max_disp31/(30000*tdel)
gp_yvel(gri_chk32) = max_disp32/(30000*tdel)
gp_yvel(gri_chk33) = max_disp33/(30000*tdel)
gp_yvel(gri_chk34) = max_disp34/(30000*tdel)
gp_yvel(gri_chk35) = max_disp35/(30000*tdel)
gp_yvel(gri_chk36) = max_disp36/(30000*tdel)
gp_yvel(gri_chk37) = max_disp37/(30000*tdel)
gp_yvel(gri_chk38) = max_disp38/(30000*tdel)
gp_yvel(gri_chk39) = max_disp39/(30000*tdel)
gp_yvel(gri_chk40) = max_disp40/(30000*tdel)
gp_yvel(gri_chk41) = max_disp41/(30000*tdel)
gp_yvel(gri_chk42) = max_disp42/(30000*tdel)
gp_yvel(gri_chk43) = max_disp43/(30000*tdel)
gp_yvel(gri_chk44) = max_disp44/(30000*tdel)
gp_yvel(gri_chk45) = max_disp45/(30000*tdel)
gp_yvel(gri_chk46) = max_disp46/(30000*tdel)
gp_yvel(gri_chk47) = max_disp47/(30000*tdel)
gp_yvel(gri_chk48) = max_disp48/(30000*tdel)
gp_yvel(gri_chk49) = max_disp49/(30000*tdel)
```

```
gp_yvel(gri_chk50) = max_disp50/(30000*tdel)
gp_yvel(gri_chk51) = max_disp51/(30000*tdel)
gp_yvel(gri_chk52) = max_disp52/(30000*tdel)
gp_yvel(gri_chk53) = max_disp53/(30000*tdel)
gp_yvel(gri_chk54) = max_disp54/(30000*tdel)
gp_yvel(gri_chk55) = max_disp55/(30000*tdel)
gp_yvel(gri_chk56) = max_disp56/(30000*tdel)
gp_yvel(gri_chk57) = max_disp57/(30000*tdel)
gp_yvel(gri_chk58) = max_disp58/(30000*tdel)
gp_yvel(gri_chk59) = max_disp59/(30000*tdel)
gp_yvel(gri_chk60) = max_disp60/(30000*tdel)
gp_yvel(gri_chk61) = max_disp61/(30000*tdel)
gp_yvel(gri_chk62) = max_disp62/(30000*tdel)
gp_yvel(gri_chk63) = max_disp63/(30000*tdel)
gp_yvel(gri_chk64) = max_disp64/(30000*tdel)
gp_yvel(gri_chk65) = max_disp65/(30000*tdel)
gp_yvel(gri_chk66) = max_disp66/(30000*tdel)
gp_yvel(gri_chk67) = max_disp67/(30000*tdel)
gp_yvel(gri_chk68) = max_disp68/(30000*tdel)
gp_yvel(gri_chk69) = max_disp69/(30000*tdel)
gp_yvel(gri_chk70) = max_disp70/(30000*tdel)
gp_yvel(gri_chk71) = max_disp71/(30000*tdel)
gp_yvel(gri_chk72) = max_disp72/(30000*tdel)
gp_yvel(gri_chk73) = max_disp73/(30000*tdel)
gp_yvel(gri_chk74) = max_disp74/(30000*tdel)
gp_yvel(gri_chk75) = max_disp75/(30000*tdel)
gp_yvel(gri_chk76) = max_disp76/(30000*tdel)
gp_yvel(gri_chk77) = max_disp77/(30000*tdel)
gp_yvel(gri_chk78) = max_disp78/(30000*tdel)
gp_yvel(gri_chk79) = max_disp79/(30000*tdel)
gp_yvel(gri_chk80) = max_disp80/(30000*tdel)
gp_yvel(gri_chk81) = max_disp81/(30000*tdel)
gp_yvel(gri_chk82) = max_disp82/(30000*tdel)
gp_yvel(gri_chk83) = max_disp83/(30000*tdel)
gp_yvel(gri_chk84) = max_disp84/(30000*tdel)
gp_yvel(gri_chk85) = max_disp85/(30000*tdel)
gp_yvel(gri_chk86) = max_disp86/(30000*tdel)
gp_yvel(gri_chk87) = max_disp87/(30000*tdel)
gp_yvel(gri_chk88) = max_disp88/(30000*tdel)
gp_yvel(gri_chk89) = max_disp89/(30000*tdel)
gp_yvel(gri_chk90) = max_disp90/(30000*tdel)
```

```
gp_yvel(gri_chk91)  = max_disp91/(30000*tdel)
gp_yvel(gri_chk92)  = max_disp92/(30000*tdel)
gp_yvel(gri_chk93)  = max_disp93/(30000*tdel)
gp_yvel(gri_chk94)  = max_disp94/(30000*tdel)
gp_yvel(gri_chk95)  = max_disp95/(30000*tdel)
gp_yvel(gri_chk96)  = max_disp96/(30000*tdel)
gp_yvel(gri_chk97)  = max_disp97/(30000*tdel)
gp_yvel(gri_chk98)  = max_disp98/(30000*tdel)
gp_yvel(gri_chk99)  = max_disp99/(30000*tdel)
gp_yvel(gri_chk100) = max_disp100/(30000*tdel)
gp_yvel(gri_chk101) = max_disp101/(30000*tdel)
gp_yvel(gri_chk102) = max_disp102/(30000*tdel)
gp_yvel(gri_chk103) = max_disp103/(30000*tdel)
gp_yvel(gri_chk104) = max_disp104/(30000*tdel)
gp_yvel(gri_chk105) = max_disp105/(30000*tdel)
gp_yvel(gri_chk106) = max_disp106/(30000*tdel)
gp_yvel(gri_chk107) = max_disp107/(30000*tdel)
gp_yvel(gri_chk108) = max_disp108/(30000*tdel)
gp_yvel(gri_chk109) = max_disp109/(30000*tdel)
gp_yvel(gri_chk110) = max_disp110/(30000*tdel)
gp_yvel(gri_chk111) = max_disp111/(30000*tdel)
gp_yvel(gri_chk112) = max_disp112/(30000*tdel)
gp_yvel(gri_chk113) = max_disp113/(30000*tdel)
gp_yvel(gri_chk114) = max_disp114/(30000*tdel)
gp_yvel(gri_chk115) = max_disp115/(30000*tdel)
gp_yvel(gri_chk116) = max_disp116/(30000*tdel)
gp_yvel(gri_chk117) = max_disp117/(30000*tdel)
gp_yvel(gri_chk118) = max_disp118/(30000*tdel)
gp_yvel(gri_chk119) = max_disp119/(30000*tdel)
temp1  = gp_yvel(gri_chk1)
temp2  = gp_yvel(gri_chk2)
temp3  = gp_yvel(gri_chk3)
temp4  = gp_yvel(gri_chk4)
temp5  = gp_yvel(gri_chk5)
temp6  = gp_yvel(gri_chk6)
temp7  = gp_yvel(gri_chk7)
temp8  = gp_yvel(gri_chk8)
temp9  = gp_yvel(gri_chk9)
temp10 = gp_yvel(gri_chk10)
temp11 = gp_yvel(gri_chk11)
temp12 = gp_yvel(gri_chk12)
```

```
temp13 = gp_yvel(gri_chk13)
temp14 = gp_yvel(gri_chk14)
temp15 = gp_yvel(gri_chk15)
temp16 = gp_yvel(gri_chk16)
temp17 = gp_yvel(gri_chk17)
temp18 = gp_yvel(gri_chk18)
temp19 = gp_yvel(gri_chk19)
temp20 = gp_yvel(gri_chk20)
temp21 = gp_yvel(gri_chk21)
temp22 = gp_yvel(gri_chk22)
temp23 = gp_yvel(gri_chk23)
temp24 = gp_yvel(gri_chk24)
temp25 = gp_yvel(gri_chk25)
temp26 = gp_yvel(gri_chk26)
temp27 = gp_yvel(gri_chk27)
temp28 = gp_yvel(gri_chk28)
temp29 = gp_yvel(gri_chk29)
temp30 = gp_yvel(gri_chk30)
temp31 = gp_yvel(gri_chk31)
temp32 = gp_yvel(gri_chk32)
temp33 = gp_yvel(gri_chk33)
temp34 = gp_yvel(gri_chk34)
temp35 = gp_yvel(gri_chk35)
temp36 = gp_yvel(gri_chk36)
temp37 = gp_yvel(gri_chk37)
temp38 = gp_yvel(gri_chk38)
temp39 = gp_yvel(gri_chk39)
temp40 = gp_yvel(gri_chk40)
temp41 = gp_yvel(gri_chk41)
temp42 = gp_yvel(gri_chk42)
temp43 = gp_yvel(gri_chk43)
temp44 = gp_yvel(gri_chk44)
temp45 = gp_yvel(gri_chk45)
temp46 = gp_yvel(gri_chk46)
temp47 = gp_yvel(gri_chk47)
temp48 = gp_yvel(gri_chk48)
temp49 = gp_yvel(gri_chk49)
temp50 = gp_yvel(gri_chk50)
temp51 = gp_yvel(gri_chk51)
temp52 = gp_yvel(gri_chk52)
temp53 = gp_yvel(gri_chk53)
```

```
temp54 = gp_yvel(gri_chk54)
temp55 = gp_yvel(gri_chk55)
temp56 = gp_yvel(gri_chk56)
temp57 = gp_yvel(gri_chk57)
temp58 = gp_yvel(gri_chk58)
temp59 = gp_yvel(gri_chk59)
temp60 = gp_yvel(gri_chk60)
temp61 = gp_yvel(gri_chk61)
temp62 = gp_yvel(gri_chk62)
temp63 = gp_yvel(gri_chk63)
temp64 = gp_yvel(gri_chk64)
temp65 = gp_yvel(gri_chk65)
temp66 = gp_yvel(gri_chk66)
temp67 = gp_yvel(gri_chk67)
temp68 = gp_yvel(gri_chk68)
temp69 = gp_yvel(gri_chk69)
temp70 = gp_yvel(gri_chk70)
temp71 = gp_yvel(gri_chk71)
temp72 = gp_yvel(gri_chk72)
temp73 = gp_yvel(gri_chk73)
temp74 = gp_yvel(gri_chk74)
temp75 = gp_yvel(gri_chk75)
temp76 = gp_yvel(gri_chk76)
temp77 = gp_yvel(gri_chk77)
temp78 = gp_yvel(gri_chk78)
temp79 = gp_yvel(gri_chk79)
temp80 = gp_yvel(gri_chk80)
temp81 = gp_yvel(gri_chk81)
temp82 = gp_yvel(gri_chk82)
temp83 = gp_yvel(gri_chk83)
temp84 = gp_yvel(gri_chk84)
temp85 = gp_yvel(gri_chk85)
temp86 = gp_yvel(gri_chk86)
temp87 = gp_yvel(gri_chk87)
temp88 = gp_yvel(gri_chk88)
temp89 = gp_yvel(gri_chk89)
temp90 = gp_yvel(gri_chk90)
temp91 = gp_yvel(gri_chk91)
temp92 = gp_yvel(gri_chk92)
temp93 = gp_yvel(gri_chk93)
temp94 = gp_yvel(gri_chk94)
```

```
temp95  = gp_yvel(gri_chk95)
temp96  = gp_yvel(gri_chk96)
temp97  = gp_yvel(gri_chk97)
temp98  = gp_yvel(gri_chk98)
temp99  = gp_yvel(gri_chk99)
temp100 = gp_yvel(gri_chk100)
temp101 = gp_yvel(gri_chk101)
temp102 = gp_yvel(gri_chk102)
temp103 = gp_yvel(gri_chk103)
temp104 = gp_yvel(gri_chk104)
temp105 = gp_yvel(gri_chk105)
temp106 = gp_yvel(gri_chk106)
temp107 = gp_yvel(gri_chk107)
temp108 = gp_yvel(gri_chk108)
temp109 = gp_yvel(gri_chk109)
temp110 = gp_yvel(gri_chk110)
temp111 = gp_yvel(gri_chk111)
temp112 = gp_yvel(gri_chk112)
temp113 = gp_yvel(gri_chk113)
temp114 = gp_yvel(gri_chk114)
temp115 = gp_yvel(gri_chk115)
temp116 = gp_yvel(gri_chk116)
temp117 = gp_yvel(gri_chk117)
temp118 = gp_yvel(gri_chk118)
temp119 = gp_yvel(gri_chk119)
end

valleysolve

; Assigning y-velocities to base

bo yv temp1  ra -0.1  0.1 -189.1 -188.9
bo yv temp2  ra  4.4  4.6 -189.1 -188.9
bo yv temp3  ra 13.4 13.6 -189.1 -188.9
bo yv temp4  ra 22.4 22.6 -189.1 -188.9
bo yv temp5  ra 31.4 31.6 -189.1 -188.9
bo yv temp6  ra 40.4 40.6 -189.1 -188.9
bo yv temp7  ra 49.4 49.6 -189.1 -188.9
bo yv temp8  ra 58.4 58.6 -189.1 -188.9
bo yv temp9  ra 67.4 67.6 -189.1 -188.9
bo yv temp10 ra 76.4 76.6 -189.1 -188.9
```

```
bo yv temp11 ra  85.4  85.6 -189.1 -188.9
bo yv temp12 ra  94.4  94.6 -189.1 -188.9
bo yv temp13 ra 103.4 103.6 -189.1 -188.9
bo yv temp14 ra 112.4 112.6 -189.1 -188.9
bo yv temp15 ra 121.4 121.6 -189.1 -188.9
bo yv temp16 ra 130.4 130.6 -189.1 -188.9
bo yv temp17 ra 139.4 139.6 -189.1 -188.9
bo yv temp18 ra 148.4 148.6 -189.1 -188.9
bo yv temp19 ra 157.4 157.6 -189.1 -188.9
bo yv temp20 ra 166.4 166.6 -189.1 -188.9
bo yv temp21 ra 175.4 175.6 -189.1 -188.9
bo yv temp22 ra 184.4 184.6 -189.1 -188.9
bo yv temp23 ra 193.4 193.6 -189.1 -188.9
bo yv temp24 ra 202.4 202.6 -189.1 -188.9
bo yv temp25 ra 211.4 211.6 -189.1 -188.9
bo yv temp26 ra 220.4 220.6 -189.1 -188.9
bo yv temp27 ra 229.4 229.6 -189.1 -188.9
bo yv temp28 ra 238.4 238.6 -189.1 -188.9
bo yv temp29 ra 247.4 247.6 -189.1 -188.9
bo yv temp30 ra 256.4 256.6 -189.1 -188.9
bo yv temp31 ra 265.4 265.6 -189.1 -188.9
bo yv temp32 ra 274.4 274.6 -189.1 -188.9
bo yv temp33 ra 283.4 283.6 -189.1 -188.9
bo yv temp34 ra 292.4 292.6 -189.1 -188.9
bo yv temp35 ra 301.4 301.6 -189.1 -188.9
bo yv temp36 ra 310.4 310.6 -189.1 -188.9
bo yv temp37 ra 319.4 319.6 -189.1 -188.9
bo yv temp38 ra 328.4 328.6 -189.1 -188.9
bo yv temp39 ra 337.4 337.6 -189.1 -188.9
bo yv temp40 ra 346.4 346.6 -189.1 -188.9
bo yv temp41 ra 355.4 355.6 -189.1 -188.9
bo yv temp42 ra 364.4 364.6 -189.1 -188.9
bo yv temp43 ra 373.4 373.6 -189.1 -188.9
bo yv temp44 ra 382.4 382.6 -189.1 -188.9
bo yv temp45 ra 391.4 391.6 -189.1 -188.9
bo yv temp46 ra 400.4 400.6 -189.1 -188.9
bo yv temp47 ra 409.4 409.6 -189.1 -188.9
bo yv temp48 ra 418.4 418.6 -189.1 -188.9
bo yv temp49 ra 427.4 427.6 -189.1 -188.9
bo yv temp50 ra 436.4 436.6 -189.1 -188.9
bo yv temp51 ra 445.4 445.6 -189.1 -188.9
```

```
bo yv temp52 ra 454.4 454.6 -189.1 -188.9
bo yv temp53 ra 463.4 463.6 -189.1 -188.9
bo yv temp54 ra 472.4 472.6 -189.1 -188.9
bo yv temp55 ra 481.4 481.6 -189.1 -188.9
bo yv temp56 ra 490.4 490.6 -189.1 -188.9
bo yv temp57 ra 499.4 499.6 -189.1 -188.9
bo yv temp58 ra 508.4 508.6 -189.1 -188.9
bo yv temp59 ra 517.4 517.6 -189.1 -188.9
bo yv temp60 ra 524.9 525.1 -189.1 -188.9
bo yv temp61 ra 532.4 532.6 -189.1 -188.9
bo yv temp62 ra 541.4 541.6 -189.1 -188.9
bo yv temp63 ra 550.4 550.6 -189.1 -188.9
bo yv temp64 ra 559.4 559.6 -189.1 -188.9
bo yv temp65 ra 568.4 568.6 -189.1 -188.9
bo yv temp66 ra 577.4 577.6 -189.1 -188.9
bo yv temp67 ra 586.4 586.6 -189.1 -188.9
bo yv temp68 ra 595.4 595.6 -189.1 -188.9
bo yv temp69 ra 604.4 604.6 -189.1 -188.9
bo yv temp70 ra 613.4 613.6 -189.1 -188.9
bo yv temp71 ra 622.4 622.6 -189.1 -188.9
bo yv temp72 ra 631.4 631.6 -189.1 -188.9
bo yv temp73 ra 640.4 640.6 -189.1 -188.9
bo yv temp74 ra 649.4 649.6 -189.1 -188.9
bo yv temp75 ra 658.4 658.6 -189.1 -188.9
bo yv temp76 ra 667.4 667.6 -189.1 -188.9
bo yv temp77 ra 676.4 676.6 -189.1 -188.9
bo yv temp78 ra 685.4 685.6 -189.1 -188.9
bo yv temp79 ra 694.4 694.6 -189.1 -188.9
bo yv temp80 ra 703.4 703.6 -189.1 -188.9
bo yv temp81 ra 712.4 712.6 -189.1 -188.9
bo yv temp82 ra 721.4 721.6 -189.1 -188.9
bo yv temp83 ra 730.4 730.6 -189.1 -188.9
bo yv temp84 ra 739.4 739.6 -189.1 -188.9
bo yv temp85 ra 748.4 748.6 -189.1 -188.9
bo yv temp86 ra 757.4 757.6 -189.1 -188.9
bo yv temp87 ra 766.4 766.6 -189.1 -188.9
bo yv temp88 ra 775.4 775.6 -189.1 -188.9
bo yv temp89 ra 784.4 784.6 -189.1 -188.9
bo yv temp90 ra 793.4 793.6 -189.1 -188.9
bo yv temp91 ra 802.4 802.6 -189.1 -188.9
bo yv temp92 ra 811.4 811.6 -189.1 -188.9
```

```
bo yv temp93  ra  820.4  820.6 -189.1 -188.9
bo yv temp94  ra  829.4  829.6 -189.1 -188.9
bo yv temp95  ra  838.4  838.6 -189.1 -188.9
bo yv temp96  ra  847.4  847.6 -189.1 -188.9
bo yv temp97  ra  856.4  856.6 -189.1 -188.9
bo yv temp98  ra  865.4  865.6 -189.1 -188.9
bo yv temp99  ra  874.4  874.6 -189.1 -188.9
bo yv temp100 ra  883.4  883.6 -189.1 -188.9
bo yv temp101 ra  892.4  892.6 -189.1 -188.9
bo yv temp102 ra  901.4  901.6 -189.1 -188.9
bo yv temp103 ra  910.4  910.6 -189.1 -188.9
bo yv temp104 ra  919.4  919.6 -189.1 -188.9
bo yv temp105 ra  928.4  928.6 -189.1 -188.9
bo yv temp106 ra  937.4  937.6 -189.1 -188.9
bo yv temp107 ra  946.4  946.6 -189.1 -188.9
bo yv temp108 ra  955.4  955.6 -189.1 -188.9
bo yv temp109 ra  964.4  964.6 -189.1 -188.9
bo yv temp110 ra  973.4  973.6 -189.1 -188.9
bo yv temp111 ra  982.4  982.6 -189.1 -188.9
bo yv temp112 ra  991.4  991.6 -189.1 -188.9
bo yv temp113 ra 1000.4 1000.6 -189.1 -188.9
bo yv temp114 ra 1009.4 1009.6 -189.1 -188.9
bo yv temp115 ra 1018.4 1018.6 -189.1 -188.9
bo yv temp116 ra 1027.4 1027.6 -189.1 -188.9
bo yv temp117 ra 1036.4 1036.6 -189.1 -188.9
bo yv temp118 ra 1045.4 1045.6 -189.1 -188.9
bo yv temp119 ra 1049.9 1050.9 -189.1 -188.9

s 30000

; Resetting boundary conditions

bo yfr
bo xfr
bo yv 0 ra 0 1050 -200 -188.9
bo xv 0 ra -0.1 0.1 -189.1 0.1
bo xv 0 ra 1049.9 1050.1 -189.1 0.1
```

```
; Solving for final equilibrium

da a

so rat 1e-5 ste 1000000

sa valley1_ini2.sav

s 20000

sa valley1_final.sav
```

APPENDIX D
RIVER VALLEY MODEL WITH PLANE BELOW BASE

```
ti
Valley 1

; Creating model geometry

ro = 0.01
set ov = 0.2

bl 0,-189 0,0 1050,0 1050,-189
cr 0,-78   1050,-78    ; Hawkesbury Sandstone (78 m thick)
cr 0,-85   1050,-85    ; Newport Formation (7 m thick)
cr 0,-97   1050,-97    ; Bald Hill Claystone (9 m thick)
cr 0,-186  1050,-186   ; Bulgo Sandstone (89 m thick + 3 m thick beam)

; Generating vertical cracks for beam at base of Bald Hill Claystone

jr 0,-189 0,-186 525,-186 525,-189
js 90,0 3,0 0,0 9,0 13.5,-189
cr 525,-189 525,-186
cr 532.5,-189 532.5,-186

jr 532.5,-189 532.5,-186 1050,-186 1050,-189
js 90,0 3,0 0,0 9,0 1045.5,-189

; Generating pre-defined cracks for valleys (70 m deep x 50 m wide)

cr   0,-70  1050,-70
cr   0,-71  1050,-71 ; New translation plane 1 m below base of valley
cr 500,-70   500,0
cr 450,-70   450,0
cr 400,-70   400,0
cr 350,-70   350,0
cr 300,-70   300,0
cr 250,-70   250,0
```

```
cr  200,-70  200,0
cr  150,-70  150,0
cr  100,-70  100,0
cr   50,-70   50,0
cr  550,-70  550,0
cr  600,-70  600,0
cr  650,-70  650,0
cr  700,-70  700,0
cr  750,-70  750,0
cr  800,-70  800,0
cr  850,-70  850,0
cr  900,-70  900,0
cr  950,-70  950,0
cr 1000,-70 1000,0

; Defining discontinuities

jr 0,-78 0,-71 1050,-71 1050,-78            ; Hawkesbury Sandstone
js 90,0 9,0 9,0 9,0 4.5 -78

jr 0,-85 0,-78 1050,-78 1050,-85            ; Newport Formation
js 0,0 1050,0 0,0 1,0
js 90,0 1,0 1,0 1,0
js 90,0 1,0 1,0 1,0 0.5,-79

jr 0,-97 0,-85 1050,-85 1050,-97            ; Bald Hill Claystone
js 0,0 1050,0 0,0 1,0
js 90,0 1,0 1,0 1,0
js 90,0 1,0 1,0 1,0 0.5,-87

jr 0,-186 0,-97 1050,-97 1050,-186          ; Bulgo Sandstone
js 0,0 525,0 0,0 9,0
js 90,0 9,0 9,0 9,0
js 90,0 9,0 9,0 9,0 4.5,-117
jr 0,-189 0,-186 525,-186 525,-189
js 90,0 3,0 0,0 9,0 13.5,-189
cr 525,-189 525,-186
cr 532.5,-189 532.5,-186
jr 532.5,-189 532.5,-186 1050,-186 1050,-189
js 90,0 3,0 0,0 9,0 1045.5,-189
```

```
; Generating zones for deformable blocks

ge q 12.7 ra 0 1050 -70    0 ; Hawkesbury Sandstone
ge q 0.2  ra 0 1050 -71  -70 ; Beam
ge q 12.7 ra 0 1050 -78  -71 ; Hawkesbury Sandstone
ge q 1.4  ra 0 1050 -85  -78 ; Newport Formation
ge q 1.4  ra 0 1050 -97  -85 ; Bald Hill Claystone
ge q 12.7 ra 0 1050 -189 -97 ; Bulgo Sandstone

; Defining material properties

pro m 1  de = 2397 b = 11.47e9 sh = 5.65e9 coh = 9.70e6  fr= 37.25 &
         ten = 3.58e6 ; Hawkesbury Sandstone

pro m 2  de = 2290 b = 7.77e9  sh = 4.66e9 coh = 8.85e6  fr= 35.00 &
         ten = 3.40e6 ; Newport Formation

pro m 3  de = 2719 b = 14.12e9 sh = 4.72e9 coh = 10.60e6 fr= 27.80 &
         ten = 2.90e6 ; Bald Hill Claystone

pro m 4  de = 2527 b = 12.60e9 sh = 7.91e9 coh = 17.72e6 fr= 35.40 &
         ten = 6.55e6 ; Bulgo Sandstone

; Assigning material properties

ch cons 3

ch m 1  ra 0 1050 -78 0    ; Hawkesbury Sandstone
ch m 2  ra 0 1050 -85 -78  ; Newport Formation
ch m 3  ra 0 1050 -97 -85  ; Bald Hill Claystone
ch m 4  ra 0 1050 -189 -97 ; Bulgo Sandstone

; Defining bedding plane properties

pro jm = 1 jkn = 21e9   jks   = 2.1e9  & ; Hawkesbury Sandstone
           jf  = 25     jrf   = 15     &
           jc  = 0.29e6 jresc = 0

pro jm = 2 jkn = 140e9  jks   = 14.0e9 & ; Newport Formation
           jf  = 25     jrf   = 15     &
           jc  = 0.29e6 jresc = 0
```

```
pro jm = 3 jkn = 204e9  jks   = 20.4e9 & ; Bald Hill Claystone
           jf  = 25     jrf   = 15     &
           jc  = 0.29e6 jresc = 0

pro jm = 4 jkn = 26e9   jks   = 2.6e9  & ; Bulgo Sandstone
           jf  = 25     jrf   = 15     &
           jc  = 0.29e6 jresc = 0

pro jm = 5 jkn = 204e9 jks   = 20.4e9 & ; Beam
           jf  = 89    jrf   = 89     &
           jc  = 1e10  jresc = 1e10   &
           jt  = 1e10  jrt   = 1e10

; Assigning bedding plane properties

ch jc = 5 ra 0 1050 -189 0 ang -1 1
se jc = 5

ch jm 1 ra 0 1050 -78 0     ang -1 1 ; Hawkesbury Sandstone
ch jm 2 ra 0 1050 -85 -78   ang -1 1 ; Newport Formation
ch jm 3 ra 0 1050 -97 -85   ang -1 1 ; Bald Hill Claystone
ch jm 4 ra 0 1050 -186 -97  ang -1 1 ; Bulgo Sandstone
ch jm 5 ra 0 1050 -189 -186 ang -1 1 ; Beam

; Vertical joint properties

pro jm = 6  jkn = 21e9  jks    = 2.1e9  & ; Hawkesbury Sandstone
            jf  = 19     jrf   = 15     &
            jc  = 0.86e6 jresc = 0

pro jm = 7  jkn = 140e9  jks   = 14.0e9 & ; Newport Formation
            jf  = 19     jrf   = 15     &
            jc  = 0.86e6 jresc = 0

pro jm = 8  jkn = 204e9  jks   = 20.4e9 & ; Bald Hill Claystone
            jf  = 19     jrf   = 15     &
            jc  = 0.86e6 jresc = 0

pro jm = 9  jkn = 26e9   jks   = 2.6e9 & ; Bulgo Sandstone;
            jf  = 19     jrf   = 15    &
            jc  = 0.86e6 jresc = 0
```

```
pro jm = 10 jkn = 204e9 jks   = 20.4e9 & ; Beam
            jf  = 89    jrf   = 89     &
            jc  = 1e10  jresc = 1e10   &
            jt  = 1e10  jrt   = 1e10

; Assigning vertical joint properties

ch jc = 5 ra 0 1050 -189 0 ang 89 91
se jc = 5

ch jm 6  ra 0 1050 -186    0  ang 89 91 ; Hawkesbury Sandstone
ch jm 7  ra 0 1050 -85   -78  ang 89 91 ; Newport Formation
ch jm 8  ra 0 1050 -97   -85  ang 89 91 ; Bald Hill Claystone
ch jm 9  ra 0 1050 -186  -97  ang 89 91 ; Bulgo Sandstone
ch jm 10 ra 0 1050 -189 -186  ang 89 91 ; Beam

; Defining gravity

se gr 0 -9.81

; Defining boundary conditions

bo yv 0 ra 0 1050 -189.1 -188.9
bo xv 0 ra -0.1 0.1 -189.1 0.1
bo xv 0 ra 1049.9 1050.1 -189.1 0.1

; Defining initial stress conditions

in st 0 0 0 yg 4.77e4 0 2.39e4 szz 0 zg 0 4.77e4 ra 0 1050 -189 0

sa valley1_ini1.sav

; Cycle to equilibrium

da a

so
```

```
; Removing valley and cycle to equilibrium

de ra 500 550 -70 0

da a

so

; Removing boundary conditions at base and attaching pre-determined y-displacements

rese vel
rese di

bo yfr
bo xfr
bo xv 0 ra -0.1 0.1 -189.1 0.1
bo xv 0 ra 1049.9 1050.1 -189.1 0.1

; Histories

; X Displacements (valley closure)
; Top of valley

hi xd 50  0 ;1
hi xd 100 0 ;2
hi xd 150 0 ;3
hi xd 200 0 ;4
hi xd 250 0 ;5
hi xd 300 0 ;6
hi xd 350 0 ;7
hi xd 400 0 ;8
hi xd 450 0 ;9
hi xd 500 0 ;10
hi xd 550 0 ;11

; Y Displacements (subsidence)

hi yd 0  0 ;12
hi yd 25 0 ;13
hi yd 50 0 ;14
```

```
hi yd 75   0 ;15
hi yd 100  0 ;16
hi yd 125  0 ;17
hi yd 150  0 ;18
hi yd 175  0 ;19
hi yd 200  0 ;20
hi yd 225  0 ;21
hi yd 250  0 ;22
hi yd 275  0 ;23
hi yd 300  0 ;24
hi yd 325  0 ;25
hi yd 350  0 ;26
hi yd 375  0 ;27
hi yd 400  0 ;28
hi yd 425  0 ;29
hi yd 450  0 ;30
hi yd 475  0 ;31
hi yd 500  0 ;32
hi yd 525  0 ;33
hi yd 550  0 ;34
hi yd 575  0 ;35
hi yd 600  0 ;36
hi yd 625  0 ;37
hi yd 650  0 ;38
hi yd 675  0 ;39
hi yd 700  0 ;40
hi yd 725  0 ;41
hi yd 750  0 ;42
hi yd 775  0 ;43
hi yd 800  0 ;44
hi yd 825  0 ;45
hi yd 850  0 ;46
hi yd 875  0 ;47
hi yd 900  0 ;48
hi yd 925  0 ;49
hi yd 950  0 ;50
hi yd 975  0 ;51
hi yd 1000 0 ;52
hi yd 1025 0 ;53
hi yd 1050 0 ;54
```

```
; Y displacements (base)

hi yd 0     -189 ;55
hi yd 4.5   -189 ;56
hi yd 13.5  -189 ;57
hi yd 22.5  -189 ;58
hi yd 31.5  -189 ;59
hi yd 40.5  -189 ;60
hi yd 49.5  -189 ;61
hi yd 58.5  -189 ;62
hi yd 67.5  -189 ;63
hi yd 76.5  -189 ;64
hi yd 85.5  -189 ;65
hi yd 94.5  -189 ;66
hi yd 103.5 -189 ;67
hi yd 112.5 -189 ;68
hi yd 121.5 -189 ;69
hi yd 130.5 -189 ;70
hi yd 139.5 -189 ;71
hi yd 148.5 -189 ;72
hi yd 157.5 -189 ;73
hi yd 166.5 -189 ;74
hi yd 175.5 -189 ;75
hi yd 184.5 -189 ;76
hi yd 193.5 -189 ;77
hi yd 202.5 -189 ;78
hi yd 211.5 -189 ;79
hi yd 220.5 -189 ;80
hi yd 229.5 -189 ;81
hi yd 238.5 -189 ;82
hi yd 247.5 -189 ;83
hi yd 256.5 -189 ;84
hi yd 265.5 -189 ;85
hi yd 274.5 -189 ;86
hi yd 283.5 -189 ;87
hi yd 292.5 -189 ;88
hi yd 301.5 -189 ;89
hi yd 310.5 -189 ;90
hi yd 319.5 -189 ;91
hi yd 328.5 -189 ;92
hi yd 337.5 -189 ;93
```

```
hi yd 346.5 -189 ;94
hi yd 355.5 -189 ;95
hi yd 364.5 -189 ;96
hi yd 373.5 -189 ;97
hi yd 382.5 -189 ;98
hi yd 391.5 -189 ;99
hi yd 400.5 -189 ;100
hi yd 409.5 -189 ;101
hi yd 418.5 -189 ;102
hi yd 427.5 -189 ;103
hi yd 436.5 -189 ;104
hi yd 445.5 -189 ;105
hi yd 454.5 -189 ;106
hi yd 463.5 -189 ;107
hi yd 472.5 -189 ;108
hi yd 481.5 -189 ;109
hi yd 490.5 -189 ;110
hi yd 499.5 -189 ;111
hi yd 508.5 -189 ;112
hi yd 517.5 -189 ;113
hi yd 525.0 -189 ;114

; Creating y-velocities at base and final solving routine

def valleysolve

; Step 1 to obtain time step

command
cyc 1
end_command

; Identifying gridpoints at base to which velocities will be attached

gri_chk1 = gp_near(0.0,-189)
gri_chk2 = gp_near(4.5,-189)
gri_chk3 = gp_near(13.5,-189)
gri_chk4 = gp_near(22.5,-189)
gri_chk5 = gp_near(31.5,-189)
gri_chk6 = gp_near(40.5,-189)
gri_chk7 = gp_near(49.5,-189)
```

```
gri_chk8  = gp_near(58.5,-189)
gri_chk9  = gp_near(67.5,-189)
gri_chk10 = gp_near(76.5,-189)
gri_chk11 = gp_near(85.5,-189)
gri_chk12 = gp_near(94.5,-189)
gri_chk13 = gp_near(103.5,-189)
gri_chk14 = gp_near(112.5,-189)
gri_chk15 = gp_near(121.5,-189)
gri_chk16 = gp_near(130.5,-189)
gri_chk17 = gp_near(139.5,-189)
gri_chk18 = gp_near(148.5,-189)
gri_chk19 = gp_near(157.5,-189)
gri_chk20 = gp_near(166.5,-189)
gri_chk21 = gp_near(175.5,-189)
gri_chk22 = gp_near(184.5,-189)
gri_chk23 = gp_near(193.5,-189)
gri_chk24 = gp_near(202.5,-189)
gri_chk25 = gp_near(211.5,-189)
gri_chk26 = gp_near(220.5,-189)
gri_chk27 = gp_near(229.5,-189)
gri_chk28 = gp_near(238.5,-189)
gri_chk29 = gp_near(247.5,-189)
gri_chk30 = gp_near(256.5,-189)
gri_chk31 = gp_near(265.5,-189)
gri_chk32 = gp_near(274.5,-189)
gri_chk33 = gp_near(283.5,-189)
gri_chk34 = gp_near(292.5,-189)
gri_chk35 = gp_near(301.5,-189)
gri_chk36 = gp_near(310.5,-189)
gri_chk37 = gp_near(319.5,-189)
gri_chk38 = gp_near(328.5,-189)
gri_chk39 = gp_near(337.5,-189)
gri_chk40 = gp_near(346.5,-189)
gri_chk41 = gp_near(355.5,-189)
gri_chk42 = gp_near(364.5,-189)
gri_chk43 = gp_near(373.5,-189)
gri_chk44 = gp_near(382.5,-189)
gri_chk45 = gp_near(391.5,-189)
gri_chk46 = gp_near(400.5,-189)
gri_chk47 = gp_near(409.5,-189)
gri_chk48 = gp_near(418.5,-189)
```

```
gri_chk49 = gp_near(427.5,-189)
gri_chk50 = gp_near(436.5,-189)
gri_chk51 = gp_near(445.5,-189)
gri_chk52 = gp_near(454.5,-189)
gri_chk53 = gp_near(463.5,-189)
gri_chk54 = gp_near(472.5,-189)
gri_chk55 = gp_near(481.5,-189)
gri_chk56 = gp_near(490.5,-189)
gri_chk57 = gp_near(499.5,-189)
gri_chk58 = gp_near(508.5,-189)
gri_chk59 = gp_near(517.5,-189)
gri_chk60 = gp_near(525.0,-189)
gri_chk61 = gp_near(532.5,-189)
gri_chk62 = gp_near(541.5,-189)
gri_chk63 = gp_near(550.5,-189)
gri_chk64 = gp_near(559.5,-189)
gri_chk65 = gp_near(568.5,-189)
gri_chk66 = gp_near(577.5,-189)
gri_chk67 = gp_near(586.5,-189)
gri_chk68 = gp_near(595.5,-189)
gri_chk69 = gp_near(604.5,-189)
gri_chk70 = gp_near(613.5,-189)
gri_chk71 = gp_near(622.5,-189)
gri_chk72 = gp_near(631.5,-189)
gri_chk73 = gp_near(640.5,-189)
gri_chk74 = gp_near(649.5,-189)
gri_chk75 = gp_near(658.5,-189)
gri_chk76 = gp_near(667.5,-189)
gri_chk77 = gp_near(676.5,-189)
gri_chk78 = gp_near(685.5,-189)
gri_chk79 = gp_near(694.5,-189)
gri_chk80 = gp_near(703.5,-189)
gri_chk81 = gp_near(712.5,-189)
gri_chk82 = gp_near(721.5,-189)
gri_chk83 = gp_near(730.5,-189)
gri_chk84 = gp_near(739.5,-189)
gri_chk85 = gp_near(748.5,-189)
gri_chk86 = gp_near(757.5,-189)
gri_chk87 = gp_near(766.5,-189)
gri_chk88 = gp_near(775.5,-189)
gri_chk89 = gp_near(784.5,-189)
```

```
gri_chk90  = gp_near(793.5,-189)
gri_chk91  = gp_near(802.5,-189)
gri_chk92  = gp_near(811.5,-189)
gri_chk93  = gp_near(820.5,-189)
gri_chk94  = gp_near(829.5,-189)
gri_chk95  = gp_near(838.5,-189)
gri_chk96  = gp_near(847.5,-189)
gri_chk97  = gp_near(856.5,-189)
gri_chk98  = gp_near(865.5,-189)
gri_chk99  = gp_near(874.5,-189)
gri_chk100 = gp_near(883.5,-189)
gri_chk101 = gp_near(892.5,-189)
gri_chk102 = gp_near(901.5,-189)
gri_chk103 = gp_near(910.5,-189)
gri_chk104 = gp_near(919.5,-189)
gri_chk105 = gp_near(928.5,-189)
gri_chk106 = gp_near(937.5,-189)
gri_chk107 = gp_near(946.5,-189)
gri_chk108 = gp_near(955.5,-189)
gri_chk109 = gp_near(964.5,-189)
gri_chk110 = gp_near(973.5,-189)
gri_chk111 = gp_near(982.5,-189)
gri_chk112 = gp_near(991.5,-189)
gri_chk113 = gp_near(1000.5,-189)
gri_chk114 = gp_near(1009.5,-189)
gri_chk115 = gp_near(1018.5,-189)
gri_chk116 = gp_near(1027.5,-189)
gri_chk117 = gp_near(1036.5,-189)
gri_chk118 = gp_near(1045.5,-189)
gri_chk119 = gp_near(1050.0,-189)

; Defining y-displacements from Model 4

max_disp1 = 1.398e-03
max_disp2 = 1.394e-03
max_disp3 = 1.372e-03
max_disp4 = 1.331e-03
max_disp5 = 1.270e-03
max_disp6 = 1.188e-03
max_disp7 = 1.086e-03
max_disp8 = 9.621e-04
```

```
max_disp9  =  8.172e-04
max_disp10 =  6.505e-04
max_disp11 =  4.614e-04
max_disp12 =  2.494e-04
max_disp13 =  1.411e-05
max_disp14 = -2.455e-04
max_disp15 = -5.299e-04
max_disp16 = -8.401e-04
max_disp17 = -1.177e-03
max_disp18 = -1.542e-03
max_disp19 = -1.937e-03
max_disp20 = -2.362e-03
max_disp21 = -2.820e-03
max_disp22 = -3.313e-03
max_disp23 = -3.843e-03
max_disp24 = -4.413e-03
max_disp25 = -5.027e-03
max_disp26 = -5.686e-03
max_disp27 = -6.396e-03
max_disp28 = -7.159e-03
max_disp29 = -7.980e-03
max_disp30 = -8.861e-03
max_disp31 = -9.804e-03
max_disp32 = -1.081e-02
max_disp33 = -1.190e-02
max_disp34 = -1.306e-02
max_disp35 = -1.430e-02
max_disp36 = -1.562e-02
max_disp37 = -1.703e-02
max_disp38 = -1.854e-02
max_disp39 = -2.014e-02
max_disp40 = -2.185e-02
max_disp41 = -2.367e-02
max_disp42 = -2.563e-02
max_disp43 = -2.778e-02
max_disp44 = -3.024e-02
max_disp45 = -3.344e-02
max_disp46 = -3.810e-02
max_disp47 = -4.513e-02
max_disp48 = -5.516e-02
max_disp49 = -6.945e-02
```

```
max_disp50 = -9.050e-02
max_disp51 = -1.225e-01
max_disp52 = -1.700e-01
max_disp53 = -2.312e-01
max_disp54 = -2.952e-01
max_disp55 = -3.600e-01
max_disp56 = -4.214e-01
max_disp57 = -4.754e-01
max_disp58 = -5.190e-01
max_disp59 = -5.502e-01
max_disp60 = -2.362e+00
max_disp61 = -5.502e-01
max_disp62 = -5.190e-01
max_disp63 = -4.754e-01
max_disp64 = -4.214e-01
max_disp65 = -3.600e-01
max_disp66 = -2.952e-01
max_disp67 = -2.312e-01
max_disp68 = -1.700e-01
max_disp69 = -1.225e-01
max_disp70 = -9.050e-02
max_disp71 = -6.945e-02
max_disp72 = -5.516e-02
max_disp73 = -4.513e-02
max_disp74 = -3.810e-02
max_disp75 = -3.344e-02
max_disp76 = -3.024e-02
max_disp77 = -2.778e-02
max_disp78 = -2.563e-02
max_disp79 = -2.367e-02
max_disp80 = -2.185e-02
max_disp81 = -2.014e-02
max_disp82 = -1.854e-02
max_disp83 = -1.703e-02
max_disp84 = -1.562e-02
max_disp85 = -1.430e-02
max_disp86 = -1.306e-02
max_disp87 = -1.190e-02
max_disp88 = -1.081e-02
max_disp89 = -9.804e-03
max_disp90 = -8.861e-03
```

```
max_disp91  = -7.980e-03
max_disp92  = -7.159e-03
max_disp93  = -6.396e-03
max_disp94  = -5.686e-03
max_disp95  = -5.027e-03
max_disp96  = -4.413e-03
max_disp97  = -3.843e-03
max_disp98  = -3.313e-03
max_disp99  = -2.820e-03
max_disp100 = -2.362e-03
max_disp101 = -1.937e-03
max_disp102 = -1.542e-03
max_disp103 = -1.177e-03
max_disp104 = -8.401e-04
max_disp105 = -5.299e-04
max_disp106 = -2.455e-04
max_disp107 =  1.411e-05
max_disp108 =  2.494e-04
max_disp109 =  4.614e-04
max_disp110 =  6.505e-04
max_disp111 =  8.172e-04
max_disp112 =  9.621e-04
max_disp113 =  1.086e-03
max_disp114 =  1.188e-03
max_disp115 =  1.270e-03
max_disp116 =  1.331e-03
max_disp117 =  1.372e-03
max_disp118 =  1.394e-03
max_disp119 =  1.398e-03

; Converting y-displacement into y-velocity via timestep and number of
cycles and assigning to corresponding gridpoints

gp_yvel(gri_chk1) = max_disp1/(30000*tdel)
gp_yvel(gri_chk2) = max_disp2/(30000*tdel)
gp_yvel(gri_chk3) = max_disp3/(30000*tdel)
gp_yvel(gri_chk4) = max_disp4/(30000*tdel)
gp_yvel(gri_chk5) = max_disp5/(30000*tdel)
gp_yvel(gri_chk6) = max_disp6/(30000*tdel)
gp_yvel(gri_chk7) = max_disp7/(30000*tdel)
gp_yvel(gri_chk8) = max_disp8/(30000*tdel)
```

```
gp_yvel(gri_chk9)  = max_disp9/(30000*tdel)
gp_yvel(gri_chk10) = max_disp10/(30000*tdel)
gp_yvel(gri_chk11) = max_disp11/(30000*tdel)
gp_yvel(gri_chk12) = max_disp12/(30000*tdel)
gp_yvel(gri_chk13) = max_disp13/(30000*tdel)
gp_yvel(gri_chk14) = max_disp14/(30000*tdel)
gp_yvel(gri_chk15) = max_disp15/(30000*tdel)
gp_yvel(gri_chk16) = max_disp16/(30000*tdel)
gp_yvel(gri_chk17) = max_disp17/(30000*tdel)
gp_yvel(gri_chk18) = max_disp18/(30000*tdel)
gp_yvel(gri_chk19) = max_disp19/(30000*tdel)
gp_yvel(gri_chk20) = max_disp20/(30000*tdel)
gp_yvel(gri_chk21) = max_disp21/(30000*tdel)
gp_yvel(gri_chk22) = max_disp22/(30000*tdel)
gp_yvel(gri_chk23) = max_disp23/(30000*tdel)
gp_yvel(gri_chk24) = max_disp24/(30000*tdel)
gp_yvel(gri_chk25) = max_disp25/(30000*tdel)
gp_yvel(gri_chk26) = max_disp26/(30000*tdel)
gp_yvel(gri_chk27) = max_disp27/(30000*tdel)
gp_yvel(gri_chk28) = max_disp28/(30000*tdel)
gp_yvel(gri_chk29) = max_disp29/(30000*tdel)
gp_yvel(gri_chk30) = max_disp30/(30000*tdel)
gp_yvel(gri_chk31) = max_disp31/(30000*tdel)
gp_yvel(gri_chk32) = max_disp32/(30000*tdel)
gp_yvel(gri_chk33) = max_disp33/(30000*tdel)
gp_yvel(gri_chk34) = max_disp34/(30000*tdel)
gp_yvel(gri_chk35) = max_disp35/(30000*tdel)
gp_yvel(gri_chk36) = max_disp36/(30000*tdel)
gp_yvel(gri_chk37) = max_disp37/(30000*tdel)
gp_yvel(gri_chk38) = max_disp38/(30000*tdel)
gp_yvel(gri_chk39) = max_disp39/(30000*tdel)
gp_yvel(gri_chk40) = max_disp40/(30000*tdel)
gp_yvel(gri_chk41) = max_disp41/(30000*tdel)
gp_yvel(gri_chk42) = max_disp42/(30000*tdel)
gp_yvel(gri_chk43) = max_disp43/(30000*tdel)
gp_yvel(gri_chk44) = max_disp44/(30000*tdel)
gp_yvel(gri_chk45) = max_disp45/(30000*tdel)
gp_yvel(gri_chk46) = max_disp46/(30000*tdel)
gp_yvel(gri_chk47) = max_disp47/(30000*tdel)
gp_yvel(gri_chk48) = max_disp48/(30000*tdel)
gp_yvel(gri_chk49) = max_disp49/(30000*tdel)
```

```
gp_yvel(gri_chk50) = max_disp50/(30000*tdel)
gp_yvel(gri_chk51) = max_disp51/(30000*tdel)
gp_yvel(gri_chk52) = max_disp52/(30000*tdel)
gp_yvel(gri_chk53) = max_disp53/(30000*tdel)
gp_yvel(gri_chk54) = max_disp54/(30000*tdel)
gp_yvel(gri_chk55) = max_disp55/(30000*tdel)
gp_yvel(gri_chk56) = max_disp56/(30000*tdel)
gp_yvel(gri_chk57) = max_disp57/(30000*tdel)
gp_yvel(gri_chk58) = max_disp58/(30000*tdel)
gp_yvel(gri_chk59) = max_disp59/(30000*tdel)
gp_yvel(gri_chk60) = max_disp60/(30000*tdel)
gp_yvel(gri_chk61) = max_disp61/(30000*tdel)
gp_yvel(gri_chk62) = max_disp62/(30000*tdel)
gp_yvel(gri_chk63) = max_disp63/(30000*tdel)
gp_yvel(gri_chk64) = max_disp64/(30000*tdel)
gp_yvel(gri_chk65) = max_disp65/(30000*tdel)
gp_yvel(gri_chk66) = max_disp66/(30000*tdel)
gp_yvel(gri_chk67) = max_disp67/(30000*tdel)
gp_yvel(gri_chk68) = max_disp68/(30000*tdel)
gp_yvel(gri_chk69) = max_disp69/(30000*tdel)
gp_yvel(gri_chk70) = max_disp70/(30000*tdel)
gp_yvel(gri_chk71) = max_disp71/(30000*tdel)
gp_yvel(gri_chk72) = max_disp72/(30000*tdel)
gp_yvel(gri_chk73) = max_disp73/(30000*tdel)
gp_yvel(gri_chk74) = max_disp74/(30000*tdel)
gp_yvel(gri_chk75) = max_disp75/(30000*tdel)
gp_yvel(gri_chk76) = max_disp76/(30000*tdel)
gp_yvel(gri_chk77) = max_disp77/(30000*tdel)
gp_yvel(gri_chk78) = max_disp78/(30000*tdel)
gp_yvel(gri_chk79) = max_disp79/(30000*tdel)
gp_yvel(gri_chk80) = max_disp80/(30000*tdel)
gp_yvel(gri_chk81) = max_disp81/(30000*tdel)
gp_yvel(gri_chk82) = max_disp82/(30000*tdel)
gp_yvel(gri_chk83) = max_disp83/(30000*tdel)
gp_yvel(gri_chk84) = max_disp84/(30000*tdel)
gp_yvel(gri_chk85) = max_disp85/(30000*tdel)
gp_yvel(gri_chk86) = max_disp86/(30000*tdel)
gp_yvel(gri_chk87) = max_disp87/(30000*tdel)
gp_yvel(gri_chk88) = max_disp88/(30000*tdel)
gp_yvel(gri_chk89) = max_disp89/(30000*tdel)
gp_yvel(gri_chk90) = max_disp90/(30000*tdel)
```

```
gp_yvel(gri_chk91)  = max_disp91/(30000*tdel)
gp_yvel(gri_chk92)  = max_disp92/(30000*tdel)
gp_yvel(gri_chk93)  = max_disp93/(30000*tdel)
gp_yvel(gri_chk94)  = max_disp94/(30000*tdel)
gp_yvel(gri_chk95)  = max_disp95/(30000*tdel)
gp_yvel(gri_chk96)  = max_disp96/(30000*tdel)
gp_yvel(gri_chk97)  = max_disp97/(30000*tdel)
gp_yvel(gri_chk98)  = max_disp98/(30000*tdel)
gp_yvel(gri_chk99)  = max_disp99/(30000*tdel)
gp_yvel(gri_chk100) = max_disp100/(30000*tdel)
gp_yvel(gri_chk101) = max_disp101/(30000*tdel)
gp_yvel(gri_chk102) = max_disp102/(30000*tdel)
gp_yvel(gri_chk103) = max_disp103/(30000*tdel)
gp_yvel(gri_chk104) = max_disp104/(30000*tdel)
gp_yvel(gri_chk105) = max_disp105/(30000*tdel)
gp_yvel(gri_chk106) = max_disp106/(30000*tdel)
gp_yvel(gri_chk107) = max_disp107/(30000*tdel)
gp_yvel(gri_chk108) = max_disp108/(30000*tdel)
gp_yvel(gri_chk109) = max_disp109/(30000*tdel)
gp_yvel(gri_chk110) = max_disp110/(30000*tdel)
gp_yvel(gri_chk111) = max_disp111/(30000*tdel)
gp_yvel(gri_chk112) = max_disp112/(30000*tdel)
gp_yvel(gri_chk113) = max_disp113/(30000*tdel)
gp_yvel(gri_chk114) = max_disp114/(30000*tdel)
gp_yvel(gri_chk115) = max_disp115/(30000*tdel)
gp_yvel(gri_chk116) = max_disp116/(30000*tdel)
gp_yvel(gri_chk117) = max_disp117/(30000*tdel)
gp_yvel(gri_chk118) = max_disp118/(30000*tdel)
gp_yvel(gri_chk119) = max_disp119/(30000*tdel)
temp1  = gp_yvel(gri_chk1)
temp2  = gp_yvel(gri_chk2)
temp3  = gp_yvel(gri_chk3)
temp4  = gp_yvel(gri_chk4)
temp5  = gp_yvel(gri_chk5)
temp6  = gp_yvel(gri_chk6)
temp7  = gp_yvel(gri_chk7)
temp8  = gp_yvel(gri_chk8)
temp9  = gp_yvel(gri_chk9)
temp10 = gp_yvel(gri_chk10)
temp11 = gp_yvel(gri_chk11)
temp12 = gp_yvel(gri_chk12)
```

```
temp13 = gp_yvel(gri_chk13)
temp14 = gp_yvel(gri_chk14)
temp15 = gp_yvel(gri_chk15)
temp16 = gp_yvel(gri_chk16)
temp17 = gp_yvel(gri_chk17)
temp18 = gp_yvel(gri_chk18)
temp19 = gp_yvel(gri_chk19)
temp20 = gp_yvel(gri_chk20)
temp21 = gp_yvel(gri_chk21)
temp22 = gp_yvel(gri_chk22)
temp23 = gp_yvel(gri_chk23)
temp24 = gp_yvel(gri_chk24)
temp25 = gp_yvel(gri_chk25)
temp26 = gp_yvel(gri_chk26)
temp27 = gp_yvel(gri_chk27)
temp28 = gp_yvel(gri_chk28)
temp29 = gp_yvel(gri_chk29)
temp30 = gp_yvel(gri_chk30)
temp31 = gp_yvel(gri_chk31)
temp32 = gp_yvel(gri_chk32)
temp33 = gp_yvel(gri_chk33)
temp34 = gp_yvel(gri_chk34)
temp35 = gp_yvel(gri_chk35)
temp36 = gp_yvel(gri_chk36)
temp37 = gp_yvel(gri_chk37)
temp38 = gp_yvel(gri_chk38)
temp39 = gp_yvel(gri_chk39)
temp40 = gp_yvel(gri_chk40)
temp41 = gp_yvel(gri_chk41)
temp42 = gp_yvel(gri_chk42)
temp43 = gp_yvel(gri_chk43)
temp44 = gp_yvel(gri_chk44)
temp45 = gp_yvel(gri_chk45)
temp46 = gp_yvel(gri_chk46)
temp47 = gp_yvel(gri_chk47)
temp48 = gp_yvel(gri_chk48)
temp49 = gp_yvel(gri_chk49)
temp50 = gp_yvel(gri_chk50)
temp51 = gp_yvel(gri_chk51)
temp52 = gp_yvel(gri_chk52)
temp53 = gp_yvel(gri_chk53)
```

```
temp54 = gp_yvel(gri_chk54)
temp55 = gp_yvel(gri_chk55)
temp56 = gp_yvel(gri_chk56)
temp57 = gp_yvel(gri_chk57)
temp58 = gp_yvel(gri_chk58)
temp59 = gp_yvel(gri_chk59)
temp60 = gp_yvel(gri_chk60)
temp61 = gp_yvel(gri_chk61)
temp62 = gp_yvel(gri_chk62)
temp63 = gp_yvel(gri_chk63)
temp64 = gp_yvel(gri_chk64)
temp65 = gp_yvel(gri_chk65)
temp66 = gp_yvel(gri_chk66)
temp67 = gp_yvel(gri_chk67)
temp68 = gp_yvel(gri_chk68)
temp69 = gp_yvel(gri_chk69)
temp70 = gp_yvel(gri_chk70)
temp71 = gp_yvel(gri_chk71)
temp72 = gp_yvel(gri_chk72)
temp73 = gp_yvel(gri_chk73)
temp74 = gp_yvel(gri_chk74)
temp75 = gp_yvel(gri_chk75)
temp76 = gp_yvel(gri_chk76)
temp77 = gp_yvel(gri_chk77)
temp78 = gp_yvel(gri_chk78)
temp79 = gp_yvel(gri_chk79)
temp80 = gp_yvel(gri_chk80)
temp81 = gp_yvel(gri_chk81)
temp82 = gp_yvel(gri_chk82)
temp83 = gp_yvel(gri_chk83)
temp84 = gp_yvel(gri_chk84)
temp85 = gp_yvel(gri_chk85)
temp86 = gp_yvel(gri_chk86)
temp87 = gp_yvel(gri_chk87)
temp88 = gp_yvel(gri_chk88)
temp89 = gp_yvel(gri_chk89)
temp90 = gp_yvel(gri_chk90)
temp91 = gp_yvel(gri_chk91)
temp92 = gp_yvel(gri_chk92)
temp93 = gp_yvel(gri_chk93)
temp94 = gp_yvel(gri_chk94)
```

```
temp95  = gp_yvel(gri_chk95)
temp96  = gp_yvel(gri_chk96)
temp97  = gp_yvel(gri_chk97)
temp98  = gp_yvel(gri_chk98)
temp99  = gp_yvel(gri_chk99)
temp100 = gp_yvel(gri_chk100)
temp101 = gp_yvel(gri_chk101)
temp102 = gp_yvel(gri_chk102)
temp103 = gp_yvel(gri_chk103)
temp104 = gp_yvel(gri_chk104)
temp105 = gp_yvel(gri_chk105)
temp106 = gp_yvel(gri_chk106)
temp107 = gp_yvel(gri_chk107)
temp108 = gp_yvel(gri_chk108)
temp109 = gp_yvel(gri_chk109)
temp110 = gp_yvel(gri_chk110)
temp111 = gp_yvel(gri_chk111)
temp112 = gp_yvel(gri_chk112)
temp113 = gp_yvel(gri_chk113)
temp114 = gp_yvel(gri_chk114)
temp115 = gp_yvel(gri_chk115)
temp116 = gp_yvel(gri_chk116)
temp117 = gp_yvel(gri_chk117)
temp118 = gp_yvel(gri_chk118)
temp119 = gp_yvel(gri_chk119)
end

valleysolve

; Assigning y-velocities to base

bo yv temp1  ra -0.1  0.1 -189.1 -188.9
bo yv temp2  ra  4.4  4.6 -189.1 -188.9
bo yv temp3  ra 13.4 13.6 -189.1 -188.9
bo yv temp4  ra 22.4 22.6 -189.1 -188.9
bo yv temp5  ra 31.4 31.6 -189.1 -188.9
bo yv temp6  ra 40.4 40.6 -189.1 -188.9
bo yv temp7  ra 49.4 49.6 -189.1 -188.9
bo yv temp8  ra 58.4 58.6 -189.1 -188.9
bo yv temp9  ra 67.4 67.6 -189.1 -188.9
bo yv temp10 ra 76.4 76.6 -189.1 -188.9
```

```
bo yv temp11 ra  85.4  85.6 -189.1 -188.9
bo yv temp12 ra  94.4  94.6 -189.1 -188.9
bo yv temp13 ra 103.4 103.6 -189.1 -188.9
bo yv temp14 ra 112.4 112.6 -189.1 -188.9
bo yv temp15 ra 121.4 121.6 -189.1 -188.9
bo yv temp16 ra 130.4 130.6 -189.1 -188.9
bo yv temp17 ra 139.4 139.6 -189.1 -188.9
bo yv temp18 ra 148.4 148.6 -189.1 -188.9
bo yv temp19 ra 157.4 157.6 -189.1 -188.9
bo yv temp20 ra 166.4 166.6 -189.1 -188.9
bo yv temp21 ra 175.4 175.6 -189.1 -188.9
bo yv temp22 ra 184.4 184.6 -189.1 -188.9
bo yv temp23 ra 193.4 193.6 -189.1 -188.9
bo yv temp24 ra 202.4 202.6 -189.1 -188.9
bo yv temp25 ra 211.4 211.6 -189.1 -188.9
bo yv temp26 ra 220.4 220.6 -189.1 -188.9
bo yv temp27 ra 229.4 229.6 -189.1 -188.9
bo yv temp28 ra 238.4 238.6 -189.1 -188.9
bo yv temp29 ra 247.4 247.6 -189.1 -188.9
bo yv temp30 ra 256.4 256.6 -189.1 -188.9
bo yv temp31 ra 265.4 265.6 -189.1 -188.9
bo yv temp32 ra 274.4 274.6 -189.1 -188.9
bo yv temp33 ra 283.4 283.6 -189.1 -188.9
bo yv temp34 ra 292.4 292.6 -189.1 -188.9
bo yv temp35 ra 301.4 301.6 -189.1 -188.9
bo yv temp36 ra 310.4 310.6 -189.1 -188.9
bo yv temp37 ra 319.4 319.6 -189.1 -188.9
bo yv temp38 ra 328.4 328.6 -189.1 -188.9
bo yv temp39 ra 337.4 337.6 -189.1 -188.9
bo yv temp40 ra 346.4 346.6 -189.1 -188.9
bo yv temp41 ra 355.4 355.6 -189.1 -188.9
bo yv temp42 ra 364.4 364.6 -189.1 -188.9
bo yv temp43 ra 373.4 373.6 -189.1 -188.9
bo yv temp44 ra 382.4 382.6 -189.1 -188.9
bo yv temp45 ra 391.4 391.6 -189.1 -188.9
bo yv temp46 ra 400.4 400.6 -189.1 -188.9
bo yv temp47 ra 409.4 409.6 -189.1 -188.9
bo yv temp48 ra 418.4 418.6 -189.1 -188.9
bo yv temp49 ra 427.4 427.6 -189.1 -188.9
bo yv temp50 ra 436.4 436.6 -189.1 -188.9
bo yv temp51 ra 445.4 445.6 -189.1 -188.9
```

```
bo yv temp52 ra 454.4 454.6 -189.1 -188.9
bo yv temp53 ra 463.4 463.6 -189.1 -188.9
bo yv temp54 ra 472.4 472.6 -189.1 -188.9
bo yv temp55 ra 481.4 481.6 -189.1 -188.9
bo yv temp56 ra 490.4 490.6 -189.1 -188.9
bo yv temp57 ra 499.4 499.6 -189.1 -188.9
bo yv temp58 ra 508.4 508.6 -189.1 -188.9
bo yv temp59 ra 517.4 517.6 -189.1 -188.9
bo yv temp60 ra 524.9 525.1 -189.1 -188.9
bo yv temp61 ra 532.4 532.6 -189.1 -188.9
bo yv temp62 ra 541.4 541.6 -189.1 -188.9
bo yv temp63 ra 550.4 550.6 -189.1 -188.9
bo yv temp64 ra 559.4 559.6 -189.1 -188.9
bo yv temp65 ra 568.4 568.6 -189.1 -188.9
bo yv temp66 ra 577.4 577.6 -189.1 -188.9
bo yv temp67 ra 586.4 586.6 -189.1 -188.9
bo yv temp68 ra 595.4 595.6 -189.1 -188.9
bo yv temp69 ra 604.4 604.6 -189.1 -188.9
bo yv temp70 ra 613.4 613.6 -189.1 -188.9
bo yv temp71 ra 622.4 622.6 -189.1 -188.9
bo yv temp72 ra 631.4 631.6 -189.1 -188.9
bo yv temp73 ra 640.4 640.6 -189.1 -188.9
bo yv temp74 ra 649.4 649.6 -189.1 -188.9
bo yv temp75 ra 658.4 658.6 -189.1 -188.9
bo yv temp76 ra 667.4 667.6 -189.1 -188.9
bo yv temp77 ra 676.4 676.6 -189.1 -188.9
bo yv temp78 ra 685.4 685.6 -189.1 -188.9
bo yv temp79 ra 694.4 694.6 -189.1 -188.9
bo yv temp80 ra 703.4 703.6 -189.1 -188.9
bo yv temp81 ra 712.4 712.6 -189.1 -188.9
bo yv temp82 ra 721.4 721.6 -189.1 -188.9
bo yv temp83 ra 730.4 730.6 -189.1 -188.9
bo yv temp84 ra 739.4 739.6 -189.1 -188.9
bo yv temp85 ra 748.4 748.6 -189.1 -188.9
bo yv temp86 ra 757.4 757.6 -189.1 -188.9
bo yv temp87 ra 766.4 766.6 -189.1 -188.9
bo yv temp88 ra 775.4 775.6 -189.1 -188.9
bo yv temp89 ra 784.4 784.6 -189.1 -188.9
bo yv temp90 ra 793.4 793.6 -189.1 -188.9
bo yv temp91 ra 802.4 802.6 -189.1 -188.9
bo yv temp92 ra 811.4 811.6 -189.1 -188.9
```

```
bo yv temp93  ra  820.4  820.6 -189.1 -188.9
bo yv temp94  ra  829.4  829.6 -189.1 -188.9
bo yv temp95  ra  838.4  838.6 -189.1 -188.9
bo yv temp96  ra  847.4  847.6 -189.1 -188.9
bo yv temp97  ra  856.4  856.6 -189.1 -188.9
bo yv temp98  ra  865.4  865.6 -189.1 -188.9
bo yv temp99  ra  874.4  874.6 -189.1 -188.9
bo yv temp100 ra  883.4  883.6 -189.1 -188.9
bo yv temp101 ra  892.4  892.6 -189.1 -188.9
bo yv temp102 ra  901.4  901.6 -189.1 -188.9
bo yv temp103 ra  910.4  910.6 -189.1 -188.9
bo yv temp104 ra  919.4  919.6 -189.1 -188.9
bo yv temp105 ra  928.4  928.6 -189.1 -188.9
bo yv temp106 ra  937.4  937.6 -189.1 -188.9
bo yv temp107 ra  946.4  946.6 -189.1 -188.9
bo yv temp108 ra  955.4  955.6 -189.1 -188.9
bo yv temp109 ra  964.4  964.6 -189.1 -188.9
bo yv temp110 ra  973.4  973.6 -189.1 -188.9
bo yv temp111 ra  982.4  982.6 -189.1 -188.9
bo yv temp112 ra  991.4  991.6 -189.1 -188.9
bo yv temp113 ra 1000.4 1000.6 -189.1 -188.9
bo yv temp114 ra 1009.4 1009.6 -189.1 -188.9
bo yv temp115 ra 1018.4 1018.6 -189.1 -188.9
bo yv temp116 ra 1027.4 1027.6 -189.1 -188.9
bo yv temp117 ra 1036.4 1036.6 -189.1 -188.9
bo yv temp118 ra 1045.4 1045.6 -189.1 -188.9
bo yv temp119 ra 1049.9 1050.9 -189.1 -188.9

s 30000

; Resetting boundary conditions

bo yfr
bo xfr
bo yv 0 ra 0 1050 -200 -188.9
bo xv 0 ra -0.1 0.1 -189.1 0.1
bo xv 0 ra 1049.9 1050.1 -189.1 0.1
```

```
; Solving for final equilibrium

da a

so rat 1e-5 ste 1000000

sa valley1_ini2.sav

s 20000

sa valley1_final.sav
```

APPENDIX E
VOUSSOIR BEAM THEORY

E.1 INTRODUCTION

It has been shown in the past that voussoir beam theory can be applied to mining subsidence problems quite effectively (Seedsman 2004), provided that there is a massive spanning unit in the overburden that remains elastic, the material properties of the spanning unit and overburden are known, and the characteristics of the cave zone is known.

Instead of providing a complete analysis and derivation of all the expressions required to calculate deflection with the voussoir beam theory, only the idealised three-joint voussoir beam model will be shown and the formulas required to determine beam deflection will be presented. The formulas presented are easily incorporated into a spreadsheet to make quick assessments of beams and the results from the analysis for Models 1 to 4 will be presented. The complete derivation can be found in Sofianos (1996) and Sofianos and Kapenis (1998), and further advancement on the topic as applied to multi-jointed beams can be found in Nomikos, Sofianos and Tsoutrelis (2002).

E.2 VOUSSOIR BEAM THEORY

Figure E.1 illustrates a three-joint voussoir beam model.

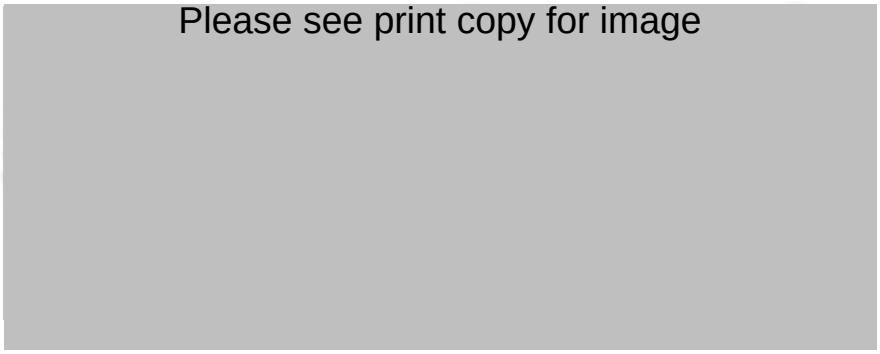

Fig. E.1 – Three-joint symmetric voussoir rock beam (Sofianos & Kapenis 1998)

The following assumptions are made:

- Rock is homogeneous, isotropic and elastic,
- The beam is horizontal and symmetric, is uniformly loaded and has only three vertical joints, one at the midspan and one at each end of the abutments,
- The abutment supports are rigid and the joints are very stiff,
- The rock Poisson's ratio is zero, and
- There is no lateral stress confining the beam prior to its deflection.

The calculation process is performed by following Equations E.1 to E.8.

$$Q_n = k_q \frac{s\gamma}{E} \qquad [E.1]$$

$$S_n = \frac{s}{t} \qquad [E.2]$$

$$n = 0.3 - 0.14 s_n \sqrt[3]{Q_n} \qquad [E.3]$$

$$z_{0n} = 1 - \frac{2}{3} n \qquad [E.4]$$

$$s_z = \frac{s_n}{z_{0n}} \qquad [E.5]$$

$$\delta_z = \frac{Q_n S_z^3}{16} \qquad [E.6]$$

$$z_0 = z_{0n} t \qquad [E.7]$$

$$\delta = \delta_z z_0 \qquad [E.8]$$

Where,

Q = Total weight of the voussoir beam
k_q = Ratio of total load on the voussoir beam to its self weight
S = Clear span of the voussoir beam
γ = Unit weight of the rock comprising the voussoir beam
E = Young's modulus of the rock comprising the voussoir beam
n = Normalised contact length at the abutment or midspan
z = Lever arm of the horizontal thrust couple
δ = Vertical deflection of the rock beam at midspan

The subscripts (unless otherwise stated) are as follows:

n = Normalisation of s or Q by division with t or tE, respectively
0 = Corresponding to the undeformed geometry of the beam
z = Normalisation of lengths by division with z_0

Once the beam deflection has been calculated, the factor of safety against buckling (FS_b) can be assessed with Equation E.9.

$$FS_b = \frac{3.15}{Q_n s_z^3} \qquad [E.9]$$

Finally, for a certain span of the beam the limiting thickness which corresponds to a factor of safety equal to one may be assessed from Equation E.10.

$$t_{\min} \approx \frac{s}{z_{0n}} \sqrt[3]{\frac{Q_n}{3.15}} \qquad [E.10]$$

It is important to note that these analytical solutions have been verified numerically with UDEC (Sofianos 1996; and Sofianos & Kapenis 1998).

In the Bulgo Sandstone analysis, the predicted deflection is quite sensitive to the chosen value of n and the goaf angle (which is used in calculating the resulting surcharge).

Using an *n* value of 0.75 has proven to be effective whilst it has also been stated that for a large number of joints, *n* is between 0.18 and 0.30 (Nomikos, Sofianos & Tsoutrelis 2002). The values of *n* used in the Bulgo Sandstone analysis have been calculated using Equation E.3.